Model predictive control of a Brayton cycle based power plant

---

by

Peter Kabanda Lusanga

A dissertation presented to the School of Electrical and Electronic Engineering, In partial fulfilment of the requirements for the degree Master of Engineering in Electric and Electronic Engineering at the Potchefstroom campus of the North-West University.

Supervisor: Dr. K. R. Uren

March 2012

ABSTRACT

The aim of this study is to implement the model predictive control in order to optimally control the power output of a Brayton cycle based power plant. Other control strategies have been tried but there still exists the need for better performance. In real systems, a number of constraints exist. Incorporating these into the control design is no trivial task. Unlike in most control strategies, model predictive control allows the designer to explicitly incorporate constraints in its formulation. The original design of the PBMR power plant is considered. It uses helium gas as the working fluid. The power output of the system can be controlled by manipulating the helium inventory to the gas cycle.

A linear model of the power plant, modelled in Simulink® is used. This linear model is used as an evaluation platform for the control strategy. The helium inventory is manipulated by means of actuators which use values generated by the controller. The controller computes these values by minimizing the cost of future outputs over a finite horizon in the presence of constraints.

The dynamic response of the system is used to tune the controller. The power output performance at different configurations of the controller under perfect conditions and with disturbances is examined. The best configuration is used resulting in an optimal power control system for the Brayton cycle based power plant.

Results showed that the method employed can be used to implement the control strategy. Furthermore, better performance can be realised with model predictive control.

Keywords: control, predictive, Brayton, cycle, advanced, optimal, power, generation, nuclear

ACKNOWLEDGEMENTS

I would like to firstly thank the school of Electrical and Electronic engineering for granting me the opportunity to further my studies.

I would also like to make mention of people who were a great help and to whom I owe my gratitude for starting and completing this project.

- Professor Charles Bodenstein, for being a source of motivation, encouragement and guidance. He was instrumental in my admission and upkeep at the beginning of my studies.

- Dr Kenny Uren, my supervisor, for his encouragement, advice, guidance and support. His leadership was cardinal throughout the course of this project.

- My parents, Dr Ngandwe K Mumba and Dr S M Lwenje, for their encouragement, support and understanding. Not forgetting my brother, Geoffrey, and sisters Natasha, Sarah, Chibale and Nandwe for their great expectations of me.

- Professor George van Schoor, for being instrumental in me completing my studies.

- Professor Alwyn Hoffman for being a source of encouragement and inspiration. His patience and faith kept me going.

- Professor Jan de Kock and the entire postgraduates committee for granting me extended time to complete my project.

- Pastor Shane Murray for being a source of encouragement and motivation. His words made me pull through even in difficult times.

- My friends and also the brethren of El tabernacle Potch for their prayers and encouragement.

- Mr Shuping Lechuti for being a great support in the most critical time of the project.

“Trust in the LORD with all thine heart; and lean not unto thine own understanding.” Proverbs 3:5

“Delight thyself also in the LORD; and he shall give thee the desires of thine heart. “ Psalm 37:4

TABLE OF CONTENTS

LIST OF FIGURES

LIST OF TABLES

LIST OF ABBREVIATIONS

GA	Genetic Algorithm
GAs	Genetic Algorithms
GFS	Genetic Fuzzy Systems
PID	Proportional, Integral and Derivative
PBMR	Pebble Bed Modular Reactor
HPT	High-pressure Turbine
HPC	High-pressure Compressor
LPT	Low-pressure Turbine
LPC	Low-pressure Compressor
PT	Power Turbine
GBPC	Gas Cycle Bypass Control Valve
FPID	Fuzzy Proportional, Integral and Derivative
FDSS	Fuzzy Decision Support System
FSs	Fuzzy Systems
FRBS	Fuzzy Rule Based Systems
KB	Knowledge Base
DB	Data Base
RB	Rule Base
MPS	Main Power System
PCU	Power Conversion Unit
RU	Reactor Unit
GUI	Graphical User Interface
AI	Artificial Intelligence
LPI	Low-pressure Injection
HPE	High-pressure Extraction
FLPI	Fuzzy Low-pressure Injection
FHPE	Fuzzy High-pressure Extraction

LIST OF SYMBOLS

e	Error
ce	Change in error
ie	Integral of error
u	Control variable
μ	Degree of membership
C	Capacitance
V	Volume
$p(t)$	Pressure
$v(t)$	Voltage
$i(t)$	Current
$q(t)$	Volumetric flow rate
N_{ind}	Number of individuals
L_{ind}	Number of parameters for optimisation
N_{MH}	Model Horizon; Number of past control moves
K_p	Open loop gain
t_s	Settling time
t_r	Rise time
T	Sampling time
θ_p	Effective dead-time
θ_d	Discrete dead-time integer
f_c	Corner frequency
τ	Largest time constant in the system
θ_{inv}	Inverse response time
P	Prediction horizon
M	Control horizon
Q_{cb}	Controllability matrix
Q_{ob}	Observability matrix
P_1	the total machine inlet pressure (in bars)
P_2	the total machine outlet pressure (in bars)
T_1	the total machine inlet temperature (in K)

T_2 the total machine outlet temperature (in K)

Q the mass flow rate (in kg/s)

N the speed of the turbo-compressor shaft (in rev/s)

C_p the specific heat capacity of the gas at constant pressure (in J/(kg K))

C_v the specific heat capacity of the gas at constant volume (in J/(kg K))

γ the ratio of specific heats of the gas = C_p/C_v

Q' the "non-dimensional mass flow rate" = $Q\sqrt{T_1}/P_1$

(Note: the units are not dimensionless, but the quantity is simply referred to as non-dimensional mass flow rate)

N' the "non dimensional speed" = $N/\sqrt{T_1}$

(Note: the units are not truly non-dimensional, but the quantity is simply referred to as non-dimensional speed)

W the shaft output power (in Watts) = $Q_{C_p}(T_1 - T_2)$

T_{ht} the high pressure turbine torque (in Nm)

T_{lt} the low pressure turbine torque (in Nm)

T_{hc} high pressure compressor driving torque (in Nm)

T_{lc} the low pressure compressor driving torque (in Nm)

J_{hp} the total moment of inertia of the high pressure turbo-compressor (in kg·m²)

J_{lp} the total moment of inertia of the low pressure turbo-compressor (in kg·m²)

Chapter 1
Introduction

1.1 Background

1.1.1 Relevance of the study

Nuclear energy is being pursued by both developed and developing nations as a solution to meet energy demands. There are a number of nuclear power technologies in use today. They can be categorised into steam and gas turbine reactors. Currently, research is being done on more efficient technologies.

High temperature gas cooled reactors have gained popularity [**1**]. One such technology is the Pebble Bed Modular Reactor (PBMR). The system is called modular since it can operate in stand alone mode or as a combination of such units [**2**]. The 14 February 2010 issue of the Business times, South Africa, described the Pebble Bed Modular Reactor (PBMR) as a company developing some of the most exciting nuclear technology in the world [**3**]. Its popularity is due to its smaller design, its assured environmental safety, short construction time, efficient part load performance, low operational logistic requirements, quick response to sudden load changes and low environmental impact [**4**], [**5**].

PBMR was started in 1999 by Eskom and had government as its chief shareholder. Foreign investment of R2 billion has taken place and reveals international interest in the technology being developed and the global benefit it holds [**6**]. The company is based in Centurion outside Pretoria [**7**]. However, a Brayton cycle test facility for the pebble bed modular reactor was set up at the North West University, Potchefstroom campus [**8**].

The PBMR was initially based on the 3-shaft Brayton cycle. In 2009 the company PBMR Pty, decided to use the conventional Rankine cycle though possibility of going back to using the Brayton cycle cannot be ruled out. Currently, the main sponsor for PBMR, which is government decided to reduce its funding of the project and the World nuclear news of 10 July 2010 reported that approximately 800 workers were to lose jobs and that PBMR would

remain with only a staff of 25 [**9**]. Despite all the recent events research has still continued at the North west University with funding coming from outside sources [**10**].

PBMR technology has a number of advantages over the pressurised water reactor (PWR) technology. Firstly, PBMR reactors are small and portable. Hence remote areas can be easily reached at reduced capital costs. A pressurised water reactor has to be located near a coast as opposed to a PBMR reactor which can be built anywhere where it is needed. When combined, the units can produce up to 400 MW. Secondly, PBMR technology has more commercial potential than its PWR counterpart partly due to its exportability. Thirdly, it has broader applications especially in cogeneration which include desalination, ethanol applications, refinery and petrochemical applications. It is used to reform methane to produce syngas, and also to produce hydrogen and oxygen by decomposing water thermo-chemically and extracting oil sands. Syngas can be used as feedstock to produce hydrogen, ammonia and methanol. Desalination requires large amounts of energy and this can easily be supplied by nuclear energy [**6**], [**11**].

Water desalination is the process of converting salt water into fresh water to make it suitable for human consumption or agricultural purposes. Table salt can be a by-product. It has got both small and large scale use. Small scale use includes seagoing ship**s** and submarines. Large scale use focuses on developing cheap and effective ways of providing fresh water for human use in places depleted of the resource [**11**].

Fourthly for South Africa it offers the country an opportunity to lead in a research area. This has economic benefit in that a whole new industry can be created consisting of engineering, manufacturing, (or) the maintenance plants where PBMR technology will be used. This would automatically lift national standards across the board.

The effect of nuclear waste on the environment is becoming less of a problem with the emergence of technologies to deal with it. Advances have been made in recycling nuclear waste. These technologies are already in use. Nuclear waste still contains ninety percent of the energy of the spent fuel [**12**].

Furthermore, PBMR offers more safety in terms of failure of the plant. Due to its design, the temperature coefficient of reactivity of the pebble-bed reactor is highly negative. This

results in the shutting down of the nuclear reaction to have no ill-effects. The shut down process occurs without any core failure or release of radioactivity to the environment [**13**].

1.1.2 Limitations of real systems

Power generation system components like all real systems have limitations in their operation. These are often undesirable since they compromise performance of the system and need to be prevented at all cost. Mass flow delivered by the compressor affects the speed of the shaft in the turbines. When choke occurs, the shaft speed may be affected. Choke is defined as the limit of mass flow velocity of a compressible fluid when it passes though an orifice [**75**]. Choked flow through system volumes occurs when the absolute pressure ratio is less than or equal to 0.528. At this instant, mass flow velocity cannot increase even when the pressure further down the channel is increased [**77**] [**14**].

For the gas turbine, surge and maximum inlet temperature are the most common limiting factors. Surge, which is due to a sudden drop in compressor delivered pressure, can result in violent dynamic pulsation which is transmitted to the whole system. This can destroy components. When very high inlet temperatures beyond the maximum specified by the manufacturer are reached, the stress exerted on the rotor-blades tends to damage them. Such a limitation is known as a constraint. Actuators such as valves in the system also have constraints. Valve opening has maximum and minimum bounds. Valves cannot open beyond fully-open, neither can they close beyond fully-closed.

Such constraints are encountered during power generation control. These needs can be addressed in control via a control system. Controllers such as the Proportional Integral control (PI) and Proportional Integral Derivative (PID) control do not include constraints in their formulation. A control algorithm which explicitly incorporates constraints in its formulation is, Model Predictive Control (MPC). The MPC control output is computed to correct the difference between the desired and actual (predicted) system output response while satisfying all the constraints. A model of the process which can be linear or non-linear is used to predict the outputs of the process. Linear models work well around an operating point during steady state operation of the plant. During transients which exhibit non-linear behaviour, linear models do not perform well. Such cases justify the need for non-linear

model predictive control. However techniques have been developed where linear models are used to sufficiently approximate non linear behaviour [**15**] .

For non-linear MPC performance aspects such as stability and robustness are not easy to evaluate when compared to linear MPC. Design and implementation of MPC using linear models is more straightforward [**16**].

1.1.3 Brayton cycle based power plant

In this study a linear state-space model of the Brayton cycle based power plant in used. The system layout is shown in Figure 1-1. The system considered is a single module which can be operated alone or as a group consisting of up to 10 such units. Each module can produce up to 110 MW of power. In the basic Brayton cycle, assuming ideal conditions, the compressor and turbine are reversible, adiabatic, and isentropic processes as shown in Figure 1-2 [**13**].

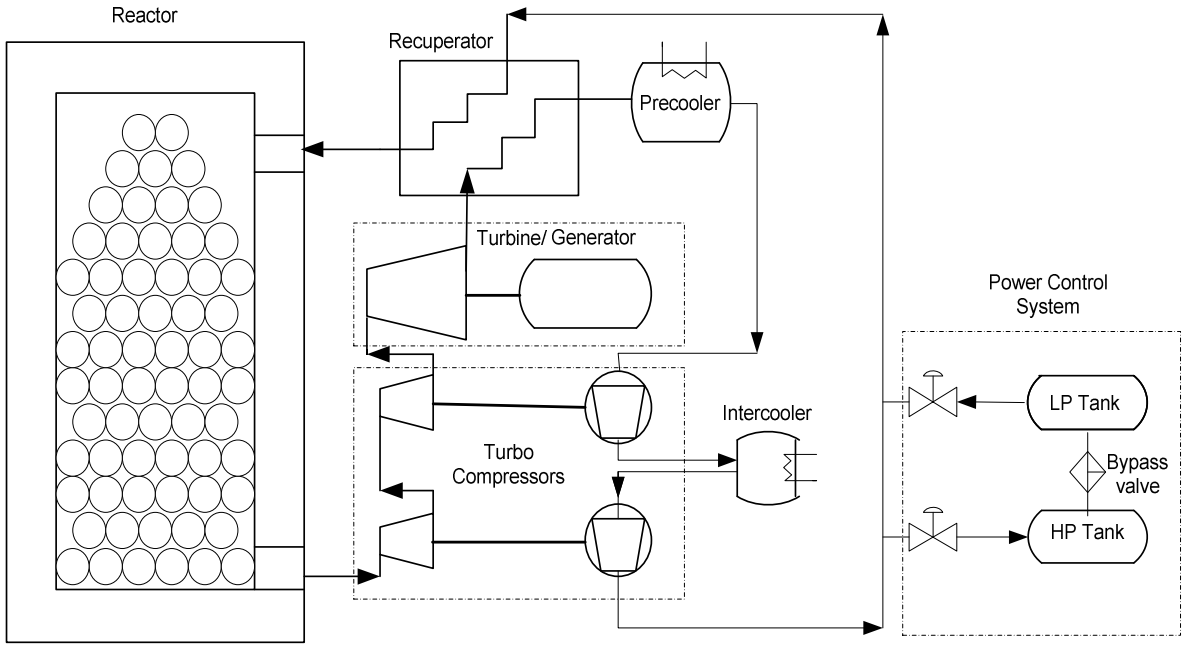

Figure 1-1 Power generation system layout [2],[13]

Gas enters the compressor and leaves at a higher temperature and pressure. From the compressor the pressurised gas (helium) is fed to the reactor where its temperature is raised at a constant pressure (isobaric) increasing its entropy or usefulness in terms of energy conversion. The high temperature gas is then fed to the turbine where much of its kinetic and thermal energy is converted to work. Part of the work done by the turbine goes

back to the system to drive the compressor. This is achieved by separate turbines in the PBMR .The pressure of the gas as well as its temperature reduces. Usually, the temperature at which the gas leaves the turbine is much higher than the temperature at which it leaves the compressor. Therefore, a recuperator is employed to raise the temperature of the cooler gas from the compressor and also to reduce the temperature of the hot gas on its way to the compressor. The gas is cooled down further by a pre-cooler at constant pressure before feeding it back again into the compressor. The bypass valve is an outlet for the gas in the system. The gas is re-circulated back into the system though the compressors. Opening the bypass valve reduces the power while closing it, if previously open, increases the power output.

Real systems deviate from the ideal and the efficiency is measured on the basis of the ideal process. As shown in Figure 1-2 the Brayton cycle which was proposed to be used by the PBMR is one with regeneration.

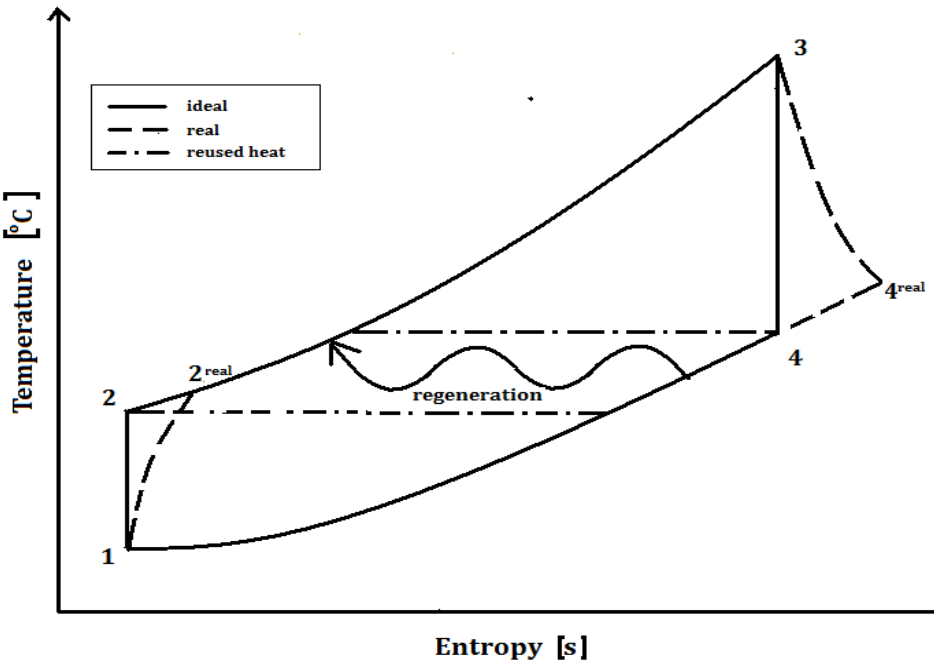

Figure 1-2 Brayton cycle

Isentropic compression takes place between 1 and 2. 2^{real} shows what the actual trajectory would be. Isobaric heat addition in the reactor is between 2 and 3. Some heat is added prior to helium entering into the reactor through regeneration (the region in-between the broken lines). The winding arrow represents heat exchange from the gas leaving the turbine

between 4 and 1. Isentropic expansion in the turbines is between 3 and 4. 4^{real} shows what the actual trajectory would be. Pre-cooling and inter-cooling takes place between 3 and 4 after the broken lines.

1.2 Power control

Power control of the system is achieved by adjusting the levels of helium in the system before it goes to the reactor. This alters the pressure as well as mass flow of the system. Two helium storage tanks at different pressure levels are used to maintain the required system pressure. Short term control is realized by adjusting the stator blades on the turbines or using bypass flow [**13**].

For this study, adjustment of turbo machinery blades will not be considered and control mechanisms shown in Figure 1-3 will be limited to:

- Low pressure injection and extraction
- High pressure extraction and injection (boosting)
- A bypass control valve

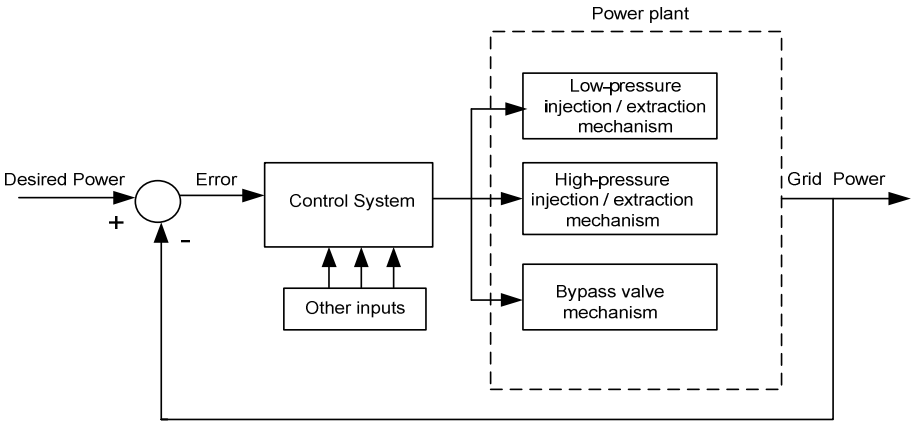

Figure 1-3 Power control System Configuration

During low pressure injection a phenomenon called the non-minimum phase effect occurs. This is undesirable and reduced by closing the bypass control valve while injecting helium into the system.

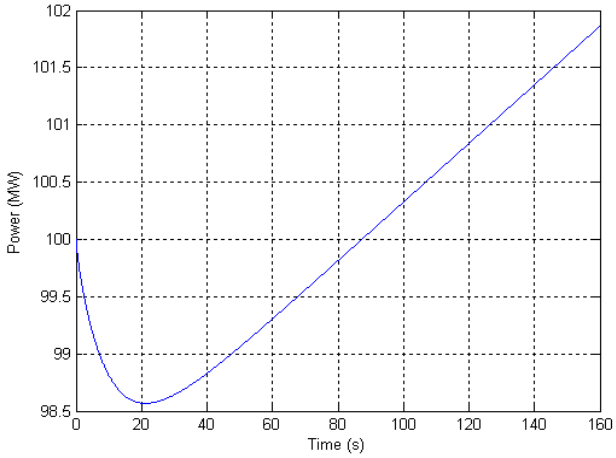

Figure 1-4 Non minimum Phase Effect

1.3 Problem statement

A control system needs to be derived which controls three helium actuators as described in the previous section. It will use the power error to adjust the helium inventory thereby controlling the power output of the plant.

The power output of the system needs to follow the desired power or set-point trajectory. This will be realised by means of a cost function representing the performance of the system. The cost function computes the most optimal input trajectory to achieve the desired power. The system contains constraints. The cost function incorporates them in order to avoid violation of the constraints during operation.

1.4 Issues to be addressed and methodology

1.4.1 Evaluation platform

An existing linear Simulink® model of the Brayton cycle will be used to test the control strategy. The existing model is complete but will need a few modifications. In the previous model, a booster tank was used [**2**]. However, this will be excluded from the model.

1.4.2 Model predictive control (MPC)

MPC will be the main focus of this study. A control strategy to handle the control mechanisms listed in section 1.2 above will be devised. In Simulink® bypass can be modelled

by injecting and extracting an equal amount of helium from the system. Therefore, the control system can be reduced to consist of two control variables. This will be implemented.

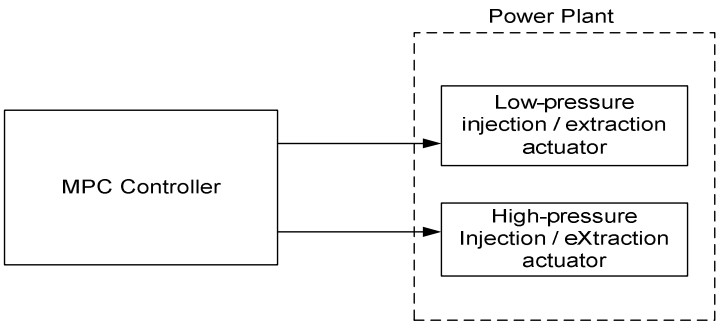

Figure 1-5 MPC Control Strategy

Tuning the controller is vital because the resulting controller must meet performance specifications. This requires a good understanding of the control formulation and the pros and cons of various controller settings. Each controller setting consists of a unique choice of parameter values. A strategy to tune the controller will be devised and applied.

The control system will be applied to different scenarios typical in real applications under normal conditions.

1.4.3 Comparison with optimal fuzzy PID control

Optimal fuzzy PID control was applied to the plant in previous works. The ITAE performance measure was used [**2**]. Results from this work will be used as a benchmark to compare with the MPC. The ITAE value will be used as the performance measure for comparison.

1.4.4 Disturbance analysis

In control systems, the presence and effect of disturbances cannot be discounted. Disturbances have an impact on how the system performs. It is therefore important that the performance of a controller be tested in such conditions. How the model predictive controller performs in the presence of disturbances will be investigated.

1.4 Overview of the dissertation

In chapter 2, a historical overview of control strategy and some applications is given. The Brayton cycle power plant to which it will be applied is discussed in more detail. Special

attention is given to the way the plant operates and power output control. Attention is now given to the theoretical aspects of the control strategy to be used.

In chapter 3, the linear model of the plant is described. The model predictive controller to be designed will be applied to this linear model. The assumptions made to arrive at a simplified model of the plant are given together with relationship between the simplified model and the evaluation platform. Simulation results of the Simulink® model are given.

Chapter 4 describes model predictive control and its advantages when compared to other control mechanisms in detail. How to determine appropriate parameter values for the controller is discussed. These values are used to tune or set the controller. Results showing the influence of each parameter on the performance of the plant are given. A performance index was formulated to compare responses of the different controller settings under normal conditions. The best set of parameters is selected and performance comparisons are made with the optimised fuzzy PID control strategy. The MPC controller is further analysed in when the plant is subject to disturbances.

In chapter 5, concluding remarks are given and recommendations for future work are made.

Chapter 2

Literature overview

2.1 Historical review

In previous work, the Brayton-cycle based power plant in consideration was controlled with PID and optimal fuzzy-PID control [**2**]. PID control has got widespread industrial use. Despite this, new control technologies have emerged which compare favourably with PID control. Model predictive control (MPC) is one such control method. Despite the fact that it has not been applied as much as PID control, MPC has a long history. Its beginnings can be traced back to the 1960s.

In the 1960s, process control practitioners focused on what was known as the linear quadratic optimal controller (LQC). This controller was unfortunately difficult to tune and had poor robustness to plant changes. It also could not handle constraints. Advances in control technology led to a control method which could easily handle constraints. Model predictive control is the term that was used for controllers which explicitly included constraints in its formulation. Major milestones in the development of MPC are described in [**17**]. Table 2-1 shows how MPC technology developed from the 1960s to the year 2000.

Table 2-1 Approximate genealogy of MPC Technology [**17**]

MPC Generation	Period	MPC version (Current)
Pre-MPC	1960 - 1970	LQG, LQC
1st Generation MPC	1970 - 1980	DMC, IDCOM
2nd Generation	1980 - 1985	Connoisseur, QDMC
	1985 - 1990	SMOC
3rd Generation	1985 - 1990	IDCOM-M, HIECON, PFC, PCT
	1985 - 1990	SMCA, RMPC
4th Generation	1990 - 2000	DMC+, RMPCT

These developments have come about from academic institutions and companies which are vendors of MPC products. Each company had its preferred MPC formulation which it

improved upon over time. This explains the different names and paths of development. The most significant MPC algorithms in industry up to 2003 can be found in the review paper, [**17**].

Improvements in the computer industry in the form of higher speeds translate into in greater computational capabilities. This has been the platform on which more advanced MPC algorithms and products have been developed by both academia and industry. The pre-first generation of controllers are referred to as the linear quadratic Gaussian controller (LGQ) described in [**17**] and the linear quadratic controller (LQC) found in [**18**]

2.1.1 Pre- MPC

LQG and LQC

Pre-MPC refers to the control technologies which preceded model predictive control. The control methodology goes by different names in literature. It is referred to as the linear quadratic Gaussian controller (LQG) in [**17**] and linear quadratic optimal controller (LQC) in [**19**]. The latter is also referred to as the linear Gaussian quadratic controller.

The origins of the LQG algorithm can be traced to Kalman's work. Quoting [**20**] and [**21**], the LQG was first used in the aerospace industry and that its formulation provides a systematic controller design methodology for high-order and multiple-input multiple-output (MIMO) systems. A simplified description of Kalman's process is given by [**17**] .

The model used was a linear state space model which can be converted to an impulse response model by successive substitutions of the state. It included noise in its output equation, and the influence of disturbances on the state of the system. The differences in LQG and LQC were in the disturbance model. In the LQG, both the noise and disturbance were zero mean Gaussian while for LQC it was defined as a sequence of zero mean vector stochastic variables of the correlation functions. Other controller configurations similar to LQC by having static coefficients throughout the operation had an omission of the disturbance terms [**18**].

These controllers had an objective function which minimised squared state and input deviations from the original. The squared differences were subject to separate weight

matrices, Q and R. This made room for tuning and trade-offs. The weight matrices were applied to the states and inputs respectively. Measured state variables were used and the objective function was computed over an infinite horizon which made the algorithm to have powerful stabilising properties. Obtaining of the solution was based on state feedback [**21**]. The solution involved two main steps. An optimal state is computed from the present output and secondly, this was used to compute the optimal process input [17].

The measurements of state variables are difficult to obtain at the right time and are often missed. The Kalman filter, or the Luenberger observer, was used to infer the unmeasured states in the calculation of the optimal control moves [**22**], [**23**]. The resulting controller has at least as high an order as the plant, which often made implementation difficult. However, to circumvent this, the controller was reduced to a lower order. Applying the LQG design to tracking systems required the use of classical control concepts such as integral control. An integral term is added to the state-space model so as to obtain the step response. More details can be found in [**18**].

It is unfortunate that in both formulations, intuitive insight about the effects of controller parameter modification was not apparent. Despite their success in the aerospace industry, LQG and LQC unfortunately had little impact on the process industry due to limitations. The main reason was that it had no constraint handling capability. In addition, the objective function included only very limited disturbance rejection specifications and hence could not handle both measurable and immeasurable disturbances. Furthermore the controller was also not capable of handling zero targets and neither did it include robustness specifications.

A procedure known as loop transfer recovery was proposed to improve the robustness [**21**]. In an effort to deal with some limitations of the LQG, [**16**] brought in how to handle practical issues. These are offset-free control and computing of steady state targets. When constraints were present they were added to some intelligent controller that would restructure the control problem based on which constraints area active at the time [**24**]. There were a part of many ad hoc solutions to some of the problems of the linear Gaussian quadratic controller or the linear quadratic controller. However, most of these solutions were not universal in nature and therefore could only be applied to a specific problem. More formalised methods began to emerge in the mid seventies. These were “identification and

command," IDCOM, and "dynamic matrix control" (DMC). This was the beginning of model predictive control, MPC.

2.1.2 First generation MPC

MPC is the only method capable of handling constraints in a systematic way in the design and implementation process. This is further elaborated in the section 2.4.4. The plant model is used to predict the effect of inputs to the plant on the future outputs. The most optimal inputs are computed to meet desired economic objectives or performance criteria. This is accomplished by minimisation of an objective function which consists of the predicted error subject to constraints [**18**].

In the first generation of MPC inclusion of constraints in the optimisation problem was introduced.

Dynamic matrix control (DMC)

In the early seventies engineers at Shell Oil developed a new control strategy known as "dynamic matrix control" (DMC), which was first applied in 1973 [**17**]. In DMC an *explicit* dynamic plant model is used to predict the effect of future control actions of the on the output. It is from this property that the name "model predictive control" came about [**25**]. The plant or dynamic model is derived from plant tests [**26**]. DMC is like linear programming which uses static parametric graphs which incorporate constraints as well as profit objectives. Like in linear programming graphs, parameters can be determined that would maximise gain. This can sometimes be non-intuitive to the user. The power of DMC is to find non-intuitive but optimum solutions.

DMC was the first to incorporate constraints and meet economic objectives. However, model accuracy was not dealt with and robustness was achieved by relaxing performance standards in recognition of model inaccuracies. In addition to errors arising from compromises in performance standards, use of fixed linear models for dynamically nonlinear processes also introduced some measure of error even when operation was fixed at a point. For most processes there is a wide range of operating conditions. Therefore, online implementation required experts to detune the model whenever necessary to meet the changing operating conditions and changing performance objectives [**26**]. The plant model

obtained was either an impulse response model or a step response model. This was later used to formulate the plant state space model.

According to [**19**], an important quality of model predictive controllers is that no stability problems exist under "perfect model conditions." However, errors do exist and need to be addressed appropriately. He identified two areas which needed research.

Firstly it is "performance specification" which involved quantifying qualitative decision making and determining whether constraints were hard or soft. Hard constraints should not be violated. However, soft constraints can be violated if that would help meet a more pertinent performance criterion. The designer must determine actual functions and tradeoffs between different performance criteria. Secondly it is "robustness to modelling errors." Control robustness is the ability of the control system to satisfy the desired performance criteria despite the inaccuracy of the model used for the design [**17**].

Model inaccuracies come about due to a number of reasons such as,

- Linearisation of the process. Problems arise when there is more than one operating condition.
- Equipment degrading or changing
- Unknown disturbance characteristics
- Identification techniques do not allow for a very accurate model due to time constraints.

Good error or disturbance prediction was found to be obtainable using optimal filtering theory to design an observer or estimator for the disturbance, if there was a model for the disturbance. The model however had to be subject to zero mean Gaussian noise. Such a requirement unfortunately is not always practical. This method was documented in [**16**]. Ten years later, a better method known as "structured singular value theory," SSV, was used. This was not restricted to a Gaussian description of the noise. Details of this method can be found in [**27**]. A simple method to determine unmeasured disturbances was by subtracting the model output from the measured output. Future disturbances would be a replication of the present [**19**]. In [**18**] the disturbance model for DMC was assumed constant.

Control involved determination of control moves or manipulated variable moves which were calculated after optimising a quadratic cost function subject to process constraints. The cost

function was representative of performance objectives and unlike the LQG, it was evaluated over a finite horizon. Both the prediction horizon and control horizon were used. A least squares problem was formulated to determine the control moves with the aim of driving the output to the set-point or reference trajectory.

In earlier approaches there was a challenge to express the desired performance objectives in a mathematical form that allowed computation of the moves. The dynamic matrix control algorithm provided such a form of expression. Multiple outputs were handled by superposition. The objective of a DMC controller is to force the output to match the setpoint with minimal error. Therefore, a penalty term was added to the manipulated variable moves resulting in a "smoother "output response. This in a way ensured robustness to model error [**17**]. Computations had to be done at each control execution.

Identification and command (IDCOM)

On another front, at a conference in 1976, another approach was presented by [**28**] which was called model predictive heuristic control (MPHC). The software used was referred to as IDCOM. The approach was called *heuristic* because like in DMC, the control law was not linear.

Though developed independently, IDCOM and DMC are similar. IDCOM also had a quadratic performance objective evaluated over a finite horizon. The major difference is in the model formulation and determination of control moves. While DMC used a step response model, IDCOM used an impulse response. The step response is equivalent to the integral of the impulse response. Expressions of future values, such as the one below contained past values, future manipulated values (control moves) and disturbances. An MPC formulation known as "model algorithmic control" (MAC) which also uses an impulse response is described in [**18**]. MAC also differs with DMC in two other aspects. Firstly, for tuning the optimisation function, only the prediction horizon is used. The model horizon is equated to the prediction horizon. Secondly, the disturbance estimate is filtered and has one additional tuning parameter added to it. This tuning parameter has a direct impact on closed loop speed of response, robustness and bandwidth [**18**].

For IDCOM, optimal control moves or plant inputs were calculated using a heuristic iterative algorithm. It is this same algorithm which was used in obtaining the impulse response of the plant. This was achieved by minimizing the difference between plant and model impulse response. Justification for using the same algorithm in calculation of control moves was because control is the mathematical dual of identification.

Though constraints were included for first generation of MPC technology, the methodology was not well formalised. The initial IDCOM and DMC algorithm are referred to as the *first generation* of MPC technology. Other first generation algorithms are MAC and internal model control, IMC. IMC was developed to avoid the weaknesses of DMC and MAC. More detailed accounts of the algorithms above can be found in [**18**]. Second generation MPC follows.

2.1.3 Second generation MPC

Quadratic dynamic matrix control (QDMC)

DMC developed into "quadratic dynamic matrix control" (QDMC). It was introduced in the 1980s. It was developed by engineers from Shell. It was first described by [**29**] and can also be found in [**19**] where it is described as a *second generation* MPC. Its aim was to handle constraints better than its predecessor, the DMC. Input and output constraints were made to appear more explicitly.

In QDMC, a single objective function was used. This was a weighted sum of all objective functions in the system or a sum of the squared difference of output variables from target values subject to inequality constraints of outputs and manipulated variables. In QDMC, weighted penalties were added to manipulated variables to improve robustness but tuning was still required. Determining the initial weight for each objective proved difficult due to many factors such as the influence a particular weight has on the other objectives and changing operating conditions. Industry settled with online updating of weights according to observed performance albeit at a high maintenance cost [**19**].

It was shown in [**19**] that the DMC objective function can be expressed in a form which allows explicit systematic definition of constraints. The dynamic matrix connects future moves to manipulated variable (MV) or control moves. This allowed all input and output

constraints to be combined into a matrix inequality containing the input (MV) move vector. In spite of the QDMC algorithm being an advanced control algorithm, the quadratic programming, QP, was one of the simplest optimisation problems that one could possibly pose. This means that a solution could be found readily using standard commercial optimisation codes. At every sampling interval new MV values were calculated based on the most recent feedback measurement. Only the first manipulated variable is used while others are for backup in case of loss of measured variables [**19**].

It was further reiterated that choice of the performance criteria was not a straight forward process. At times one would have to choose between a frequency or time-domain objective function. Other times decisions would have to be made on whether to include a particular constraint into the objective function.

Apart from problems arising due to the choice of objective function parameters others were due to model inaccuracies which resulted in degradation of system performance. Therefore, tuning may be necessary as an online measure. The structured singular value (SSV) approach was to be used in handling model inaccuracies. SSV is suited for processes with static control loop variables. It provides a measure of true process satisfaction which allowed the designer to specify uncertainties in a structured way. Performance was described by weighted frequency response functions in which uncertainties were described in less strict terms unlike in linear quadratic control which required that disturbances be described as Gaussian noise. The only requirement on the form of representation was that the inaccuracy had to be represented in block diagram form. Two problems had to be solved. The first was "analysis" which involved evaluation of the SSV value. The second was known as "synthesis" which used the computed performance value, model description and disturbance uncertainties to optimise a controller transfer function so that the SSV criterion was met. At the time, this method was useful in QDMC at the design stage in the absence of constraints. This type of analysis helped in the tuning of the controller. However, it was not possible to consider all possible scenarios. Specifications were limited to most common operating conditions. It is known that the SSV method, cannot work in an environment with criteria which does not easily translate to frequency response functions. An online solution for synthesis would produce a controller that can accept changing objective and constraint criteria.

The major contribution of second generation of MPC technology was that it comprised of algorithms which provided a systematic way to implement all the constraints [**17**].

2.1.4 Third generation MPC

With QDMC input and output constraints could be arrived at in a systematic way. However, in the case of an infeasible solution to the quadratic program, QDMC had no way out. In addition to this, some constraints were more important than others. Therefore they could be classified into hard and soft constraints or in order of priority. In practice, low priority constraints would have to be sacrificed for high priority ones. This was not a trivial task. Some researchers developed an algorithm which solved multiple objectives. The objectives were normalised based on their good and bad values which the designer had to specify. This made more engineering sense in that values would be selected which were directly related to the problem. However, this method needed a good man-machine interface.

On real time plants, process information could be lost due to hardware failure, operator interference or valve saturation.

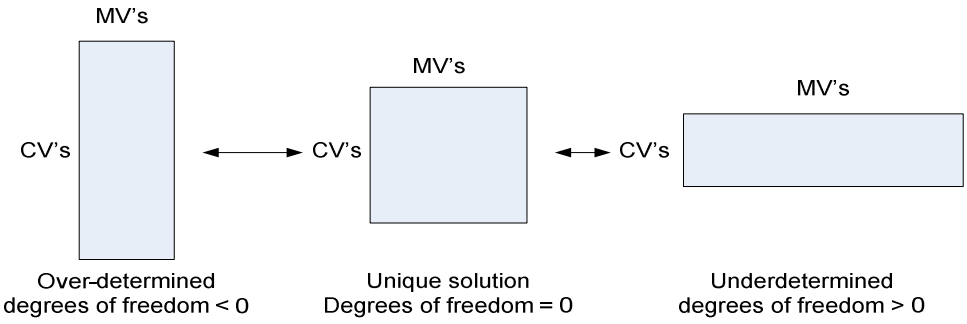

Figure 2-1Process structure and the degrees of freedom [17**], [**30**]**

In reference to Figure 2-1, when plant outputs equal control moves, it leads to a unique solution. This is known as the *square plant* case. When control moves are more than the outputs, this is known as the *fat plant* case. When this occurs, it is still possible to move the plant to an optimal operating point. For a plant in operation, it may occur that fault occurs in sub-plant. Rather than turning off, an MPC controller should make the best of the sub-plant. This is the underdetermined case. In the case of poorly conditioned sub-plants, the controller must recognise and screen them out before erratic control action ensues. There is another case where plant outputs are more than the control moves, it is known as an over-

determined case. Performance criteria cannot be met. This would require relaxing of specifications such as using least squares to minimise output violations. This is all in an effort to keep the plant running despite a few operational problems.

These issues caused engineers in academia and various companies to start working on new versions of MPC. Some companies involved were Setpoint, Adersa, and Shell (France). These developed the following technologies, IDCOM-M, hierarchical constraint control (HIECON), Setpoint Multivariable Control Architecture (SMCA), Shell Multivariable Optimising Controller (SMOC), PCT and RMPC are regarded as *third generation* of MPC technology. With the exception of SMOC which evolved from LQR, these technologies were based on IDCOM. More detail with each technology can be found in [**17**].

Third generation MPC technologies were able to distinguish between the different levels of constraints. These are hard, soft, and ranked. Unlike the preceding generation, this generation provided a mechanism to recover from infeasible solutions. They also addressed the issues resulting from a time varying control structure, they provided a better set of options for feedback, had more controller specifications and allowed for a broader range of process dynamics such as stable, integrating and unstable [**17**].

2.1.4 Fourth generation MPC

From the mid-nineties, it was noted that MPC was still not well understood among process engineers and operators. **There was a gap**. This can be attributed in part to the complexity of the algorithm. Therefore DMC vendors went into developing products which would require minimum human intervention once it has been commissioned. They shifted from emphasis of knowledge transfer to things that would simplify the design process such as state space modelling, improved tuning techniques, new integration techniques for systems, integration with neural networks and so on. However, the discomfort among operators continued. This knowledge gap led to a drive to train personnel, improve user interface, and reduce or hide system complexity [**26**]. Products like DMC-plus and RMPCT were among some of the outcomes. These are known as *fourth generation* MPC technology. An example can be found in [**31**] where an MPC product developed at AspenTech called Advanced

Process Control State-Space controller (SSC) was described. One of the objectives was to develop a working environment to enable even engineers not experienced in control theory and MPC to build, install and maintain a wide range of control applications efficiently.

Apart from an improved interface between the operator and the control system, other properties of fourth generation included multiple optimisation levels to address different priorities in control objectives, more flexibility in steady-state target optimisation, quadratic programming was included and economic objectives were specified. Model inaccuracy was also dealt with by direct consideration of model uncertainty (robust control design), better prediction error based identification technology and sub-space identification methods. Non-linear MPC had also emerged and only needed stability aspects to be addressed. A detailed account of these features can be found in [**17**].

At present, all these advances have led to better MPC formulation which makes it more reliable as a control option and also easy to use [**32**]. The fact that it has been applied previously in industry with a good measure of success further compounds its usefulness. Applications of model predictive control can be found in many process industries such as, chemical, refining, food processing and many more. Of late, it has found application in power generation which includes nuclear plants. An overview of some applications of MPC in nuclear powered plants follows.

2.2 Nuclear applications

There are various forms in which model predictive control has been used in nuclear plant applications. These applications range from linear to non-linear predictive control with different model formulations. The following are some examples of nuclear applications found in literature.

MPC was applied to linear and non-linear model predictive solution to nuclear steam generators. The linear model worked well under fixed operating conditions. Its results were verified by the non-linear model. Model predictive control was preferred due to its suitability to deal with non-minimum phase effects which are high at low power levels synonymous to start-ups of nuclear plants. The controlled output was kept within range of the set-point. Tracking of the set-point was faster at high power levels than at low power

levels. Steam flow-rate changes were coped with well. The non-linear model used for verification was a 2-region model. However, the linear model was used to design the controller. Parameters used in the optimisation differed greatly based on the power level changes in the generator. The designed controller could still be used for different power levels by simply adjusting the input weighting factor [**33**].

MPC was used by [**34**] to tune parameters of a PID controller being used to control the reduced linear model of the steam Generator found in [**35**]. PID controllers have fixed control gains. However, as described earlier for steam generators, parameters vary greatly at different power levels and therefore require different control values at each power level. A staggered model predictive control method was applied. A predetermined plant model was used to determine a number of finite operating regions which spanned over the whole range of operation of the plant. These operating regions were used to design an equal number of model predictive controllers in advance. When operating conditions moved to other finite operating regions, operation was switched to the corresponding MPC controller. This was done for all the expected power levels [**36**]. Like in [**33**], the controller response to water level was fast. If there was a sudden change in the set-point of the steam generator water-level, only the input-weighting factor in the controller was changed depending to the power level [**34**].

Different power levels are normally encountered. A way of dealing with them can be found in [**37**]. A generalised predictive control method was developed. It was combined with a recursive parameter estimation algorithm which was based on the extended least-squares method. It dealt with the steam generator water level control problems mentioned in previous works. At every time step, the algorithm estimated the mathematical model of steam generators which was used to design the generalised predictive controller, GPC. The controller was applied to the linear and nonlinear models for nuclear steam generators as in [**33**]. It was designed to cope with deviation of the water level from the set-point and steam flow disturbance effectively. Simulations were carried out using software aids to analyse the set-point tracking performance. The changing dynamics due to power levels were handled by the online estimation of the mathematical model of steam generators at every time instant. The estimated model was used to design a generalised predictive controller. Results were compared to those obtained using a PI controller and exhibited better performance.

Compared with the nonlinear model, the linear model showed good performance at the operating water level.

In [**38**] an MPC method meant to account for a changing point and dynamic characteristics was designed and implemented. This was achieved by combining the controller with a parameter estimator. At each time step the parameter estimator recursively identified a controller design model and optimised control inputs were recalculated by the model predictive controller using the measurements signals available at that instant. The method was earlier used by others in a SISO system [**38**]. They controlled the water level of nuclear steam generators. An improvement on this was carried out by Na *et al*, 2005. This was accomplished by controlling two variables, the power level and axial power distribution. They also optimised the set-point tracking control performance of pressurised water reactors (PWRs).

The axial shape index and power level were systematically and simultaneously controlled by regulating the control and part-strength control rod banks. Load-following and operation of the Korea Standard Nuclear Power plants were also verified. They were simulated numerically by MASTER code which can evaluate the space and time-dependent diffusion equation in hexagonal and 3-D Cartesian geometries [**38**].

In [**39**] it was suggested to design a nonlinear predictive controller based on a Takagi-Sugeno fuzzy model. It was used to predict the effect of future control moves on the output of the plant. An optimisation approach coupled with a simple gradient technique was used to determine the future controller outputs. The main advantages of the algorithm were that the fuzzy model was easy to implement and computing of the gradient sector during the optimisation was non-trivial. The control method was simulated and applied to the water level control in a U-tube steam generating unit (UTSG) for a power nuclear plant. Many input variables were used in training the model. These covered the whole input range sufficiently. Its stability was verified by simulating it for long periods under conditions similar to those in real plants. The control experiments were conducted successfully and the results and performance were satisfactory [**39**].

A multiple model predictive control strategy was presented in [**40**]. It was referred to as improved implicit multiple model predictive control (IIMMPC) to control movable nuclear reactors. This was especially needful due to the requirement for a load following ability. A nuclear plant is nonlinear in general. However, it can be approximated using a combination of many different linear models. In this method, the state space model is built from the physical model of the pressurised water reactor core. Following this, the influence of parameters during changes in the power level were analysed so as to build some local models. IMPC was then used to design the local controller. The results showed that IIMMPC based on the multiple models is an efficient way to design the controller of movable nuclear plants whose power output trajectory changes often [**40**].

A robust model predictive control method (RMPC) was implemented by [**15**] to handle the water level for a steam generator. The model used was the polytropic uncertain linear time varying (LTV) model of the plant. This had to be able to approximate the system's non-linear behaviour. There was another way to deal with constraints. It limited the constraints on the system. This approach helped deal with the problem of stability due to unmodeled dynamics and parametric uncertainty in a more direct and systematic fashion. The closed-loop stability was insured by using a parameter-dependent Lyapunov function and the optimisation problem involving the linear matrix inequality (LMI) technique. It was built within the multi model framework where a linear parameter varying, LPV, model was built around several operating points or operating regimes. The simulations carried out proved that the controller was effective in different operating conditions. The LPV MPC showed an improvement in keeping the water level at the set point and it dealt with disturbances coming from changes in the steam flow-rate better, when compared to RMPC. It also had strong robustness [**15**].

A multivariable integrated model predictive control method for a nuclear power plant can be found in [**41**]. The work involved modeling of the steam generator and turbine. The method was investigated because the PID control has limitations. Solving the coupling problem of rotation speed of turbine and steam pressure at the outlet of the steam generator was more visible. The generalised predictive control algorithm had been improved upon in multivariable integrated model predictive control. The results obtained from

simulations showed that compared to PID control, the rotation speed of the turbine is faster. Adding to that, outlet pressure of the steam generator is steadier and has a smaller overshoot. Generally it exhibited better performance for the nuclear power plant [**41**].

In 2001, [**42**] developed an architecture for integrating neural networks with a PI controller commonly used in industrial applications. This approach was preferred to circumvent the problem of cost incurred in replacing old control technologies for newer better ones. In this approach MPC was used to predict future variables of the system using a model based on a recurrent neural network capable of modeling the system in all operating conditions. PI controller parameters were then tuned by a backpropagation through time approach using "parallel learning." Such a system easily tracks operation of the system. This way, regulation and stabilisation of the controlled process was achieved while the parameters were being updated online during operation. This method was used in the stabilisation and transient control of the generator's water level. Often there is lots of actuator noise and process parameter drifts which come from wear-and-tear effects resulting from long use. The PI controller's adaptiveness made it possible to handle these and other unwanted operational transients. Stability however, could not be easily ascertained for this method and the system only relied on the minimisation of errors which can be done using recurrent neural networks. The results obtained, when compared with the PID controller which was being used at the time, demonstrated superior stabilisation and transient through all operating regimes of the plant [**42**].

A model predictive controller for direct power control (DPC) of a doubly-fed induction generator (DFIG) was proposed and implemented by [**43**]. The DFIG falls under wind energy systems. Control of these systems is largely based on stator-flux-vector control or stator-voltage-oriented control. The control law is obtained by optimising the objective function. This function incorporates the magnitude of the control effort and the difference between the predicted active and reactive powers and the expected values. The active and reactive powers were decoupled and control was achieved by means of a rotor current controller. The predicted outputs (active and reactive power) were calculated from a linearised state space model. A constant switching frequency was used which proved to be an advantage in that drawbacks of conventional DPC were overcome. The influence of estimation errors for

these leakage inductance and resistance was also investigated and found to be negligible. The simulations showed that the controller was both effective and robust during several operating conditions and variations of machine parameters. This placed DPC as a candidate for DIFG implementation [**43**].

A model predictive controller was designed by [**44**] for controlling the main primary circuit dynamics of the Paks nuclear power plant (Paks NPP) located in Hungary which is a pressurised water nuclear power plant. The model used was designed for control during load-change transients. This was done in order for the controller to maintain stability of the plant in the presence of hard constraints for both the input and state variables while producing the required amount of power.

The hybrid plant model was embedded into a non-hybrid discrete time LPV form. Good quality measurement data made parameter identification of the primary circuit dynamics and the control-oriented modeling possible. What motivated the work was that despite having a satisfactory performance, studies and simulations of the current control method showed that the dynamic behaviour during longer periods mainly due to load changes could be improved upon by using a multivariable controller. Control of pressure in the primary circuit of each unit was cardinal. In works prior to this, the pressure control loop was successfully carried out from the modelling phase through the identification, controller design phase right up to the implementation phase of the plant. The end result was an increase of delivered power to 1-2%. A linear matrix inequality (LMI) based model predictive regulator was built for the primary circuit of a pressurised water nuclear power plant. The hybrid model was discretised and embedded in the non-hybrid LPV structure of which more familiar control design methods could be used. The LPV model was then applied to the LMI based MPC algorithm with a few problem specific modifications of the original control algorithm. Dynamic behaviour of the controlled system did satisfy the input and state constraints [**44**].

In 2010, [**45**] proposed and investigated how a multiple disturbance model can be applied in model predictive control. Most classical model-based control strategies assume a single disturbance model while in the real system applications, the sources of disturbance are

more. Previous multiple model-based approaches have generally focused on handling multiple operating conditions, with the aim of simulating non linear behaviour of the system more accurately. Four different disturbance models expected in a common nonlinear system were applied. These are namely, additive output, step input, ramp input, and periodic. These were applied to a linear state-space model. Disturbances can occur in two forms periodic and sudden. Periodic errors would be due to a poorly tuned controller or other systematic errors. Simulation results demonstrated successful estimation and control of single and multiple simultaneous disturbances [**45**].

There have been a number of MPC products developed. One such is called 3dMPC for ABB Automation products. It is described in [**46**]. They used state-space models for the model predictor. One of their aims was to show some benefits of using multivariable state space models in model predictive control the main being that the quality of predicted outputs was improved.
It further allowed for independent tuning of responses to set-point changes, measurable disturbances and to non-measurable disturbances or model-mismatch. The structure was such that it allowed for tuning while still retaining robustness [**46**].

This section shows that there have been a number of applications of MPC in power generation. Parameters which were controlled varied from speeds of the turbo machines, temperature and levels of the fluid in the systems. Methods of how to deal with changing operating points for linear models have been discussed as well as use of non-linear models in MPC. Disturbance specification has also been looked into. It has been shown that MPC can produce satisfactory closed loop performance for nuclear plant based control. Therefore, it is feasible to assume that Model predictive control can be applied to a three-shaft Brayton Cycle based power plant. This power plant is described in the following section.

2.3 Three-shaft Brayton cycle based power station

2.3.1 Introduction

The original design of the PBMR (Pebble Bed Modular Reactor) is a typical three-shaft Brayton cycle based nuclear power station. The PBMR has changed their design to a single-shaft system. This study is based on the original design. However the method developed can easily be applied on the single-shaft design. Each plant is intended to produce up to 400 MW of power using modular units of approximately 110 MW a piece. The PBMR is a Brayton cycle based nuclear plant. The reactor is graphite-moderated and it uses helium as the cooling fluid. Heat in the core is generated from nuclear fission. Heat is transferred to the coolant gas (helium), and converted into electrical energy by means of a gas turbo-generator [**13**], [**47**].

2.3.1 Operation of the power plant

During the start-up transition which occurs before normal power operation, the reactor is already heated up and the power turbine is externally maintained at 50 Hz. A separate start-up system and control not part of the steady-state Brayton cycle is used in this phase. This consists of start-up blower system (SBS) and control valves to provide initial flow in the cycle. The low pressure bypass and gas bypass control valves (LPB and GBPC) are systematically controlled until the HPT and LPT are running through their critical frequency ranges (between 20% and 80% of nominal speed). When the Brayton cycle becomes self sustaining the start-up system is deactivated [**47**].

During normal operation, beginning at the reactor outlet, helium then leaves the reactor at a temperature of approximately 900 °C. The helium then moves through the High then Low-pressure Turbines (HPT, LPT) which drives the High and Low-pressure Compressor (HPC, LPC) respectively. The helium then moves through the Power Turbine (PT) which drives the generator.

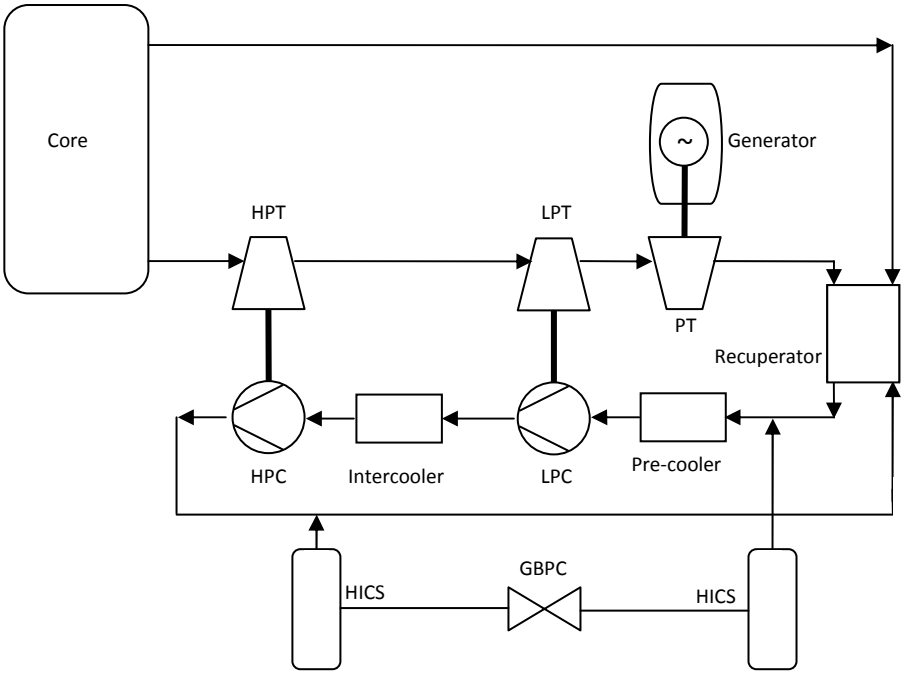

Figure 2-2 A detailed power plant layout [2]

Still at high temperature, helium passes through the recuperator where it loses some heat to the low temperature helium returning to the reactor.

From the recuperator, the helium is now cooled by means of a pre-cooler. Cooling increases the density of the helium which improves the efficiency of the compressor. The helium is then compressed by the LPC. The helium is further cooled in the intercooler and the HPC then compresses the helium.

The cold high-pressure helium is made to pass through the recuperator for the purposes of pre-heating it. The helium then returns to the reactor.

The reactor core consists of two zones. The inner zone that contains inert graphite spheres and the outer zone (annulus) that contains fuel spheres. The nuclear reaction takes place in the core annulus and is controlled by the control rods that are housed in the side reflector of the reactor. Helium at a temperature of approximately 500 °C and 70 bar enters the reactor and flows downwards through the pebble bed picking up the heat generated there and reaching up to about 900 °C at the outlet. Fuel spheres are composed of a graphite base embedded with uranium which is the fuel [**13**]. During reactor shutdown, residual heat is removed by active and/or passive cooling of the system. The plant should be shutdown once a year for maintenance purposes and during failure [**48**].

2.3.2 Power output control

Power output control is achieved by helium injection (extraction) to the circuit. This increases (or decreases) the pressure and amount of helium at various points in the cycle while the gas temperatures and the pressure ratios of the system remain the same. The increased (decreased) pressure and subsequent increased mass flow rate increases the heat transfer rate, thus increasing (reducing) the power.

Helium storage tanks ranging from low to high pressure are used to maintain the required gas pressure in the circuit. The power control system determines the rates of flow. At the machine level, stator blades on the turbo machinery can be adjusted and bypass flow employed to achieve short-term control [**13**].

The helium Inventory Control System (HICS) and the Gas Cycle Bypass Control Valve (GBPC) shown in Figure 2-2 are used to adjust the helium inventory of the cycle. Helium is normally injected into the cycle at the inlet of the pre-cooler and removed at the outlet of the HPC. It was found that high pressure injection (boosting) as well as low pressure extraction are essential mechanisms for the system to achieve the desired performance. A limited amount of helium can also be injected into the manifold by the HICS booster tank for instant changes in the amount of gas flowing in the system and consequently the power levels. This and similar changes is implemented using the GBPC There are also no minimum phase effects.

The HICS and GBPC can be summarised into the following helium inventory actuators, these are:

- A Gas cycle bypass control valve
- Low-pressure injection or extraction at the low-pressure side of the system
- High-pressure extraction or injection (boosting) at the high-pressure side of the system

Helium injection or extraction is governed by the power error. This is the difference between the required power set point and the actual electrical power generated. The power error is used by some type of controller to generate control values for the actuators as shown in Figure 2-2.

Control values have to be intelligently adjusted because each response affects the system as a whole. An intelligent control strategy is needed to generate control values that will result in smooth power responses and sufficient reserve capacity in stand by mode.

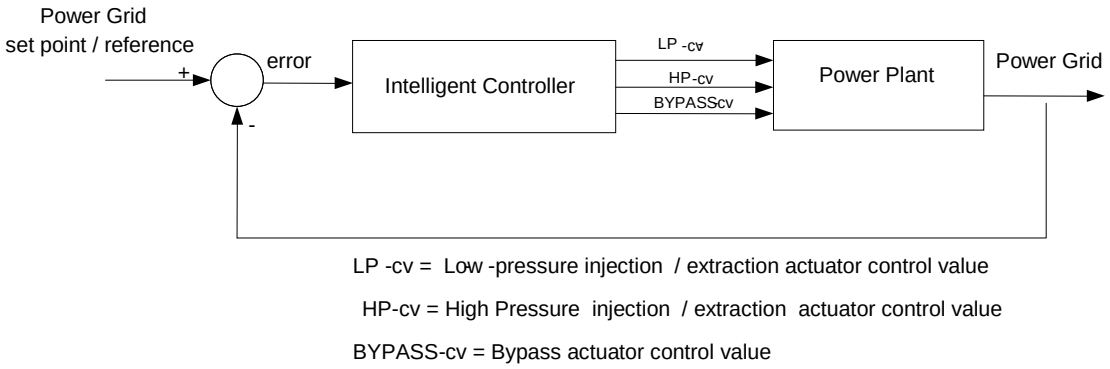

Figure 2-3 Power control layout for the power plant

The diagram shows the intelligent controller via the two control actuators LP-cv and HP-cv. The controller computes the control variables based on the error between the power grid set-point and the output. A possible control technique that will be able to intelligently adjust the three control actuators and satisfy the control demands is model predictive control, MPC. In the next sections, this control strategy is described and implemented used to control the three shaft Brayton-cycle power plant.

2.4 Formulation of the state-space model for MPC

In model predictive control, the controller uses a plant model to generate control variables for the plant. Three different modeling approaches are used in model predictive control. These are the finite impulse response (FIR), step response and state space models. For this research, the state space approach is used. In this approach predicting ahead is made possible by current information in the form of state variables at current time. The state space model used can be either a continuous or discrete time state space model. However, implementation is performed in the digital environment. Conversion from continuous time to discrete time is therefore carried out at some point during implementation [**32**]. For this reason, discrete time state space models will be used in describing the theoretical aspects of this control strategy. The model however is kept as a continuous time state space model to avoid problems which arise with a digital state space model due to sampling rates.

A model can be defined for single input single output systems (SISO) or for multiple input multiple output systems (MIMO). The following state-space formulation is found in [**32**].

$$x_m(k+1) = A_m x_m(k) + B_m u(k) + B_d \omega(k) \quad (2\text{-}1)$$

$$y_m(k) = C_m x_m(k) + D_m u(k), \quad (2\text{-}2)$$

where x_m is the state variable. A_m, B_m, C_m, and D_m are the system or state matrix, control matrix, output matrix, and feed-forward matrix respectively. The exponential of the state matrix, e^{Amt} is called the state transition matrix. It is assumed that the plant has *m* inputs, *q* outputs and n_1 states. Normally the number of outputs is less than or equal to that of inputs (i.e., $q \leq m$). B_d can be referred to as the disturbance matrix and ω(k) is the input disturbance [**32**].

In receding horizon control, information of the plant at each time instant is needed for control and prediction. It is also assumed that current inputs $u(k)$, do not have an immediate effect on the output $y_m(k)$. As a result, D_m is a zero matrix and the state space model is rewritten as:

$$x_m(k+1) = A_m x_m(k) + B_m u(k) + B_d \omega(k), \quad (2\text{-}3)$$

$$y(k) = C_m x_m(k), \quad (2\text{-}4)$$

where A_m, B_m and C_m have dimension $n_1 \times n_1$, $n_1 \times m$ and $q \times n_1$, respectively. This model is changed to suit our design purpose in which an integrator is embedded. We begin by first defining the terms;

$$\Delta x_m(k+1) = x_m(k+1) - x_m(k), \quad (2\text{-}5)$$

$$\Delta x_m(k) = x_m(k) - x_m(k-1), \quad (2\text{-}6)$$

$$\Delta u(k) = u(k) - u(k-1), \quad (2\text{-}7)$$

$$\varepsilon(k) = \omega(k) - \omega(k-1). \quad (2\text{-}8)$$

From the above, the difference equation of the state space model is

$$\Delta x_m(k+1) = A_m \Delta x_m(k) + B_m \Delta u(k) + B_d \varepsilon(k) \quad (2\text{-}9)$$

To connect $\Delta x(k)$ to the output $y_m(k)$, a new state variable vector is chosen to be,

$$x(k) = \begin{bmatrix} \Delta x_m(k) \\ y(k) \end{bmatrix}. \tag{2-10}$$

On the other hand,

$$\Delta y(k+1) = y(k+1) - y(k) = C_m\big(x_m(k+1) - x_m(k)\big) = C_m \Delta x_m(k+1), \tag{2-11}$$

$$\Delta y(k+1) = C_m A_m \Delta x_m(k) + C_m B_m \Delta u(k) + C_m B_d \varepsilon(k), \tag{2-12}$$

$$y(k+1) = \Delta y(k+1) + y(k), \tag{2-13}$$

$$y(k+1) = C_m A_m \Delta x_m(k) + C_m B_m \Delta u(k) + C_m B_d \varepsilon(k) + y(k). \tag{2-14}$$

Therefore, the difference state space model can be written as,

$$\underbrace{\begin{bmatrix} \Delta x_m(k+1) \\ y(k+1) \end{bmatrix}}_{x(k+1)} = \underbrace{\begin{bmatrix} A_m & o_m^T \\ C_m A_m & I_{q\times q} \end{bmatrix}}_{A} \underbrace{\begin{bmatrix} \Delta x_m(k) \\ y(k) \end{bmatrix}}_{x(k)} + \underbrace{\begin{bmatrix} B_m \\ C_m B_m \end{bmatrix}}_{B} \underbrace{\Delta u(k)}_{u(k)} + \underbrace{\begin{bmatrix} B_d \\ C_m B_d \end{bmatrix}}_{B_\varepsilon} \underbrace{\varepsilon(k)}_{\varepsilon(k)}, \tag{2-15}$$

$$\underbrace{[y(k)]}_{y(k)} = \underbrace{[o_m \quad I_{q\times q}]}_{C} \underbrace{\begin{bmatrix} \Delta x_m(k) \\ y(k) \end{bmatrix}}_{x(k)}, \tag{2-16}$$

where q×q is the identity matrix. It has dimensions q×q, which is the number of outputs; and o_m is a q × n_1 zero matrix. The augmented state-space equation above can be written in more simplified notation as shown below, its dimensionality is taken as n (= n_1 + q). There are q integrators embedded in the model.

$$x(k+1) = Ax(k) + Bu(k) + B_\varepsilon \omega(k), \tag{2-17}$$

$$y(k) = Cx(k). \tag{2-18}$$

2.5 Unconstrained Control

In [**32**] it is stated that in order to obtain the desired closed loop performance, the model should be both controllable and observable Controllability depends on whether the system is or can be made stable.

2.5.1 Stability

A closed-loop system which is not stable has got little value. A system is stable if its output response is bounded when the input applied is equally bounded. The stability of a system in state-space form (A, B, C, D) is dependant on the state matrix, A. The location of poles or eigenvalues of the state matrix determines the stability of the system**.** Eigenvalues are counterparts of poles. A continuous system is said to be stable when all the poles or eigenvalues of the state matrix have negative real parts. For a stable discrete system the eigenvalues fall within the unit circle [**49**], [**50**].

2.5.2 Controllability

It is possible to stabilise a system which is open-loop unstable if there is an input that can affect the response of the states. A system is controllable if all its states can be changed by adjusting the inputs. This means that there exists input can cause the system states to go from an initial condition or state $\boldsymbol{x}(0)$ at $t = 0$ to zero or any desired state $\boldsymbol{x}(t)$ at any time, $t > 0$. Since controllability is a measure of the effect of inputs, it is determined by the state matrix, A, and input matrix, B. These matrices are used to generate the controllability matrix, Q_{cb}, which is used to determine the controllability of the system. Q_{cb} is defined as,

$$Q_{cb} = [B\ AB\ \dots\ A^{n-1}B], \tag{2-19}$$

where n is the number of states. A system is controllable if the rank of Q_{cb} is equivalent to the number of rows it contains or its determinant is non-zero. That is,

$$rank(Q_{cb}) = n, \tag{2-20}$$

$$Det(Q_{cb}) \neq 0. \tag{2-21}$$

Controllability means system poles or eigenvalues can be placed anywhere in the system. This is done by means of a state-feedback controller gain, K. The closed-loop system eigenvalues are now determined by,

$$A' = A - BK. \tag{2-22}$$

where A' is the closed-loop system state-matrix which is used to determine the new eigenvalues of the system [**49**][**50**]. If a system is uncontrollable the eigenvalues associated with the uncontrollable modes of the system cannot be adjusted. An alternative approach

which is more numerically stable is use of the Controllability Gramian. Details of this method can be found in [**51**]. If a discrete time transfer function, $G(z)$, for the plant model can be defined from A_m, B_m, C_m such that,

$$G_m(z) = \frac{C_m B_m}{(zI - A_m)}, \tag{2-23}$$

$$G(z) = \frac{z}{(z-1)} G_m(z), \tag{2-24}$$

and that $G_m(z)$ has no zero at z = 1 then the model is minimally realizable and therefore controllable [**51**]. A controller can be designed for a controllable system.

2.5.3 Stabilisability

A system which had unstable eigenvalues but is controllable is said to be stabilisable. This means that a stable closed-loop system can be realised from an open-loop unstable system.

2.5.4 Observability

Desired closed loop performance is dependent on the observability of the system. Given the input, if the initial state $\boldsymbol{x}(0)$ can be determined from the output at a time $t > 0$ then the system is observable. The output depends on the output matrix, C, a matrix known as the observability matrix, Q_{ob}, which is defined as,

$$Q_{ob} = [C\ CA\ \ldots CA^{n-1}]^T. \tag{2-25}$$

A system is controllable if Q_{cb} has full row rank or its determinant is non-zero [**49**], [**50**]. That is,

$$rank(Q_{ob}) = n, \tag{2-26}$$

$$Det(Q_{ob}) \neq 0. \tag{2-27}$$

An alternative approach which is more numerically stable is use of the observability gramian. Details of this method can be found in [**51**]. Observability is essential in feedback control systems and especially in model predictive control where the current state is necessary for computing future states, control moves and outputs [**32**].

2.5.5 Future system parameter values

In order to predict future control moves at a time (*k*), current plant information is necessary. This can be either taken from measurements or by state estimation or state vectors, $x(k)$. Wang [**32**], gives the following outline in determining the future states, future outputs and the future control trajectory which is denoted by,

$$\Delta U = [\Delta u(k_i)^T \ \Delta u(k_i+1)^T \ \dots \ \Delta u(k_i+ N_c - 1)^T \ ]^T \tag{2-28}$$

The state-space model (A, B, C), is used to calculate the set of future states by making use of future control parameters. This is done sequentially. Future state variables are denoted as,

$$x(k_i+1|k_i) = Ax(k_i) + B\Delta u(k_i) + B_d\varepsilon(k_i) \tag{2-29}$$
$$x(k_i+2|k_i) = Ax(k_i+1|k_i) + B\Delta u(k_i+1) + B_d\varepsilon(k_i+1|k_i)$$
$$x(k_i+2|k_i) = A^2x(k_i) + AB\Delta u(k_i) + B\Delta u(k_i+1) + AB_\varepsilon\varepsilon(k_i) + B_d\varepsilon(k_i+1|k_i) \tag{2-30}$$
$$\vdots$$
$$\begin{aligned} x\big(k_i+N_p\big|k_i\big) = A^{N_p}x(k_i) + \ & A^{N_p-1}B\Delta u(k_i) \ + A^{N_p-2}B\Delta u(k_i+1) + \ \dots \\ & + \ A^{N_p-N_c}B\Delta u(k_i+N_c-1) + A^{N_p-1}B_d\varepsilon(k_i) + \cdots \\ & + \ A^{N_p-2}B_d\varepsilon(k_i+1|k_i) + \cdots + A^{N_p-N_c}B_d\varepsilon(k_i+N_c-1|k_i), \end{aligned} \tag{2-31}$$

where N_c is the control horizon and N_p is the prediction horizon. Note that $N_c \geq N_p$.

The future states are then used to calculate determine future outputs by substitution. This too is done sequentially as follows,

$$y(k_i+1|k_i) = Cx(k_i+1|k_i) \tag{2-32a}$$
$$y(k_i+1|k_i) = C\ Ax(k_i) + CB\Delta u(k_i) + CB_d\varepsilon(k_i) \tag{2-32b}$$
$$y(k_i+2|k_i) = Cx(k_i+2|k_i) \tag{2-33a}$$

$$\begin{aligned} y(k_i+2|k_i) = CA^2x(k_i) + CAB\Delta u(k_i) + CB\Delta u(k_i+1) + \cdots \\ + CAB_\varepsilon\varepsilon(k_i) + CB_d\varepsilon(k_i+1|k_i) \end{aligned} \tag{2-33b}$$
$$\vdots$$
$$y\big(k_i+N_p\big|k_i\big) = Cx\big(k_i+N_p\big|k_i\big)$$
$$\begin{aligned} y\big(k_i+N_p\big|k_i\big) = CA^{N_p}x(k_i) + CA^{N_p-1}B\Delta u(k_i) + CA^{N_p-2}B\Delta u(k_i+1) + \cdots \\ + C\ A^{N_p-N_c}B\Delta u(k_i+N_c-1) + CA^{N_p-1}B_d\varepsilon(k_i) + \cdots \\ + CA^{N_p-2}B_d\varepsilon(k_i+1|k_i) + \cdots + CA^{N_p-N_c}B_d\varepsilon(k_i+N_c-1|k_i), \end{aligned} \tag{2-34}$$

Therefore the future predicted outputs denoted by Y are,

$$Y = \Big[y(k_i+1|k_i)^T \ y(k_i+2|k_i)^T \ \dots \ y\big(k_i+N_p\big|k_i\big)^T\Big]^T, \tag{2-35}$$

while the future states are,

$$\text{X}= \Big[x(k_i+1|k_i)^T \ x(k_i+2|k_i)^T \ \dots \ x\big(k_i+N_p\big|k_i\big)^T\Big]^T. \tag{2-36}$$

Assuming $\varepsilon(k_i)$ is zero-mean white noise, the predicted value of at future sample p is $\varepsilon(k_i + p|k_i)$. Since it has zero mean, at any value of p, predicted noise is taken as zero. Therefore, (2-27) and (29) can be written in compact matrix form as shown below,

$$Y = Fx(k_i) + \phi\Delta U \,, \tag{2-37}$$

where

$$F = \begin{bmatrix} CA \\ CA^2 \\ CA^3 \\ \vdots \\ . \\ CA^{N_p} \end{bmatrix}; \phi = \begin{bmatrix} CB & 0 & 0 & \dots & 0 \\ CAB & CB & 0 & \dots & 0 \\ CA^2B & CAB & CB & \dots & 0 \\ & \vdots & & & \\ & . & & & \\ CA^{N_p-1}B & CA^{N_p-2}B & CA^{N_p-3}B & \dots & CA^{N_p-N_c}B \end{bmatrix}.$$

Similarly future states are written as

$$X = C^{-1}Fx(k_i) + C^{-1}\phi\Delta U. \tag{2-38}$$

2.5.6 Optimisation

During optimization, at a time k_i the control system aims to minimise the error between the predicted output value and a given reference or set-point signal $r(k_i)$ which also is of length N_p. It is assumed that the set-point remains constant. A control signal ΔU is computed to satisfy this objective which is represented by a cost function J . The set-point information is contained in a vector R_s. This is obtained by multiplying $r(k_i)$ with a row vector of one's containing N_p elements.

$$R_s^T = [1\ 1 \dots 1]\, r(k_i), \tag{2-39}$$

The cost function is defined as,

$$J = (R_s - Y)^T(R_s - Y) + \Delta U^T \bar{R}\Delta U \,, \tag{2-40}$$

where $\bar{R}$ is a diagonal matrix or the form

$$\bar{R} = r_w I_{N_c \times N_c}\ (r_w \geq 0), \tag{2-41}$$

where r_w is a tuning parameter used to help achieve the desired closed-loop performance. An optimal $\Delta \boldsymbol{U}$ needs to be computed to minimise J. It is found by substituting (2-37) in (2-40).

$$J = (R_s - Fx(k_i) + \phi\Delta U\ )^T(R_s - Fx(k_i) + \phi\Delta U\ ) + \Delta U^T \bar{R}\Delta U \,, \tag{2-42}$$

$$J = (R_s - Fx(k_i)\ )^T\big(R_s - Fx(k_i)\big) - 2\phi^T\Delta U^T\big(R_s - Fx(k_i)\big) + \Delta U^T(\phi^T\phi + \bar{R})\Delta U \,, \tag{2-43}$$

The 1st derivative of J with respect to ΔU is expressed as,

$$\frac{\partial J}{\partial \Delta U} = -2\phi^T\left(R_s - Fx(k_i)\right) + 2(\phi^T\phi + \bar{R})\Delta U = 0(for\ minimum\ J)\ . \quad (2\text{-}44)$$

Therefore

$$\Delta U = (\phi^T\phi + \bar{R})^{-1}\phi^T\left(R_s - Fx(k_i)\right), \quad (2\text{-}45)$$

To find a connection between the reference r(k_i) and the control variable ΔU, R_s is redefined as,

$$R_s^T = [1\ 1\ \dots\ 1]\ r(k_i) = \bar{R}_s\ r(k_i)\ . \quad (2\text{-}46)$$

Therefore,

$$\Delta U = (\phi^T\phi + \bar{R})^{-1}\phi^T\left(\bar{R}_s\ r(k_i)\ - Fx(k_i)\right), \quad (2\text{-}47)$$

where, $(\phi^T\phi + \bar{R})^{-1}\phi^T\bar{R}_s\ r(k_i)$ corresponds to the change in the reference signal or set-point, and $(\phi^T\phi + \bar{R})^{-1}\phi^T F$ corresponds to state feedback control in this framework. The matrix $(\phi^T\phi + \bar{R})^{-1}$ is called the Hessian matrix in literature. It contains derivatives of the cost function.

The optimal solution, ΔU, is substituted into the cost function J to obtain the minimum of the cost function as,

$$J_{min} = \left(R_s - Fx(k_i)\right)^T\left(R_s - Fx(k_i)\right) - \left(R_s\ - Fx(k_i)\right)^T\phi(\phi^T\phi + \bar{R})^{-1}\phi^T\left(R_s\ - Fx(k_i)\right) \quad (2\text{-}48)$$

A single control move can be found by isolation using (2-47). This is done with a row vector of length, N_c as shown below,

$$\Delta u(k_i) = [1\ 0\ 0\ \dots\ 0](\phi^T\phi + \bar{R})^{-1}\left(\phi^T\bar{R}_s\ r(k_i)\ - \phi^T Fx(k_i)\right),$$

$$\Delta u(k_i) = k_y r(k_i) - K_{mpc}x(k_i). \quad (2\text{-}49)$$

There is a relationship between k_y and K_{mpc}. The feedback gain K_{mpc} can be broken down into, $K_{mpc} = \left[K_x\ K_y\right]$, where K_y is the last element of K_{mpc}.

The closed-loop equation of the augmented matrix can be found by substituting (2-49) into (2-17) and expressing k_i as k.

$$x(k+1) = Ax(k) + Bk_y r(k) - BK_{mpc}x(k) + B_\varepsilon \omega(k), \quad (2\text{-}50)$$

Assuming zero white Gaussian noise, (2-50) reduces to

$$x(k+1) = Ax(k) + Bk_y r(k) - BK_{mpc}x(k). \quad (2\text{-}51)$$

Therefore, the closed-loop eigenvalues can be evaluated by using the closed-loop characteristic equation,

$$det\left[\lambda I - \left(A - BK_{mpc}\right)\right] = 0. \quad (2\text{-}52)$$

2.6 Constraint handling

In the presence of constraints, the system performance deteriorates significantly if the constraints are not part of the design specification. For SISO systems, the constraints on the control are taken note of and this leads to modified state variables. The resulting system has good performance. However, for MIMO systems the problem is more complex and a better control framework is necessary. The predictive control problem is an optimisation problem includes constraints present in its formulation. Different types of constraints can be encountered in control systems applications. They can be classified as constraints on manipulated or control variables, outputs, state variables, and inputs. These can be in form of rates and directions of change or limits on magnitudes.

2.6.1 Constraints on the control variable incremental variation

Constraints on the controller output signal must not, and in most cases cannot, be violated therefore they are known as hard constraints. A positive change in the control variable Δu corresponds to a positive direction and sign in the variable. A change of sign signifies a change in direction. This type of constraint can be expressed as,

$$\Delta u^{min} \leq \Delta u(k) \leq \Delta u^{max}\ . \quad (2\text{-}53)$$

If $\Delta u^{min} = 0$ then the control signal cannot decrease in magnitude. On the other hand if $\Delta u^{max} = 0$ then the control signal can only decrease. For m control variables, this type of constraint is expressed as,

$$\Delta u_1^{min} \leq \Delta u_1(k) \leq \Delta u_1^{max}$$

$$\Delta u_2^{min} \le \Delta u_2(k) \le \Delta u_2^{max}$$
$$\vdots$$
$$\Delta u_m^{min} \le \Delta u_m(k) \le \Delta u_m^{max} \quad (2\text{-}54)$$

Over a control horizon of size N_c the constraints can be expressed as,

$$\begin{bmatrix} \Delta u_1^{min} \dots \Delta u_1^{min} \\ \Delta u_2^{min} \dots \Delta u_2^{min} \\ \vdots \quad \ddots \quad \vdots \\ \Delta u_m^{min} \dots \Delta u_m^{min} \end{bmatrix} \le \begin{bmatrix} \Delta u_1(k) & \Delta u_1(k+1) & \dots & \Delta u_1(k+N_c-1) \\ \Delta u_2(k) & \Delta u_2(k+1) & \dots & \Delta u_2(k+N_c-1) \\ \vdots & \vdots & \ddots & \vdots \\ \Delta u_m(k) & \Delta u_m(k+1) & \dots & \Delta u_m(k+N_c-1) \end{bmatrix} \le \begin{bmatrix} \Delta u_1^{max} \dots \Delta u_1^{max} \\ \Delta u_2^{max} \dots \Delta u_2^{max} \\ \vdots \quad \ddots \quad \vdots \\ \Delta u_m^{max} \dots \Delta u_m^{max} \end{bmatrix} \quad (2\text{-}55)$$

where all the matrices in this inequality are of size $m \times N_c$. This can be expressed in a more compact form,

$$\Delta U^{min} \le \Delta U \le \Delta U^{max}, \quad (2\text{-}56)$$

where ΔU^{min} and ΔU^{max} are $m \times N_c$ matrices containing the minimum and maximum constraints respectively. ΔU is the compact form of m control variables over the prediction horizon. (2-56) can be expressed in matrix form as,

$$\begin{bmatrix} -I \\ I \end{bmatrix} \Delta U = \begin{bmatrix} -\Delta U^{min} \\ \Delta U^{max} \end{bmatrix}. \quad (2\text{-}57)$$

2.6.2 Constraints on the amplitude of the control variable

These are the most common type of constraints. They are mainly subject to the limitations posed by the transducers. These are defined as follows,

$$u^{min} \le u(k) \le u^{max}. \quad (2\text{-}58)$$

Multi variable systems are specified as follows,

$$u_1^{min} \le u_1(k) \le u_1^{max} \quad (2\text{-}59)$$

$$u_2^{min} \le u_2(k) \le u_2^{max}$$
$$\vdots$$
$$u_m^{min} \le u_m(k) \le u_m^{max} \ . \quad (2\text{-}60)$$

As in (2-56) and (2-57) the amplitude constraint can also be extended over the whole prediction horizon. In compact form the constraints can be expressed as,

$$U^{min} \le U \le U^{max}, \quad (2\text{-}61)$$

where all the matrices in this inequality are of size $m \times N_c$. As in (2-58), (2-61) can be expressed as,

$$\begin{bmatrix} -I \\ I \end{bmatrix} U \leq \begin{bmatrix} -U^{min} \\ U^{max} \end{bmatrix}. \tag{2-62}$$

It is possible to express ΔU in terms of U^{min} and U^{max}. For each control variable increment Δu_n (where $n = 1,2, \ldots m$) the future control variable can be derived as follows,

$$\Delta U_n = [\Delta u_n(k), \Delta u_n(k+1) .. \Delta u_n(k+N_c-1)], \tag{2-63}$$

where

$$\Delta U = \left[\Delta U_1 \ \Delta U_2 \ \ldots \Delta U_{N_c}\right]^T. \tag{2-64}$$

$$u_n(k) = u_n(k-1) + \Delta u_n(k) = u_n(k-1) + \overbrace{[1\ 0\ 0 \ldots 0]}^{\beta_1} \Delta U_n,$$
$$u_n(k+1) = u_n(k) + \Delta u_n(k+1) = u_n(k-1) + \Delta u_n(k) + \Delta u_n(k+1),$$
$$u_n(k+1) = u_n(k-1) + \underbrace{[1\ 1\ 0 \ldots 0]}_{\beta_2} \Delta U_n,$$
$$\vdots \qquad\qquad \vdots$$
$$u_n(k+N_c-1) = u_n(k+N_c-2) + \Delta u_n(k+N_c-1),$$
$$u_n(k+N_c-1) = u_n(k-1) + \Delta u_n(k) + \Delta u_n(k+1) + \cdots + \Delta u_n(k+N_c-1)\ ,$$
$$u_n(k+N_c-1) = u_n(k-1) + \overbrace{[1\ 1\ 1 \ldots 1]}^{\beta_{N_c}} \Delta U_n. \tag{2-65}$$

(2-65) can be expressed in compact form as,

$$U_n = U_n(k-1) + \beta \Delta U_n, \tag{2-66}$$

where

$$\beta \text{ (triangular matrix)} = \left[\beta_1 \ \beta_2 \ \ldots \beta_{N_c}\right]^T \tag{2-67}$$

and

$$U_n(k-1) = [u_n(k-1)\ u_n(k-1)\ \ldots u_n(k-1)]^T, \tag{2-68}$$

where $U_n(k-1)$ is an $N_c \times 1$ matrix and

$$U_n = [u_n(k), u_n(k+1) .. u_n(k+N_c-1)]. \tag{2-69}$$

For m control (or manipulated) variables the expression (2-71) is expanded to include all m control variables as follows,

$$U = U(k-1) + \beta \Delta U, \tag{2-70}$$

Constraints on the amplitude of the controller output or control variable can be included by substituting (2-70) into (2-61)

$$U^{min} \leq U(k-1) + \beta \Delta U \leq U^{max}, \tag{2-71}$$

This above can also be written as,

$$\begin{bmatrix} -\beta \\ \beta \end{bmatrix} \Delta U = \begin{bmatrix} -U^{min} + U(k-1) \\ U^{max} - U(k-1) \end{bmatrix}. \tag{2-72}$$

2.6.3 Constraints on the output variables

Constraints for output variables $y(k)$ and state variables $x(k)$ are specified in the same way. State variables and output constraints and are often relaxed due to their large impact on the optimisation problem. When constraints on the output are enforced, constraints on control variables can be violated due to the large changes they are forced to undergo by the former resulting in constraint conflicts. Therefore, a slack variable s_v is included to "soften" the constraints. $s_v > 0$

$$y^{min} - s_v \leq y(k) \leq y^{max} + s_v, \tag{2-73}$$

where s_v is called the slack variable. Output and state variable constraints are therefore referred to as "soft" constraints.

Over the prediction horizon of N_p a compact (2-68) becomes

$$Y^{min} \leq Y \leq Y^{max}, \tag{2-74}$$

where Y^{min}, $Y$and Y^{max} are $q \times N_p$ matrices containing all the minimums, predicted values and maximum values of the outputs respectively. Output constraints can also be expressed in terms of ΔU.

$$Y^{min} \leq Fx(k) + \phi \Delta U \leq Y^{max}, \tag{2-75}$$

This can be expressed as,

$$\begin{bmatrix} -\phi \\ \phi \end{bmatrix} \Delta U = \begin{bmatrix} -Y^{min} + Fx(k) \\ Y^{max} - Fx(k) \end{bmatrix} \tag{2-76}$$

2.6.4 Including constraints in the objective function

The optimisation is a minimisation of ΔU in the objective function J(2-35) in the presence of constraints.

$$J = (R_s - Fx(k_i))^T \left(R_s - Fx(k_i)\right) - 2\phi^T \Delta U^T \left(R_s - Fx(k_i)\right) + \Delta U^T \left(\phi^T \phi + \bar{R}\right) \Delta U. \tag{2-76}$$

The constraints defined in (2-63), (2-77) and (2-81) can be put together in one expression as shown below,

$$\begin{bmatrix} M_1 \\ M_2 \\ M_3 \end{bmatrix} \Delta U \leq \begin{bmatrix} N_1 \\ N_2 \\ N_3 \end{bmatrix}, \tag{2-77}$$

where the data matrices are defined as,

$$M_1 = \begin{bmatrix} -I \\ I \end{bmatrix}; M_2 = \begin{bmatrix} -\beta \\ \beta \end{bmatrix};\ M_3 = \begin{bmatrix} -\phi \\ \phi \end{bmatrix}; \text{ and}$$

$$N_1 = \begin{bmatrix} -\Delta U^{min} \\ \Delta U^{max} \end{bmatrix}; N_2 = \begin{bmatrix} -U^{min} + U(k-1) \\ U^{max} - U(k-1) \end{bmatrix}; N_3 = \begin{bmatrix} -Y^{min} + Fx(k) \\ Y^{max} - Fx(k) \end{bmatrix}.$$

(2-77) can be further compacted as,

$$M\Delta U \leq \gamma, \tag{2-78}$$

where

$$M = \begin{bmatrix} M_1 \\ M_2 \\ M_3 \end{bmatrix}; \gamma = \begin{bmatrix} N_1 \\ N_2 \\ N_3 \end{bmatrix}.$$

The receding horizon control law implements only the first control movement while ignoring the other future control signals. However, it is still being debated as to whether constraints must of necessity be imposed on all future control signals and system output trajectories. Normally, the total number of constraints for inequality constraints is greater than the dimension of the decision variable ΔU. The Hessian matrix is known as $\left(\phi^T \phi + \bar{R}\right)\Delta U$ and is assumed to be both positive definite and symmetric. A general form for quadratic equations is shown below,

$$J = \frac{1}{2} x^T E x + x^T F, \tag{2-79}$$

$$Mx \leq \gamma, \tag{2-80}$$

where E is symmetric and positive definite. F, M, γ and E are all compatible matrices and vectors.

(2-80) is an inequality constraint similar to (2-78). An example of an equality constraint is shown below.

$$Mx = \gamma\ . \tag{2-81}$$

For inequality constraints Kuhn-Tucker conditions (see appendix A.4) are used. It is shown that both the active and inactive constraints can be defined in terms of the Lagrange multipliers. Inequality constraints such as those in (2-78) and (2-80) comprise of active and inactive constraints depending on their value during the whole process. An equality is said to be active if the limit or boundary has been reached as in (2-81) e.g. $M_i x = \gamma_i$, and inactive when the variable is within the bounds or limits e.g. $M_i x < \gamma_i$. M_i and γ_i correspond to the ith rows of the matrices M and γ.

In order to minimise the objective function in the presence of equality constraints, Lagrange expressions can be incorporated into the equation. Expressions (2-79) and (2-81) can be augmented as follows:

$$J = \frac{1}{2}x^T Ex + x^T F + \lambda^T(Mx - \gamma) \tag{2-82}$$

λ is a vector whose elements are called Lagrange multipliers. Minimisation is achieved by taking partial derivatives of the cost function, *J,* with respect to x and λ and equating them to zero. Optimal values for λ and x are shown below,

$$\lambda = -(ME^{-1}M^T)^{-1}(\gamma + ME^{-1}F), \tag{2-83}$$

$$x = -E^{-1}(M^T\lambda + F). \tag{2-84}$$

The expressions for the state variables x and λ contain two terms. One of them is the optimal solution without constraints while the other is a correction term which incorporates the effect of constraints. Incorporating the constraints in (2-78) into the objective function in (2-40) the following is obtained,

$$J = (R_s - Y)^T(R_s - Y) + \Delta U^T\bar{R}\Delta U + \lambda^T(M\Delta U - \gamma), \tag{2-84a}$$

where λ contains Lagrange multipliers which are computed in a manner similar to (2-83).

A number of different programming procedures are and can be used depending on the nature of the problem. A detailed account is found in Wang [**32**]. At every set of the algorithm the constraints which are active at that time need to be identified and added to the objective function in order to solve the optimisation problem while satisfying all

constraints. The necessary conditions (known as Kuhn-Tucker conditions) are listed based on the nature of the control problem (see appendix, A.4). The active set of constraints needs to be updated at each step since it is constantly changing. Prior knowledge of this set would shorten the iterative procedure. Methods which employ this approach are known as active set methods which are a subset of primal methods.

However, the optimisation problem becomes more complex as the number of constraints increases. To counter this, an approach referred to as the dual of primal methods is used where by inactive constraints are identified and removed as opposed to finding the active constraints. With the Lagrange multipliers being used as decision variables a dual objective function is defined and minimised. More details of this are found in Wang [**32**]. It is the opinion of this writer that the choice of which approach to use or the steps to determine it need to be addressed. Perhaps that is why in [**32**] they are referred to as primal-dual methods. Primal being the original objective function. One of the algorithms proposed to solve this dual problem is the Hildreth's quadratic programming procedure which are described in the works of Luenberger in 1969 and, Wismer and Chattergy in 1978, [**52**][**53**]. It is a sequential approach in which individual Lagrange multipliers are adjusted to minimise the objective function. It requires that the number of constraints be less than the number of decision variables, which are control or manipulated variables in this case, to converge. In the presence of active constraints, a compromised, near-optimal solution without any violations of the constraints will be arrived at by the algorithm. This is deemed safe for real–time applications. Again, if active constraints are identified at the beginning the closed-form solution for the optimisation problem can easily be computed.

2.7 Laguerre functions in DMPC design

Sometimes, the computational load is too much when using the approaches described up to this point. To circumvent this, the model can be expressed in terms of functions whose properties can simplify and minimise computations. One such type of functions is Laguerre functions which are derived from a state-space realisation of Laguerre networks. A more detailed account of Laguerre functions can be found in Wang [**32**]. Some of the properties of Laguerre functions are the orthonormal nature. This simplifies computations. In addition to

this the exponential decay factor in the Laguerre functions ensures convergence of the solution to the required change in the control after the transient period.

2.7.1 Plant input and Laguerre functions

Assuming the network is used to model the response of the n^{th} input to a system, a set of discrete-time Laguerre functions $L(k)$ are expressed as

$$L_n(k) = [{l_1}^n(k)\ {l_2}^n(k) \dots {l_N}^n(k)]^T\ , \tag{2-85}$$

where *N* is the number of coefficients used [**32**]. The value of *N* has an effect on the accuracy of the model. $L_n(k)$ is a function of a which is a pole of the discrete Laguerre network. For stability a is bounded as, $0 \leq a < 1$. When $a = 0$ Laguerre functions become a set of pulses as can be shown below,

$${l_1}^n(k) = \delta(k), {l_2}^n(k) = \delta(k-1), {l_N}^n(k) = \delta(k-N). \tag{2-86}$$

Orthonomality is illustrated below,

$$\sum_{k=0}^{\infty} l_i(k) l_j(k) = 0 \text{ for } i \neq j \tag{2-87}$$

$$\sum_{k=0}^{\infty} l_i(k) l_j(k) = 0 \text{ for } i = j. \tag{2-88}$$

For MIMO systems the nth computed control signal ΔU_n is defined by,

$$\Delta U_n = [\Delta u_n(k_i)\ \Delta u_n(k_i+1)\ \Delta u_n(k_i+2) \dots \Delta u_n(k_i+N_c-1)]^T\ . \tag{2-89}$$

A single control element can be expressed as a function of time shifted impulse response as shown,

$$\Delta u_n(k_i+i) = [\delta(i)\ \delta(i-1)\ \delta(i-2) \dots \delta(i-N_c+1)]\Delta U_n. \tag{2-90}$$

The total set off control signals for a system with *m* inputs at an instant k is,

$$\Delta u(k) = [\Delta u_1(k)\ \Delta u_2(k) \dots\ \Delta u_m(k)]^T. \tag{2-91}$$

For design purposes, the control trajectory ΔU_n is taken to be the impulse response of a stable dynamic system. Therefore, a future control signal at a sampling instant k can be written in terms of Laguerre functions and coefficients determined from design as,

$$\Delta u_n(k_i + k) = \sum_{j=1}^{N} c_j(k_i) l_j(k) \quad (2\text{-}92)$$

which is equivalent to:

$$\Delta u_n(k_i + k) = L_n(k)^T \eta_n, \quad (2\text{-}93)$$

where $\eta_n = [c_1\ c_2\ c_3 \dots\ c_N]^T$ represents the set of coefficients. The coefficients are functions of k_i which is the initial time value in the moving horizon window [**32**]. The full set of coefficients for all inputs is

$$\eta^T = [\eta_1^T\ \eta_2^T \dots\ \eta_m^T]. \quad (2\text{-}94)$$

2.7.2 Future parameter values with Laguerre functions

Given the state-space model (A,B,C) , the control variable $\Delta u_n(.)$ and the initial state $x(k_i)$, Laguerre functions can be used to express the future state and plant output for the system at a given sampling instant m as,

$$x(k_i + m|k_i) = A^m x(k_i) + \sum_{i=0}^{m-1} A^{m-i-1} B.L(i)^T \eta\ , \quad (2\text{-}95)$$

$$y(k_i + m|k_i) = CA^m x(k_i) + \sum_{i=0}^{m-1} CA^{m-i-1} B.L(i)^T \eta. \quad (2\text{-}96)$$

where

$$B = [B_1\ B_2 \dots\ B_m] \quad (2\text{-}97)$$

In expanded form (2-95) can be written as,

$$x(k_i + m|k_i) = A^m x(k_i) + \sum_{j=0}^{m-1} A^{m-j-1} [B_1 L_1(j)^T\ B_2 L_2(j)^T \dots\ B_m L_m(j)^T]\, \eta$$

$$x(k_i + m|k_i) = A^m x(k_i) + \Phi(m)^T \eta \quad (2\text{-}98)$$

where

$$\Phi(m)^T = \sum_{j=0}^{m-1} A^{m-j-1} [B_1 L_1(j)^T\ B_2 L_2(j)^T \dots\ B_m L_m(j)^T]. \quad (2\text{-}99)$$

The expression for the future state (2-95) is the same as equations (2-29) to (2-31) without the error terms while (2-96) can be compared to equations (2-32a) to (2-34). In order to compute the prediction, it is necessary to evaluate the convolution sum S_c. which is the same as $\Phi(m)^T$ in (2-95) and (2-98).

$$S_c(m) = \Phi(m)^T = \sum_{i=0}^{m-1} A^{m-i-1} B.L(i)^T. \quad (2\text{-}100)$$

Wang [**32**], shows that for this computation, Laguerre functions can be expressed in state-space form A_l where $L(k+1) = A_l L(k)$. Therefore,

$$S_c(m) = AS_c(m-1) + S_c(1)(A_l^{m-1})^T. \quad (2\text{-}101)$$

A_l is an $(N \times N)$function of the Laguerre poles, a.

2.7.3 Optimisation with Laguerre functions

In (2-40) the cost function can is written as,

$$J = (R_s - Y)^T(R_s - Y) + \Delta U^T \bar{R} \Delta U.$$

When Laguerre functions are used the terms $\Delta u_n(k_i + k)$ in ΔU are substituted with $L_n(k)^T \eta_n$ and $y(k_i + m|k_i)$ expressed in terms of (2-96) . The function *J* is simplified due to some terms in the squared control term tending to zero when a large enough prediction horizon is used. This is a result of the orthonormality of Laguerre functions. The new *J* is written as,

$$J = (R_s - Y)^T(R_s - Y) + \eta^T R_L \eta, \quad (2\text{-}102)$$

or

$$J = \sum_{m=1}^{N_p} \big(r(k_i) - y(k_i + m|k_i)\big)^T \big(r(k_i) - y(k_i + m|k_i)\big) + \eta^T R_L \eta, \quad (2\text{-}103)$$

where R_L is an $(N \times N)$ diagonal matrix with $r_w \geq 0$ on its diagonal [**32**]. The state variable can be altered in a manner similar to that done in equation (2-10) to include the set-point error term $r(k_i) - y(k_i + m|k_i)$ as follows,

$$x(k_i + m|k_i) = [\Delta x_m(k_i + m|k_i)\, r(k_i) - y(k_i + m|k_i)]. \quad (2\text{-}104)$$

This leads to a re-formulated cost function similar to the discrete-time linear quadratic regulators (DLQR). In this case, the aim is to find the coefficient vector η to minimise the cost function:

$$J = \sum_{m=1}^{N_p} x(k_i + m|k_i)^T Q x(k_i + m|k_i) + \eta^T R_L \eta\ , \quad (2\text{-}105)$$

where the weighting matrices $Q \geq 0$ and $R_L > 0$. The weight matrix Q is chosen to be such that

$$Q = C^T C \quad (2\text{-}106)$$

for minimisation of the error between the set-point or reference signal and the output. Equation (2-40) defines r_w. Constrained control can also be applied to Laguerre defined

systems. The above can be extended to MIMO systems. The values of N and a can be used as tuning parameters. The larger the N, the better the model. Like Laguerre networks, other orthonormal functions such as Kautz functions can be used. However, Laguerre have the advantage of simplified programming.

The objective function can be rewritten as,

$$J = \eta^T \Omega \eta + 2\eta^T \psi x(k_i) + \sum_{m=1}^{N_p} x(k_i)^T (A^T)^m Q A^m x(k_i) \quad (2\text{-}107)$$

where,

$$\Omega = \left(\sum_{m=1}^{N_p} \Phi(m) Q \Phi(m)^T + R_L \right), \quad (2\text{-}108)$$

and

$$\psi = \left(\sum_{m=1}^{N_p} \Phi(m) Q A^m \right). \quad (2\text{-}109)$$

$\Phi(m)$ is defined in (2-99). When the objective function, is minimised by taking a partial differentiation with respect to η and equating it to zero the following is obtained,

$$J_{min} = x(k_i)^T \left(\sum_{m=1}^{N_p} (A^T)^m Q A^m - \psi^T \Omega^{-1} \psi \right) x(k_i), \quad (2\text{-}110)$$

$$J_{min} = x(k_i)^T P_{dmpc} x(k_i) \, , \quad (2\text{-}111)$$

where

$$P_{dmpc} = \sum_{m=1}^{N_p} (A^T)^m Q A^m - \psi^T \Omega^{-1} \psi, \quad (2\text{-}112)$$

The optimal solution for the parameter η is,

$$\eta = -\Omega^{-1} \psi x(k_i) \quad (2\text{-}113)$$

The elements of η are decision variables.

By replacing k_i with k the receding horizon control law can be defined in terms of a state feedback with gain K_{mpc} as,

$$\Delta u(k) = -K_{mpc} x(k), \quad (2\text{-}114)$$

where

$$K_{mpc} = L(0)^T \begin{bmatrix} L_1(0)^T & o_2^T & \dots & o_m^T \\ o_1^T & L_2(0)^T & \dots & o_m^T \\ \vdots & \vdots & \ddots & \vdots \\ o_1^T & o_2^T & \dots & L_m(0)^T \end{bmatrix}^{-1} \Omega \quad \psi \quad (2\text{-}115)$$

$$L_n(0) = \sqrt{(1-a^2)}[1 \; -a \; a^2 \; -a^3 \dots -(1)^{N-1} a^{N-1}] \quad (2\text{-}116)$$

Therefore from (2-94)

$$\Delta u(k+m) = \begin{bmatrix} L_1(m)^T & o_2^T & \dots & o_m^T \\ o_1^T & L_2(m)^T & \dots & o_m^T \\ \vdots & \vdots & \ddots & \vdots \\ o_1^T & o_2^T & \dots & L_m(m)^T \end{bmatrix} \eta \,, \tag{2-117}$$

$$\Delta u(k) = M\eta \,, \tag{2-118}$$

where M represents the diagonal matrix of Laguerre multipliers. Since the feedback gain is now defined, the closed loop feedback control is,

$$x(k+1) = \left(A - BK_{mpc}\right)x(k). \tag{2-119}$$

2.7.4 Constraint handling

In the case where constraints on the change in control signal $\Delta u(k+m) \in \Delta U$ or its amplitude $u(k) \in U$ are to be incorporated in the optimisation problem they can simply be stated as,

$$\begin{bmatrix} -M\eta \\ M\eta \end{bmatrix} \Delta U \leq \begin{bmatrix} -\Delta U^{min} \\ \Delta U^{max} \end{bmatrix}. \tag{2-120}$$

$$u(k) = \sum_{i=0}^{k-1} \Delta u(i) \,. \tag{2-121}$$

The inequality constraint for the future time k, k =1,2,..., and similar to (2-76) is expressed as

$$u^{min} \leq u(k_i - 1) + \beta.\eta \leq u^{max}, \tag{2-122}$$

where $u(k_i - 1)$ represents all the previous control signals and

$$\beta = \begin{bmatrix} \sum_{i=0}^{k-1} L_1(i)^T & o_2^T & \dots & o_m^T \\ o_1^T & \sum_{i=0}^{k-1} L_2(i)^T & \dots & o_m^T \\ \vdots & \vdots & \ddots & \vdots \\ o_1^T & o_2^T & \dots & \sum_{i=0}^{k-1} L_m(i)^T \end{bmatrix}, \tag{2-123}$$

where o_m^T is a zero row vector with dimension similar to $L_m(0)^T$.

The state variable $x(k)$ which was previously defined in (2-10) as,

$$x(k) = \begin{bmatrix} \Delta x_m(k) \\ y(k) \end{bmatrix}.$$

$x(k)$ has to be redefined for the closed-loop system as,

$$x(k) = \begin{bmatrix} \Delta x_m(k) \\ e(k) \end{bmatrix}, \tag{2-124}$$

$$e(k) = y(k) - r(k). \tag{2-125}$$

2.8 Exponential weights in MPC design

Where constraints of a linear time invariant system are active, stability properties are compromised. This is because for such a system the control law is non-linear. However, it is possible to establish stability of the closed-loop system under certain conditions such as terminal of states and a large prediction horizon. An example of a terminal state is, $x(k_i + N_p|k_i) = 0$. It is known that the number of decision variables should be larger than that of active constraints. As a result of the presence of terminal states, which are active constraints, there is an increase in the number of decision variables. There is however the danger of not satisfying all the input, output and terminal constraints because of the interdependence between them brought about by the presence of terminal states. For this reason, terminal states are seldom used. Instead, for large prediction horizons, predictive control and DLQR become similar. Such problems are solved using the Riccati equation.The value,

$$x(k_i + N_p|k_i)^T Q x(k_i + N_p|k_i) \approx 0, \tag{2-127}$$

which from the Lyapunov function analysis, leads to a stable closed-loop system [**32**].

Exponential data weighting has been introduced in the LQR design, [**54**], and receding Horizon control, [**55**]. The weighting factor was $\{\alpha^j, j = 1,2, \dots\}$, where $\alpha = e^{\lambda \Delta t}$ [**54**]. These can either be applied to the cost function or control variables and states as transformed variables. This is shown below as follows,

$$J = \sum_{m=1}^{N_p} \alpha^{-2j} x(k_i + m|k_i)^T Q x(k_i + m|k_i) + \sum_{m=1}^{N_c} \alpha^{-2j} \Delta u(k_i + m)^T R \Delta u(k_i + m), \tag{2-128}$$

Or

$$\Delta \widehat{U}^T = \left[\alpha^{-0} \Delta u(k_i)^T \ \alpha^{-1} \Delta u(k_i + 1)^T \ \dots \ \alpha^{-N_p} \Delta u(k_i + N_p - 1)^T\right], \tag{2-129}$$

$$\hat{X}^T = \left[\alpha^{-1} x(k_i + 1|k_i)^T \ \alpha^{-2} x(k_i + 2|k_i)^T \ \dots \ \alpha^{-N_p} x(k_i + N_p|k_i)^T\right]. \tag{2-130}$$

(2-129) and (2-130) can be expressed as,

$$\Delta \widehat{U}^T = \left[\Delta \hat{u}(k_i)^T \ \Delta \hat{u}(k_i + 1)^T \ \dots \ \Delta \hat{u}(k_i + N_p - 1)^T\right], \tag{2-131}$$

and

$$\hat{X}^T = \left[\hat{x}(k_i + 1|k_i)^T \ \hat{x}(k_i + 2|k_i)^T \ \dots \hat{x}(k_i + N_p|k_i)^T\right] \tag{2-132}$$

respectively.

The cost function of (2-128) can be expressed in terms of the new state control variables in (2-131) and 2-132) as follows:

$$J = \sum_{m=1}^{N_p} \hat{x}(k_i + m|k_i)^T Q \hat{x}(k_i + m|k_i) + \sum_{m=1}^{N_c} \Delta\hat{u}(k_i + m)^T R \Delta\hat{u}(k_i + m), \quad (2\text{-}133)$$

where $\hat{x}(k_i + j|k_i)$ and $\Delta\hat{u}(k_i + j)$ are governed by the difference equation:

$$\hat{x}(k_i + j + 1|k_i) = \frac{A}{\alpha}\hat{x}(k_i + j|k_i) + \frac{B}{\alpha}\Delta\hat{u}(k_i + j) \quad (2\text{-}134)$$

The values $\alpha > 1$ and $\alpha < 1$ make the state $x(k_i + j|k_i)$ more significant at current time and future time respectively. The result is to minimise the un-weighted cost function, while changing the scale of the design model. The value of α chosen should be to ensure that the transformed design model has all its poles inside the unit circle to ensure that the prediction is based on a stable model. The optimisation using transformed variables decay at a faster rate than the original variables. This results in fewer terms in the Laguerre functions. This means a lower number of constraints is forced on the future samples. Alternatively, the Q and R matrices can be chosen to produce a closed-loop system having a stability margin of α^{-1}. Another method would be to choose new values for Q and R such that there is no need of the exponential weighting. These methods can result in a better conditioned system [**32**].

Let the new Q be Q_α and the new value of R be R_α.

$$\gamma = \alpha^{-1}, \quad (2\text{-}135)$$

$$Q_\alpha = \gamma^2 Q(1 - \gamma^2)P_\infty \quad (2\text{-}136)$$

$$R_\alpha = \gamma^2 R, \quad (2\text{-}137)$$

where P_∞ is the steady-state Riccati solution of the original cost function. The exponentially weighted solution will lead to solutions identical to those of the actual $x(k_i + j|k_i)$ and $\Delta u(k_i + j)$.

For a system without constraints, when a sufficiently large prediction horizon is chosen with weighting matrices *Q* and *R* greater than zero, the minimisation of the cost function *J* in (2-125) is reduces to a discrete-time linear quadratic regulator (DLQR) problem. Using Laguerre functions in formulating MPC has the advantage of optimising the cost function *J* in real

time, in the presence of a set of constraints [**32**]. These can be expressed in the same form as in (2-78) where,

$$M\Delta U \leq \gamma.$$

Exponential weights can be applied to M. The constraints expressed as

$$M_\alpha \Delta \widehat{U} \leq \gamma \tag{2-138}$$

where

$$M_\alpha = M \begin{bmatrix} I & 0 & \dots & 0 & 0 \\ 0 & \alpha^1 I & \dots & 0 & 0 \\ \vdots & \vdots & \ddots & \vdots & \vdots \\ 0 & 0 & \dots & \alpha^{N_p-1} I & 0 \\ 0 & 0 & \dots & 0 & \alpha^{N_p} I \end{bmatrix}.$$

The optimisation functions *J* in (2-133) can be written in compacted form as,

$$J = \hat{x}^T Q \hat{x} + \Delta \hat{u}^T R \Delta \hat{u}. \tag{2-139}$$

Transformed constraints can be incorporated into (2-139) in a manner similar to (2-82) and (2-84a). The resulting objective function which is minimised is,

$$J = \hat{x}^T Q \hat{x} + \Delta \hat{u}^T R \Delta \hat{u} + \lambda^T \left(M_\alpha \Delta \widehat{U} - \gamma \right). \tag{2-140}$$

It should be noted that closed-loop stability needs to be monitored by examining the eigenvalues of the closed-loop system whenever the constraints are not activated [**32**].

2.9 State estimation

Sometimes state variables are not measurable or would become unavailable during operation due to faults in the equipment. State variables are essential in the computation of future control moves and their unavailability would be detrimental to the control system. In such cases state variables can be obtained by use of state estimates or by means of non-minimal state-space realisation together with the corresponding input and output. The control block with which state estimation is carried out is called an observer. A necessary condition is that the system should be observable. The state estimate $\hat{x}_m(k)$ is used in place of the original state $x_m(k)$ in subsequent calculations.

2.9.1 The observer

The state estimate is defined in terms of the plant model. State estimation is more accurate with state feedback. This ensures that the state error,

$$\tilde{x}_m(k) = x_m(k) - \hat{x}_m(k), \tag{2-141}$$

converges to zero. $\tilde{x}_m(k)$ is the state error while $x_m(k)$ is the original state. An observer gain, K_{ob}, is used to tune the rate of convergence which is determined by the designer's choice of the location of observer poles. The observer to estimate state variable $\hat{x}_m(k)$ can be defined by ,

$$\hat{x}_m(k+1) = \overbrace{A_m\hat{x}_m(k) + B_m u(k)}^{\text{Model}} + \overbrace{K_{ob}\big(y(k) - C_m\hat{x}_m(k)\big)}^{Correction\ term}, \tag{2-142}$$

The observer gain can be determined from the future state error, $\tilde{x}_m(k+1)$. Following (2-141),

$$\tilde{x}_m(k+1) = x_m(k+1) - \hat{x}_m(k+1), \tag{2-143}$$

Substituting (2-141) and (2-3) into (2-143) and ignoring the disturbance term, we obtain

$$\tilde{x}_m(k+1) = A_m\tilde{x}_m(k) - K_{ob}C_m\tilde{x}_m(k). \tag{2-144}$$

The values of K_{ob} can be obtained using the eigen values of the matrix, $A - K_{ob}C_m$. For a single output case, given a set of desired observer poles $\{p_1, p_2, \ldots p_n\}$, K_{ob} can be obtained by,

$$det[\lambda I - (A - K_{ob}C_m.)] = \Pi_{i=1}^{n}(\lambda - p_i). \tag{2-145}$$

For a multi-output system, K_{ob} can be calculated iteratively using Kalman's filter (see the appendix, A.3).

Once designed, the observer can be connected to the rest of the feedback system. The feedback gain K_{mpc} can be broken down as,

$$K_{mpc} = \begin{bmatrix} K_x & K_y \end{bmatrix}, \tag{2-146}$$

where K_y is the last element of K_{mpc}. By combining the feedback state matrix (2-50), feedback input $\Delta u(k_i) = k_y r(k_i) - K_{mpc}x(k_i)$, in (2-49), the state error (2-141) and future state error equation (2-144) the following system equation is obtained,

$$\begin{bmatrix}\tilde{x}(k+1)\\ x(k+1)\end{bmatrix} = \begin{bmatrix}A - K_{ob}C & o_{n\times n}\\ BK_{ob} & A - BK_{mpc}\end{bmatrix}\begin{bmatrix}\tilde{x}(k)\\ x(k)\end{bmatrix} + \begin{bmatrix}o_{n\times m}\\ BK_y\end{bmatrix} r(k) \tag{2-147}$$

where $o_{n\times n}$ and $o_{n\times m}$ are $n \times n$ and $n \times m$ zero matrices respectively [**32**]. The subscripts m have been dropped. To compute the closed-loop eigenvalues the characteristic equation is obtained by

$$det\left[\lambda I - \begin{bmatrix}A - K_{ob}C & o_{n\times n}\\ = BK_{ob} & A - BK_{mpc}\end{bmatrix}\right] = 0. \tag{2-148}$$

The solution to this equation shows that the eigen values arise independently from both the control-loop and observer-loop as follows. Observer-loop eigenvalues are,

$$det\big[\lambda I - [A - K_{ob}C]\big] = 0. \tag{2-149}$$

Control-loop eigen values are,

$$det\left[\lambda I - \big[A - BK_{mpc}\big]\right] = 0. \tag{2-150}$$

If we make q^{-1} to represent a backward shift and $\frac{1}{1-q^{-1}}$ to denote the discrete time integrator, the closed-loop block diagram for the system is shown in Figure 2-4.

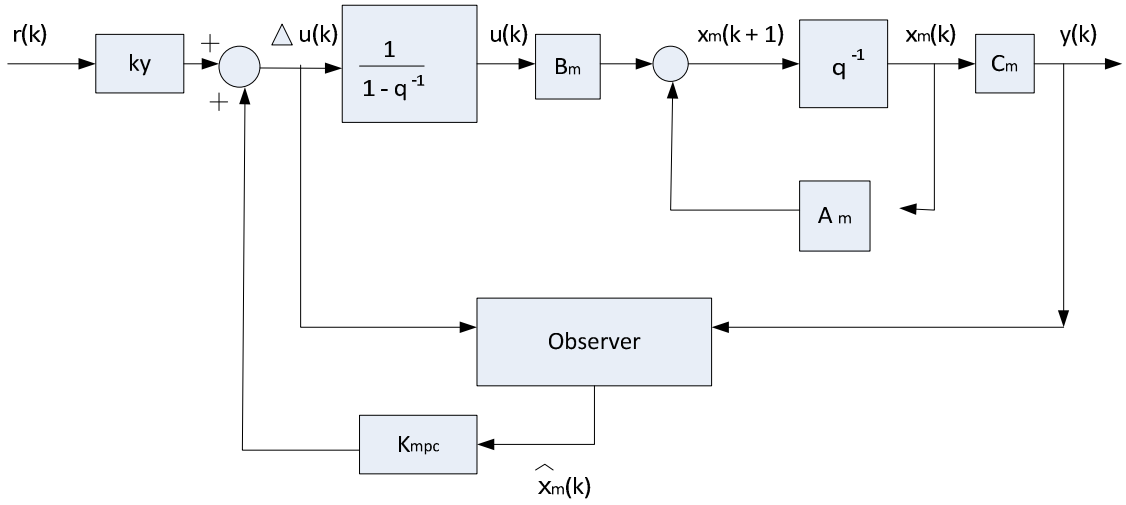

Figure 2-4 Discrete-MPC with an observer [32**]**

The observer takes the change in $\Delta u(k)$ from (2-49) and the output, $y(k)$, to compute the state estimate, $\hat{x}_m(k)$. The inner loop shows the state-space model (A_m, B_m, C_m). From the

diagram above it can be seen that even in the absence of the measured state $x_m(k)$, the observer can reliably estimate the states which can subsequently be used in the controller.

2.9.2 Tuning observer dynamics

Design of multivariable systems using Kalman filter is a trial and error process and therefore time consuming. Anderson and More [**54**], outline a simple approach in which the poles are placed inside a circle with a specified radius $\propto$ $(0 < \propto < 1)$. This is discussed below.

A transformation is performed on A_m and C_m which results in an observer equation similar to (2-144) to include $\propto$. Let $\hat{A}_m = \frac{A_m}{\propto}$ and $\hat{C}_m = \frac{C_m}{\propto}$. The observer equation becomes,

$$\tilde{x}_t(k+1) = \tilde{x}_t(k)\left(\hat{A}_m - \hat{K}_{ob}\hat{C}_m\right). \tag{2-151}$$

This can be solved iteratively using Riccati's equations(see appendix) and the eigenvalues of $\left(\hat{A}_m - \hat{K}_{ob}\hat{C}_m\right)$ obtained are guaranteed to be within the unit circle. Therefore the system is stable. The trial and error method is therefore just limited to choosing $\propto$, θ and Γ. θ and Γ are covariance matrices for the disturbances in the state and output equations for the state-space model in a stochastic setting. See the appendix for details.

2.10 Non-minimal state-space form

In 2005 Wang and Young [**56**] , proposed an approach wherein the state-space model of the system was to be constructed from a discrete-time transfer function or a difference equation in a non- minimal form. Using this approach, the need for an observer as a deterministic state reconstructor or a stochastic Kalman filter is negated [**57**]. The opposite of a non-minimal state-space model realisation is a minimal state-space model.

Different state-space models or varying dimensions can be realised from a transfer function $G_m(z)$. A minimal state space model is described by Kailath, 1980, is one having the smallest number of state variables among all possible realisations. Other properties are that is controllable and observable. A realisation is minimal if and only if the numerator $B(z) = C_m(zI - A_m)^{-1}B_m det(zI - A_m)$ and denominator $A(z) = det(zI - A_m)$ are relatively prime [**32**]. The transfer function is,

$$G_m(z) = \frac{y(k)}{u(k)} = \frac{B(z)}{A(z)} = C_m(zI - A_m)^{-1}B_m \,. \tag{2-152}$$

The numerator and denominator polynomials for the transfer function are,

$$B(z^{-1}) = b_1 z^{-1} + b_2 z^{-2} + \cdots + b_m z^{-m}, \tag{2-153}$$

$$A(z^{-1}) = 1 + a_1 z^{-1} + a_2 z^{-2} + \cdots + a_n z^{-n}. \tag{2-154}$$

For purposes of brevity the SISO system will be considered since application to MIMO systems is straightforward. The choice of the state vector is determined by the designer. This consequently has an impact on the non-minimal state-space model realised. Wang [**32**], presents the approach as follows,

Let $A(z^{-1})(1 - z^{-1}) = 1 + \bar{a}_1 z^{-1} + \bar{a}_2 z^{-2} + \cdots + \bar{a}_n z^{-n} + \bar{a}_{n+1} z^{-(n+1)}$,

and the state variable vector

$$x_m(k) = [y(k)\, y(k-1)\ \ldots y(k-n-1)\ \Delta u(k)\ \ldots\ \Delta u(k-m)]^T, \tag{2-155}$$

with a state–space model expressed as,

$$x_m(k+1) = A_m x(k) + B_m u(k) + B_d \epsilon(k), \tag{2-156}$$

$$y(k) = C_m x_m(k)\,, \tag{2-157}$$

where $\epsilon(k)$ is white noise. If $m = n$ then A_m is a $(2n+1) \times (2n+1)$ matrix, B_m is a matrix of $(2n+1) \times 1$, and C is a $1 \times (2n+1)$ matrix.

$$A_m = \begin{bmatrix} -a_1 & -a_2 & \ldots & -a_{n-1} & -a_n & b_2 & \cdots & b_{m-1} & b_m \\ 1 & 0 & 0 & 0 & 0 & 0 & \vdots & 0 & 0 \\ \vdots & \vdots & \ddots & \vdots & \vdots & \vdots & \ddots & \vdots & \vdots \\ 0 & 0 & 0 & 1 & 0 & 0 & \vdots & 0 & 0 \\ 0 & 0 & 0 & 0 & 1 & 0 & \vdots & 0 & 0 \\ 0 & 0 & 0 & 0 & 0 & 1 & \vdots & 0 & 0 \\ 0 & 0 & 0 & 0 & 0 & 0 & \vdots & 0 & 0 \\ \vdots & \vdots & \ddots & \vdots & \vdots & \vdots & \ddots & \vdots & \vdots \\ 0 & 0 & 0 & 0 & 0 & 0 & 0 & 1 & 0 \end{bmatrix}; B = \begin{bmatrix} b_1 \\ 0 \\ \vdots \\ 0 \\ 1 \\ 0 \\ \vdots \\ 0 \\ 0 \end{bmatrix};\ B_d = \begin{bmatrix} 1 \\ 0 \\ 0 \\ 0 \\ \vdots \\ 0 \\ 0 \\ 0 \\ 0 \end{bmatrix}$$

$$C = [1 \quad 0 \quad 0 \quad \ldots \quad 0 \quad 0 \quad 0]$$

The state variable can be augmented to include an embedded integrator in the same way as was done to obtain (2-15) and 2-16) [**32**][**56**]. For systems with dead-time, the model is derived to include it. A system with dead-time, d, has the form as shown below,

$$G_m = \frac{B(z)}{A(z)} z^{-d}\,. \tag{2-158}$$

A detailed account can be found in Wang [**32**].

The state variable model can take different forms determined by the motivation. In order to include *proportional integral-plus* control, Wang and Young [**56**], chose the state variable vector to be, $\Delta x_m(k) = [\Delta y(k)\ \Delta y(k-1)\ \ldots \Delta y(k-n+1)\ \Delta u(k)\ \ldots\ \Delta u(k-m+1)]^T$. The output variable vector $y(k)$ is included by augmenting the state variable x_m as shown in (2-10). The reference signal can also be included in the state in as part of the integral-of-error state variable $z(k)$ as

$$x_m(k) = [y(k)\ y(k-1)\ \ldots y(k-n+1)\ \Delta u(k)\ \ldots\ \Delta u(k-m+1)\ z(k)]^T, \quad (2\text{-}159)$$

where $z(k) = z(k-1) + y_d(k) - y(k)$ and $y_d(k)$ is the reference signal or set-point [**57**].

This follows a state space description of the form,

$$x_m(k) = A_m x(k-1) + B_m u(k-1) + D y_d(k), \quad (2\text{-}160)$$

$$y(k) = C_m x_m(k)\ . \quad (2\text{-}161)$$

The integral of error passes though the system therefore the non-minimal state-space model is of the form,

$$A_m = \begin{bmatrix} -a_1 & \ldots & -a_{n-1} & -a_n & b_2 & \cdots & b_{m-1} & b_m & 0 \\ 1 & \ldots & 0 & 0 & 0 & \ldots & 0 & 0 & 0 \\ \vdots & \ddots & \vdots & \vdots & \vdots & \ddots & \vdots & \vdots & \vdots \\ 0 & \vdots & 1 & 1 & 0 & \vdots & 0 & 0 & 0 \\ 0 & \vdots & 0 & 0 & 1 & \vdots & 0 & 0 & 0 \\ 0 & \vdots & 0 & 0 & 0 & \vdots & 0 & 0 & 0 \\ \vdots & \vdots & \vdots & \vdots & \vdots & \ddots & \vdots & \vdots & \vdots \\ 0 & \ldots & 0 & 0 & 0 & 0 & 1 & 0 & 0 \\ a_1 & \ldots & a_{n-1} & a_n & -b_2 & 0 & -b_{m-1} & -b_m & 1 \end{bmatrix}; B = \begin{bmatrix} b_1 \\ 0 \\ \vdots \\ 0 \\ 1 \\ 0 \\ \vdots \\ 0 \\ -b_m \end{bmatrix};$$

$$D = [0\quad 0\quad 0\quad \ldots\quad 0\quad 0\quad 1]^T;\ C = [1\quad 0\quad 0\quad \ldots\quad 0\quad 0\quad 0].$$

Following theis formulation, the future states have to include the reference or set-point signal. This is done sequentially by manipulation of the state-space equation. In compact form it is written as,

$$X = C^{-1}Fx(k_i) + C^{-1}\phi\Delta U + HS, \quad (2\text{-}162)$$

$$Y = Fx(k_i) + \phi\Delta U + HS, \quad (2\text{-}163)$$

where F and ϕ are obtained as in equations (2-35) and S is the vector of set-point values in the time window k to $k + N_p$. The resulting vector H is,

$$H = \begin{bmatrix} CD & 0 & 0 & \dots & 0 \\ CAD & CD & 0 & \dots & 0 \\ CA^2D & CAD & D & \dots & 0 \\ \vdots & \vdots & \vdots & \ddots & \vdots \\ CA^{N_p-1}D & CA^{N_p-2}D & CA^{N_p-3}D & \dots & CA^{N_p-N_c}D \end{bmatrix}, \quad (2\text{-}164)$$

and

$$\mathrm{S}= \left[y_d(k_i+1|k_i)^T \;\; y_d(k_i+2|k_i)^T \;\; \dots \;\; y_d\left(k_i+N_p\middle|k_i\right)^T \right]^T. \quad (2\text{-}165)$$

Consequently, this new formulation of Y which includes the set-point would have to be used instead of the former which had no HS term.

2.11 Tuning parameters

In the earlier sections of this chapter, a number of tuning parameters were encountered. The list of parameters a designer has to tune depends on the type of model and the MPC formulation used. From a discrete time transfer model tuning parameters include m and n which are the number of numerator and denominator coefficients respectively. In the case where the impulse response model is used, both m and n would be equal to the model horizon [**32**]. A step response model can have what is known as a model horizon, N_{MH}, which represents the effects of past control moves [**58**]. From the transfer function or bode and phase diagram of a model, the open-loop gain K_p, overall time-constant τ, settling time t_s , rise time t_r, effective dead-time θ_p, and corner frequency f_c [**50**] .

When Laguerre functions are used to approximate the model or control trajectory, two tuning parameters, a (scaling factor) and N, which (number of Laguerre terms), are introduced. To ensure stability a is limited to $0 \leq a < 1$. When $a = 0$, the number of parameters, N, required to approximate the control signal increases. For $a > 0$, Laguerre functions decay to zero at a much slower rate howbeit with smaller initial values [**32**].

Exponential data weighting introduces a weighting parameter alpha, α. For $\alpha < 1$ emphasis is put on future states while for $\alpha > 1$ emphasis is on the present states. When $\alpha > 1$ is applied to the cost function numerical instability is reduced whereas $\alpha < 1$ compounds it [**32**]. When exponential data weighting is applied to the state-space matrices it can be seen that the eigen values are minimised by an increasing α since the transformed matrices are divided by α. Therefore a good choice of α i.e. slightly above the value which results in a

stable system, makes the design model asymptotically stable (eigenvalues < 1). Numerical stability is measured by calculating the numerical condition number of the Hessian matrix. This number is significantly improved (reduced) with an increasing α. In the DLQR, it is shown that an infinite prediction horizon or an infinite upper-bound in *J* guarantees stability. Since the effect of future states and controls approaches zero, approximating the DLQR with large enough finite prediction and control Horizon (upper bounds of the cost function) is validated as sufficient to guarantee closed loop stability [**32**].

2.11.1 Sampling time

For a discrete-time model in the sampling time, T, is of great importance. A large sampling time would yield a discrete time model which does not capture the dynamics of the model. This would result in a highly inaccurate or unstable model response. A very small T increases execution time. For a system with very fast system dynamics, the designer can decide to only consider slower system dynamics which define the underlying response. The sampling time or sampling rate is related to the closed-loop bandwidth of the feedback system,f_c as follows,

$$\frac{1}{30f_c} < T < \frac{1}{5f_c} \ . \tag{2-166}$$

These are shown to relate to the rise time as,

$$0.06t_r < T < 0.4t_r, \tag{2-167}$$

where t_r is the rise-time [**59**]. In a case where dead-time is present Dougherty and Cooper, 2003, show that the maximum of 0.1τ and $0.5\theta_p$ would be used as the time constant as shown,

$$T = max\big(0.1\tau, 0.5\theta_p\big), \tag{2-168}$$

where θ_p is the effective dead-time [**58**]. The discrete dead-time integer is computed as follows,

$$\theta_d = Int\left(\frac{\theta_p}{T}\right) + 1, \tag{2-169}$$

where θ_d is the discrete dead-time integer [**58**]. By observation it can be seen that this value of T can be smaller than the ranges given by [**59**] when $0.5\theta_p < 0.1\tau$, since $0.06t_r = 0.24\tau > 0.1\tau$. Therefore the range of T which can be used is,

$$min\big(0.1\tau, 0.5\theta_p\big) \leq T \leq 0.4t_r. \tag{2-170}$$

2.11.2 Prediction horizon

The prediction horizon, P, is the period ahead when it is desired for the output to follow the set-point or reference trajectory. It is sometimes referred to as the costing horizon. There are varying opinions are to the proper value for the prediction horizon. Increasing the prediction horizon results in less aggressive control actions. This is desirable for more robust closed-loop behaviour. However, the consequence is slower system response. While most literature focuses on the maximum limit i.e. they assume a value of zero or one as the lower limit of the costing horizon, Trierweiler and Farina, 2003, introduce a term P_0, which is the lower limit. It does not necessarily take on the value of the immediate or next output instance but may be larger depending on the amount of dead-time. Therefore,

$$P_0 > \begin{cases} \theta_p \\ \theta_{inv} \end{cases} \tag{2-171}$$

where θ_p is dead-time and θ_{inv} is the inverse response time [**59**].

This is because the output can only be reached after these two periods of time. The cost function takes on a form,

$$J = \sum_{m=P_0}^{N_p} \big(r(k_i) - y(k_i + m|k_i)\big)^T \big(r(k_i) - y(k_i + m|k_i)\big) + \sum_{m=1}^{N_c} \Delta\hat{u}(k_i + m)^T R \Delta\hat{u}(k_i + m). \tag{2-172}$$

When considering the cost function of (2- 139) the new *J* becomes,

$$J = \sum_{m=P_0}^{N_p} \hat{x}(k_i + m|k_i)^T Q \hat{x}(k_i + m|k_i) + \sum_{m=1}^{N_c} \Delta\hat{u}(k_i + m)^T R \Delta\hat{u}(k_i + m). \tag{2-173}$$

The maximum horizon, P, should be bigger than P_0. Ideally, the prediction horizon should be chosen to be infinity to ensure nominal stability of the closed loop system. On the contrary Trierweiler and Farina, 2003, state that the prediction horizon should be,

$$P < t_s, \tag{2-174}$$

since it is not profitable to cost the future error in J that is not affected by future control actions.

An infinite horizon is not possible practically therefore, P is chosen to be as large as possible. Considering limitations of real time systems further, the prediction horizon should be chosen to be as small as necessary for real time implementation. A limit that can be placed on the minimum value for P are that,

$$P \geq \tau, \tag{2-175}$$

where τ, is the largest time constant in the system. A more exact evaluation of P can be found in [**58**]. It is given as,

$$P = N_{MH} = Int\left(\frac{5\tau}{T}\right) + \theta_d, \tag{2-176}$$

where θ_d is the discrete dead-time integer and $int(.)$ is the integer value of the parameter between the brackets. The value of P obtained above is a discrete time integer version of P [**58**], [**59**], [**14**].

The best value of P depends on computational resources available and the requirements of the system to be controlled. From the above, a range of values can be used. In a case where computational speed is an issue t_s can be used as the upper bound in the range, leading to,

$$0 \leq \begin{Bmatrix} \theta_p \\ \theta_{inv} \end{Bmatrix} \leq P_0 < \tau \leq P \leq t_s + \theta_p \, . \tag{2-177}$$

When converted to discrete time as in [**58**] the equation above becomes,

$$0 \leq \begin{Bmatrix} \theta_d \\ int\left(\frac{\theta_{inv}}{T}\right) \end{Bmatrix} \leq P_0 < Int\left(\frac{\tau}{T}\right) \leq P \leq Int\left(\frac{5\tau}{T}\right) + \theta_d \, . \tag{2-278}$$

It has to be noted that $t_s = 5\tau = Int\left(\frac{5\tau}{T}\right)$ when converted to discrete time.

2.11.3 Control horizon

The control horizon, M, refers to the interval when the control can be changed after which it is assumed to be constant. Increasing the control horizon results in more aggressive control actions, faster system response, and less robust closed-loop behaviour. It should be chosen as small as possible to reduce computing time. In quoting Van der Meulen, Vroemen stated that though M can go up to P, the control horizon should be chosen as,

$$\frac{1}{6}P \leq M \leq \frac{1}{3}P. \tag{2-179}$$

However for stable systems, $M = 1$ can be used though $M > 1$ gives better performance [**14**]. In [**59**] the minimum bound is related to the number of unstable poles in the system resulting in a range of,

$$Number\ of\ RHP\ poles \leq M < P, \tag{2-180}$$

where $Number\ of\ RHP\ poles$ refers to the number of unstable or right- hand- poles in the system. The control horizon can be equated the to the overall time response as follows,

$$M = Int\left(\frac{\tau}{T}\right) + \theta_d. \quad (2\text{-}181)$$

Any of the above approaches can be used depending on the stability of the system [**58**].

2.11.4 Controllable weight

Controllable weight Q refers to the weight applied to the outputs. It is used to achieve better control of a specific measured output [**59**]. Where several outputs are concerned, their importance can be reflected in the individual parameters in Q and when the parameters are increased, the influence of M on the closed loop behaviour decreases [**14**]. Trierweiler gave it a value corresponding to the output directions of the right hand pole zeros. More details of this method can be found in [**59**]. However, for the general case the following value

$$Q = C^T C, \quad (2\text{-}182)$$

is sufficient as can be deduced from derivations of the cost function *J*.

2.11.5 Move suppression

Move suppression or input weights, R, is used to penalise incremental control actions. It can be used to effect whatever closed loop behaviour is desired. Decreasing input weights has the same effect as when the control horizon is increased [**14**]. Trierweiler gave it a value corresponding to the input directions of the right hand pole zeros. More details of this method can be found in [**59**]. Dougherty and Cooper, 2003, related it to the open-loop gain, Model Horizon and overall time constant as follows,

$$R = \frac{M}{10}\left(\frac{3.5\tau}{T} + 2 - \frac{(M-1)}{2}\right)K_P^2\,, \quad (2\text{-}183)$$

where K_P is the open-loop gain of the system. This is valid when $M > 1$ [**58**]. For stable processes, $R = 0$ can be used in conjunction with $M = 1$. However, better performance is achieved with $R > 0$ [**59**].

2.12 Conclusion

A brief introduction to Model predictive control was given in this chapter. The history ad applications of MPC relevant to this study are given. This was to highlight some issues which were of concern with previous applications and to give confidence that extending MPC to the three shaft Brayton cycle based power plant is a feasible endeavour. A description of the plant was given with reference to the control aspects. The relevance of MPC was given as well. A literature study of the theoretical aspects of MPC was carried out. Most of the work on this study was based on the work of Wang [**32**]. The next chapter looks at the plant model in detail to which MPC will be applied.

Chapter 3

Linear model of a Brayton cycle based power plant

3.1 Introduction

The power production system of a Brayton cycle based power plant is referred to as the Main Power System (MPS). It consists of two parts namely the Reactor Unit (RU) and the Power Conversion Unit (PCU) which are directly coupled to each other. The RU generates thermal energy by means of a nuclear reaction. The PCU converts this thermal energy to mechanical work and then to electric energy [**60**].

The RU and PCU are controlled separately. Control of the RU ensures that the right amount of energy is added to the helium passing through it, while control of the PCU ensures that the power output of the PBMR meets the demand. A model of the PCU needs to be derived to be able to test different control techniques. In this chapter a linear model of the PCU will be described [**2**].

3.2 Derivation of a simplified model

The PCU utilises a Brayton cycle with recuperation and helium as the coolant gas. A schematic diagram of the PCU is shown in Figure 3-1. At (1), preheated helium enters the reactor and exits at (2). The hot high-pressure helium is made to expand in a high pressure turbine (HPT). At (3) the helium from the HPT is further expanded as it passes through the low pressure turbine (LPT) and at (4) the pressure has dropped considerably. The HPT drives the HPC and similarly, the LPT drives the LPC. After the going through the LPT, power turbine further expands the helium to the pressure at (5), which is approximately the same as the pressure at (6) and (7). Upon entering the low pressure compressor (LPC) low pressure helium at a low and temperature is compressed by a LPC to an intermediate pressure (8). The intercooler then cools it to state (9) thereby improving the overall cycle efficiency. A high pressure compressor (HPC) is then used to compress the helium and at (10) the helium is at its highest pressure. Between (10) and (1), the temperature of helium is raised in the recuperator before it enters the reactor at (1). In the reactor, the

temperature of the helium is raised higher as it passes through the reactor from the reactor inlet at (1) to the reactor outlet and HPT inlet at (2).

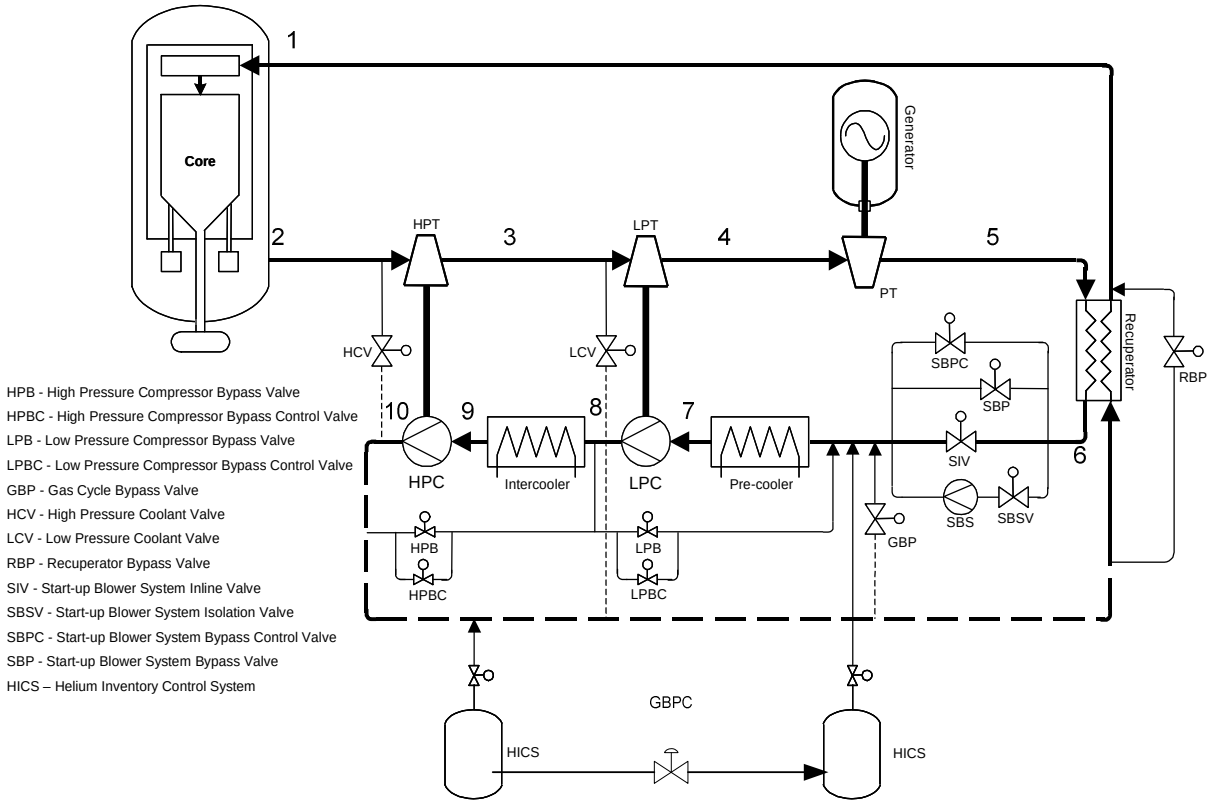

Figure 3-1 A schematic of the PBMR power conversion unit [60**]**

Output power levels are adjusted depending on the demand for power. The demand is anticipated beforehand and the desired power trajectory over time can be set well in advance. A controller is needed to ensure that the output power is equal to the desired power. This is known as load following. The desired power will be referred to as the reference power or set-point power. A controller using a feedback loop is needed to keep the power grid at the set-point. This is done by manipulating the valves which control the amount of helium in the circuit. Output power is determined by how much helium is flowing in the system. This is by helium injection, extraction or bypass as described in the earlier sections. In order to design the controller, a plant model is necessary. There are three main modes of operation of the MPS namely, start-up, steady-state and shutdown. During steady-state, normal operation takes place. In normal operation, not very large changes are required in the power output. The purpose of the controller is to ensure that the power output follows the set-point trajectory during normal operation. Therefore, a linear model is sufficient to model small changes to the set-point.

The dynamics of the PCU are non-linear in general. In order to derive the linear model, a number of assumptions were made [**60**]. They are listed in Table 3-1.

Table 3-1 Assumptions made to derive a linear model

Component	Assumption	Reason
Reactor	Constant outlet temperature	Dynamics of the reactor tend to be much slower than those of the system
HP compressor	Constant inlet temperature	Intercooler ensures the temperature keeps remains constant
LP compressor	Constant inlet temperature	Pre-cooler ensures the temperature keeps remains constant
Connecting pipes	Negligible pressure losses	The pressure losses are small enough to be ignored
HICS tanks /valves	Modelled as mass flow sources	Active control is assumed on the valves
Generator	Constant speed	It is connected to the grid which operates at a constant speed
System volumes	Modelled as lumped volumes	(Refer to section 3.2.1) Every volume can be modelled as a capacitor. As is seen in circuit theory, capacitors in series or parallel can be combined to form one. This simplifies the model and captures all the dynamics.

3.2.1 A linear model of the volumes in the system

For all systems, interactions involve power or energy flow and conservation. Modeling of such systems can be achieved by means of balance equations as shown in [**61**].

Rate of inflow – **rate of outflow** = **rate of accumulation**. (3-1)

This is applicable to a number of cases. For electrical systems the two sides of the equation are electrical current and rate of accumulation of electrical charge. In the case of the HICS this is the same as mass flow and rate of accumulation of the fluid in a volume. When modeling fluid systems, a volume is the same as capacitance in an electric circuit, pressure is the same as voltage and volumetric flow rate (or mass flow rate) is can be treated as current [**60**]. Because of this an electrical equivalent can be used to model certain mechanical and thermodynamic systems. The analogy is illustrated in Figure 3-2 below.

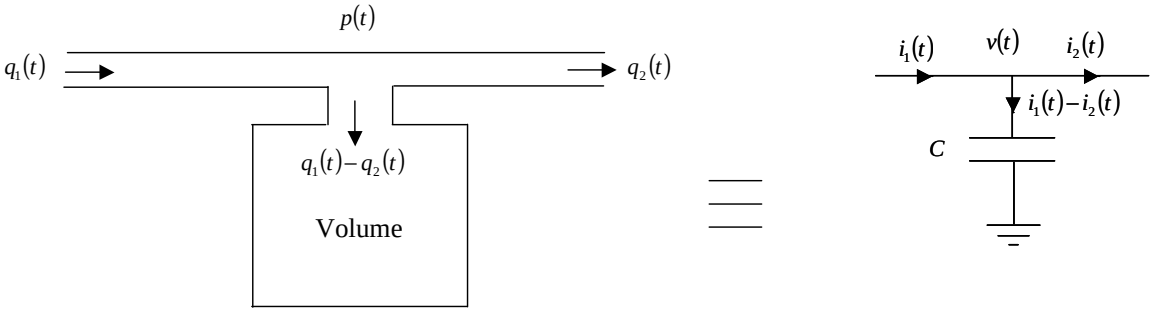

Continuity equation:

$$q_1(t) - q_2(t) = C\frac{d}{dt}p(t)$$

Kirchoff's current law:

$$i_1(t) - i_2(t) = C\frac{d}{dt}v(t)$$

Figure 3-2 The analogy between a volume and a capacitor [60**]**

The capacitance is proportional to volume and inversely proportional to temperature. Therefore, a volume in a low temperature circuit has a much higher capacitance than the same volume in a high temperature circuit. It should be noted that the analogy between a volume and a capacitor holds provided that the there are no large changes in the temperature of the fluid during the transient. With this condition satisfied, the capacitance value can be assumed to be fixed around a particular operating point.

The following observations can be made with regard to the expression for capacitance.
The dynamic model for a volume is expressed as,

$$p(t) = \frac{1}{C}\int\big(q_{in}(t) - q_{out}(t)\big)dt \tag{3-2}$$

Note equation above yields pressure in Pascals. The turbo machine models require pressure to be in bars. Thus, we introduce a modified capacitance as follows:

$$p(t) = \frac{1}{C'}\int\big(q_{in}(t) - q_{out}(t)\big)dt \tag{3-3}$$

where $C' = 1 \times 10^5 \cdot C'$, and the factor 10^5 converts the pressure from Pascals to bars.

With all of these assumptions, the simplified model of the PCU will be structured according to Figure 3-3. The figure shows the significant capacitances C_{LP}, C_{HP}, C_{MP}, C_{HT} and C_{LT}. The subscripts in this case indicate low pressure, high pressure, medium pressure, high pressure turbine, and low pressure turbine respectively. The bypass valves and HICS tanks are modelled as constant mass flow rate sources.

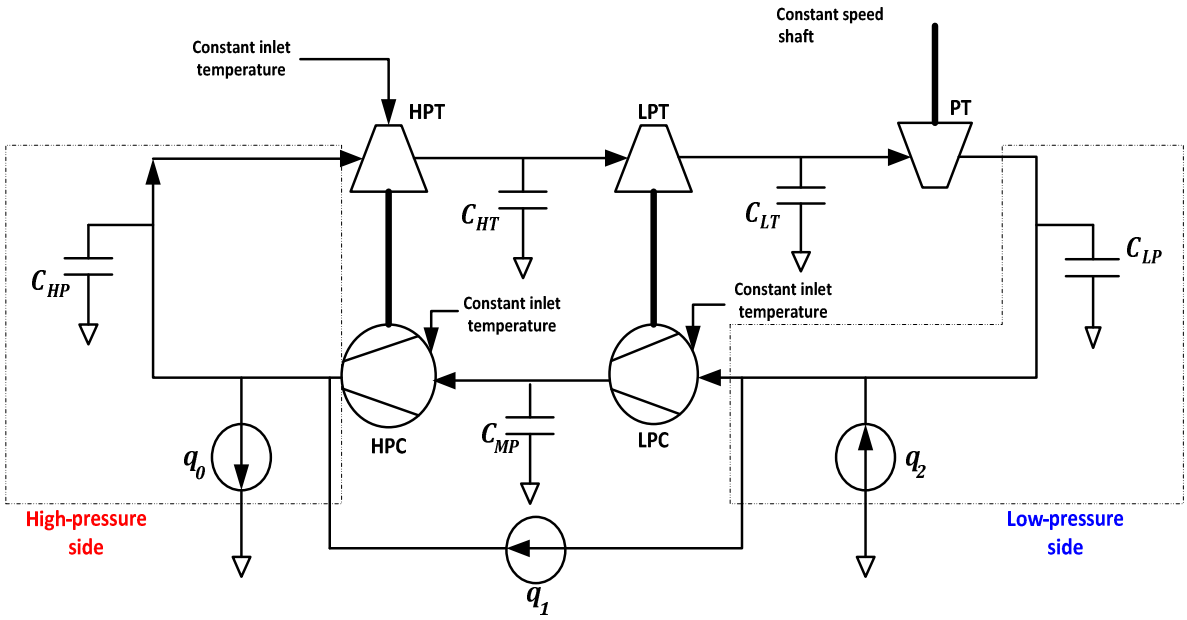

Figure 3-3 A schematic of the conceptual model of the PCU

Volume C_{HP} is the largest volume. It comprises of the volume of the reactor, the path of the gas between the reactor and the high-pressure compressor, the pipes connecting the reactor to the high-pressure turbine and also the internal volume of the high-pressure compressor which the gas occupies. Volume C_{LP} includes the volume of the recuperator on the low-pressure side, the pre-cooler and the volume containing gas within the turbine. Volume C_{MP} comprises of the intercooler volume, and the internal volume of the low-pressure compressor filled with gas. Volumes C_{HT} and C_{LT} are the smallest. This is because they come after the high and low pressure turbines. They are necessary in the model to make it possible to compute conditions at these points.

Since the temperature of helium from the reactor and the inlet temperatures of helium to the compressors are assumed to be constant, temperature is not included as a state. The gas in C_{HP} is considered to be constant for fast transients. This is also due to the reactor core materials having a large heat capacitance. In the same way, the pre-cooler and intercooler make it possible to approximate temperature of the gas in volumes C_{LP} and C_{MP} as constant. The temperatures of the gas in volumes C_{HT} and C_{LT} comprise mainly of the volumes of the low and high pressure turbines. Their magnitudes can be determined from other state variables. The simplified model does not cover all the aspects of plant operation.

However, it is sufficient in design of the plant controllers and estimators, and can also be used as a system engineering tool [**47**].

By assuming constant inlet temperature to the high pressure turbine, we are implicitly assuming that the reactor is acting as a perfect heat source. The reactor output temperature remains constant under all conditions. The mass flow "source" q_o represents the mass flow being injected from the HICS into the low pressure side of the circuit. The source q_2 represents the extraction of helium from the high pressure side of the circuit to the HICS. The source q_1 represents the flow through the compressor bypass valves. The flow through this valve is directed from the low pressure (LP) side to the high pressure (HP) side. The direction of q_1 is shown in Figure 3-3. The reason for this is that in steady state, the compressor bypass valves are open, allowing flow from the HP to LP side. If the valves are closed instantaneously, the flow goes from being a positive value to zero. In the perturbed sense however, all steady state values are removed prior to the transient and hence, when the valves are closed, it appears (only in the perturbed sense) as if the flow has gone from zero to some negative value. Since our model is a perturbed model, it is correct to show the incremental mass flow rate through these valves in the sense indicated in Figure 3-3.

The volumes illustrated are "lumped" volumes and are calculated by summing all the individual volumes between two turbo machines. The state variables are due to energy storage elements. The only energy storage elements in the system are the inertias making up the shafts of the turbine-compressor pairs and the capacitors. Since the low-pressure turbine (LPT) is connected to the low-pressure compressor, and likewise the high pressure (HP) turbine to the HP compressor, the inertia between them is the same. As a result, this system has two state variables due to inertia in the shafts and five state variables due to storage elements. This gives seven state variables in total. Rubin and Pritchard [**62**], showed how this simplified model is implemented using Simulink®. This is discussed further in the later sections.

3.3 Development of the model

Since the objective is to develop a linear model that will accurately model the dynamics of the PCU and the system is assumed to be in steady state, attention is focused on the

variations in the state variables due to small changes in some of the other state variables and not the actual value of the state variables of the system [**60**]. Linearisation of the model enables calculation of the frequency response. The elements within the plant were linearised, as this gave a better perspective of the global response (Rubin and Pritchard, 2002). For control purposes, the interest is in the system response due to small changes in the steady state mass flow rates. The model therefore makes use of the partial derivatives of the system differential equations evaluated at the operating point. The mass flow-rates of the injection, extraction and bypass mechanisms are therefore modelled as the perturbations q_1 and q_2 and not the actual flow rates Q_2 and Q_1.

3.3.1 General notes on linear model development

For a non-linear system in steady state, small perturbations in a variable can be approximated by taking the first term of the Taylor series about the operating point or steady state value. The result is a linear expression. For example a non-linear system

$$Y = f(X_1, X_2, X_3) \tag{3-4}$$

can be expressed as,

$$y = Y_0 + \frac{\partial Y}{\partial X_1}x_1 + \frac{\partial Y}{\partial X_2}x_2 + \frac{\partial Y}{\partial X_3}x_3 = Y_0 + K_{yx_1}x_1 + K_{yx_2}x_2 + K_{yx_3}x_3. \tag{3-5}$$

Since the variable of interest is the change in y the steady state value can be omitted and the change, y', denoted as,

$$y' = K_{yx_1}x_1 + K_{yx_2}x_2 + K_{yx_3}x_3. \tag{3-6}$$

Furthermore, if any of the variables above x_1, x_2 and x_3 can be expressed as functions of other variables, the equation above can be expanded further by taking partial derivatives of these functions. For example, if x_1, x_2 and x_3 can be expressed in terms of c_1 and c_2, Taking only the change in the x variables, (3-3) then becomes,

$$y' = K_{yx_1}\left(K_{x_1c_1}c_1 + K_{x_1c_2}c_2\right) + K_{yx_2}\left(K_{x_2c_1}c_1 + K_{x_2c_2}c_2\right) + K_{yx_3}\left(K_{x_3c_1}c_1 + K_{x_3c_2}c_2\right) \tag{3-7}$$

Therefore,

$$y' = K_{yc_1}c_1 + K_{yc_2}c_2 + G_{yc_1}c_1 + G_{yc_2}c_2 + L_{yc_1}c_1 + L_{yc_2}c_2 \tag{3-8}$$

where

$$K_{yc_1} = K_{yx_1} \cdot K_{x_1c_1}, K_{yc_2} = K_{yx_2} \cdot K_{x_2c_2},$$

$$G_{yc_1} = K_{yx_2} \cdot K_{x_2c_1},\ G_{yc_2} = K_{yx_2} \cdot K_{x_2c_2}$$

$$L_{yc_1} = K_{yx_3} \cdot K_{x_3c_1}, L_{yc_2} = K_{yx_3} \cdot K_{x_3c_2}$$

Linear models for the components of the plant are found the same way. These models were then can be combined to make the state space for representation of the plant. The models derived were used to build a Simulink model from which a state-space representation was obtained. Detailed derivations are found in [**62**]. However, models of the components will be discussed briefly.

3.3.2 Linear models of the turbo-machines

In order to derive non-linear or linear models for both the turbine and compressor, the following assumptions are made [**47**],

- The volume of the machine is zero. Any internal volume element such as chambers or diffusers must be represented using external volumes.
- Pressure changes at the inlet of the machine are immediately transferred to the outlet. This is based on the zero volume assumption above.
- The steady state compressor or turbine maps are valid under transient conditions. These can be obtained from manufacturers.
- The only energy flow across machine boundaries is in the form of gas flow and the rotating turbo-compressor shaft.
- The shaft dynamics are excluded from the turbo-compressor models. They are handled independently.

Based on the assumptions above, there is no energy storage within the turbine model. Therefore, the turbine is simply maps input to output variables. External models account for the energy storage elements within the system. Turbo-compressor shaft inertia and volumes or pressure vessels store energy.

A generic turbine or compressor model appropriate for our purposes would have the input – output relationship depicted in the block diagram in Figure 3-4 below.

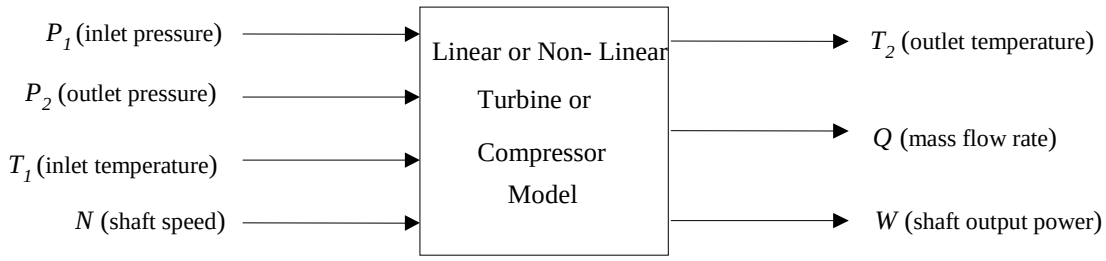

Figure 3-4 Input–output relationship for a turbine or compressor model

The inlet pressure ratio determines the operation of a turbine.

Turbine specific variables:

$$P_{rt} = P_1/P_2 > 1 \tag{3-9}$$

$$\eta_t = \frac{T_2/T_1 - 1}{P_{rt}^{-\left(\frac{\gamma-1}{\gamma}\right)} - 1} \tag{3-10}$$

Compressor specific variables:

$$P_{rc} = P_2/P_1 > 1 \tag{3-11}$$

$$\eta_c = \frac{P_{rc}^{\left(\frac{\gamma-1}{\gamma}\right)} - 1}{T_2/T_1 - 1} \tag{3-12}$$

The steady state behaviours of the turbine and compressor are sufficiently described by their operating maps. Two maps are used to describe each machine. The first one is one that relates non-dimensional mass flow (Q') and non-dimensional speed (N') to pressure ratio (P_{rt}, P_{rc}) and another that relates non-dimensional mass-flow and speed to efficiency η_t or η_c taken at constant heat source and sink pressures [**60**].

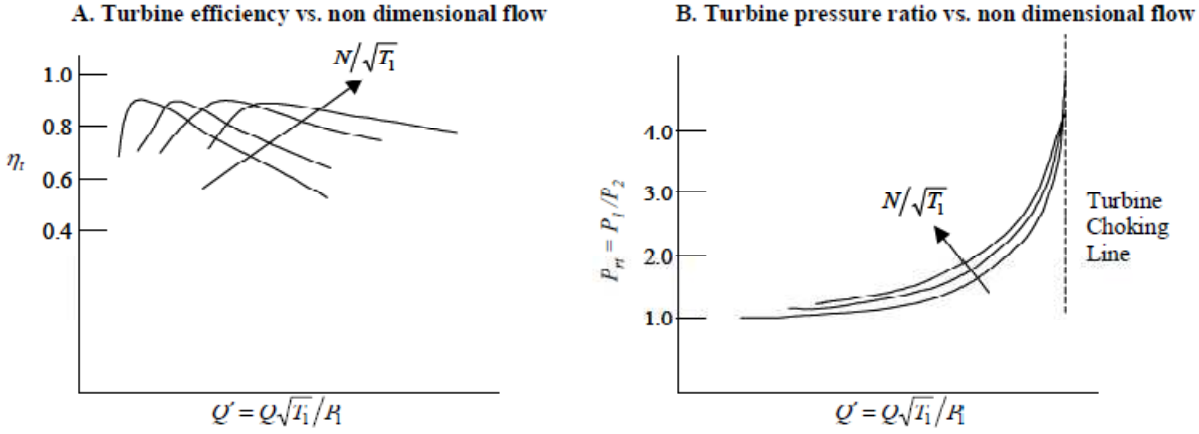

Figure 3-5 Shapes of the turbine and compressor performance maps

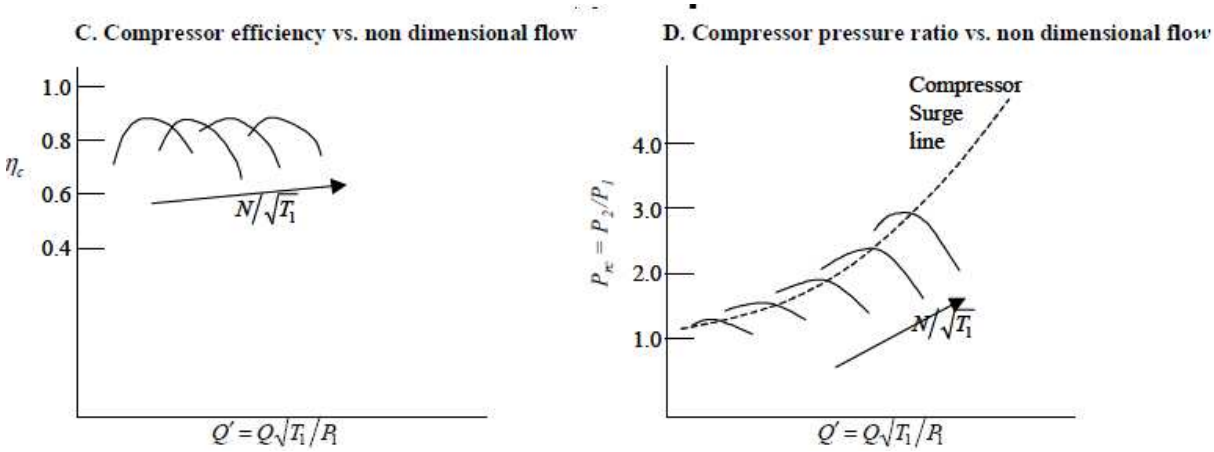

Figure 3-6 Shapes of the turbine and compressor performance maps [62]

It is important to note however that the "non dimensional" mass flow rate and actual mass flow rate are not proportional. Similarly, actual shaft speed must not be confused with "non-dimensional" shaft speed. In actual fact, while physical shaft speed may remain fixed (as in the case of a power turbine attached to a generator), non-dimensional speed may change due to inlet temperature changes,

Some useful deductions can be made from the maps. The compressor pressure ratio map is substantially more sensitive to changes in non-dimensional speed than the turbine pressure ratio map is. On the other hand, pressure ratio defined for the compressors is the inverse of the pressure ratio defined for the turbines.

The actual compressor operating point (for axial compressors) will, is usually designed to be on the right of the compressor surge line. The permissible operating points usually lie to the right, parallel to the surge line, for safety reasons. The turbines typically operate substantially to the left of the "choking line".

The linear model is used to simulate the effect of small perturbations in the input variables or tracking of changes in the set-point on the outputs of the system components. The meaning of "small" perturbations would vary for different plants. In this case it is assumed that changes in the region of 1/10 of the operating point constitute "small" perturbations. Choices of working values are dependent on the requirements i.e. specified outputs and available hardware or resources. The following methodology can be used to determine appropriate values for the operating point for turbines and compressors. It is found in [**60**].

Given the performance maps as shown in Figure 3-5 [**62**],

- Determine the pressure ratio ($P_{rt} = P_1/P_2 > 1$ or $P_{rc} = P_2/P_1 > 1$) and non-dimensional speed, N'.
- Using the pressure ratio map, determine the non-dimensional mass flow, $Q'$and hence solve for actual mass flow, Q.
- Given the non-dimensional mass flow and speed, determine the isentropic efficiency η_t or η_c using the efficiency map.
- Given the efficiency, solve for the temperature drop using the relationship,

  $T_1 - T_2 = \eta_t T_1 \left(1 - P_{rt}^{-\left(\frac{\gamma-1}{\gamma}\right)}\right)$ for turbines or

  $T_1 - T_2 = \frac{1}{\eta_c} T_1 \left(1 - P_{rc}^{\left(\frac{\gamma-1}{\gamma}\right)}\right)$ for compressors.

  • Hence, solve for the work done on the turbine or by the compressor using, $W = QC_p(T_1 - T_2)$. Note that the mechanical efficiency of the turbine is excluded at this stage, and is done at the level of the shaft model.
- Repeat the above until feasible values are obtained.

The values obtained can be used as operating pint values. Different sets of values can be obtained for different operating points. These can be denoted with a subscript "0" e.g. the operating point value for shaft power, W, referred to as, W_0.

Outputs due to small variations in the inputs can be solved linearly. This forms the basis for the Simulink® and state-space models used.

3.3.3 The linear turbine model

A more detailed model development can be found in [**60**]. The linear models developed below use only the perturbed quantities. There are three outputs discussed by Pritchard. These are mass flow-rate Q, output temperature T_2, and shaft power W. However, in the Simulink model which is used in this work, torque T_t is used for the High and low pressure turbines. In this section, all the four outputs will be discussed.

3.3.4 Output temperature

Output temperature is a function of three variables namely p_1, p_2, and t_1. i.e.

$$t_2 = f(p_1, p_2, t_1). \tag{3-13}$$

For a turbine the non-linear outlet pressure ratio is given by:

$$P_{rt} = P_1/P_2 \tag{3-14}$$

$$P_{rc} = P_2/P_1 \tag{3-15}$$

Small perturbations in pressure ratio can be approximated as ;

$$P_{rt} = K_{P_{rt}P_1} \cdot P_1 + K_{P_{rc}P_2} \cdot P_2 \tag{3-16}$$

where $K_{P_{rt}P_1}$ and $K_{P_{rc}P_2}$ are partial derivatives of pressure ratio w.r.t. Input and output pressure respectively. Efficiency is assumed to be constant and the non-linear outlet temperature is given by:

$$T_1 - T_2 = T_1 \left\{ \eta_t \left({P_{rt}}^{-\left(\frac{\gamma-1}{\gamma}\right)} - 1 \right) + 1 \right\} . \tag{3-17}$$

Small perturbations in output temperature can be approximated as:

$$t_2 = c_{T_2T_1} + c_{T_2p_{rt}} \cdot p_{rt} \tag{3-18}$$

Consequently, the complete linear model can be expressed as:

$$t_2 = K_{21}.p_1 + K_{22}.p_2 + K_{23}.t_1. \tag{3-19}$$

A similar approach is used for the compressor model where T_2 is replaced by:

$$T_2 = T_1 \left\{ \frac{1}{\eta_c} \left({P_{rc}}^{\left(\frac{\gamma-1}{\gamma}\right)} - 1 \right) + 1 \right\}. \tag{3-20}$$

Similar modifications can be implemented in the determination of changes in mass-flow, shaft power and torque.

3.3.5 Mass-flow

Mass- flow is a function of four variables namely p_1, p_2, n, and t_1. When taking into account the pressure ratio which too is a function of the non- dimensional values, mass flow-rate and speed.

$$q = f(p_1, p_2, n, t_1). \tag{3-21}$$

$$P_{rt} = C_{P_{rtQ}'} q' + C_{P_{rtN}'} n' \tag{3-22}$$

where $\boldsymbol{C_{P_{rt}Q'}}$ is the slope of the pressure ratio with respect to, (w.r.t), non dimensional mass flow at the operating point and is derived numerically. $\boldsymbol{C_{P_{rt}N'}}$ is the slope of the pressure ratio w.r.t non dimensional speed and is derived numerically at the operating point.

Since $Q' = Q\sqrt{T_1}/P_1$ and $N' = N/\sqrt{T_1}$, the equation above can be expanded further to yield:

$$P_{rt} = C_{P_{rt}Q}q + C_{P_{rt}P_1}p_1 + C_{P_{rt}T_1}T_1 + C_{P_{rt}N}n. \tag{3-23}$$

Solving for q results in,

$$q = \frac{1}{C_{P_{rt}Q}}\left(P_{rt} - C_{\mathrm{P}_{rt}P_1}p_1 - C_{P_{rt}T_1}T_1 - C_{P_{rt}N}n\right). \tag{3-24}$$

which can be expressed as,

$$q = K_{11}.p_1 + K_{12}.p_2 + K_{13}.n + K_{14}.t_1. \tag{3-25}$$

3.3.6 Shaft power

Shaft power is a function of four variables namely p_1, p_2, n, and t_1. The non-linear shaft output power is given by. $W = QC_p(T_1 - T_2)$ Assuming that C_p remains constant, the linearised, approximate change in power can be expressed as,

$$w_t = C_{WQ} \cdot q + C_{W\Delta T} \cdot (T_1 - T_2)\ . \tag{3-26}$$

Substituting the expressions for q and t_2 , W can be expressed as

$$W_t = K_{31}.p_1 + K_{32}.p_2 + K_{33}.t_1 + K_{34}.n. \tag{3-27}$$

In the case where torque is the preferred output as in the Simulink® models, torque is given as

Hence the torque supplied by the turbine to the shaft is given by:

$$T_t = \frac{\eta_m W_t}{2\pi N} \tag{3-28}$$

Assuming that mechanical efficiency remains constant, the torque perturbation due to a change in speed or shaft power is expressed as:

$$\tau_t = C_{T_tW_t} \cdot w_t + C_{T_tN} \cdot n \tag{3-29}$$

where $C_{T_tW_t}$ and $C_{T_tN}$are partial derivatives of torque w.r.t. shaft power and shaft speed evaluated at the operating point.

Since the shaft is connected to a compressor, we must consider the compressor change in torque too. In a similar fashion the compressor change in torque which comes from changes in its shaft power or shaft speed is,

$$\tau_c = C_{T_cW_c} \cdot w_c + C_{T_cN} \cdot n \tag{3-30}$$

This can be shown to arrive at an expression similar to that of power. However, the values of the constants differ. The same subscripts used for power in (3-27) are used as illustrated:

$$\tau_t = K_{31}.p_1 + K_{32}.p_2 + K_{33}.t_1 + K_{34}.n. \tag{3-31}$$

From the above, a turbine or compressor model can be shown to be:

$$\begin{bmatrix} q \\ t_2 \\ w \end{bmatrix} = \begin{bmatrix} K_{11} & K_{12} & K_{13} & K_{14} \\ K_{21} & K_{22} & K_{32} & K_{24} \\ K_{31} & K_{32} & K_{33} & K_{34} \end{bmatrix} \begin{bmatrix} p_1 \\ p_2 \\ n \\ t_1 \end{bmatrix} \tag{3-32}$$

OR

$$\begin{bmatrix} q \\ t_2 \\ \tau_t \end{bmatrix} = \begin{bmatrix} K_{11} & K_{12} & K_{13} & K_{14} \\ K_{21} & K_{22} & K_{32} & K_{24} \\ K_{31} & K_{32} & K_{33} & K_{34} \end{bmatrix} \begin{bmatrix} p_1 \\ p_2 \\ n \\ t_1 \end{bmatrix}. \tag{3-33}$$

This equation was implemented in Simulink® by Rubin and Pritchard as shown in Figure 3-7,

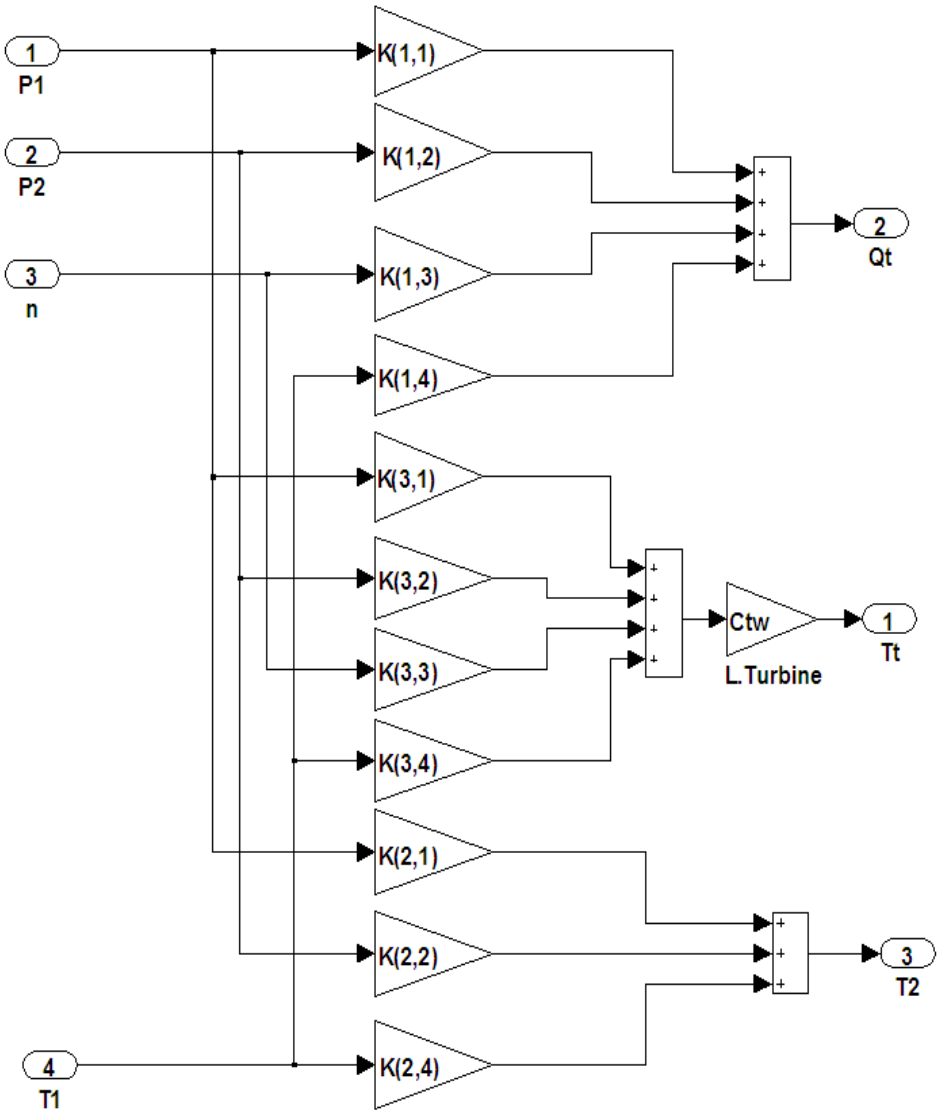

Figure 3-7 The structure of a turbine [62]

3.3.7 Shaft speed

Energy storing was earlier identified to be the volumes and the high and low pressure turbine shafts. The overal accelerating shaft torque is given by computing the sum of the torques acting on the shaft. The change in shaft speed can be solved using Newton's second law:

$$n(t) = \frac{1}{2\pi J}\int\left(\tau_c(t) + \tau_t(t)\right)dt, \tag{3-34}$$

where J is equal to the total inertia of the spinning shaft (in Nm/rad/s). The factor 2π is introduced to convert speed from rad/s to rev/s (Hz). Recognising that during steady state the turbo-compressor powers are equal, it follows that $W_{oc} = -\eta W_{01}$. This is due to the

steady shaft speed. The $C_{\tau N}$ terms cancel out. It follows that equation above can be written as:

$$n(t) = \frac{1}{Jt}\int \left(C_{T_c W_c} \cdot w_c(t) + C_{T_t W_t} \cdot w_t(t) \right) dt \quad (3\text{-}35)$$

where $J' = 2\pi J$, and the factor 2π converts between rad/s and Hz. It should be noted that the shaft model can be represented by the block diagram below.

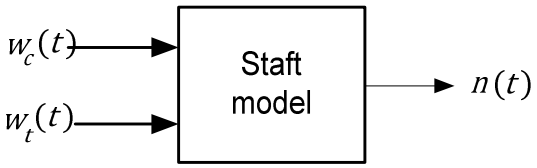

Figure 3-8 A block diagram of the linear shaft model.

The Simulink model to determine speed was however implemented by Rubin and Pritchard, [**62**], as shown below.

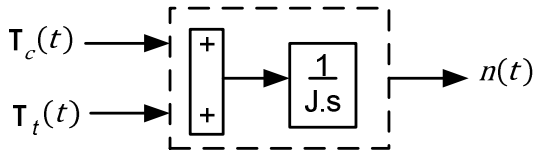

Figure 3-9 A Simulink® block diagram of shaft

In [**60**] the individual models for turbines and compressors in series were combined and relevant assumptions were made to simplify final expression. Taking into account the capacitor equations and shaft dynamics, a complete state space model of the plant was realised.

Table 3-2 Operating Points [2]

Parameter	HPT	LPT	PT	HPC	LPC
Inlet Pressure [bar]	66.6297	54.6362	40.1385	43.53	22.6753
Outlet Pressure [bar]	54.8958	40.4244	23.2309	71.1325	44.9211
Inlet Temperature[K]	1167.8709	1077.6134	951.0655	294.0547	294.5871
Outlet Temperature [K]	1081.2458	958.1085	773.8077	364.6934	397.3649
Shaft speed [rps]	100.0288	117.1042	50	100.0288	117.1042
Mass flow [kg/s]	145.9751	148.9716	153.1759	152.2948	157.472
Efficiency	0.87584	0.90909	0.8902	0.8902	0.88956
Power Output [MW]	57.8144	86.041	137.4871	-57.2363	-85.1805

The state space model extracted was of the form

$$\dot{X}(t) = AX(t) + B\,U(t)$$

$$\dot{Y}(t) = CX(t) + DU(t) \tag{3-36}$$

where

$$X(t) = \left[P_{hp}(t)\;\; P_{ht}(t)\;\; P_{lt}(t)\;\; P_{lp}(t)\;\; P_{mp}(t)\;\; N_l(t)\;\; N_h(t)\right]',\; U(t) = \left[S_{fh,in}\;\; S_{fh,out}\right]',$$
$$Y(t) = [W_t],$$

The output vector can be expanded to include other parameters such as mass-flows, temperature, turbo-machine speeds and pressure. Model verification is shown in Figure 3-9.

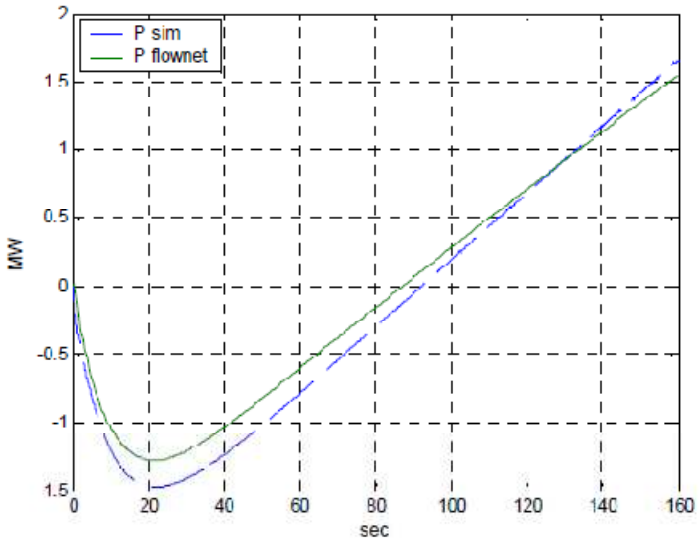

Figure 3-10 Helium injection: Flownet vs linear plant model [62**]**

The y-axis represents only the change in power. Therefore MW on this axis means the power is still at operating point level which in this case is 100 MW.

3.4 Simulink® linear model of the PCU

3.4.1 Introduction to Simulink®

Simulink® is a software package used to model and simulate dynamic systems. It supports both linear and non-linear systems. It supports both continuous and discrete time models and a hybrid of the two.

On the right is the low-pressure side of the circuit (blue dashed line) while on the left is the high-pressure side of the circuit (red dashed line). The advantage of Simulink® for modelling is a graphical user interface (GUI) in which simple drag and drop mouse operations can be used in building models such as block diagrams. This enables models to be drawn up just as one would with pencil and paper. After the model is complete, simulation follow and plots of the results can be generated.

3.4.2 Modelling the PCU in Simulink®

A Simulink® model of the PCU already exists. Relation between the Simulink Model and the plant model shown in Figure 3-3 is shown in Figure 3-10. At the top the three models of the turbines HPT, LPT and PT are shown [**2**].

At the bottom there is a model for the low-pressure compressor (LPC) and a model for the high-pressure compressor (HPC). The power turbine model block (PT) has an output labelled (Wt) and numbered (8). This output represents the power output of the system.

At the bottom right of the figure there is an input numbered (1) in green. This input represents the mass flow source q_2. Helium is injected through (1) from the HICS into the low-pressure side of the circuit. At the bottom left of the figure there is an input numbered (2) in green. This input represents the mass flow source q_0. Helium is extracted by means of the input (2) from the high-pressure side of the circuit. The bypass is shown as q_1. During the bypass, helium not passed through the compressors. In the Simulink® model, the two inputs (1) and (2) are used to model the bypass as opposed to a separate set of input and output to the system. In the Simulink® model the volumes between the turbines (C_{HT} andC_{LT}), the leak flows and pipe losses at the outlets of the compressors and turbines are taken into consideration in this model. The high and low pressure lumped volumes C_{HP} and $C_{LP}$are modelled as weighted integrators in the Simulink® model. On the right, C_{LP} is represented by the block C-LP while on the left C_{HP} is represented by the block C_HP . The same is done for all volumes.

Using Matlab/Simulink a state space model can be automatically extracted from the Simulink model.

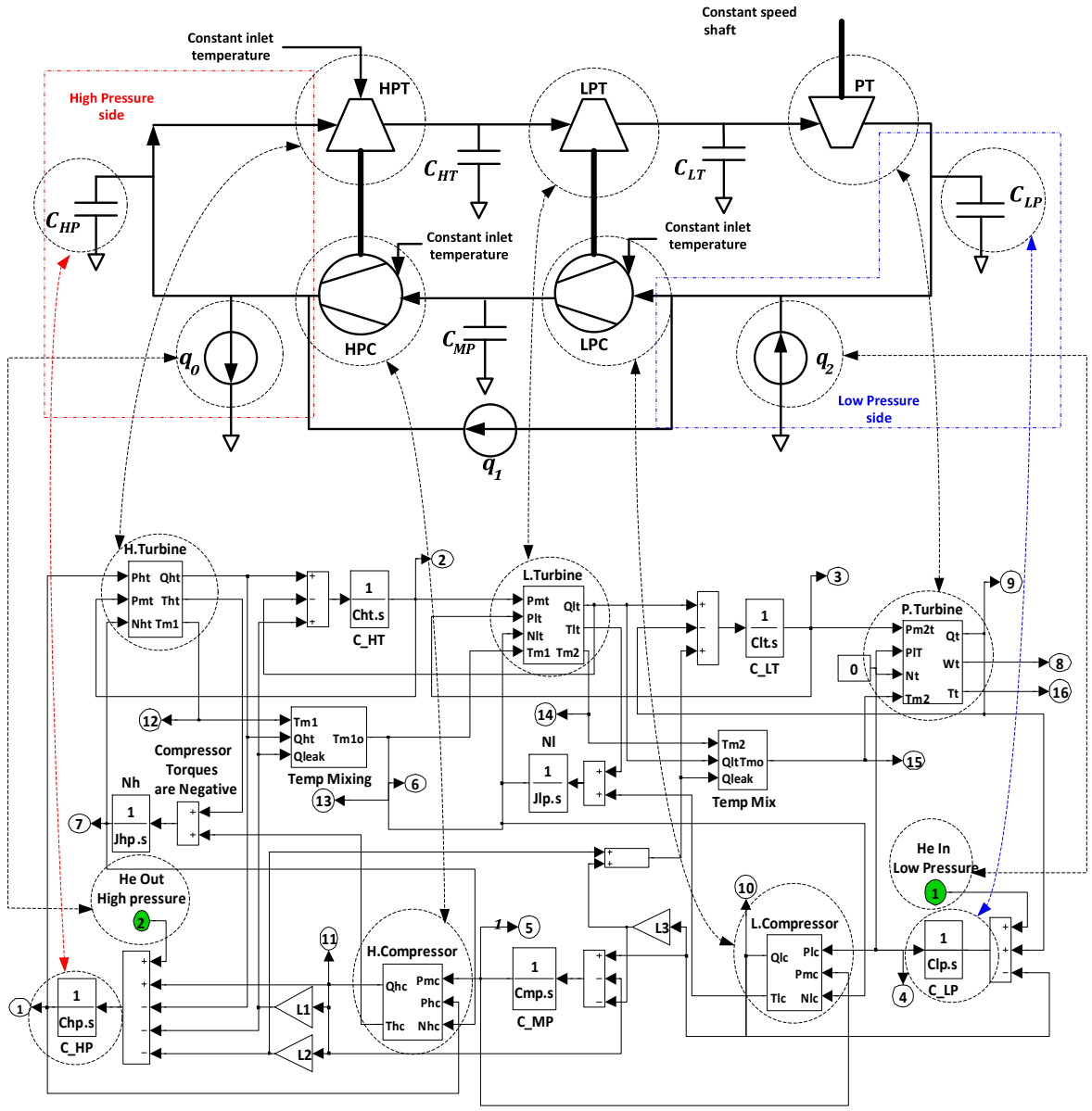

Figure 3-11 Simulink® model of the PCU [2][62]

3.4.3 Simulation of the PCU model

The model as described is part of work done by J.F Pritchard [12]. This model does not have a high-pressure injection capability. In this section the adjustments made to the PCU model will be discussed. The following paragraphs will be concerned with the booster tank model that was added to the PCU model to give it a high-pressure injection capability.

The Simulink® model has three actuators to manipulate the power output of the power plant at normal load following conditions. If there is a sudden change in the power demand

the system must adjust to meet that power demand. The three actuators will be briefly explained.

Low pressure injection

Helium is injected at the low-pressure side of the system to increase the mass flow in the system. However, low pressure helium injection does not result in an instantaneous increase in the power output of the system. The powers will in fact first drop before it starts to increase. This is called the non-minimum phase effect. It is undesirable. Let the perturbation of helium injected at input (1) in Figure 3-10 be equal to one. All the other inputs are assumed to be zero and the power output at the beginning of the simulation is 100 MW. The change in power in the three models due to helium injection at the low-pressure side is given in Figure 3-11.

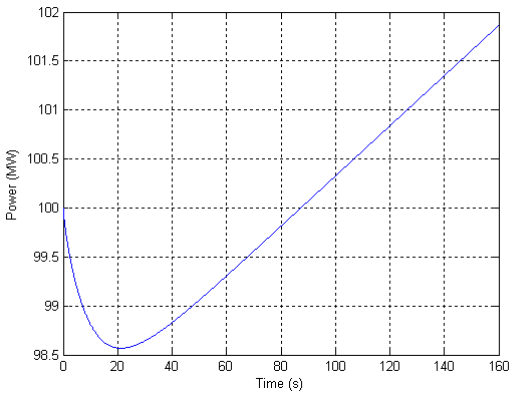

Figure 3-12 Power output during low pressure injection [2]

Gas bypass

In the real world system a gas bypass valve is used for bypassing. Opening the gas bypass valve reduces the generated electrical power and closing it will increase the power. By opening the gas bypass valve some of the helium that would normally pass through the reactor and turbines is re-circulated through the compressors. This reduces the mass flow-rate which results in the compressors using proportionately more of the available thermal energy and a decreased shaft power in the power turbine. The power can instantaneously be increased or decreased by using the bypass valve countering the non-minimum phase effect resulting from injecting helium at pre-cooler inlet.

In the Simulink® model gas bypassing is implemented by injecting gas at the low-pressure side and extracting the same amount of gas at the high-pressure side.

Figure 3-12 shows the power output by setting the gas bypass valve perturbation to one. This means that the valve is opened and effectively the power will drop.

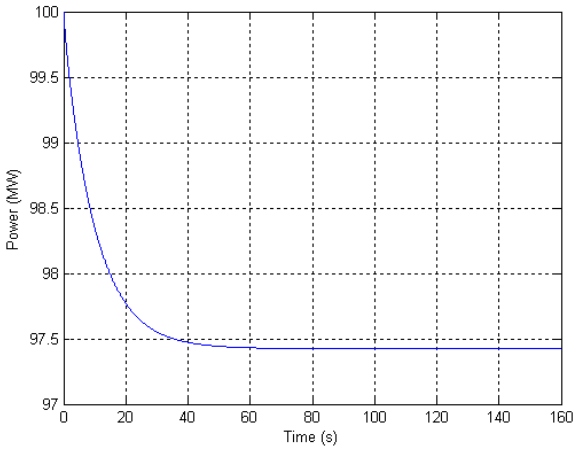

Figure 3-13 Power output due to opening the bypass valve [2]

Figure 3-13 shows the power output by setting the gas bypass valve perturbation to minus one. This means that the valve is closing and the power will increase. In Simulink, this is equivalent to setting the LP control mechanism to a negative value (LP extraction) and the HP control mechanism to a positive value (HP injection).

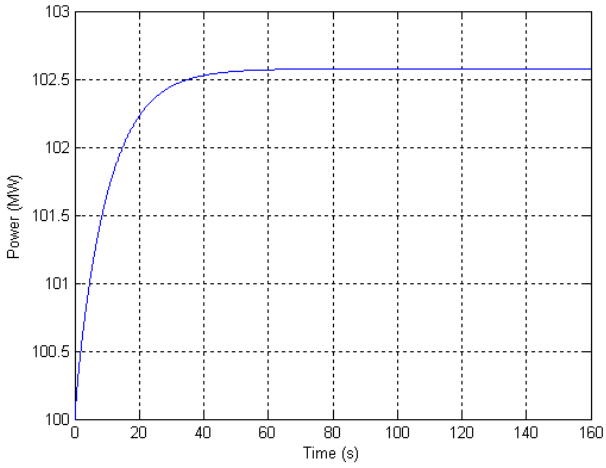

Figure 3-14 Power output due to closing the bypass valve [2]

When the By-pass valve is set to zero, no change is observed on the output.

High pressure extraction

Helium gas easily extracted at the high-pressure side of the system to decrease the mass flow in the system. Extraction of gas at the high-pressure side results in an instant decrease in the power of the system. Figure 3-11 shows the power output by setting the high-pressure extraction perturbation to one.

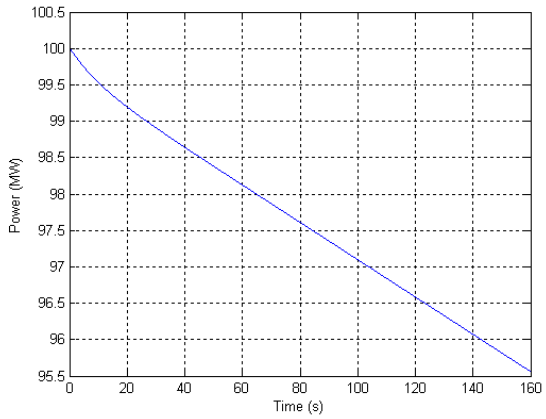

Figure 3-154 Power output due to high pressure extraction [2]

3.5 Conclusion

In this chapter, the basic operation of a three-shaft Brayton based power plant was described. The as the assumptions made in order to make the simplified model were given. It was shown that volumes in the plant model can be modelled by their electrical equivalents. Based on the assumptions, it was shown how linear models can be derived from the non-linear models. The linearised models and were used to construct a Simulink model. This model was shown to be accurate when its response was compared with a Flownet simulation. The power output during helium injection, extraction and Bypass mechanisms when applied to the model, was shown. A state-space model was automatically extracted from the Simulink® model. This model can be used in designing a controller for the power plant.

The next chapter deals with the design procedure of an MPC controller for the plant. The performance of this controller is then evaluated over various operating conditions.

Chapter 4

MPC implementation

4.1 Introduction

In this section a model predictive controller is designed for the system. It starts with the analysis of the extracted model. This gives insight to what kind of performance to expect from the controller. The controller parameters are determined from the response of the system. Performance is dependent on the tuning parameters and the effect of each parameter is studied. The best parameters are chosen and the performance of the MPC controller is compared to that of a genetically optimised fuzzy PID controller.

4.2 Model analysis

A state-space model was extracted from the Simulink® model. This model had 16 outputs but for control purposes, the state space model was manually reduced to one output as shown. This model is used by the MPC controller.

$$\dot{X}(t) = A_m X(t) + B_m U(t)$$

$$\dot{Y}(t) = C_m X(t) + D_m U(t) \tag{4-1}$$

where

$$A_m = \begin{bmatrix} -0.1113 & 9.617 & 0 & 0 & 0.3732 & 0 & 0.001071 \\ 0.08108 & -19.08 & 6.999 & 0 & 0 & -9.327 \times 10^{-5} & -2.086 \times 10^{-5} \\ 0.0005615 & 9.438 & -16.98 & 0.144 & 0 & 9.354 \times 10^{-5} & 4.085 \times 10^{-9} \\ 0.005835 & 0.02124 & 9.978 & -0.5977 & 0.1206 & -0.00104 & 4.245 \times 10^{-9} \\ 0.02381 & 0 & 0 & 0.4537 & -0.4938 & 0.001039 & -0.00105 \\ -3.747 & 0.0002171 & -2.308 \times 10^{4} & 9.069 & -171.2 & -0.7398 & -2.726 \times 10^{-5} \\ 124.4 & -2.216 \times 10^{4} & 0 & 0 & 32.28 & 0 & -0.7298 \end{bmatrix},$$

$$B_m = \begin{bmatrix} 0 & 1 \\ 0 & 0 \\ 0 & 0 \\ 1 & 0 \\ 0 & 0 \\ 0 & 0 \\ 0 & 0 \end{bmatrix},$$

$C_m = [\ -5370 \quad -1.955 \times 10^{4} \quad 2.194 \times 10^{7} \quad -5.305 \times 10^{5} \quad 0 \quad 0.2439 \quad -0.03906\ ]$, and

$$D_m = [0 \quad 0].$$

This model was analysed to determine whether it would be possible to design a controller for this model. The system can also be represented in transfer function format.

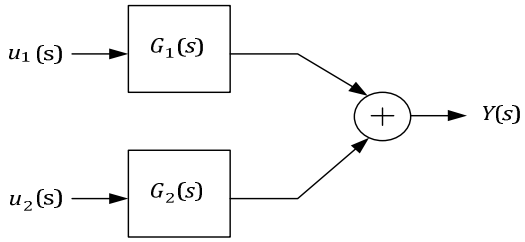

Figure 4-1 Block Diagram representation of the system

In Figure 4-1, $u_1(s)$ represents the controller output to the low pressure side of the plant and $G_1(s)$ is the corresponding transfer function. On the other hand $u_2(s)$ represents the controller output to the high pressure side of the plant and $G_2(s)$ is the corresponding transfer function. $Y(s)$ is the power output.

Matlab was used to obtain the transfer function model of the state space model (4-1). The transfer function is evaluated as follows [**63**].

$$H(s) = \frac{B(s)}{A(s)} = \frac{b_1 s^{n-1} + \cdots + b_{n-1}s + b_n}{a_1 s^{m-1} + \cdots + a_{m-1}s + a_m} = C(sI - A)^{-1}B + D\,. \tag{4-2}$$

In the same environment the transfer function can be converted to pole-zero formats wherein the poles, zeros and gain of the system are specified as,

$$G(s) = K\frac{(s-z_1)(s-z_2)\cdots(s-z_i)}{(s-p_1)(s-p_2)\cdots(s-p_j)} = K\frac{\prod_{q=1}^{i}(s-z_q)}{\prod_{v=1}^{j}(s-p_v)} \tag{4-3}$$

where K is the gain, z_q is the q^{th} zero, p_v is the v^{th} pole, $G(s)$ is the transfer function for one input. The real poles stand for the time constants in the system. This is known as the pole-zero format. The above would yield j time constants defined as, $\tau_v = -\frac{1}{p_v}$, where $v = 1,2,\ldots,j$.

4.2.1 System characteristics

From the transfer functions in pole zero format the poles of the system are visible. The two transfer functions imply that there are two sets of poles and zeros. Figure 4-2 shows the poles and zeros of $G_1(s)$ which is the transfer function from the high pressure side to the output. The poles are denoted by "**x**" while the zeros are indicated by "**o**". All the poles are on the left hand side of the plane while all but one zero are on the left side of the graph. For actual values see appendix A.6. The positive zero is only slightly on the right side of the plane at 0.0121. Figure 4-3 shows a similar plot of poles and zeros of $G_2(s)$ which is the

transfer function from the low pressure side to the output. The positive zero in $G_2(s)$ is much larger than that in $G_1(s)$. A zero on the positive side results in the non-minimum phase effect.

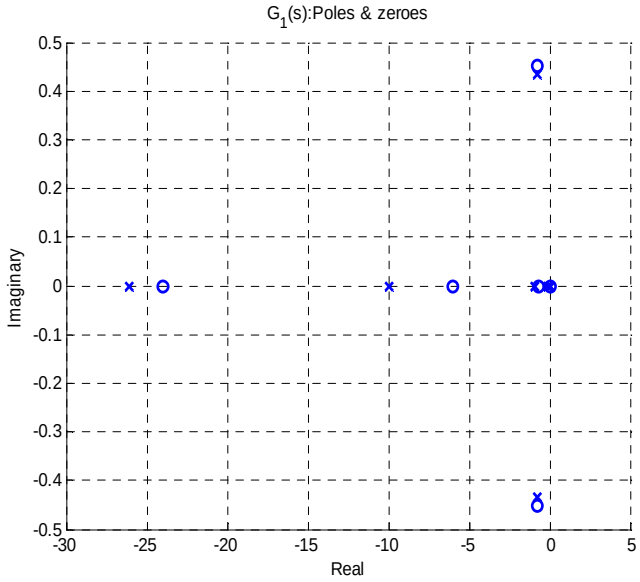

Figure 4-2 Pole-zero plot of $G_1(s)$

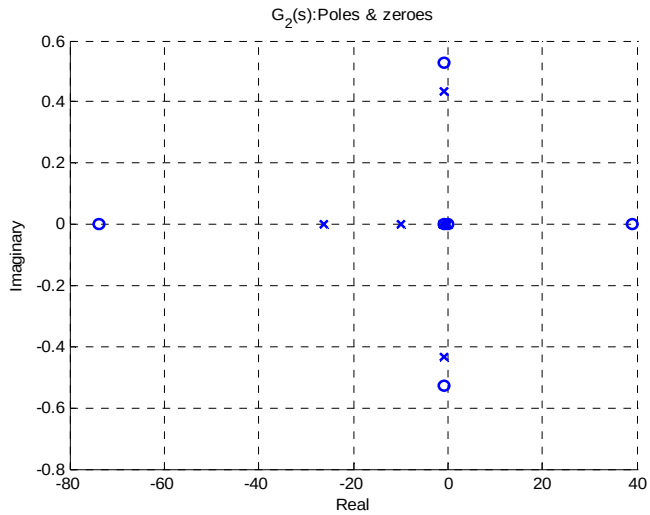

Figure 4-3 Pole-zero plot of $G_2(s)$

Due to the zero in $G_2(s)$ being much further along the positive real axis than the one in $G_1(s)$, the non-minimum phase effect is more apparent in $G_2(s)$ than in $G_1(s)$. This is the reason why low-pressure injection has a more pronounced non-minimum phase effect. It must be noted that these are approximations of poles and zeros in the system and are therefore not exact. However, the location of the poles gives a very good idea of the system's characteristics.

Stability

From Figure 4-2 and Figure 4-3, the system poles are all on the left hand side. Therefore it the system is open-loop stable. This means that the open loop settling time can be used in determining MPC parameters [**59**].

Controllability

For a system defined in state-space form, A, B, C and D, controllability can be determined from the state and control matrices. These are A and B respectively. Let A be an $n \times n$ matrix. The rank of a matrix X, denoted as $\mathrm{rank}(X)$, is the number of linearly independent rows or columns of a full matrix. The number of uncontrollable states, N_{uc}, is calculated as,

$$N_{uc} = \mathrm{n} - \mathrm{rank}(Q_{cb}), \tag{4-4}$$

where Q_{cb} is the controllability matrix evaluated as shown in equation (2-19). The number of uncontrollable states was zero therefore the system is fully controllable.

Stabilisability

Since the system is stable, it implies that the system is closed loop stabilisable.

Observability

Observability can be determined from the state and control matrices, A and c respectively. The number of unobservable states, N_{uo}, is determined as follows:

$$N_{uo}\mathrm{n} - \mathrm{rank}(Q_{cb}) \tag{4-5}$$

where length(A) is the number of rows in the state matrix and Q_{ob} is the observability matrix evaluated as shown in equation (2-25). The number of unobservable states is zero therefore the states are observable.

Since the system is stabilisable, controllable and observable, designing a controller for the system is feasible. The MPC controller has a number of tuneable parameters as listed in section 2.9. Determining these parameters requires that the plant response be expressed as a first order plus time delay model, FOPTD. The time-constant, open-loop gain and dead time can be determined from this model. The responses of control actions such as opening and closing the bypass valve as discussed in chapters 1 to 3 is similar to first order response. This means a FOPTD model is a good enough approximation. Parameters such as the time

constant, gain, and time delay can be easily obtained from the FOPTD model. These parameters are used in determining the MPC parameters. The transfer function model of the system was extracted from the state-space model. Furthermore, more transfer function models of the plant response can be found in Rubin and Pritchard, [**62**]. These will be used in obtaining a first order plus time delay model.

4.2.2 First order plus time delay (FOPTD)

Given a transfer function model of a system, Skogestad, [**64**], shows how to derive a first order plus time delay, FOPTD, and a second order plus time delay, SOPTD, approximation of the transfer function model. In the same paper it is ensured that the tuning rules are model based and analytically derived. This type of approximation is simple to derive and can be applied to a many different types of processes.

From the pole zero format, the model should be converted to the form,

$$\frac{\prod_j\left(-T_{j0}^{inv}+1\right)}{\prod_i(\tau_{i0}s+1)}e^{-\theta_s s}, \tag{4-6}$$

where τ_{i0} are sorted in decreasing order according to their magnitude. $T_{j0}^{inv} > 0$ denote the inverse response time constants.

$$T_{j0}^{inv} = -\tau_{j0}, \tag{4-7}$$

where τ_{j0} denotes the j^{th} numerator time constant. In order to obtain a FOPTD model,

$$G(s) = \frac{K_p e^{-\theta_p s}}{\tau s+1}, \tag{4-8}$$

the half rule is employed. According to the half rule, "the largest denominator time constant is distributed evenly to the effective delay and the smallest retained time constant. " This is mathematically realised as follows,

$$\begin{aligned} \tau &= \tau_{10} + \frac{\tau_{20}}{2}, \\ \theta_p &= \theta_0 + \frac{\tau_{20}}{2} + \sum_{i\geq 3}\tau_{i0} + \sum_j T_{j0}^{inv} + \frac{h}{2}., \end{aligned} \tag{4-9}$$

Second – order model parameters are approximated as follows,

$$\tau_1 = \tau_{10} + \frac{\tau_{20}}{2},$$

$$\tau_2 = \tau_{20} + \frac{\tau_{30}}{2}$$

$$\theta_p = \theta_0 + \frac{\tau_{20}}{2} + \sum_{i\geq 4} \tau_{i0} + \sum_j T_{j0}^{inv} + \frac{h}{2}. \tag{4-10}$$

For a model with positive numerator time constants, it is suggested to cancel the numerator term $(T_o s + 1)$ with a corresponding denominator term $(\tau_o s + 1)$, where τ_o is a positive. The following approximations are used:

$$\frac{T_0 s+1}{\tau_o s+1} \approx \begin{cases} \frac{T_0}{\tau_0} & \text{for } T_0 \geq \tau_0 \geq \theta_p \quad \text{(rule T1)} \\ \frac{T_0}{\theta} & \text{for } T_0 \geq \theta_p \geq \tau_0 \quad \text{(rule T1a)} \\ 1 & \text{for } \theta_p \geq T_0 \geq \tau_0 \quad \text{(rule T1b)} \\ \frac{T_0}{\tau_0} & f\text{or } \tau_0 \geq T_0 \geq 5\theta_p \quad \text{(rule T2)} \\ \frac{(\tilde{\tau}_0/\tau_o)}{(\tilde{\tau}_0-\tau_o)s+1} & \text{for } \tilde{\tau}_0 \overset{\text{def}}{\Rightarrow} \min(\tau_0\,, 5\theta_p\,) \quad \text{(rule T3)} \end{cases} \tag{4-11}$$

If there is two or more positive numerator time constants, elimination takes place one at a time and the parameters T_0, τ_o, θ_p are updated accordingly. Normally, the closest larger denominator time constant, τ_o, to T_0 is chosen and rules T2 and T3 in (4-11) are used. In the absence of a larger time constant, the closest smaller time constant can be used. Skogestad, gives the following guidelines in determining the *closest* smaller denominator when two smaller time constants τ_{oa} and $\tau_{ob}$are available for choosing. The time constant is chosen as $\tau_o = \tau_{ob}$(small) if

$$\frac{T_0}{\tau_{ob}} < \frac{\tau_{0a}}{T_0}, \tag{4-12}$$

and

$$\frac{T_0}{\tau_{ob}} < 1.6\,, \tag{4-13}$$

are both satisfied. However, Skogestad does not deal with complex roots [**64**]. On the other hand, Isakssson and Grebe show how to deal with complex conjugate pairs in polynomials [**65**]. When reducing to first order, if the dominant root is complex, only the real part is kept. If a dominant real root is followed by a complex part as shown below,

$$A(s) = (\tau_1 s + 1)\tau_2^2 s^2 + 2\zeta\tau_2^2 s + 1,\ \tau_1 > \tau_2\,, \tag{4-14}$$

The roots are chosen as follows,

$$\hat{A}(s) = \begin{cases} \tau_2^2 s^2 + 2\zeta\tau_2^2 s + 1 & \text{if } \tau_1 < \frac{\tau_2}{2\zeta}\,, \\ (\tau_1 s + 1)(\tau_2 s + 1) & \text{if } \tau_1 > \frac{\tau_2}{2\zeta}\,. \end{cases} \tag{4-15}$$

The methods in Skogestad above were applied to the transfer functions, $G_1(s)$ and $G_2(s)$. The FOPTD models obtained were as follows,

$$G_{1_{FOPTD}}(s) = \frac{(-5.31\times10^3)e^{-82.7s}}{(5.534\times10^{16}s + 1)} \approx \frac{(-5.31\times10^3)e^{-82.7s}}{s}, \tag{4-16}$$

$$G_{2_{FOPTD}}(s) = \frac{(5.75\times10^3)e^{-6.4s}}{(-5.534\times10^{16}s + 1)} \approx \frac{(-5.74\times10^3)e^{-6.4s}}{s}. \tag{4-17}$$

The FOPDT transfer function models in equations 4-16 and 4-17 were used together to approximate the whole plant. The three control mechanisms were applied to the FOPTD plant model. Unfortunately, the response obtained was far from that expected. The cause of this is that due to the high order of the system most of the system dynamics are lost in the reduction. The purpose of obtaining an FOPTD model is to obtain parameters which can be used to calculate MPC controller parameters. The time constant from the above models is very large and can be approximated as infinity. Therefore the gain, time constant and time delay obtained from the above models in equations 4-16 and 4-17 would yield unrealistic MPC controller parameters. This coupled with the bad system approximation means that the models derived from the zero pole gain format transfer functions, $G_1(s)$ and $G_2(s)$ cannot be reliably used to obtain MPC controller parameters which would ensure good system performance. Consequently, a different approach to obtain the FOPTD model of the plant is necessary. One such method is by fitting the system's response for each control mechanism with a single FOPTD model.

A similar approach to this was employed by Rubin and Pritchard for a three shaft Brayton-cycle based power plant. Below is a simplified model of the plant found in Rubin and Pritchard [**62**],

$$P(s) = \frac{-0.28(s-0.012)(s+0.677)}{s(s+0.0969)(s+0.953)} \tag{4-18}$$

This function can be rewritten as,

$$P(s) = \frac{-0.28(-83.3s_1)(1.477s+1)}{s(10.32s+1)(1.049s+1)}. \tag{4-19}$$

Using the methods in Skogestad and Isakssson would yield a system with only a pole at the origin as shown,

$$P(s) = \frac{-0.28\mathrm{e}^{-83.31s}}{s}. \tag{4-20}$$

The time constant cannot be determined. It is infinite and therefore cannot be used in the tuning process.

Deciding on a response which would result in a useful FOPTD model is rather intuitive. Three responses that can give insight into the time constant of the system are helium injection and extraction for a fixed period and helium bypass. These three responses result in adding or subtracting a fixed amount of helium from the system. Once there is no further change In the amount of helium in the circuit, the power output settles to a fixed value. Adding or subtracting a fixed amount of helium to the system can be compared to a step increase or decrease in the amount of helium. The responses mentioned in earlier sections for helium injection and extraction are different as shown in Figure 3-11 and Figure 3-14. Helium is injected (extracted) continuously for the whole time period considered. In terms of the amount of helium in the system, continuous injection is equivalent to a ramp increase (decrease) which results in a continuous increase (decrease) in the power delivered to the load. It is not possible to capture the time constant of the system from an ever increasing (decreasing) amount of helium. Only step changes in helium amounts can be used to determine the time constant dominant in the system. The bypass mechanism was also used because it is equivalent to a step decrease in the helium amount in the system. From these responses the time constants can be computed. When helium injection, extraction and bypass mechanisms are implemented on the system as described, the following is obtained:

Helium injection

Helium was injected for a period of 1second at a rate of 1kg/s. The response is shown below.

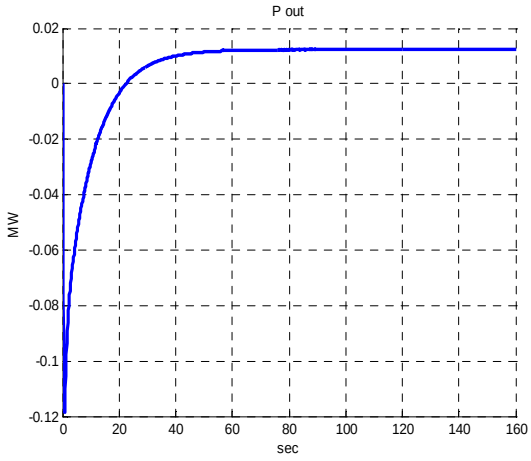

Figure 4-4 Helium injection for one second at 1kg/s

The minimum phase effect is apparent in this response. This is a result of the positive zero or right hand plane zero at 39.098 on the real axis. This is illustrated in Figure 4-3 and

section A.5 in the appendix. The output power level drops for about 0.12 MW before it starts rising again. Power only increases beyond the operating point (0 MW) after 23.16 seconds. The original model has got two transfer functions corresponding to control mechanisms at the low and high pressure points respectively. However, a input single output model, and therefore a single transfer function, can be used to approximate the response of a multi input single output model as shown in Rubin and Pritchard, [**62**]. In this study the FOPDT model was obtained via trial and error. Firstly, the input value was set to a positive value since helium was being added to the system. From observation the time it takes for the response to become positive after the initial drop is 23.16s. This value is used in determining the dead-time, θ_p. The time-constant and gain are determined from the positive portion of the response. An FOPDT model was fitted to this portion of the response as shown in Figure 4-3.

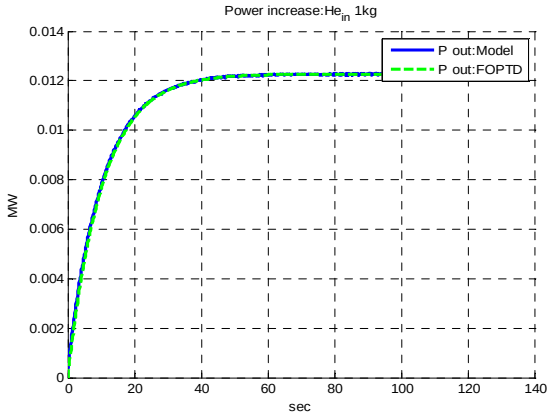

Figure 4-5 FOPDT model of helium injection response for 1s

The FOPTD model for the above response is,

$$G(s) = \frac{12.277\times10^{-3}e^{-0.0006s}}{(10.31s+1)} \tag{4-21}$$

The minimum phase effect takes 23.16 seconds. In the FOPTD model, a minimum phase effect is modeled as a time delay. Adding the 23.16 seconds initially observed to the time delay 0.006 seconds in (4-22) gives the total dead-time, $\theta_p = 23.1606\,s$. Therefore, the overall response for helium injection as,

$$G(s) = \frac{12.277\times10^{-3}e^{-23.1606s}}{(10.31s+1)} \quad . \tag{4-22}$$

The mean squared error for the full response was 0.0124 MW. The average squared error per instant of time was 9.738×10^{-5} MW. The same procedure was followed for helium extraction.

Helium extraction

Helium was extracted for one second at a rate of 1kg/s. The system responded as follows:

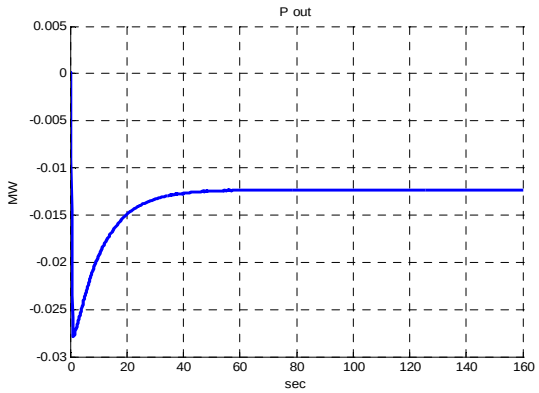

Figure 4-6 The response of helium extraction for 1s

It should be noted that power level is dependent on the amount of helium flowing in the system but is also affected by pressure levels which are altered during injection and extraction. It can be observed in section A.5 in the appendix and marginally in Figure 4-2 that there is a right hand zero in the extracted model at 0.0121 on the real axis. This is the cause of the minimum phase effect observed in the response in Figure 4-6. The time constant for the above response can be estimated by shifting the response upwards and fitting the resulting model with an FOPTD model as shown in Figure 4-7. An input of value -1 was chosen to signify helium extraction and applied to the FOPDT model,

$$G(s) = \frac{15.6\times10^{-3}e^{-1.6s}}{(10.31s+1)}. \tag{4-23}$$

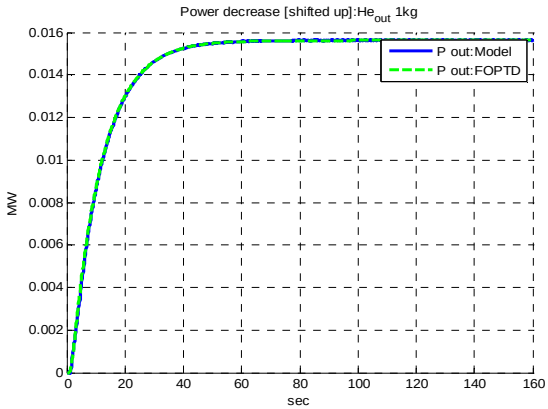

Figure 4-7 An FOPDT model of the shifted extraction response

For the above FOPTD model approximation of the system response, the mean squared error for the full response was 5.14×10^{-9} MW and the average squared error per instant in

time is 4.05×10^{-11}MW. The value for gain was $k_p = 15.6 \times 10^{-3}$. From the system response shown in Figure 4-4, the gain should be $k_p = 12.3 \times 10^{-3}$. The output power is expressed in Mega-watts.

Helium bypass

In helium injection and extraction, only a very small amount of helium was added or removed from the helium circuit. Bypassing helium flowing at a rate of 1kg/s may however result in more helium being bypassed than the amounts observed during helium injection and extraction. How much helium is bypassed depends on the flow-rate and the length of the bypass channel. The only variable known is the mass flow-rate. It will therefore be assumed that the effect of the channel is negligible. Helium bypass is modelled by injecting and extracting equal amounts of helium in the low and high pressure sides respectively. For the FOPTD model approximation of the bypass response, an input control signal of -1kg/s was used. The negative sign was chosen since helium bypass results in lesser helium flowing in the turbines.

$$G(s) = \frac{2.632\times10^{6}e^{-0.0060285s}}{(10.31s+1)} \tag{4-24}$$

For the above FOPTD model approximation of the system response, the mean squared error for the full response was 3.68×10^{-10} MW and the average squared error per instant in time is 2.91×10^{-13}MW. Figure 4-6 shows how the FOPTD model response compares with the actual model response when helium bypass occurs.

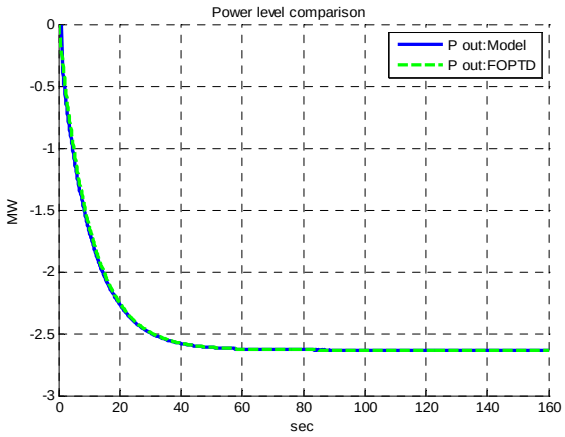

Figure 4-8 An FOPDT model for the response of helium bypass

From the system response shown in Figure 4-6, the gain should be $k_p = 2.63$ when the power is expressed in Mega-watts. Furthermore, the value for K_p for helium bypass clearly shows that the assumption that the bypass channel length has negligible effect on the amount of helium taken from the system is not good enough. The amount of helium removed from the system during bypass is much greater than the amount during helium extraction. As a result power drops by 2.63 MW as compared to 0.012 MW during helium extraction.

4.3 Model predictive controller design

4.3.1 Tuning parameters

The FOPTD models in the previous section (see equations 4-22, 4-23 and 4-24) in are used to compute the values for the tuning parameters which can be used by the MPC controller. The values obtained are the scope of parameters that can be used. The designer must then proceed to choose the best set of parameters. Details about these formulas used are found in section 2.9. There were different values of *R* obtained. This is due to the different values for the gain, k_p. Table 4-1 shows how the FOPTD model parameters k_p, τ and θ_p for helium injection shown in equation 4-21 were used to obtain MPC controller parameters.

The same procedure was used to obtain controller values from the helium extraction and bypass FOPTD models in equations 4-23 and 4-24 respectively. The value for the time constant for helium extraction and bypass was 10.31 seconds. The time constant and time delay, fix the sampling time and settling time. Sampling time is chosen as the interval between $min(0.1\tau, 0.5\theta_p)$ and $0.4t_r$. Due to the smaller inverse response times during helium extraction and its absence during the bypass mechanism, the lower bound of the interval differs. The smallest sampling value was found from the helium extraction FOPTD model approximation which also records the largest move suppression value, R. The smallest move suppression interval is during helium injection.

In general, parameter values obtained from the model approximations for the three control mechanism's responses are different. However, the results obtained can be used to determine which values to consider during MPC controller parameter selection. Table 4-2 is a summary of the results from the three mechanisms.

Table 4-1 Calculating MPC tuning parameters for helium injection

Parameter	Range	Actual value of range
Sampling Time (Ts)	$min(0.1\tau, 0.5\theta_p) \leq T \leq 0.4t_r$. $\tau = 10.31\ s$ $0.1\tau = 1.031 \approx 1$ $\theta_p = 23.16\ s$, therefore $0.5\theta_p = 11.58\ s$. $t_r = 22.66$ therefore, $0.4t_r = 9.064\ s \approx 9\ or\ 10$.	$1 \leq T \leq 9$ $\theta_p = 23.16\ s$
Prediction Horizon (P)	Horizon $0 \leq \begin{Bmatrix}\theta_p \\ \theta_{inv}\end{Bmatrix} \leq P_0 < \tau \leq P \leq t_s + \theta_p$ $t_s + \theta_p = 5\tau + \theta_p = 51.55 + 23.16 = 74.71\ s$ $23.16\ s \leq P_0 < P \leq 74.71$	$24\ s \leq P_0 < P \leq 74\ s$
Control Horizon (M)	$RHP\ zeros < \frac{1}{6}P_{min} \leq M \leq \frac{1}{3}P_{max}$. $RHP\ zeros = 1$ $1 < 3.86 \leq M \leq 24.9$	$4\ s \leq M \leq 24\ s$
Output Weight (Q)	$Q = C^T C$	1
Move Suppression (R)	$R = \frac{M}{10}\left(\frac{3.5\tau}{T} + 2 - \frac{(M-1)}{2}\right)K_P^2$ $K_p = 12.277 \times 10^{-3}$ $R_{min} \geq R \geq R_{max}$ $R_{min} = \frac{M_{min}}{10}\left(\frac{3.5\tau_{min}}{T_{max}} + 2 - \frac{(M_{max}-1)}{2}\right)K_P^2$ $R_{min} = -0.02808$ $R_{max} = \frac{M_{max}}{10}\left(\frac{3.5\tau_{max}}{T_{min}} + 2 - \frac{(M_{min}-1)}{2}\right)K_P^2$ $R_{max} = 1.11597$	From $R_{min} \geq R \geq R_{max}$, $-0.02808 \geq R \geq 1.11597$. The value of *R* in should be greater than zero therefore, $0 \geq R \geq 1.11597$.

In Table 4-2 the first row indicates the control mechanism and the “Min” and “Max” labels in the second row directly below a control mechanism name represent the minimum and maximum values for corresponding parameters listed in the first column.

Table 4-2 MPC parameter values for injection, extraction and bypass

	LP helium Injection		HP helium extraction		Helium Bypass	
Parameter	**Min**	**Max**	**Min**	**Max**	**Min**	**Max**
T [s]	1	9	0.8	9	0.003	9
τ [s]	10.31	10.31	10.31	10.31	10.31	10.31
P [s]	24	74	1.6	56.15	0.006	51.56
M [s]	4	24	0.267	18.7167	0.001	8.5933
R	0	1.116	0	4.011	0	8.1621×10^4
Q	1	1	1	1	1	1

The basic notation which is used in expressing the chosen values is as follows. X stands for an MPC parameter value listed in Table 4-2 during low pressure helium injection. X_{final} is the final range of values after considering all control mechanisms. X_{inject} is the set of all values in the set $\{X_{min} \dots X_{max}\}$ during low pressure injection. X_{min} and X_{max} are the minimum and maximum values of the parameter X listed in Table 4-2 under columns "Min" and "Max" respectively for helium injection. The same is true for other control mechanisms. $X_{extract}$ and X_{bypass} represent the range of X during high pressure extraction and bypass mechanisms. An empirical approach was preferred in this design. The final range of parameters is chosen as follows:

For the sampling time, the minimum range of sampling times is chosen. This is because the sampling time should be small enough to visibly capture all the system dynamics.

$$T_{final} = min\big(T_{inject}, T_{extract}, T_{bypass}\big). \tag{4-25}$$

Therefore, $T_{final} = \{0.003 \dots 9\}$. Ideally, an infinite prediction horizon should be used to guarantee stability but is not practically feasible [**21**], [**32**], [**58**]. Since P must be as large as possible,

$$P_{final} = max\big(P_{inject}, P_{extract}, P_{bypass}\big), \tag{4-26}$$

hence $P_{final} = \{24 \dots 74\}$. Control horizon, M, is a fraction of the prediction horizon, P. Therefore, it was chosen as,

$$M = max\big(M_{inject}, M_{extract}, M_{bypass}\big), \tag{4-27}$$

meaning $M_{final} = \{4 \dots 24\}$. The criterion used to choose the final value for move suppression weight range, R_{final} was by selecting values common to all three mechanisms. In other words,

$$R_{final} = R_{inject} \cap R_{extract} \cap R_{bypass}, \tag{4-28}$$

hence $R_{final} = \{0 \dots 1.116\}$. Table 4-3 shows a complete list of the values chosen. The ranges in this table will be used to select the best parameter values. Knowledge on how each parameter affects the system performance can be used to determine the best values for the controller.

Table 4-3 Tuning parameters

Parameter	Min	Max
Control horizon , M [s]	4	24
Sampling time , Ts	0.003	9
Prediction horizon, P [s]	24	73
Input weight, R	0	1.116

Note: Prediction and control horizons above are expressed in seconds. The horizons in terms of the number of future values are found by dividing the horizon (defined by a unit of time e.g. seconds, [s]) by the sampling time, T. The resulting horizon is unit-less. For the sake of simplicity, horizons will be defined in terms of time and not as the number of samples in the later sections.

4.3.2 Tuning parameter behaviour

The effect of each controller parameter on the performance of the plant is analysed in this section. The evaluation platform was in Simulink® and the MPC design tool was used in conjunction with an m-file to design the controller. Gains were kept at default values (see appendix A.6) [**63**]. The MPC design tool incorporates the extracted state-space model and uses it in computing future control moves required for the output to follow the reference trajectory.

Constraints and rate weights were also added to the controller. The constraints are chosen so as to resemble real systems. In this case, constraints were applied to the actuators being controlled by the controller. A limit was placed on the mass flow-rate. The signs used show the direction of flow. Rate weights determine how fast change can take place. For example, mass flow-rate cannot instantaneously rise from 0kg/s to 2kg/s. There is a finite period greater than zero seconds through which this takes place. The rate weight represents the rate of change in the flow. The rate weights were determined by observing previous results responses found in [**2**].

$$rate\ weight = \frac{mass\ flow}{time} \tag{4-29}$$

Table 4-4 MPC controller constraints and rates

	LP min (Kg/s)	LP max (Kg/s)	HP min (Kg/s)	HP max (Kg/s)
Constraint	-2.5	2.5	-2.5	2.5
Move rate	-0.57(down rate)	0.95 (up rate)	-0.4 (down rate)	0.6375 (up rate)

Table 4-5 MPC controller move rate weights

Low pressure actuator		High pressure actuator	
down rate	**up rate**	**down rate**	**up rate**
-0.57	0.95	-0.4	0.6375 (up rate)

The low pressure actuator is connected between the pre-cooler and the low pressure compressor. The high pressure actuator is connected after the high pressure compressor. The extracted model is a continuous time model. However, the MPC toolbox automatically converts it to a discrete time model. Figure 4-6 shows the Simulink® implementation. In the figure, the MPC controller block uses an already designed controller. The controller is specified in the controller block's dialog box (See appendix A.6).

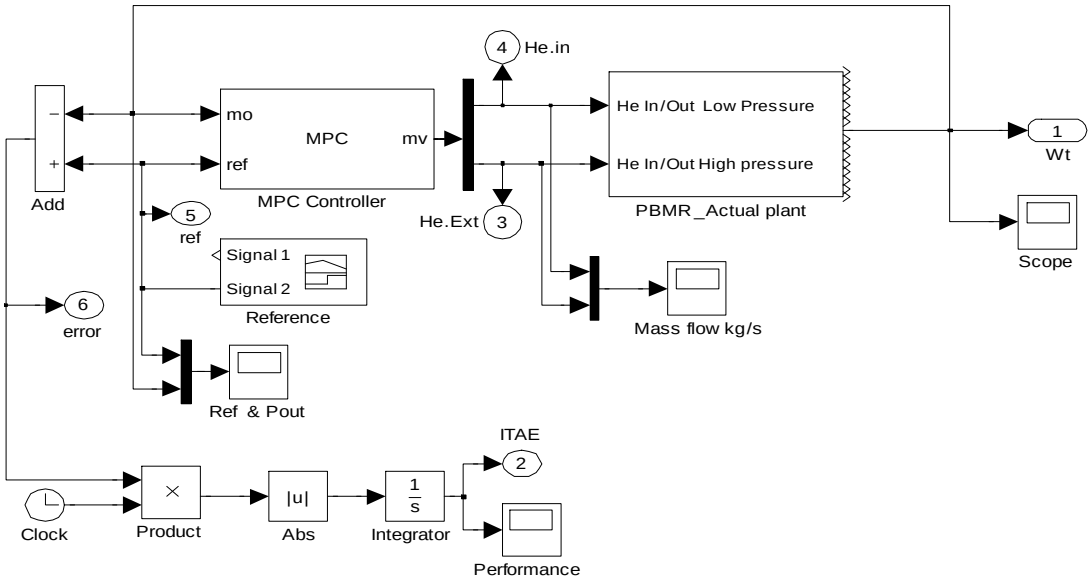

Figure 4-6 Simulink diagram of MPC control system

4.3.3 Simulations

Performance and tuning parameters

Effect of MPC controller parameter values on the performance is analysed in this section. The values which were sampled for analysis for each of the parameters are given in Table 4-6. Some values outside those specified in the table were included for comparison purposes. A prediction horizon, $P = 20\ s$, and a control horizon of $M = 2\ s$ were included. In order to avoid the case of the MPC controller reducing to a minimum variance controller which is unstable on non-minimum phase processes when $M = P = 20\ s$, the maximum control horizon was chosen to be $M = 19\ s$, [**59**]. A very small sampling time would increases the computational demands of the controller. To speed up the computations, the minimum sampling time used was 0.1 seconds as opposed to 0.003 seconds. Values of *R* used are limited to the range $\{0 \dots 0.015\}$. This range proves sufficient enough to capture the general behaviour or effect of *R*. The intervals between the values used for each parameter is large. This is because the aim of the analysis is simply to observe the general behaviour of the performance as the MPC parameters are varied. This was deemed sufficient for the design since such an understanding would influence the criterion used in determining the best choice of tuning parameter values. Consequently the number of simulation scenarios is only 810. In each simulation scenario a different set of MPC controller parameter variables are used.

Table 4-6 Tuning values used in analysis.

Tuning parameter	Values used
Sampling time, Ts (s)	0.1, 1, 3, 6, 9
Control horizon, M (s)	2, 4, 9, 14, 19,
Prediction Horizon, P (s)	20, 24, 35, 45, 60, 73
Input or manipulated variable weight , R	0 0.003, 0.006, 0.009, 0.01312, 0.015

The performance measure used is the $ITAE$ performance index as given by (4-30)

$$ITAE = \int_0^T t|e(t)|dt \tag{4-30}$$

where T is the total simulation period and $e(t)$ is the power error at time step t. It was decided to normalise the power error because the power error can have a very large number. Equation (4-23) then becomes the following:

$$ITAE = \int_0^T t \left| \frac{e(t)}{1\times10^8} \right| dt \tag{4-31}$$

Simulations of the system in Figure 4-6 for each scenario are carried out. The performance for each control scenario is measured and used for comparison purposes. The lower the value of the $ITAE$ performance index the better the performance [**2**]. It must be noted that the $ITAE$ index would be lower for more robust systems which tends to have slower response but excellent disturbance rejection capabilities. Performance in this case is more a measure of load following capabilities of the system and not a measure of all system performance characteristics.

As mentioned earlier, understanding the effect of each MPC controller parameter on the performance of the system helps the designer to intuitively choose which values to use. The choice would depend on the desired performance, characteristics, computational constraints, and limitations posed by the hardware implementation of the system. The impact that a particular parameter has on performance can be monitored by seeing how performance changes as the variable of interest is varied while other parameters are held constant. Figures 4-7 to 4-11 visibly depict this phenomenon as follows:

Variation of the performance of the system when the control horizon is varied at fixed values of the prediction horizon, P, and move weight, R.

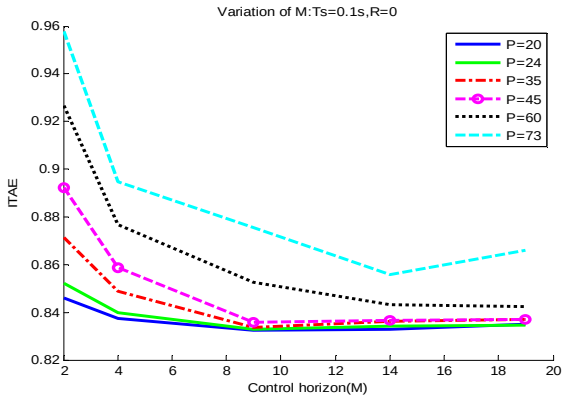

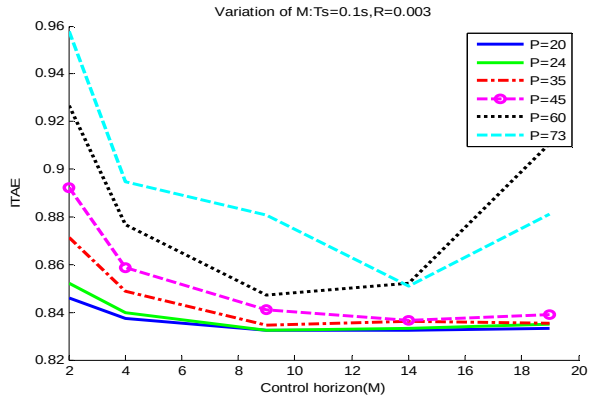

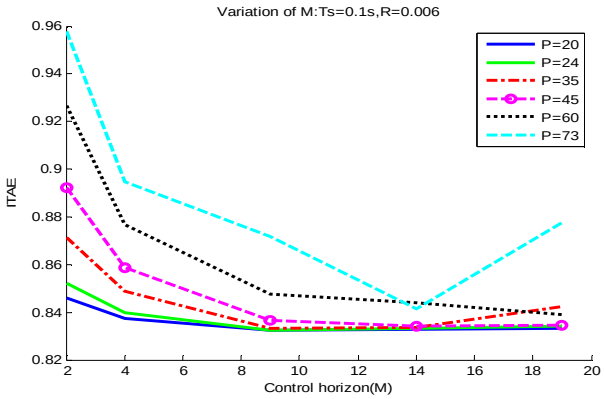

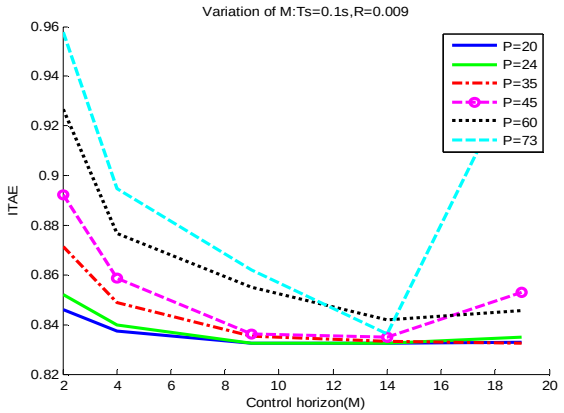

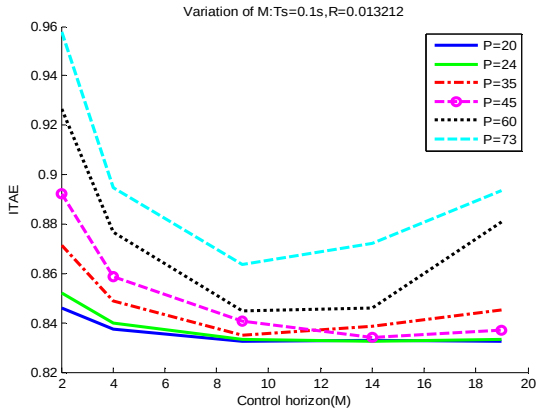

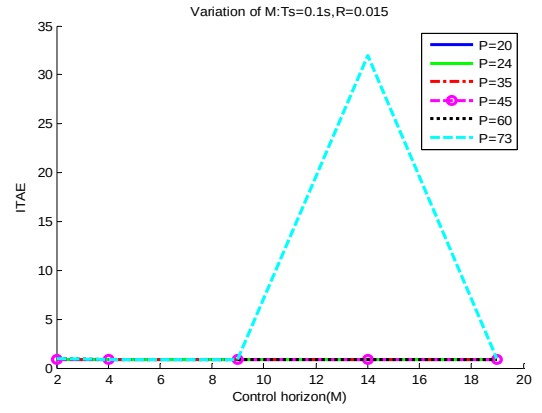

Figure 4-7 Effect of changing the control horizon on the performance

A step increase in load is applied to the system for all the simulations from Figure 4-7 to Figure 4-11.

Figure 4-7 above shows the performance of the plant when the control horizon is varied. The controller has sampling time 0.1s and this performance is monitored while keeping the value of the manipulated variable weight, R, constant. There are six graphs in the figure showing the performance at the different values of R. The size of the prediction horizon, P, is kept constant while M is varied.

Generally for a fixed R and P the $ITAE$ value decreases as M increases. When the value of P is large the ITAE performance value is also high, signifying poorer performance. This trend is however not consistent as can be seen in the 1st row 2nd column where the $ITAE$ value for $P = 60$ is greater than that of $P = 73\ s$ for $M = 19\ s$. As an R increases the performance index tends to increase slightly after $M = 10\ s$. In the 2nd row and 3rd column of Figure 4-7, for $P = 73\ s$ the performance at $M = 14\ s$ deteriorates sharply. The closed loop system at this time contains an unstable pole. This could be one of the reasons to the sharp deterioration in performance.

The difference in performance become less apparent as the control horizon is increased and this becomes more pronounced after $M = 9\ s$. After this value of M, the performance index is nearly horizontal. This means that after $M = 9$ increasing the control horizon has little effect on the performance of the system. However, this observation does not hold for $P \geq 60\ s$.

The performance index for $P = 20\ s$ and $P = 24\ s$, after $M = 4\ s$ is almost equal. At these control values the controller performance is the best. It appears that, a small prediction horizon results in more aggressive control action and is therefore faster when compared to MPC controllers with larger prediction horizons, [**59**].

Figure 4-8 below shows the performance of the controller when the prediction horizon is varied. When $R = 0\ s$ and $M = 2\ s$ the performance decreases (value increases) as the prediction horizon increases. However, for $M = 4\ s$ to $M = 19\ s$ the performance deteriorates ($ITAE$ value increases) for a while before it begins to improve ($ITAE$ value decreases). The performance then settles at about $ITAE = 0.84$ for all values of M.

The variation in performance for each value of M is like a series of triangular waves moving towards the right as R is increased. When $R = 0\ s$ and $R = 0.015\ s$ the graphs are similar. The "triangular wave" appears to have moved full circle from $R = 0\ s$ to $R = 0.015\ s$. It can be concluded that performance does not remain constant but consists of rises and falls, periodically being shifted to the right as the input weight increases. The magnitude of the peaks generally decreases as M is increased.

Variation of the performance of the system when the prediction horizon, P, is varied at fixed values of the control horizon, M, and move weight, R.

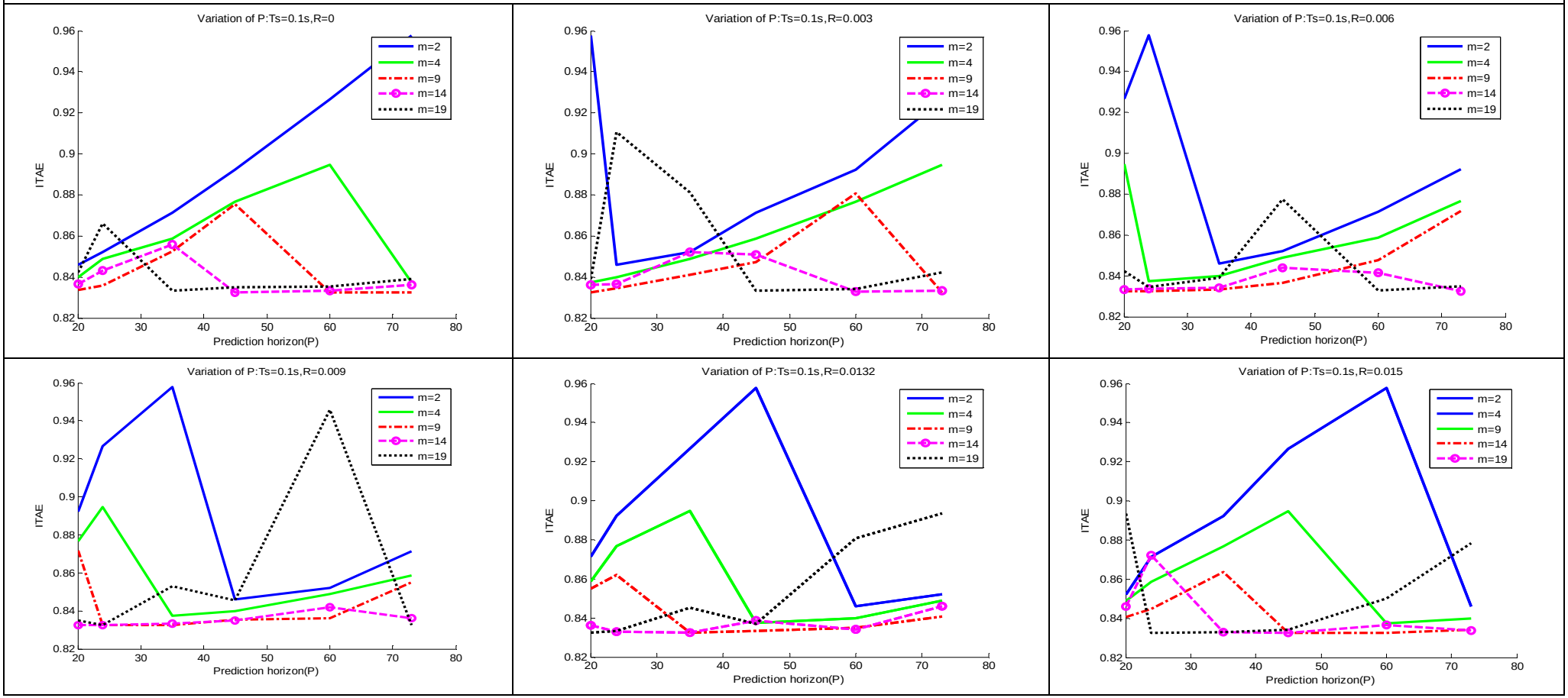

Figure 4-8 Effect of changing the prediction horizon on performance

Variation of the performance of the system when the sampling time, T, is varied at fixed values of the control horizon, M, prediction horizon, P, and move weight, R.

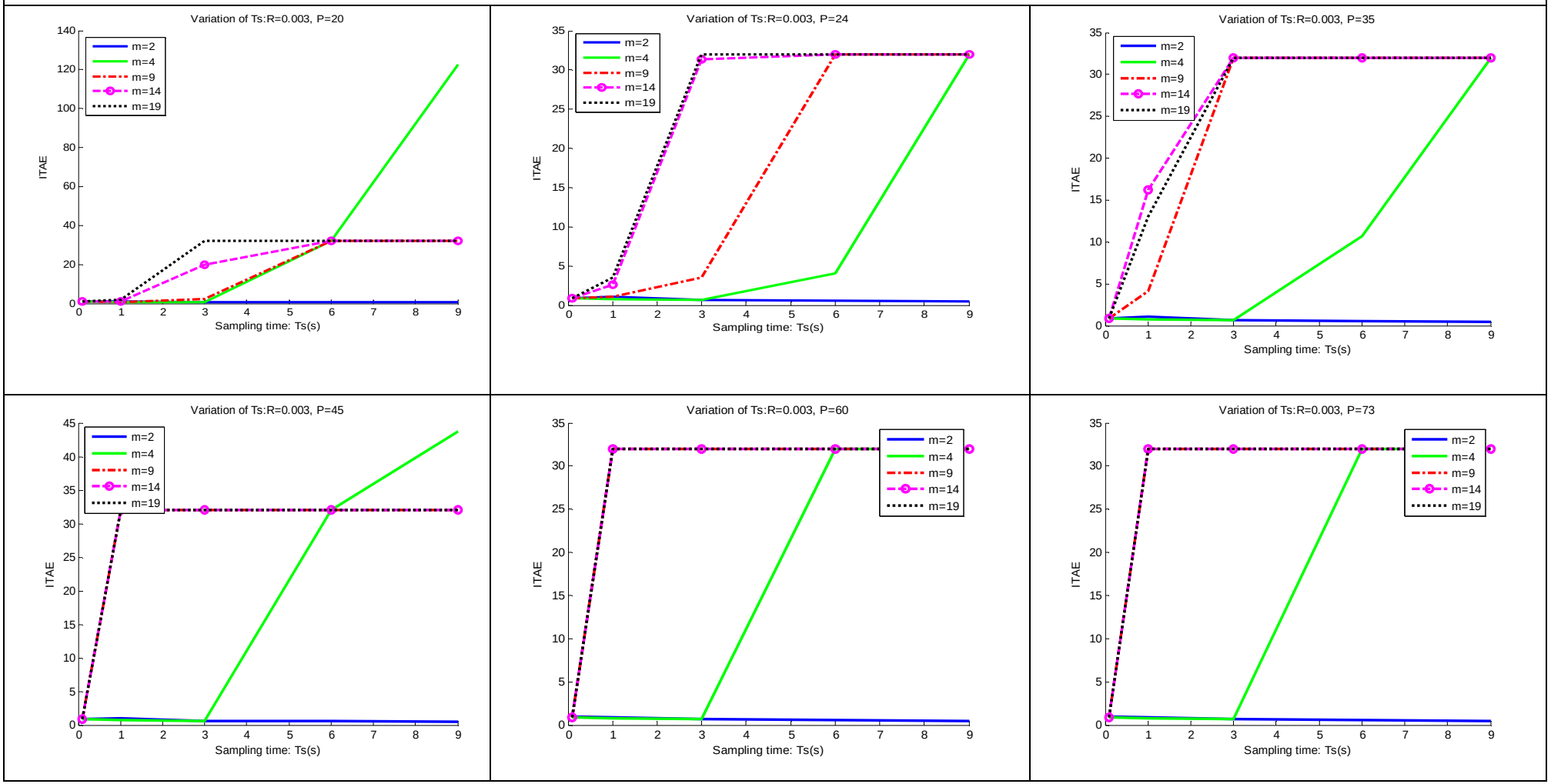

Figure 4-9 Effect of changing the Sampling time on performance

Figure 4-9 shows the performance when the sampling time is varied for different control horizons. Except for $M = 2\ s$, the $ITAE$ value rises between $T = 1\ s$ and $T = 3\ s$ for all the six prediction horizon values. This indicates deteriorating performance when $T > 1\ s$. As P increases, the $ITAE$ values for $M = 9\ s\ , 14\ s$, and $19\ s$, start rising much earlier i.e. at $T = 0.1\ s$. This trend continues until there is no visible change in performance from $P = 60\ s$ to $P = 73\ s$. The rising $ITAE$ values are due to the increased control horizon. Large control horizons result in less aggressive control actions which tend to more robust and stable overall performance of the system. Unfortunately, a slow response scores low on the $ITAE$ performance index. It has a high value $ITAE$ value as evidenced in all the diagrams in Figure 4-9.

For all prediction horizon values considered, the performance at $M = 2\ s$ and $M = 4\ s$ remains the same up to $T = 3\ s$. From then on, the $ITAE$ index values for $M = 4\ s$ increase and at $P = 20\ s$ and $P = 45\ s$ when $T = 6\ s$, the performance index value rises even higher. A low $ITAE$ value can be observed when $T \leq 3\ s$ for $M = 2\ s$ and $M = 4\ s$ at any value of P. An interesting observation is that for $M = 2\ s$ the graphs show little change in performance with a varying sampling time. However, numeric data does indicate varying performance for different values of T.

What can be deduced from this is that performance deteriorates then T is increased and the best or faster performance is obtained when $M \leq 4\ s$. It is recommended that the sampling time should be kept less than or equal to $3\ s$. For small values of M, the system response to changes is fastest and has less computational time. This is also reiterated in [**14**]. In [**63**] small control horizons are encouraged. It should be noted however that a very small sampling time is counterproductive when considering computational time. On the other hand a large sampling time means changes in load demands, implemented via the reference power, causes the system to recognise changes late causing a slower response.

Figure 4-10 shows how performance of the controller varies with a changing value of R. For $M > 4$ at $P \geq 45\ s$ the $ITAE$ valuee remains constant while for $P < 45\ s$ performance varies, for $\forall R$. When $M = 2\ s$, the best recorded performance is for $P = 73\ s$ and the worst is for $P = 24\ s$. However, performance for low values of $P\ (20{,}24)$ is better than that of higher values of $P\ (60{,}73)$ when $M \geq 4\ s$. The best performance $\forall P$ is when $M = 4\ s$ with the lowest $ITAE$ values at at $P = 20\ s$, $P = 24\ s$. and $P = 73\ s$. $ITAE$ values

increase or decrease with M from $M = 4\ s$ resulting in the worst or slowest performance $\forall P$ when $M = 19\ s$, as R is varied. When $P = 20\ s$ and $24\ s$ the plant retains the lowest $ITAE$ values for $M = \{4\ s, 9\ s, 14\ s, 19\ s\}$ over the entire range of R.

The results show that the move suppression weight has more impact on the performance of for small prediction horizons e.g. when $P = \{20\ s\ , 24\ s, 35\ s\}$. Its effect is to reduce aggressiveness of control actions and therefore has the same effect as changing the control horizon as reiterated in [**63**].

Variation of the performance of the system when the move weight, R, is varied at fixed values of the prediction horizon, P at different values of control horizon, M

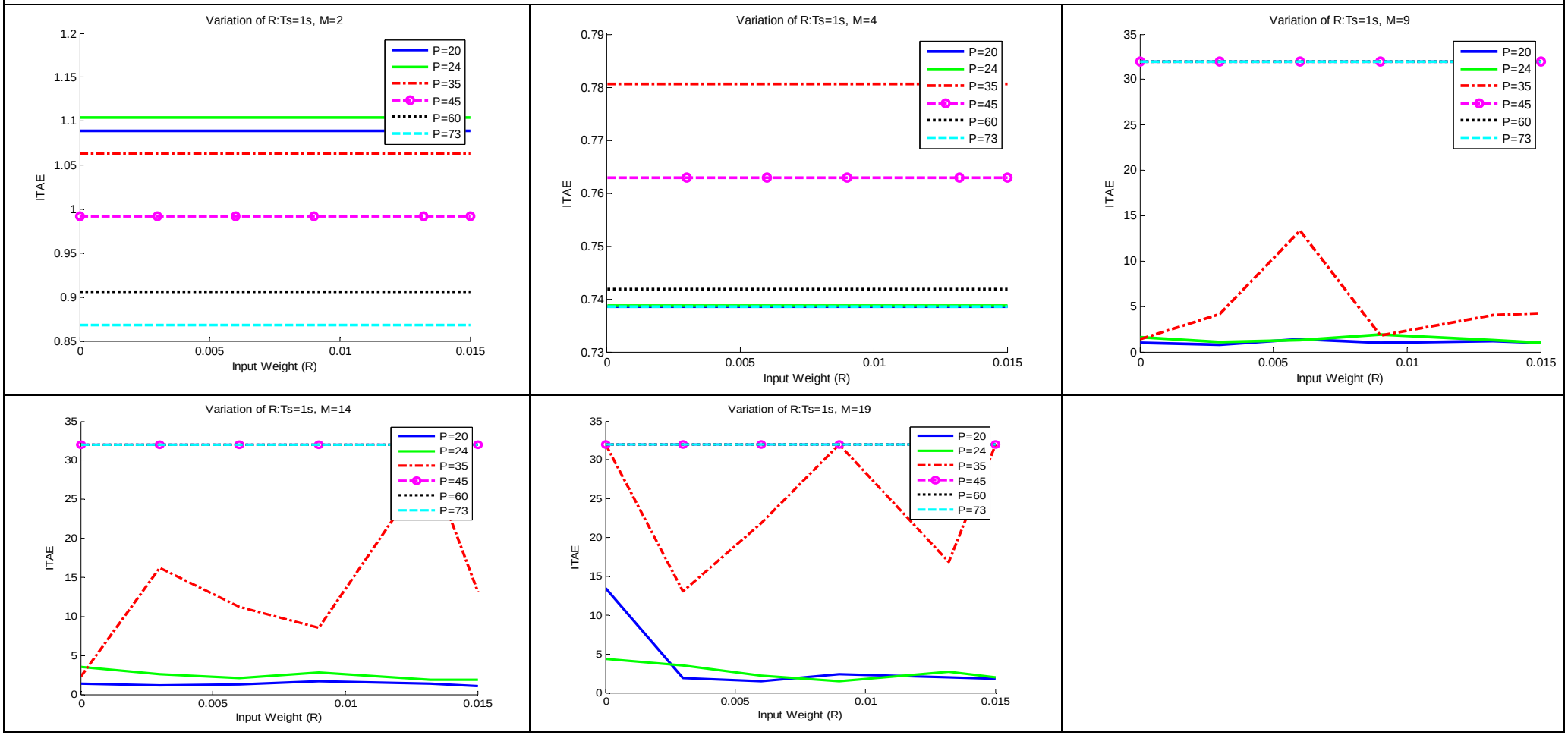

Figure 4-10 Effect of changing R on performance at a fixed P

Variation of the performance of the system when the move weight, R, is varied at fixed values of the control horizon, M, and different values prediction horizon, P.

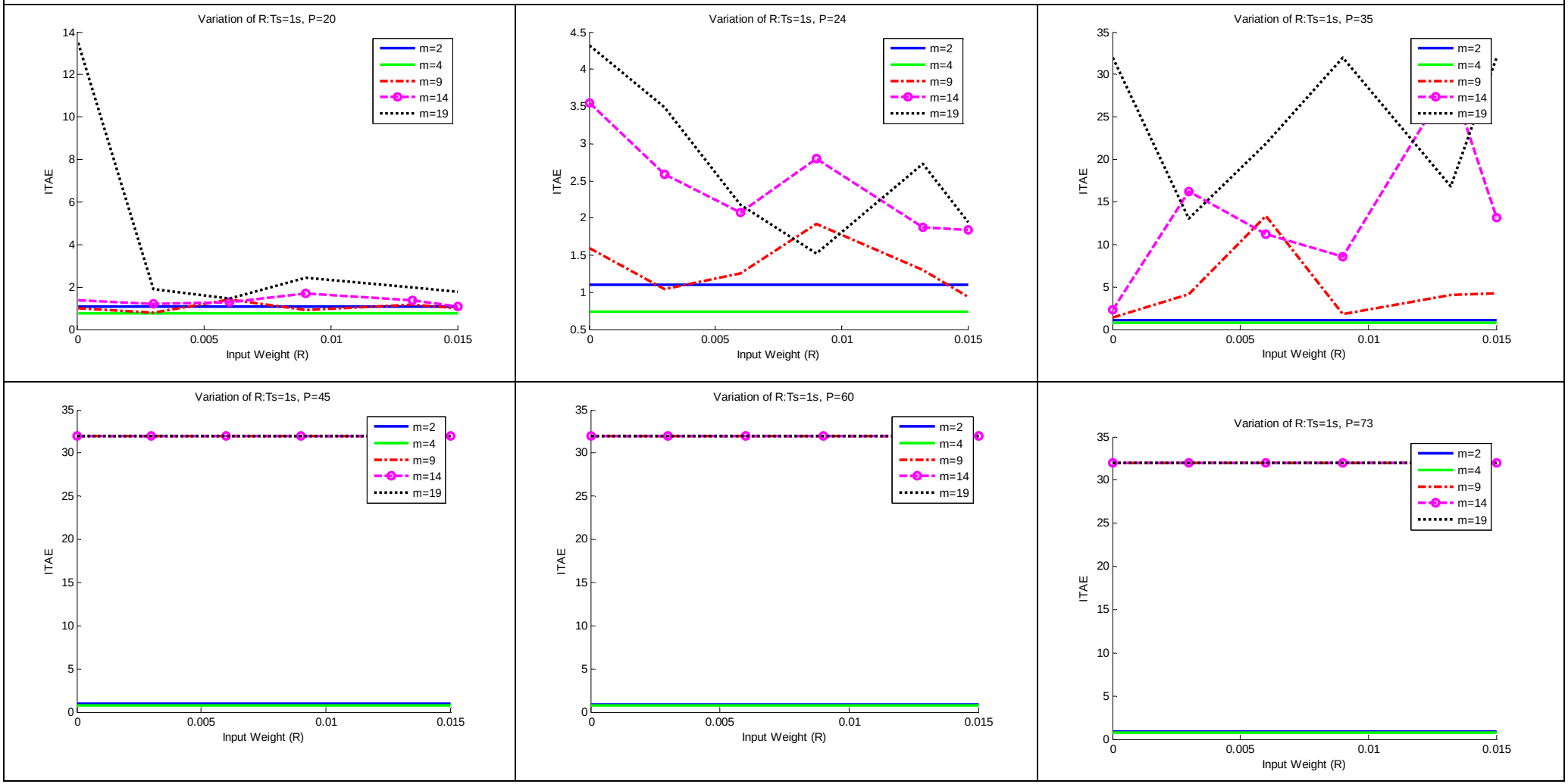

Figure 4-11 Effect of changing R, on the performance at a fixed M

Figure 4-11 also shows the performance of the controller when R is varied. This figure is just a different view of what is observed in Figure 4-10. The data used was the same. For $P < 45\ s$ and $M > 4\ s$ the ITAE index changes as R is varied. However, when $= \{2\ s, 4\ s\}$, the rate weight R has no effect on the performance. For $\forall P \geq 45\ s$ it can again be seen that R has no impact and performance is only dependent on the value of the control horizon, M. The lowest $ITAE$ index values are when $M = 2\ s$ and $M = 4\ s$. The results show that the move suppression weight has negligible impact when the control horizon is small e.g. $2\ s$ and $4\ s$. When M is between $4\ s$ and $14\ s$ the value of R affects the performance. However, its effect appears to be nonlinear. $ITAE$ values are generally higher for large control horizons. Hence it can be said that the performance deteriorates with an increase in M.

From the results, the effect of R is to reduce aggressiveness of control actions and therefore has the same effect as changing the control horizon as reiterated in [**63**]. However, in the case where M is small enough i.e. $M = \{2\ s, 4\ s\}$ the influence of R appears to be negated by the aggressiveness of the small control horizon. In effect, it can be said that the two effects cancel each other out. The same can be said of large prediction horizons, i.e. $P \geq 45\ s$, the effect of R is negligible.

Stability and tuning parameters

The choice of tuning parameters is important in that it affects the stability of the plant. The closed loop eigenvalues given in (2-52) can be used to determine the stability of the system. The controller feedback gain K_{mpc} has an effect on the system poles and consequently on the stability of the system. In (2-52) the eigenvalues of the plant are given as,

$$det\left[\lambda I - \left(A - BK_{mpc}\right)\right] = 0. \tag{4-32}$$

The future outputs are computed in (2-37) as, $= Fx(k_i) + \phi\Delta U$. The optimisation function minimises future control moves and the controller gain is computed from (2-49) as,

$$K_{mpc} = [1\ 0\ 0\ \ldots 0](\phi^T\phi + \bar{R})^{-1}\phi^T F. \tag{4-33}$$

The structure of the matrices ϕ and F is dependant on the prediction and control horizon. Furthermore, It can be seen from (2-40) that $\bar{R}$ is the weight on the control moves. Equation (4-33) shows the controller gain to be dependent on $\phi, \bar{R}$ and . These two parameters are

defined in terms of state space matrices, the prediction horizon, control horizon and weights on the control moves as shown in equation (2-38). However, the relationship is rather complex and even made to be more unpredictable when constraints are included and active. When constraints are active, the system becomes non-linear. There is no discernable pattern in what would cause the system to be unstable. A step reference signal was chosen and the controller was applied to the plant. Controller parameters were varied and performance of the system as well as the position of system poles determined. It was found that certain control parameter values cause an unstable system pole. This was found to be controllable in some cases while in others the system was uncontrollable. In such cases, the plant was not able to follow the reference trajectory. It is therefore important that the choice of MPC parameters be carried out carefully.

4.3.4 Choice of MPC tuning parameters

Due to the variation in the performance when different trajectories of desired or reference power are used, more than one reference power trajectory is needed. A set of six different trajectories are used on the system and the performance of each set of MPC parameters for a particular reference power trajectory is determined (See appendix A.8 for the reference signals used). This is in order to capture the advantages and disadvantages of each set of MPC tuning parameters. The ITAE values are then summed up. In Table 4-2, the sum is in the last column. The performance measures for each reference signal are labelled as ITAE1 to ITAE6 in Table 4-7. The results are then sorted in order of decreasing ITAE value. The first column indicates the position of a particular parameter set in terms of performance. For example, No 2 means the set of parameters in row number two produced the second best performance.

The set of parameters that was chosen was No 7, see Table 4-7. This is the seventh best performance. The best performance was in row number 1. Nevertheless, according to Trierweiler [**59**] and Wang [**32**], the prediction horizon should be greater than the inverse response time. This is also reiterated in the Release notes for Matlab® which is the implementation software [**63**]. Due to the fact that the inverse response after a unit low pressure injection for one second at a rate of 1kg/s when $T = 1\ s$ is 23.16 seconds, the prediction horizon, $P = 24\ s$ is preferred over $P = 20\ s$. Therefore, the set of parameters

with the best performance at this prediction horizon is chosen. At this prediction horizon $M = 4\ s$. In the last column of Table 4-7 is the sum of all the ITAE values for the six desired or reference power trajectories. The difference in the overall performance between the chosen parameter-set and the best, is only 0.353 which is negligible.

Table 4-7 List of the best performance

No	Ts	R	M	P	M\P	ITAE1	ITAE2	ITAE3	ITAE4	ITAE5	ITAE6	SUM_ITAE
1	1	0.003	4	20	0.2	23.44546	11.43457	1.260192	10.24302	0.683172	0.738479	47.804895
2	1	0	4	20	0.2	23.44564	11.43458	1.260194	10.24302	0.683173	0.738479	47.805088
3	1	0.01321	4	20	0.2	23.44565	11.43458	1.260196	10.24302	0.683174	0.738479	47.805092
4	1	0.006	4	20	0.2	23.44566	11.43457	1.260194	10.24302	0.683175	0.738477	47.805094
5	1	0.009	4	20	0.2	23.44569	11.43457	1.260191	10.24302	0.683178	0.738478	47.805119
6	1	0.015	4	20	0.2	23.44572	11.43458	1.260194	10.24302	0.683171	0.738477	47.805153
7	1	0.003	4	24	0.16667	23.45794	11.56892	1.260154	10.44916	0.683278	0.738612	48.158068
8	1	0	4	24	0.16667	23.45794	11.56899	1.260171	10.44916	0.683277	0.738618	48.158147
9	1	0.006	4	24	0.16667	23.45796	11.56899	1.260171	10.44916	0.683279	0.738619	48.158182
10	1	0.015	4	24	0.16667	23.45796	11.56899	1.260171	10.44916	0.683277	0.738627	48.158187
11	1	0.01321	4	24	0.16667	23.45798	11.569	1.260174	10.44916	0.683283	0.738618	48.158208
12	1	0.009	4	24	0.16667	23.45812	11.569	1.260173	10.44916	0.683277	0.73862	48.158342
13	1	0	4	73	0.05480	24.186	11.60344	1.263375	10.2975	0.683598	0.738522	48.772425
14	1	0.006	4	73	0.05480	24.18603	11.60346	1.263381	10.2975	0.683603	0.738515	48.772485
15	1	0.015	4	73	0.05480	24.18607	11.60343	1.263375	10.2975	0.6836	0.738524	48.772497
16	1	0.009	4	73	0.05480	24.18604	11.60349	1.263388	10.2975	0.683599	0.738521	48.772532
17	1	0.003	4	73	0.05480	24.18604	11.6035	1.26339	10.2975	0.683597	0.738524	48.772547
18	1	0.01321	4	73	0.05480	24.18612	11.6035	1.263394	10.2975	0.683598	0.738521	48.772633
19	1	0.006	4	60	0.06667	24.10988	11.68698	1.26343	10.31823	0.68357	0.741893	48.803976
20	1	0.003	4	60	0.06667	24.10988	11.68699	1.263435	10.31823	0.683571	0.741893	48.803995

The smallest value of M used is $2\ s$. From Table 4-3, the best 20 parameter sets all have $M = 4\ s$. This can be attributed to the fact that M must be long enough in order that the control actions have a reasonable effect on the output response [58]. Though the prediction horizon for the best performance is only $24\ s$, larger prediction horizons result in more stable closed-loop predictive control systems.[**32**].

The chosen parameter set is as follows,

$$T = 1\ s, R = 0.003, M = 4\ s \text{ and } P = 24\ s.$$

The parameters are defined in continuous time but can also be expressed in terms of numbers of samples. The sampling time, T is $1\ s$ therefore, the prediction and control horizons in terms of numbers of samples are 4 and 24 respectively.

This set of results was used in the MPC controller. Three different scenarios were chosen in order to investigate the type of control mechanism used. The controller was trained using a state- space model extracted from the Simulink® model which serves as the actual plant. The results of the controller on the actual plant and on the model used by the controller are compared. The first column shows results when the MPC controller is applied to the state space model which is used by the model predictive controller in determining future moves. The second column shows results when the controller is applied to the actual plant.

The state space model which is used by the controller was extracted from a Simulink® model of the plant. As seen in the figures, there is very little difference in the two sets of graphs. This is implies that the model used by the controller is a very good approximation of the plant. In most systems however, there is a significant difference. The response of the system to an increase or decrease in load is investigated. The first scenario looks at a small power increase while the second looks at a large power increase. In the third scenario a plant output during a decrease in load is investigated. So far, the changes in load which have been covered look at a single step change. However, normally a number of these changes take place in a time period. The plant should be able to track multiple changes in load demand. Therefore, in the fourth and fifth scenarios, plant output during multiple changes is observed. Lastly, the performance of MPC control is compared with fuzzy optimised PID control.

Scenario 1: Power level is increased by 2 MW.

Figure 4-12 shows the responses or a 2 MW increase. The negative values of flow on the low pressure actuator and positive values on the high pressure actuator are equivalent to the bypass valve being closed or constricted. Therefore, the Bypass control valve is being adjusted. The bypass valve begins to close for the first four seconds before opening up slightly for about two seconds. After 15 seconds, the position of the bypass control valve remains in a slightly closed position. Consequently more helium is allowed to flow through the circuit, and an increase in the output power is recorded. Therefore, for a small increase, the main mechanism used is slightly closing the bypass control valve. This is the choice the controller makes since it is the most optimal when compared to helium injection.

Scenario 2: Power level is increased by 6 MW.

As can be seen in Figure 4-13, the gas pressure bypass valve in this scenario is again constricted. However, the allowed bypass flow is less than in the case of the small power increase. For the small power increase the absolute values of the actuators are less than in the large power increase case. Furthermore, the closure is held on longer than in the small signal case since it takes longer to reach the desired trajectory. The desired trajectory is reached after 25 seconds in this case. After 30 seconds, the bypass valve is then held at a nearly closed position. Therefore, for a large increase, the main mechanism used is almost closing the bypass control valve. This is the choice the controller makes since it is the most optimal when compared to helium injection.

Scenario 1: Power level increased by 2 MW.

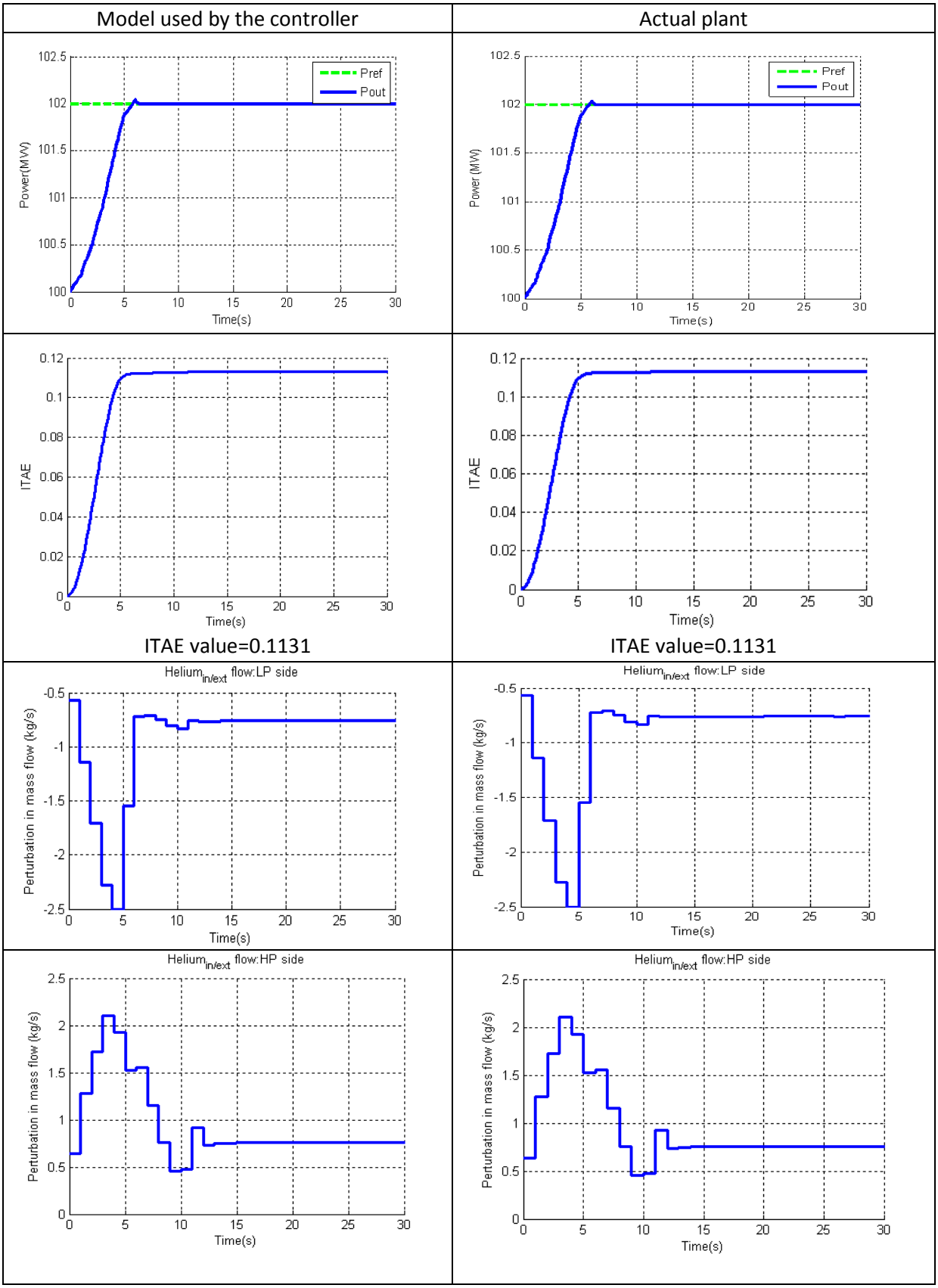

Figure 4-12 Results for small Power increase

Scenario 2: Power level increased by 6 MW.

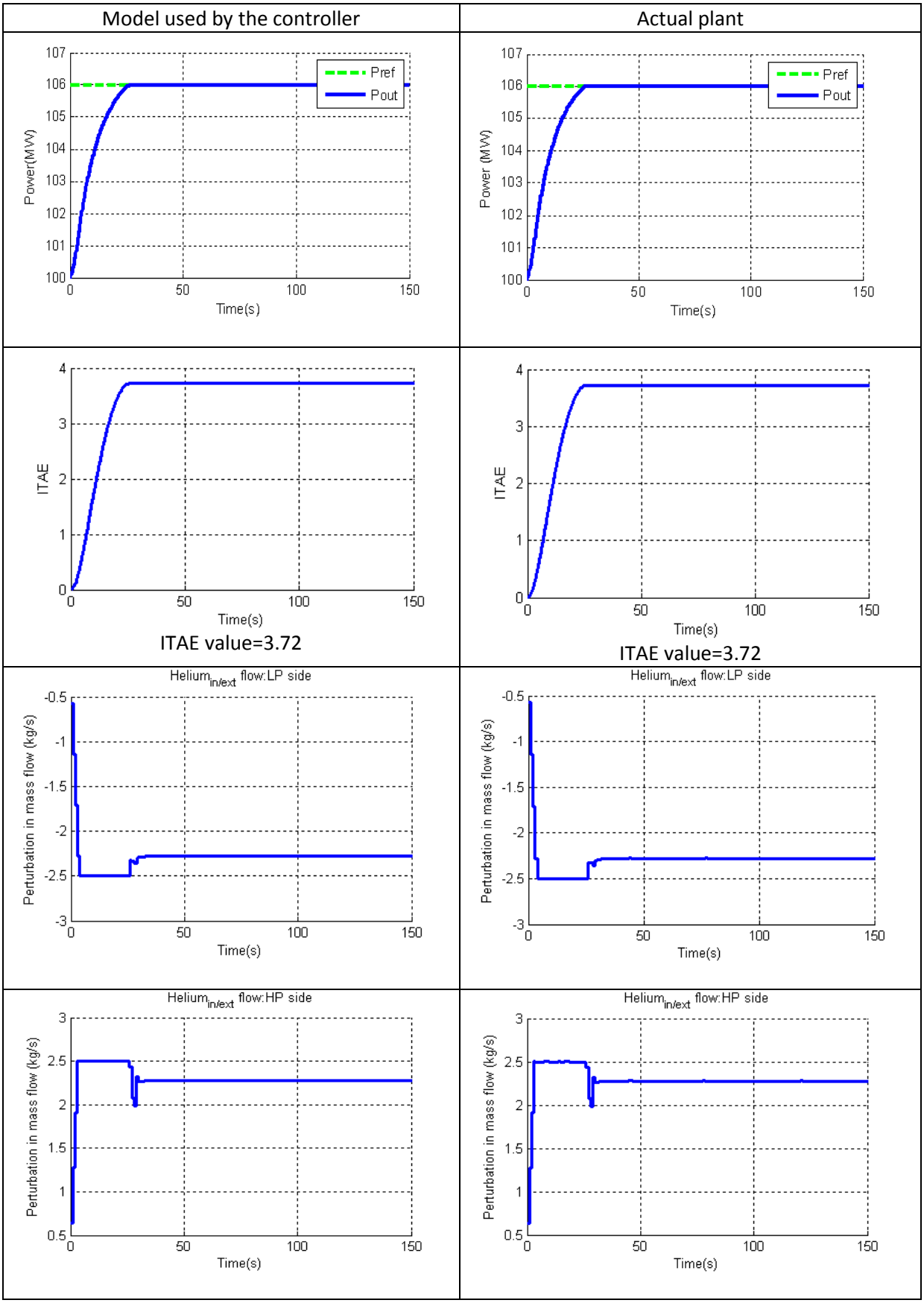

Figure 4-13 Results for a large Power increase

Scenario 3: Power level is decreased by 3 MW.

In the third scenario depicted in Figure 4-14, the power is decreased by 3 MW. The positive values of flow on the low pressure actuator and negative values on the high pressure actuator are equivalent to the bypass valve being opened up. The bypass valve begins to open for the first few seconds and then it is slightly closed till about 12 seconds. Afterwards it is held in a more open position than it held during steady state. Opening the bypass valve is the choice the controller makes since it is the most optimal when compared to high pressure helium extraction. The trajectory for HP helium extraction has a less steep gradient than the bypass therefore it is not well suited for step changes. However this may not be the case for a steadily falling reference power level (negative ramp).

The first three scenarios show that low pressure extraction and high pressure injection are the preferred control mechanisms during increasing load demands. These two mechanisms have been explained to be equivalent to closing the bypass valve. On the other hand, decreasing load demand was best controlled by low pressure injection and high pressure extraction which is simply the bypass mechanism. When the controller tries to keep the power output at the same level as the demand for power (given as the reference power), this in known as load following. The bypass valve plays a major role during load following.

Scenario 3: Power level decreased by 3 MW.

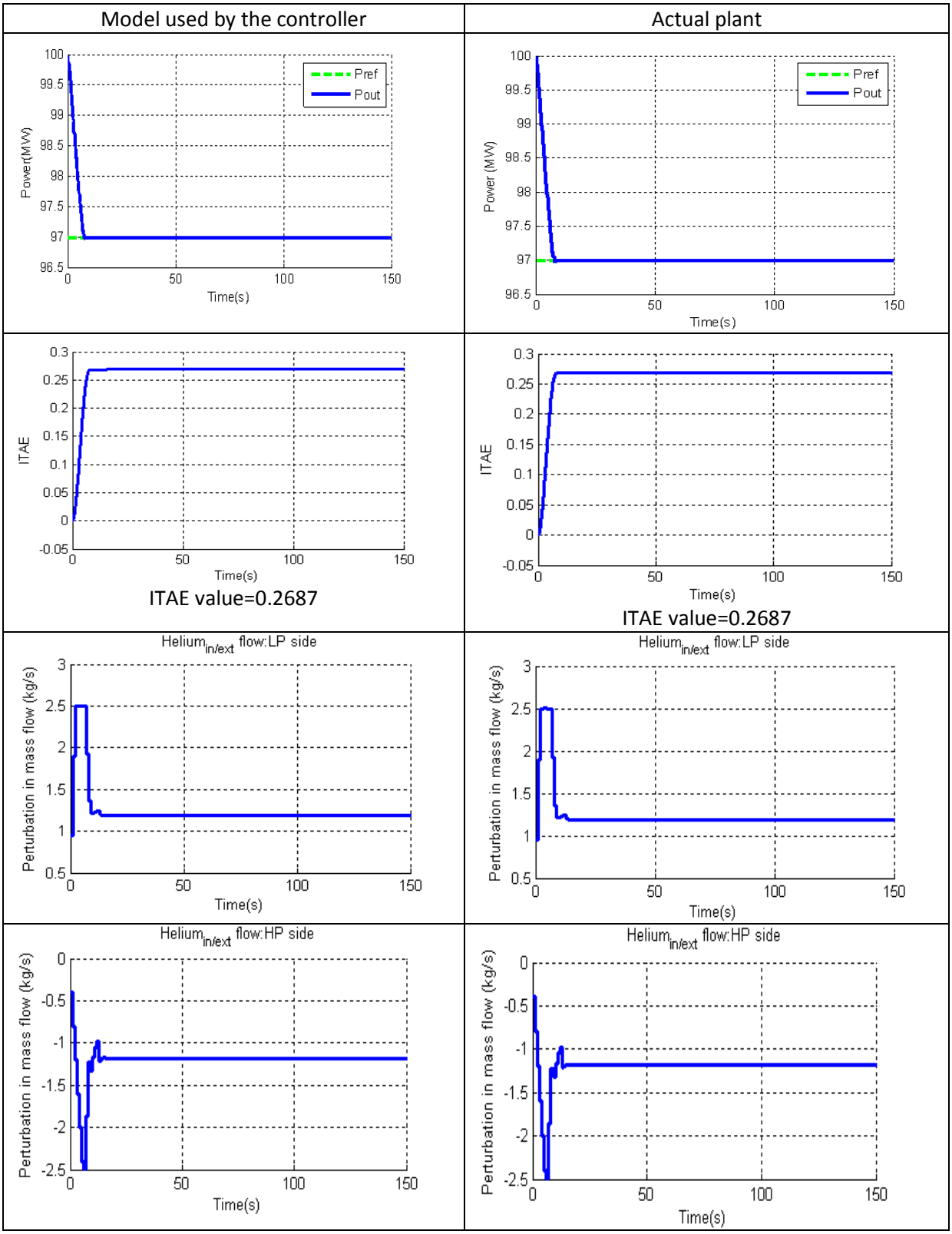

Figure 4-13 Results for load power decrease

Scenario 4: Multiple change in reference or desired power, P_{ref}.

Figure 4-14 and 4-15 shows load following of a changing load. The desired or reference power over a time period is known as a reference trajectory. The reference trajectory is in green while the plant output is in blue.

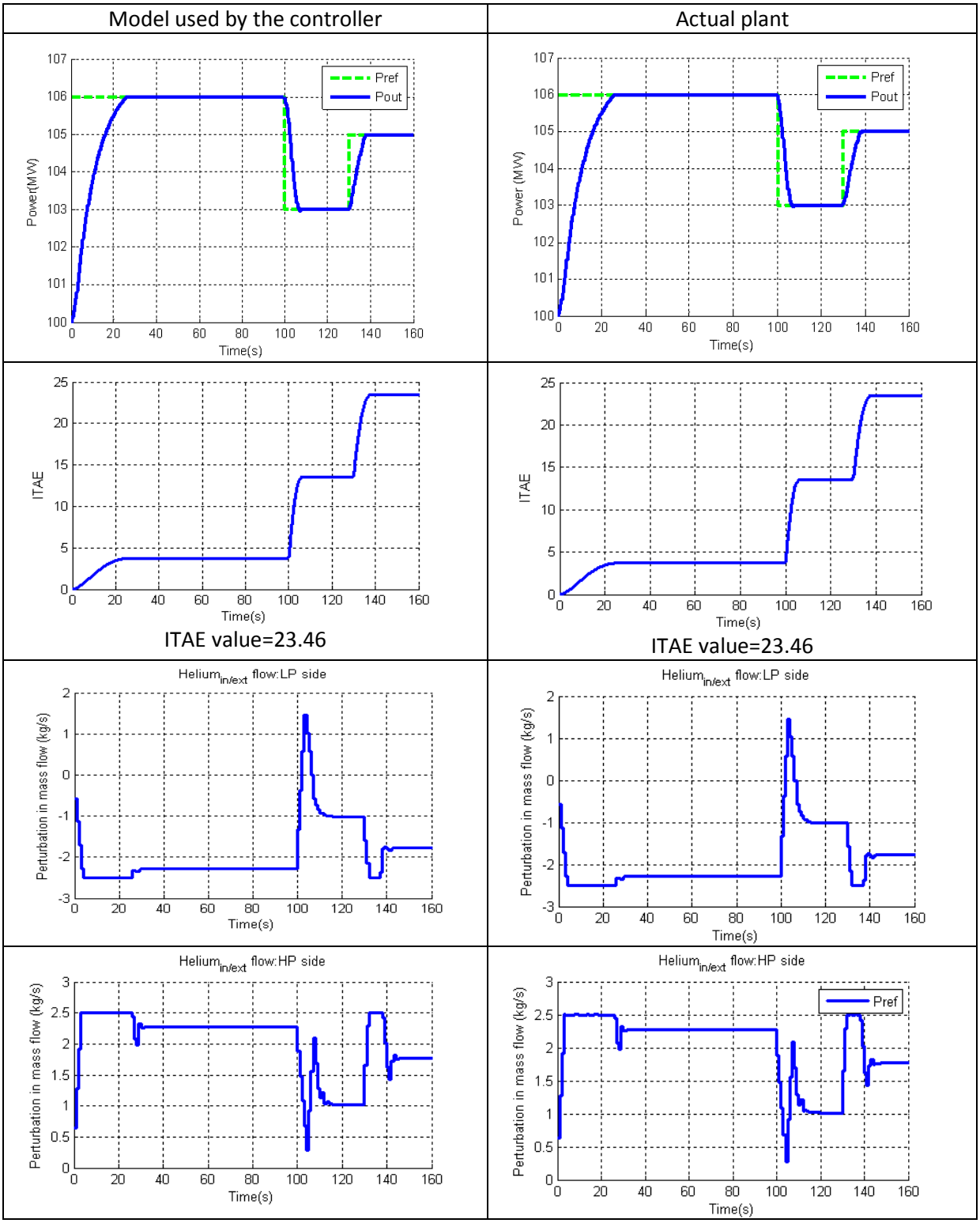

Figure 4-14 MPC control changing reference power

Scenario 5: Multiple change in reference or desired power, P_{ref}.

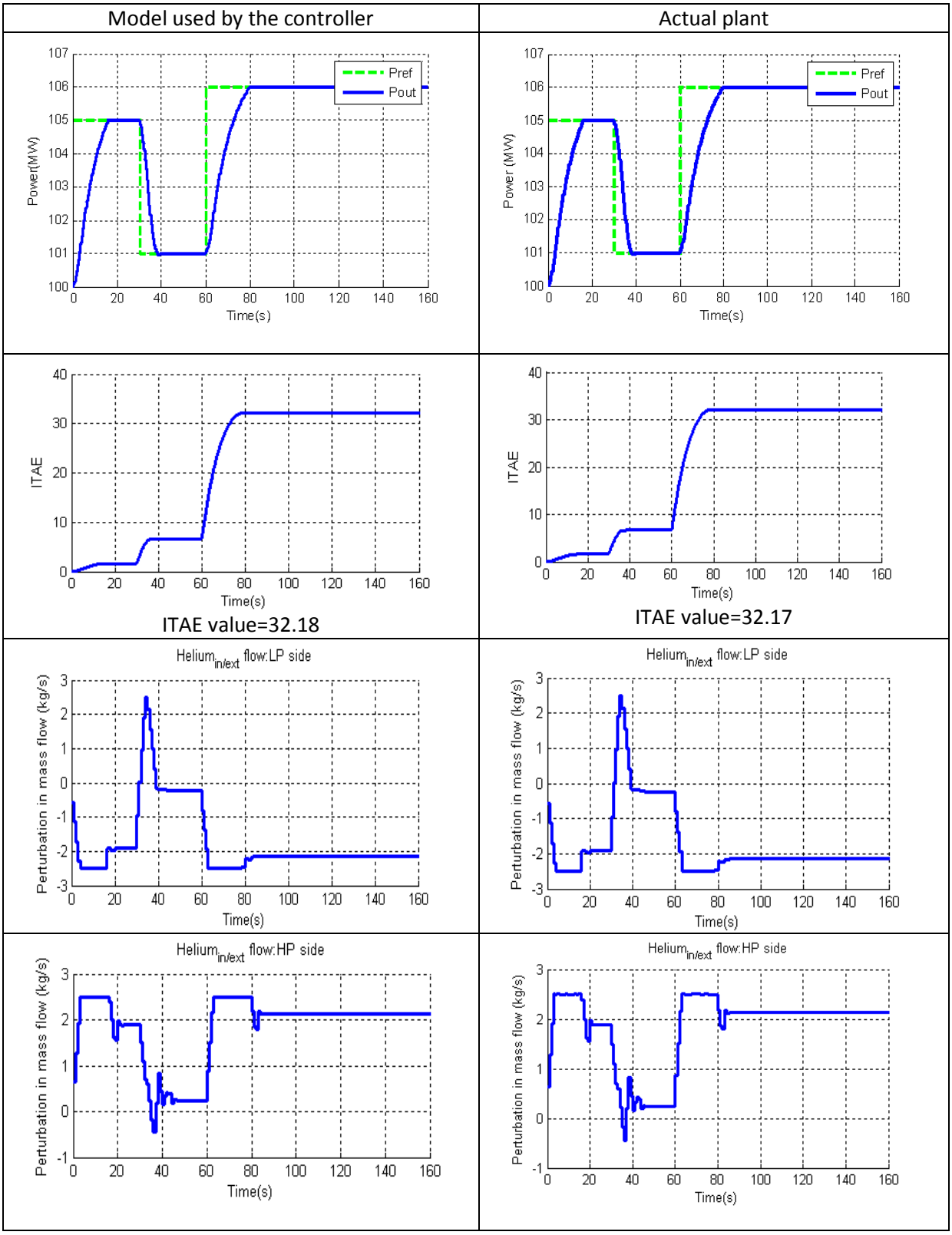

Figure 4-15 MPC control changing reference power

An improvement in the ITAE index from what is expected, 32.18 to 32.17, is observed when the controller is applied to the actual plant. The ITAE index is improved by 0.01.

4.5 Comparison of MPC and genetically optimised fuzzy PID control

In this section, two reference trajectories are applied to the plant. The reference trajectories are specified as shown in green. It was desired to simulate a changing reference signal. This is the same trajectory that was used when genetically optimised fuzzy PID control was implemented on the system. In the optimal fuzzy PID control system, four actuators were used namely, low pressure injection, high pressure extraction, bypass and boosting mechanisms. "Boosting" was carried out on the high pressure side of the plant using a separate booster tank [**2**]. All four control mechanisms can be simulated using two actuators as has been implemented using the MPC controller. Therefore, despite the differences in the number of actuators used, the two control strategies can be compared. The fuzzy PID optimised control serves as a benchmark for determining the performance of the implemented MPC control.

The results of the MPC controller and optimal fuzzy controller are compared in Figure 4-16 and 4-17 below.

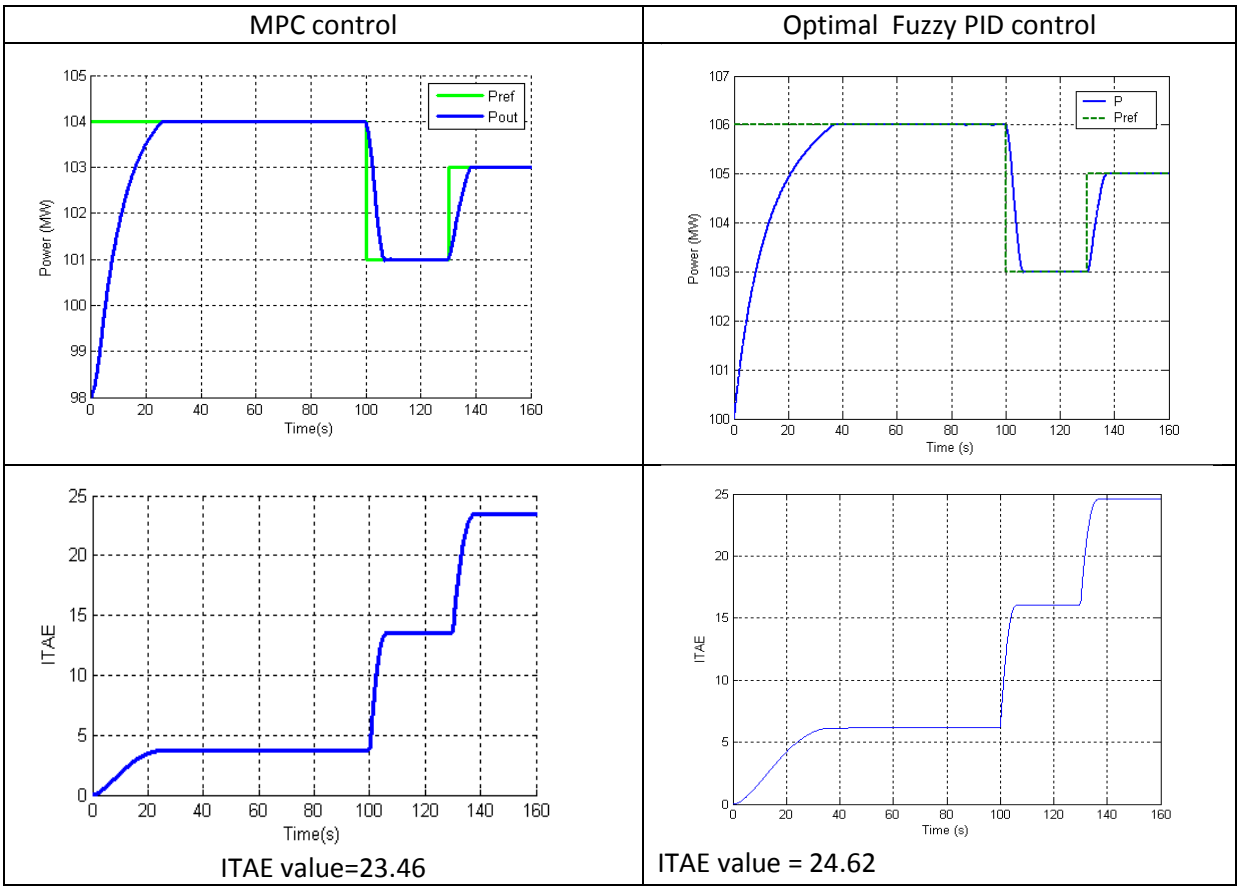

Figure 4-16 Comparing optimised fuzzy control and MPC control

The results obtained for the first reference trajectory in Figure 4-16 above shows that the performance (load following ability) is better in MPC control. The $ITAE$ index in MPC control is 23.46 while in optimal fuzzy PID control it is 24.62. The implemented MPC controller thus improves the index by 1.16. Similarly, the results obtained when a second reference trajectory is used show that the MPC control improves the index by 2.49. The response is shown in Figure 4-17. The $ITAE$ index in MPC control is 32.17 while in optimal fuzzy PID control it is 34.66.

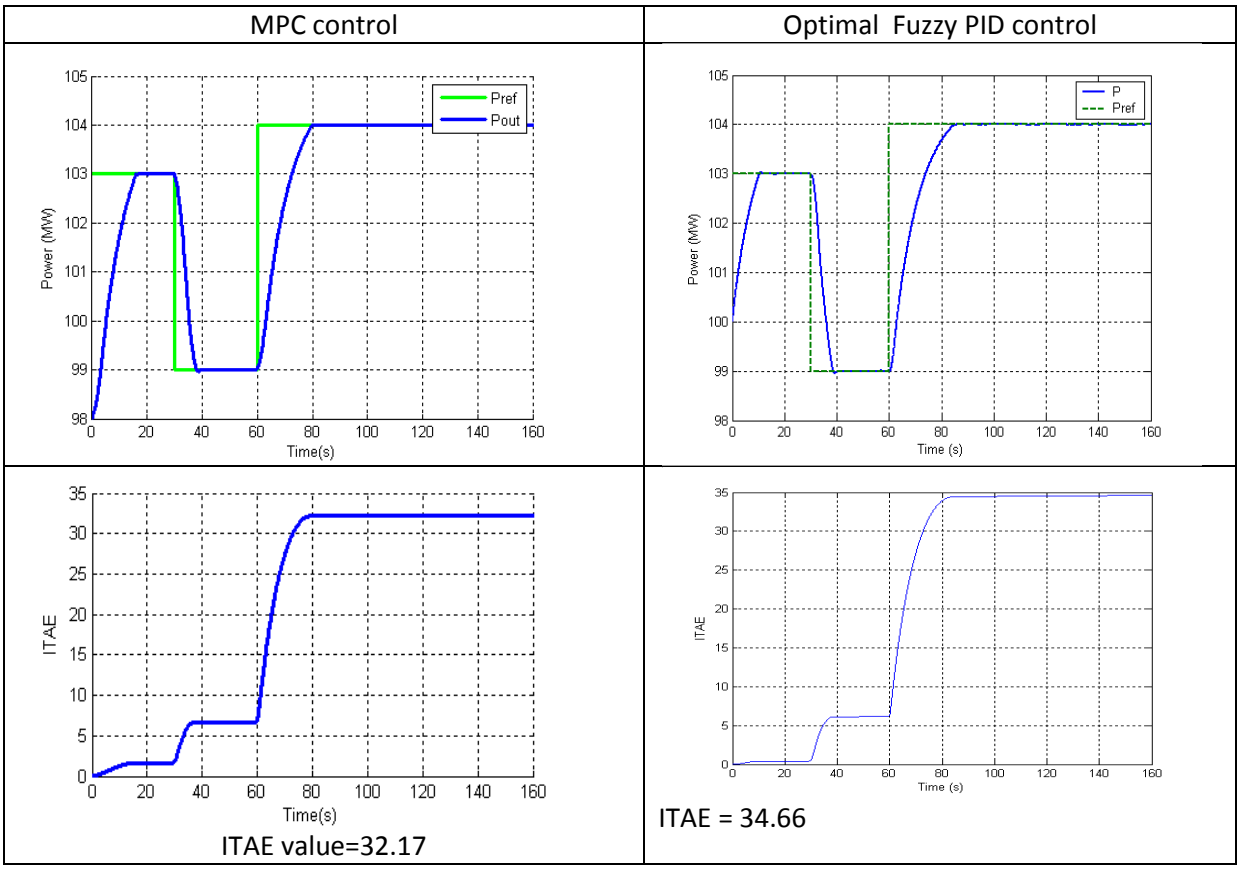

Figure 4-17 Comparing optimised fuzzy control and MPC control

In both instances, MPC control performance (load following) was better. Only one aspect, load following, has been looked at so far and already the advantages of MPC control over optimised fuzzy PID control are evident. However, care must be taken in the choice of the MPC controller tuning parameters since performance is highly dependent on the choice of these values.

In the next section, other aspects of control are looked at. How the plant performs in the presence of disturbances is very critical. The plant should be able to give the required output even in the presence of disturbances.

4.6 Disturbances

Introduction

Maintaining the output power at the desired level is very important for power generation systems as well as reacting well to disturbances during distribution. These disturbances can come from the plant itself or from the power grid. Disturbances are unique to the design of the plant. How a plant reacts to a change in the load and or reference signal is a telling point to the quality of control system and plant design. In addition to poor performance, disturbances can lead to failure or malfunctioning of components which would ultimately lead to failure to the plant as a whole and can also pose danger to the environment when not managed well. This chapter investigates some of the disturbances which might occur during the running of the PBMR a brief description is given followed by simulations of different scenarios, i.e. effect of individual disturbances on the plant performance.

4.6.1 Plant disturbances

In real situations, a system experiences disturbances. These can lead to poor system performance. Disturbances cause outputs to move from the desired setpoint especially due to the fact that they cannot be controlled or manipulated by the process engineer. Some are measurable while others are unmeasured. It is necessary for the control structure to account for all disturbances that would have an effect on the process. A large disturbance can cause system instability [**66**]. In MPC, measured disturbances can be incorporated in the design by use of the prediction horizon can be used to determine the future disturbances and the reference signal (desired output) changes [**14**]. The control horizon can be used to determine the most optimal control moves to ensure that future outputs track the reference signal well. In the Matlab implementation used, an integrator is naturally embedded into the design, This ensures that the control system rejects constant disturbances, as well as white noise without steady-state errors[**32**]. However, unmeasurable disturbances pose a threat to the constraints. Ideally the output constraints ought to be accounted for i.e. they should not be broken. Nevertheless, in the presence of unmeasured or unpredictable disturbances, the actual outputs cannot be directly constrained through the controller. This is because only the predicted output is considered in determining the control moves [**67**].

Common disturbances in a gas powered power plant are differences (losses or gains) in amount of the gas, temperature and pressure. [**66**] describes a steam turbine powered by heated gas. In that system, there were seven control variables. Disturbances were also identified which would affect some system parameters. Variations due to disturbances were specified to be within 2% for concentration of fuel and air, 25% to 50% for temperature and 4% for pressure. However, larger differences can be recorded in the event of depressurisation due to a pipe break or leak. Pressure loss is expressed as a percentage as shown below,

$$P_{loss} = \frac{P_{in} - P_{out}}{P_{in}} \times 100 \ \% \,, \tag{5-1}$$

where P_x reads as "pressure x." Pressure losses are due to resistance in flow which is a result of friction and changes in cross-sectional area of flow. There are also mechanical losses in power due to friction [**68**].

There are a number of disturbances which can occur in a PBMR plant and these have been identified. In order to protect the plant, a number of monitoring and protection systems have been put in place to prevent the plant exceeding defined operating margins. If these margins are breached, plant components can be damaged [**13**]. Disturbances from varying sources affect parameters such as temperature, speed of the turbo-machines, pressure, mass flow and density of helium. The transition of a disturbance action from its previous value to zero is a result of corrective measures triggered and sometimes implemented by the monitoring and protection systems. Details of the monitoring and protection systems are found in [**13**]. Some of these systems include radiation, meteorological, and seismic monitoring systems, equipment and reactor protection systems. A number of support systems for mass flow and temperature regulation are also part of the plant and work hand in hand with the control, monitoring and protection systems for safe operating of the plant. The following is a list of plant components and disturbances which are present in each one.

Reactor

In the reactor, reactivity is varied by control rod movement. There are also external reactivity disturbances which cannot affect reactivity and should not be discounted. Small disturbances can affect the temperature coefficient. The reactor loses heat through its walls

however, this is negligible [**68**]. Temperatures of the reactor vessel should not rise beyond what the reactor vessel can handle. Fuel spheres which are spent have to be discharged from the reactor core and fresh ones fed in. This is done at full power by the fuel handling and support system, FHSS [**13**]. During this process, minor temperature variations can be experienced by the reactor. This is a known disturbance since discharge of fuel and refuelling can be anticipated. However in the event that a control rod drops, output temperature can be affected since reactivity in the reactor vessel is controlled by the control rods [**13**]. As such, an unexpected momentary variation in temperature can ensue.

In the Simulink® model, some of the "disturbances" were included and values were assigned to each one. Below is a table showing the names and values of the "disturbances" which have been used in the plant model implemented in the previous sections. They are used to cause the system to be as close as possible to the real system. Refer to Figures 3-10 and Figure A-14 for details.

Table 4-8 Plant losses

Name	Description	Value
Clp tuning factor	Tuning factor for low pressure volumes	1.2
Chp tuning factor	Tuning factor for high pressure volumes	0.7
Cmp tuning factor	Tuning factor for medium pressure volumes	1.2
HPT diffuser loss	High pressure turbine diffuser loss	0.004
LPT diffuser loss	Low pressure turbine diffuser loss	0.004
PT diffuser loss	Power turbine diffuser loss	0.007
HPC diffuser loss	High pressure compressor diffuser loss	0.3
LPC diffuser loss	Low pressure compressor diffuser loss	0.1
Leak flow$_{HPC_LPTin}$ (L1)	Fraction of leak flow from high pressure compressor to the low pressure turbine inlet	0
Leak flow$_{HPC_LPTout}$ (L2)	Fraction of leak flow from high pressure compressor to the low pressure turbine outlet	0
Leak flow$_{LPC_PT}$ (L3)	Fraction of leak flow from low pressure compressor to the power turbine	0

The losses (disturbances) in the table are embedded in the Simulink model, as shown in Figure 3-10 and Figure A-14 in the appendix for details.

Turbo-machines

Turbo machines are interconnected. I.e. the turbines are connected to the compressors by shafts. Mechanical power losses assumed to be in the range of 1% occur due to mechanical friction. This is concentrated in the gear box and frequency converter, both of which are required to run the turbine at high speeds. Power loss comes about due to loss in efficiency. There are also pressure losses in the turbo- machines due to resistance. This resistance is due to friction and changes in flow concentration area. In the turbo machines, about 1% to 2% of the mass flow from the compressors is bled off for cooling turbine discs [**68**]. A support system helps replenish helium lost on a daily basis. The turbines are designed to run on electro-magnetic bearings, EMBs. The sealing system of EMBs has to be done well in order to prevent power losses of up to 10 MW.

The leak flows L1, L2 and L3 in Table 4-8, are right after the low and high pressure compressors labelled as L. Compressor and H. Compressor respectively in the Simulink models shown in Figures 3-10 and A-14. As the last three rows of the table show, one of the assumptions made in the plant model is that the fraction of leak flow is zero, i.e. no leak flow. However, in simulating the leak flow, the fraction of leak flow should be given a value between 0.01 and 0.02 corresponding to 1% and 2% of the flow which is bled off to the compressors.

Leak flows can be regarded as a known disturbance

Heat exchangers

In heat exchangers, i.e. pre-cooler intercooler and recuperator, pressure losses are present. The magnitude of the pressure loss is inversely proportional to the volume of the hear exchanger which also is dependant on the operating pressure. The lower the operating pressure, the larger the volume required. Pressure losses are due to temperature differences and can be of magnitudes of 0.8% to 1.8% on the hot side and 0.334% to 0.8% on the cold side. Pressure losses can be extremely high and even up to 7Mpa in the case of a pipe burst. A pipe burst would result in depressurisation.

Such an accident is not confined to the heat exchangers only but also other sections of the plant. As a safety measure, the containment of the plant should be such that air inflow is

inhibited to prevent graphite ignition which would be detrimental to the plant. This however is still debated. Details of the safety of pebble bed reactors can be found in [**13**], [**69**] and [**70**]. Such an occurrence however would be a major disturbance and beyond the scope of this study.

4.6.2 Control disturbances

Control mechanisms are actuated by valves. A malfunctioning valve can cause the system to receive an incorrect amount of helium which would result in the plant giving out an output different from that desired. Depending on the actual disturbance, the system should be able to recover from this. A worst case scenario would be a valve to be either always closed or always open. Such a problem would cause the system to become unstable. Other disturbances are due to delays. However, these are small and their effect of delays will be assumed to be negligible. In operation, a valve stuck in its position remains there throughout the control period thereby fixing the mass flowthrough the valve. Load following is almost impossible when a valve is faulty, i.e. stuck, permanently closed or permanently open.

4.6.3 Grid disturbances

The reference signal is adjusted depending on the anticipated load. However, in some cases it can occur that the load exceeds that anticipated (overload) or is far less than expected (short-circuit or underload). During anticipated load changes, it is required that a smooth transition takes place from one load level to another. In the system modelled, a constant power turbine shaft speed is assumed. However a constant shaft speed is a control task required to avoid grid separation during normal operations. Plant frequency is dependant on power turbine shaft speed. A mismatch of frequency between the power plant and the grid would cause grid separation. Tripping of a plant also causes grid separation. This is because the load is reduced to zero in a very short period and the turbine speed increases. A separate control mechanism is needed to prevent turbine shaft over-speed [**69**]. Closing of fuel valves is one of the ways to achieve this. However, after the fault is cleared the power generation system remains with the large load. Since valves are closed at this time, returning the system to its original state is not an easy process. The power turbine has to be

reaccelerated under low fuel conditions. Load shedding techniques can be used to reduce the drop in frequency. Shokooh *et al*, 2005, suggests how intelligent load shedding can be used to address problems that would arise due to grid disturbance described above. Stability of the system can be impacted negatively when the system frequency drops [**71**]. Some grid disturbances are a result of unfavourable weather conditions.

4.6.4 Disturbance simulations

The disturbances described in the previous section can be divided into known and unknown disturbances. Grid disturbances such as overloads and underloads cannot be anticipated and therefore are classified as unknown disturbances. Helium bled off to cool turbine blades is also a disturbance but since the amount is known, it is classified as a known disturbance. The bled off helium is pumped back into the cycle using the helium make up system. Leakages in compressors and disturbances in the inlet temperature of helium entering the turbines (i.e. outlet temperature of the reactor) due to the transitions that occur during spent fuel extraction and refuelling can be anticipated before hand and therefore are known disturbances. Malfunctioning valves or control system disturbances will be classified as unknown disturbances since they are accidental or due to component failure. In this section, the power output response is investigated in different disturbance scenarios. White Gaussian noise which was not included in the last section is also added.

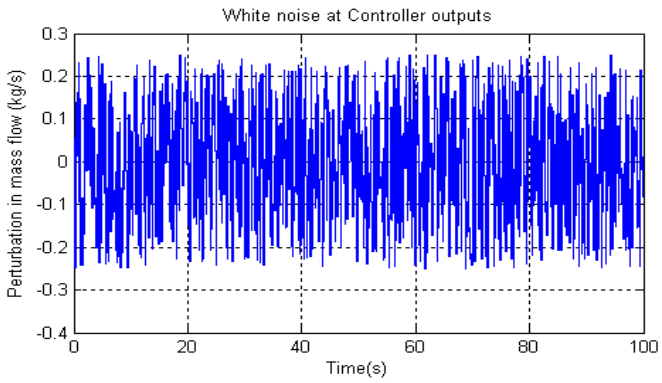

Figure 4-18 White noise at plant control inputs (controller outputs)

White Gaussian noise

Implementation of Model predictive control requires use of electronic hardware in conjunction with the inventory control system. In most electronic systems, inherent noise is generated within the integrated circuits (ICs) and transistors. This is known as white noise.

White noise is “an uncorrelated random noise process with equal power at all frequencies” [**76**]. White noise arises from movement of charge carriers at temperatures greater than absolute zero [**50**], [**72**]. White noise is usually assumed to have zero mean [**32**]. Furthermore, a random signal is considered as "white noise" if it is observed to have a flat power spectral density over the full bandwidth of the medium of transmission [**73**]. Signals which have much higher frequency components than the upper bound frequency of a system subcomponent’s bandwidth are classified are white noise as well [**72**]. White Gaussian noise can occur in both the plant inputs (control signals) and the plant outputs. As shown in Figure 4-18 and Figure 4-19.

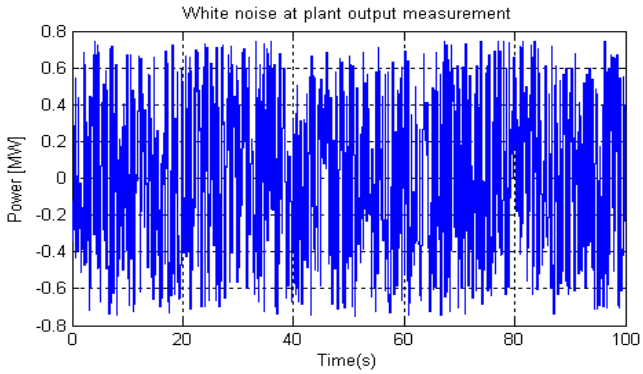

Figure 4-19 White noise at plant output

The plant was modified to include white noise as shown in Figure 4-20. The added noise blocks are shaded in green.

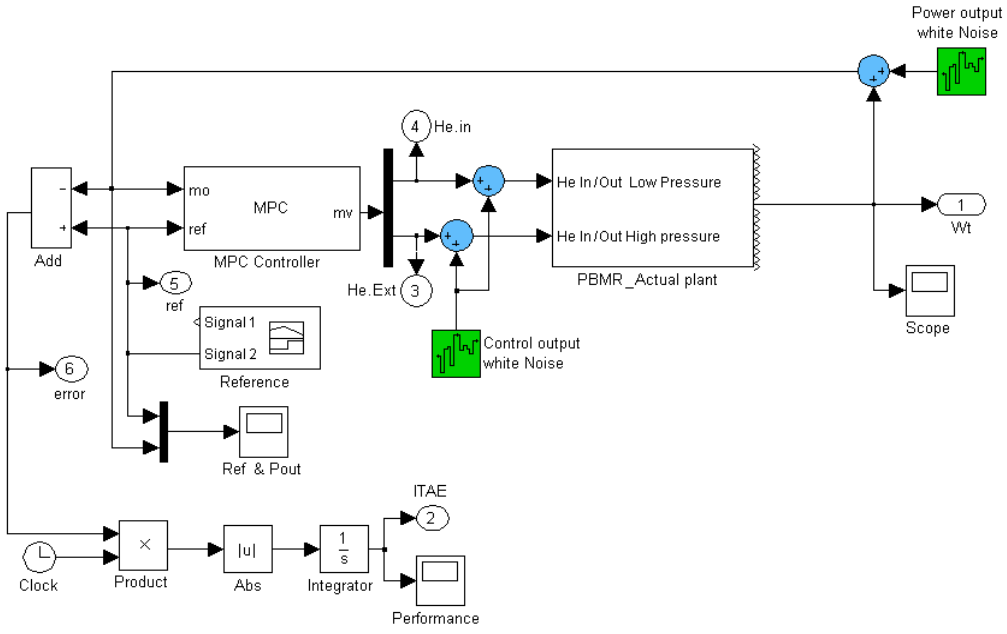

Figure 4-20 Plant: white noise at the controller output & plant output

The noise levels were taken to be about a tenth of the highest value of the measurement to which the noise was added. This can be seen in Figures 4-18 and 4-19 where the average peak of the noise is 0.23kg/s and 0.7 MW respectively. The results are shown in Figure 4-21.

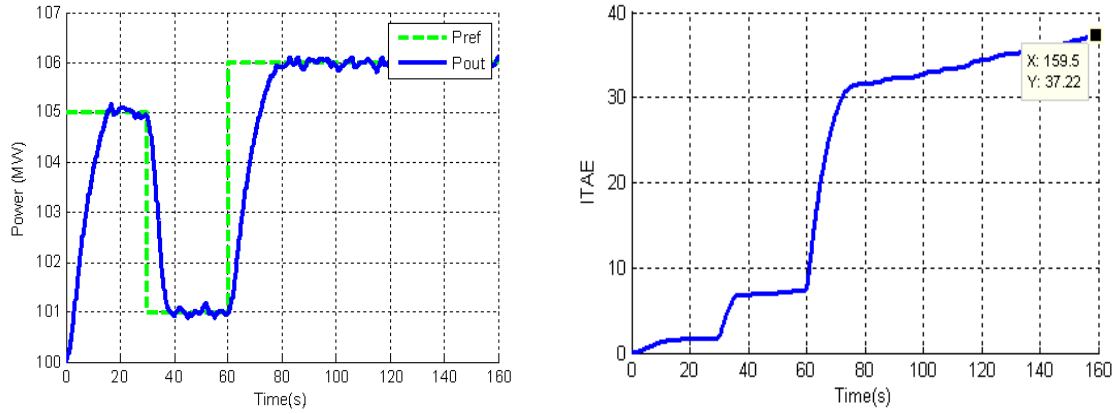

Figure 4-21 Plant response in presence of white noise

Results show that the plant still manages to follow the trajectory but it never settles down. For interest's sake, larger prediction and control horizons were applied to the plant to see the response. Table 4-10 below shows a summary of the results. The actual plots of the response and ITAE index can be found in the appendix A.10.2. The table has been divided into two parts. The first part consists of control and prediction horizons within the ranges of $M$and P calculated in Table 4-1 in the last column on the left. The second part consists of prediction and control horizons outside the ranges given in Table 4-1. The symbols "x" and "√" identify the worst and best performances and the corresponding MPC parameters. The asterisk shows the result and parameters of the chosen controller with $P = 24$s and $M = 4\ s$.

From the first part of Table 4-10 it can be seen that the effect of increasing the prediction horizon or control horizon has a negative effect on the ITAE performance. This is because both actions result in less aggressive control actions resulting in a slower system. In Figure 4-21, the ITAE index increases because the plant output does not settle. There is always an error therefore, the integral of time error keeps increasing. In a worst case scenario, if the control actions are too relaxed or slow and the noise signal large enough, the plant output may fail to match the load demand in the presence of white noise as seen in Figure A-17. The second part reveals that values of $M$and P outside the prescribed ranges as depicted in Table 4-1 when used in the MPC controller result in a favourable response. This is because, low values of $M$and P result in aggressive control actions which favour good plant response

in the presence of white noise. However, short prediction horizons have their disadvantages [**32**], [**59**].

Table 4-9 Controller performance in presence of White noise

Control horizon	Prediction horizon	ITAE index
4	73	38.49
4	60	38.49
14	45	694.3 x
19	24	217.9
14	24	61.35
9	24	42.73
4	24	37.22 *√
2	20	39.46
4	10	37.1 √
4	10	37.27
4	6	37.58

White noise is the most common noise experienced in measurement and control. However there are many sources of noise. The next section looks at disturbances on the output. These are grid disturbances.

Grid disturbances

Grid disturbances also affect the speed of the power turbine. An unexpected increase in load cause the power turbine speed to reduce and a decrease in the load can cause the turbine speed to "run away" that is to continually increase. Special measures need to be taken to prevent this. Power turbine speed is linked to the frequency of the output power. The grid operates at a fixed frequency. The grid frequency and power turbine frequency must be the same. A difference in the speeds can cause isolation of the plant from the grid, which is undesirable. In this section the effect of "grid disturbances" on the speed is ignored. The assumption is that there exists some control mechanism which keeps the turbine speed fixed. Only the effect on the power output is considered. The grid disturbance was applied as shown in Figure 4-23. The grid disturbances are shown in Figure 4-22.

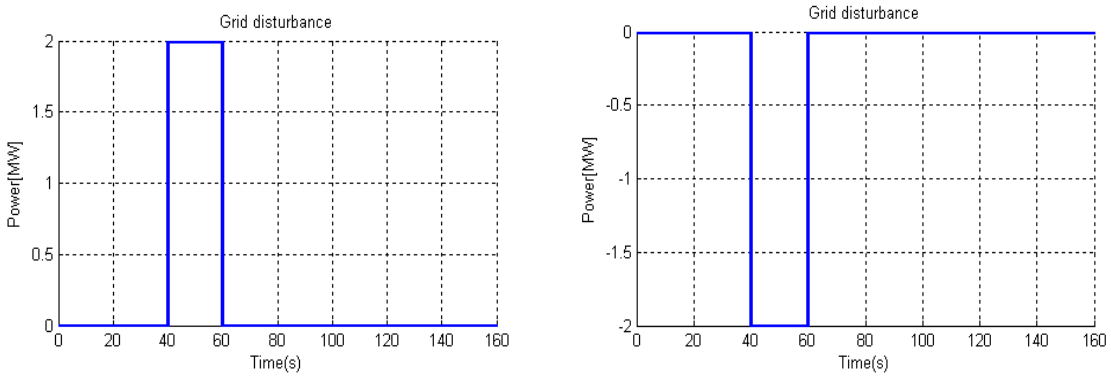

a) Increase in load from the grid b) Reduction in load from the grid

Figure 4-22 Grid disturbances: Load increase and decrease

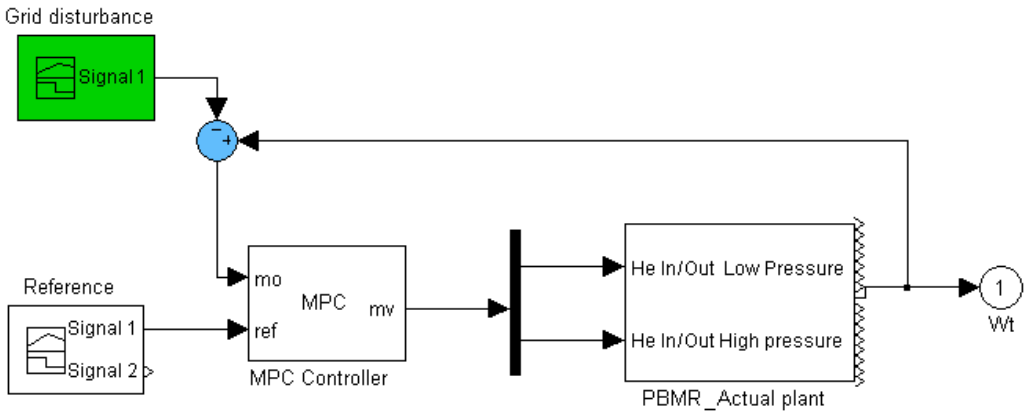

Figure 4-23 Plant layout to investigate grid disturbance

In Figure 4-23 above, the shaded block stands for the unexpected change in load. Figure 4-24 and Figure 4-25 show results for both and increase and decrease in load.

The response when a controller with prediction horizon of 24s and control horizon of 4s is shown in Figure 4-24. The ITAE index is 11.31 and appears to be rising. However, index can be seen to be settling gradually and if the simulation went beyond 160s seconds, it would stop rising. The continued rise means that the output power level is not yet equal to P_{ref}, which is the expected load demand or reference power. There is a drop in the rate of rise as power converges to P_{ref}.

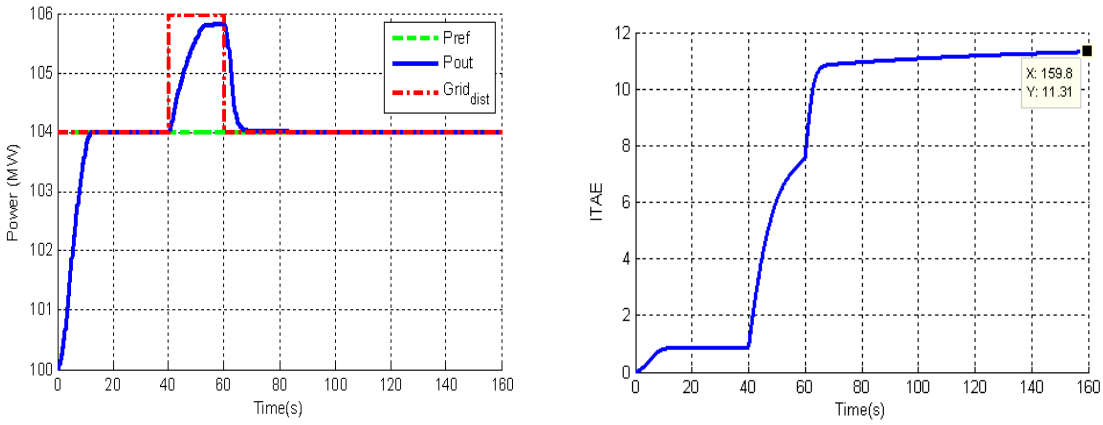

Figure 4-24 Plant response & performance when grid load rises

The performance of an MPC controller when different values for the control and prediction horizons are used is investigated. The chosen controller parameters $P = 24\ s$ and $M = 4\ s$ had been chosen with the assumption of perfect conditions. However, real systems encounter a number of disturbances. It is therefore necessary to see how the performance would be if different MPC parameters are used. This is briefly carried out and the results are shown in Table 4-10. The structure of this table is similar to Table 4-9 where values outside the ranges specified in Table 4-1 are included in the investigation and recorded in the bottom section of the table.

Table 4-10 Controller performance with grid disturbance

Control horizon	Prediction horizon	Load increase ITAE	Load decrease ITAE
4	73	13.68	12.39 x
4	60	13.01	11.75
14	45	12.97	9.4
19	24	16.98 x	9.86
14	24	9.211 √	8.86 √
9	24	10.27	9.04
4	24	11.31 *	9.60*
2	20	11.45	11.51
4	10	11.53	8.89
2	10	11.63	10.14
4	6	14.39 x	9.65

Plant performance during grid load increase and decrease are in the third and fourth columns of Table 4-10.

During grid load increase, the best result is obtained when $M = 14\ s$ and $P = 24\ s$. The already chosen controller has the third best performance with an index of 11.31. Increasing the prediction horizon does not improve on the ITAE index performance. The same can be said about reducing the control horizon. However, increasing the control horizon significantly improves the results. This is mainly due to the slower rate of change. The output response does not easily change. It is more robust. However, when this rate of change is too low as in the case when the horizon is $M = 19\ s$ while $P = 24\ s$, the advantages brought about by a slower rate of change are negated when the response over a larger period are considered i.e. when the overall error is integrated over time. A good balance is necessary between speed and robustness. Figure A-20 in the appendix shows the response when is $M = \{4\ s, 19\ s\}$.

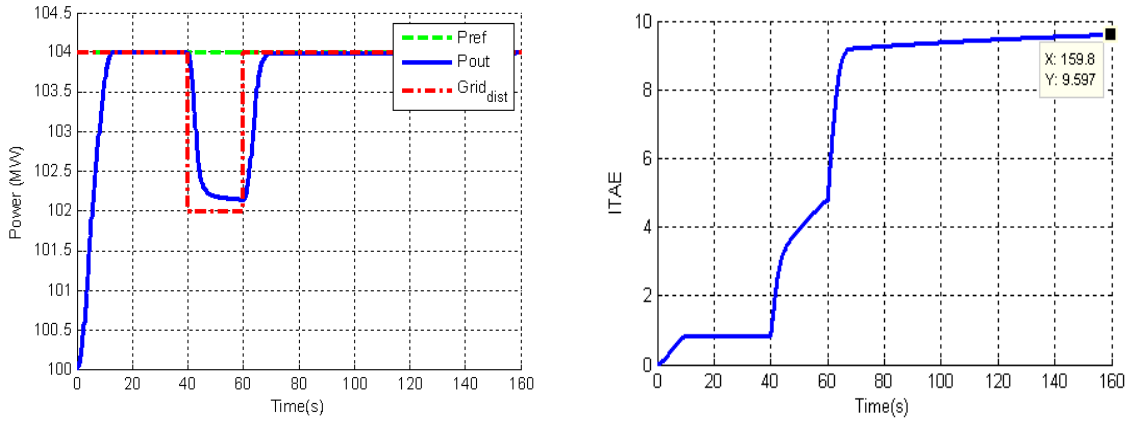

Figure 4-25 Plant response & performance when grid load drops

During grid load decrease shown above, the best performance is obtained when when $M = 14\ s$ and $P = 24\ s$. The same conclusions can be drawn from the results of load decrease as has been discussed during grid load increase. A very large prediction horizon does not improve the performance while increasing the control horizon to a peak value can improve performance and load rejecting capabilities. Knowledge about what is likely to occur in a particular plant can be used to determine which performance characteristics are of priority.

Like grid disturbances, other short term disturbances which can occur are leaking control actuators or pipes that lead to the system. Longer term disturbances are faulty valves. Load following during inventory control is investigated in the next section.

Control disturbances

Control disturbances have been discussed in section 4.6.2. A faulty valve means that more constraints have been added to the valve. The advantage of MPC is that if the fault is not so severe, then this constraint can be added in the controller definition and optimal control would be achieved. However, the overall performance of the system in this case would depend on the extent of the fault. Critical faults are “always fully open” or “always closed” or “open but not adjustable”. They are critical in the sense that they do not guarantee load following. The only time when the plant output can be correct is if it does not change from its steady state condition. On a plant, these would need to be replaced for normal operation to continue. Leaks can happen anytime. They can be simulated as shown in Figure 4-26. The coloured blocks in the figure represent how much and when a leak occurs.

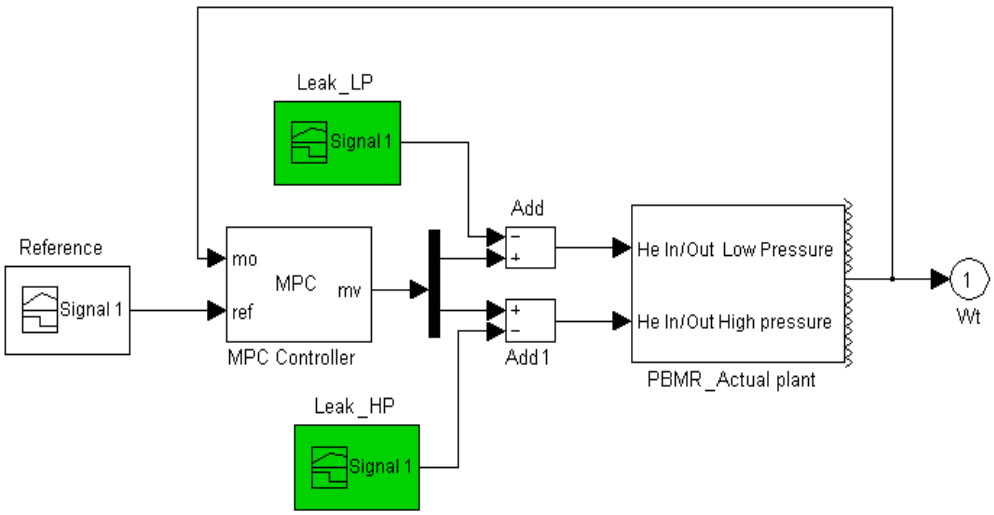

Figure 4-26 Leak flows on the controller outputs

The leaks looked are those which occur for short periods. i.e. it is assumed that the leak is noted and quickly rectified. Figure 4-27 shows the leaks which are applied to the controller outputs. There are two pipes connected to the system. One is connected on the low pressure side ($Leak_{LP}$) while the other is on the high pressure side ($Leak_{HP}$). Figure 4-28 shows the plant response and ITAE performance index.

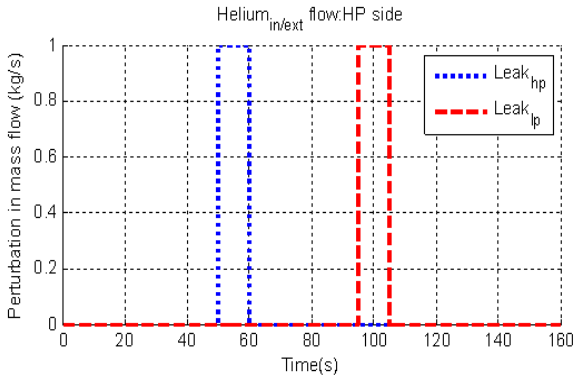

Figure 4-27a Magnitude and time interval of controller output leak flows

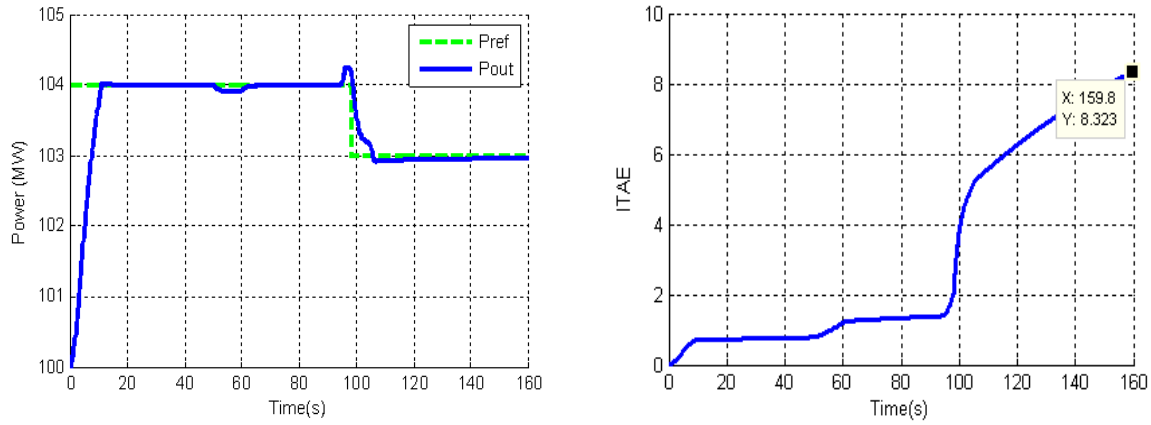

Figure 4-27b Plant response and performance when controller outputs leak

Figure 4-27 shows the response when $P = 24\ s$ and $M = 4\ s$. In the power output response between 50 and 60 seconds, there is a dip in the output power. This is the time when a leak occurs in the high pressure pipe as shown in Figure 4-26. The control action at this time is similar to helium bypass hence the drop in power. However, once the leak is stopped the system recovers and the plant output once matches the expected load trajectory. At 95 seconds, the low pressure side begins to leak. This causes a slight increase in output power. The control action this time is equivalent to the bypass valve closing hence the increase in power. At 98 seconds the load trajectory drops by one mega-watt while the leak is still present in the low pressure side. The leak is stopped at 1-5 seconds and the system tries to track the expected load. Though it is close to the desired value, the output power is still approaching the desired power up to the end of the simulation. Therefore, the ITAE index is seen to rise continually despite the output power almost being equal to the desired power. It is expected that given more time the plant output would equal the expected load and the ITAE plot would flatten off. Like the case of other disturbances, performance of the plant

was investigated for other values of P and M. The results are shown in Table 4-11. The table is also divided in two parts in the same way it is done for the other disturbances.

Table 4-11 Performance with control leak disturbance

Control horizon	Prediction horizon	ITAE
4	73	8.24 √
4	60	8.247
14	45	451.5 x
19	24	49.13
14	24	39.21
9	24	8.84
4	24	8.323*
2	20	10.26
4	10	8.72
2	10	10.12
4	6	7.925

For this type of disturbance, it appears that aggressive control actions, resulting from small control horizons, are needed to keep the plant output under control if a leak occurs. When the control horizon is large, the plant output fails to track the expected load trajectory as in the case when $P = 45\,s$ and $M = 14\,s$. Therefore slow control actions, which were favoured when more robust response was required, put the plant at risk of even shutting down just after a small leak which can be easily fixed.

The next section looks into leak flows from compressors and how they affect the plant response.

Compressor leaks

Compressor leaks are inevitable. Therefore, leaks of 1.5% of the flow are added to the plant. Two scenarios are investigated. In the first one, the plant performance when the leaks are "unknown" to the controller is observed. In the second scenario the leaks are introduced to the controller and plant model. Normally, the MPC controller has a port where the measured disturbance can be input [**63**]. However, the inclusion of this "disturbance" on to the plant is made easier in that the Simulink model from which the state space plant model

used by the MPC is extracted has the leaks as variables. Therefore, the adding the known disturbance is equivalent to updating the fraction of helium that is leaked from zero to 0.015 (15%). The two scenarios are compared. One advantage on MPC is that known disturbances can be included and considered by the MPC controller in computing optimal control moves [**32**]. The fraction of compressor flow which is leaked is shown as the "New value" in Table 4-12 while the value used in earlier sections is depicted as "Old value" in the table.

Table 4-12 Compressor leak flows

Name	Description	Old value	New value
Leak flow$_{HPC_LPTin}$ (L1)	Fraction of leak flow from high pressure compressor to the low pressure turbine inlet	0	0.015
Leak flow$_{HPC_LPTout}$ (L2)	Fraction of leak flow from high pressure compressor to the low pressure turbine outlet	0	0.015
Leak flow$_{LPC_PT}$ (L3)	Fraction of leak flow from low pressure compressor to the power turbine	0	0.015

Three scenarios are investigated. The first is when no leaks are included in the plant model or the state-space model used by the MPC controller. In the second scenario leaks are added to the plant model but not the state-space plant model used by the controller. In the third scenario leaks are introduced in both the state-space model used by the controller and the plant. Results are shown in Figures 4-28 to 4-30.

Scenario 1

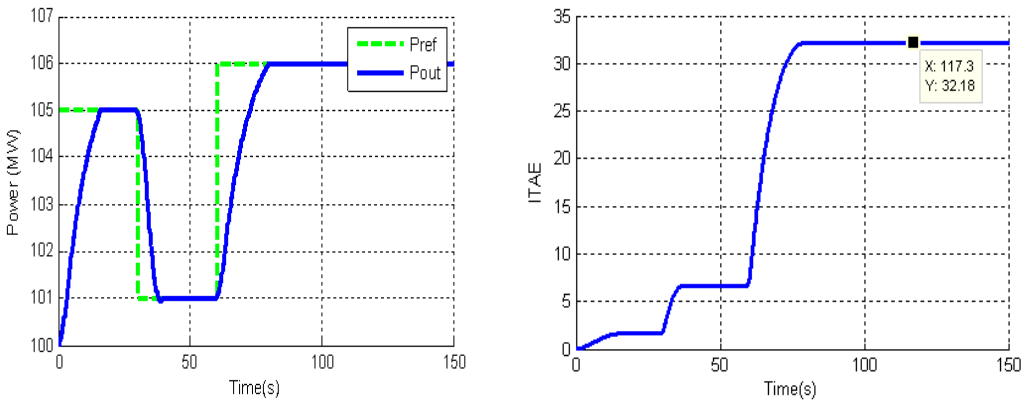

Figure 4-28 Performance when no leaks are present

Output when leaks are not included in either the MPC model or actual plant. The ITAE performance index is 32.18.

Scenario 2

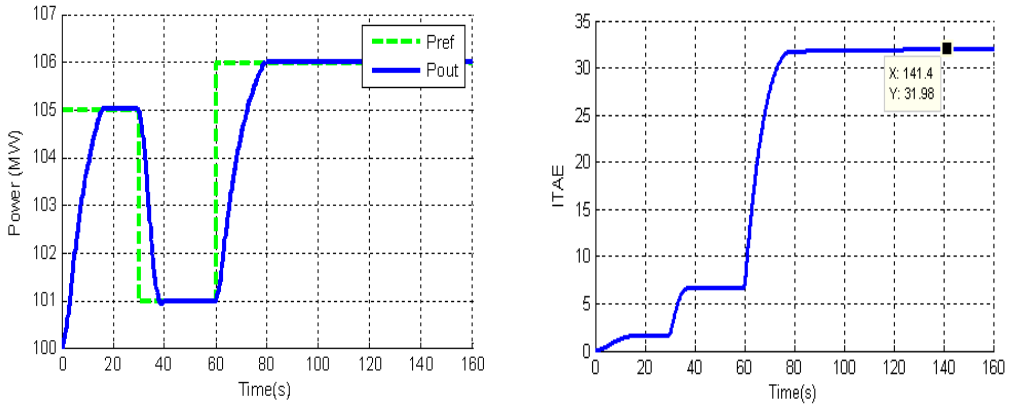

Figure 4-29 Performance when present leaks are not specified in controller

In this scenario the response of the plant model incorporating leaks is investigated. The model used by the controller does not incorporate leaks. The index of the output response is 31.99. It is interesting that the performance is better than in the first scenario. It appears that this disturbance favours performance. This is an issue which should be looked at in the future. Under normal circumstances, performance should deteriorate when a disturbance is introduced.

Scenario 3

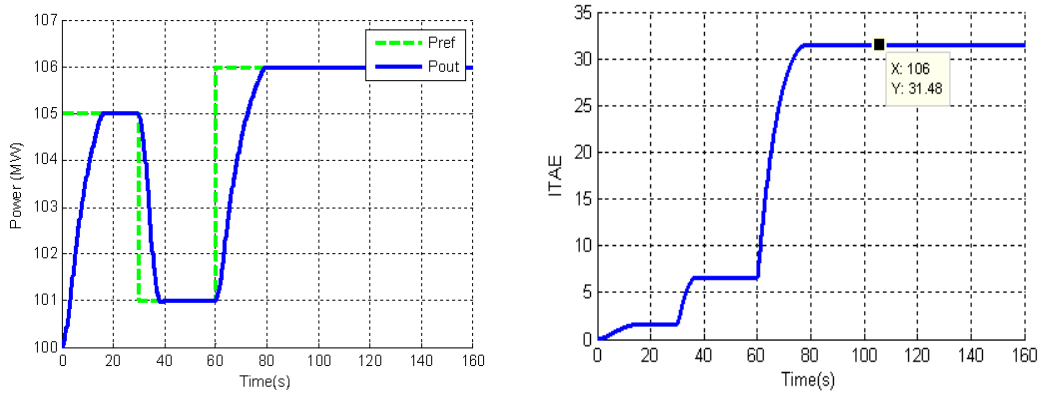

Figure 4-30 Performance when leaks are specified in MPC controller

In this scenario both the MPC controller model and the plant model included leaks. The controller performed better when the controller incorporated the disturbance. There was

an improvement from 31.99 to 31.48. The above result shows that performance is better when known disturbances are incorporated by the MPC controller. Table 4-13 shows a summary of the results.

Table 4-13 Summary of including leak flows

Scenario No.	Model used by MPC controller	Actual plant	ITAE index
1	No leaks	No leaks	32.18
2	No leaks	Leaks included	31.98
3	Leaks included	Leaks included	31.48

In order to have a more complete view of the effect of all the disturbances, six different trajectories for the load (expected load or reference power) were applied to the system. The reference signals are shown in Figure A-21. The results are recorded in Table A-3 to A-6 in the appendix. Conclusions which can be drawn from the results are the same as above.

4.7 Conclusion

Model predictive control was implemented in this chapter. All the control mechanisms were implemented using only two actuators. Firstly, the system response was used to determine the most suitable MPC parameters. The plant model responses for three control mechanisms were approximated using FOPTD models which were used to obtain ranges of tuning parameters for the MPC controller. After looking at the influence of each tuning parameter on the plant response, the best set of parameters was chosen and implemented on the Brayton-cycle power plant. The ITAE index was used as a performance measure. Previously, genetically optimised PID control had been applied to the plant. The results of this control strategy were compared with the results obtained when the MPC controller is used. MPC control had a performance index of 23.46 while optimised PID control had an index of 24.62.

The plant models used did not incorporate disturbances. Therefore, the performance of the plant in the presence of disturbances was investigated. It was found that disturbances to

affect the plant output response but with carefully tunned MPC controller load following can be assured under normal circumstances. The magnitude and speed of control actions was found to have a telling effect on the overall performance with and without disturbances. Tradeoffs have to be made. Therefore, more plant and controller analysis is necessary in order to assess all possible scenarios. This should be a prerequisite in designing the controller.

Chapter 5

Conclusions and recommendations

5.1 Introduction

In this dissertation the problem of controlling the power output of a Brayton cycle based power plant optimally, under normal load following conditions was addressed. Further work was carried out to analyse the effect of disturbances. The control problem was tackled in a number of phases. Firstly, the evaluation platform to be used in evaluating model predictive control was finalised. This platform was a Simulink® model. The next phase was to investigate the response of the system in order to determine which control mechanisms were needed to answer this control problem. The third phase was to find a method to systematically determine parameters necessary for this control strategy. Lastly performance of this control strategy under unfavourable conditions was investigated. This chapter highlights how these problems were tackled. It also looks at possible future work that can be done.

5.2 Concluding remarks

In order to investigate model predictive control a linear model of the plant was needed. It was decided to use a linear Simulink® model of the plant that had been used previously in investigating other control strategies, namely PID control and genetically optimised PID control. A state-space model of the plant needed to implement the control strategy was also automatically extracted from the Simulink® model using Matlab. The linear Simulink® model was used as a test platform for model predictive control.

Previous work had showed that all the necessary control actions could be implemented using only two actuators. These actuators are valves. It was found that two way valves are necessary to implement all the control mechanisms. Real valves are constrained systems. These constraints had to be quantified and in order to incorporate them in an optimisation function used to calculate control moves. A trial and error approach was used.

This control strategy used the extracted state-space model to predict the response of future control moves. Therefore, apart from quantifying the constraints, the best sampling time, prediction and control horizons had to be determined. Further adjustments would have to be implemented therefore determining suitable weights was part of the work. Also investigated was how to derive a state-space plant model from physical principals. This was done for verification purposes.

A systematic method was found and suitably adjusted to solve this problem. Good performance "bands" or range of values was established for each parameter. Plant performance as parameters within these bands varied was investigated. This was in order to strategise on which method or approach to use obtain the best parameters in each range that would ensure that the desired control performance is achieved. Due to the high number of tuning parameters affecting the plant performance, it was found that establishing relationships between performance and certain tuning parameter values was a non-trivial endeavour. In some cases the relationship appeared to be non-linear. Adding to the complexity in this task is the fact the influence of one parameter may as well negate the effect of another.

An empirical approach was decided on and used to choose the best parameters from each band or range. The set of parameters which outperformed the rest was $P = 24\ s, M = 4\ s$, $R = 0.003$ and $T = 1\ s$. Lower sampling periods proved unreliable. This was attributed to the initial sampling time specification when the state-space model was extracted. It was one second. Smaller sampling periods probably resulted in poorly conditioned mathematical states causing the plant to be unstable.

Using the chosen parameters, plant performance under various conditions was then carried out. Good responses were shown by the controller. Following this, comparisons were made with other control strategies used previously in the plant. An improvement of 1.16 in the ITAE index was realised using the model predictive control strategy when compared to the optimised PID control strategy. This is depicted in the Figure 6-1.

Effect of plant disturbances was carried out. It was found that this should be incorporated within the initial strategy of obtaining the best MPC controller. Plant disturbances were investigated and quantified. These where then used to further analyse MPC tuning

parameters. Based on the findings, thorough knowledge of the plant conditions during operation of the plant are necessary when designing a good MPC controller. This is because all the tuning parameters cause the system to exhibit certain properties of concern to the designer. These properties include load following abilities, disturbance rejection and stability. Their effect on different disturbances was found to differ therefore trade-offs have to be made.

The disturbance analysis also shows that the chosen MPC parameter values perform reasonably well even in the face presence of disturbances. Table 6-1 shows the variation in performance that each parameter exhibited for different types of disturbances.

Table 6-1 Overall performance of the control strategy with disturbances

Plant performance in presence of disturbances					
Control horizon	**Prediction horizon**	**Controller output leaks ITAE**	**Grid Load increase ITAE**	**Grid Load decrease ITAE**	**ITAE index**
4	73	8.24 √	13.68	12.39 x	38.49
4	60	8.247	13.01	11.75	38.49
14	45	451.5	12.97	9.4	694.3 x
19	24	49.13	16.98 x	9.86	217.9
14	24	39.21	9.211 √	8.86 √	61.35
9	24	8.84	10.27	9.04	42.73
4	24	8.323*	11.31 *	9.60*	37.22 *√
2	20	10.26	11.45	11.51	39.46

The “√” indicates best performance while “x” indicates worst performance. The asterisk shows the performance of the chosen parameter.

5.3 Future work

Model predictive control is not a very widely used control strategy. There is still a lot of research to be done on MPC. The empirical method used in this study can be further refined to include the population of all possible values. Furthermore, already established techniques such as genetic algorithms can be investigated as a means of optimising the MPC parameter selection.

The limitations imposed by the sampling time in the evaluation platform which resulted in mathematical ill-conditioning during calculations can be negated or improved upon in future research.

One of the assumptions made was a constant grid speed. However, when it came to modeling grid disturbances, this assumption is not realistic. Therefore, the evaluating platform needs to be improved upon in this regard.

The linear model of the power plant used as a test-bed for the control strategy can be improved upon by modeling more effects. The plant was modelled at a single operating point. The control strategy can be implemented on multiple operating points to model all operating modes. Better still, a non-linear model can be derived.

5.4 Closing remarks

The goals in terms of using Model Predictive Control in controlling the power output of a Brayton cycle based power plant were achieved and the foundation for further research in control optimisation was laid.

References

[1] A. C. Kadak, "Excitement builds for high temperature," in *High Temperature Reactor Conference*, Washington, DC, 2008, pp. 5.

[2] K. Uren, "Optimal Control of a Brayton Based Power Plant," M.Eng. dissertation. school Elect. and Electr. Eng.,NWU,Potch.,SA, 2005.

[3] C. Barron. (2010, Feb). More nuclear power 'a no-brainer' for future, Business *Times (South Africa)* [Online]. Available: http://www.pbmr.com/index.asp?Content=212

[4] K. Kemm. (2010, Apr). South African-developed PBMR will ensure that nuclear is the power source of the future , *Engineering News* [Online]. Available: http://www.engineeringnews.co.za/article/south-african-developed-pbmr-will-ensure-that-nuclear-is-the-power-source-of-the-future-2011-04-01

[5] P. K. N. Kumar, A. Tourlidakis, and P. Pilidis, "Performance Review: PBMR Closed Cycle Gas Trubine Power Plant," in *IAEA Technical Committee Meeting on "Gas Turbine Power Conversion Systems for Modular HTGRs* [Online], Palo Alto, CA, 2000. Available: **www.iaea.org/inis/collection/NCLCollectionStore/_Public/./32047835.pdf** [Date of access: Aug. 2011].

[6] Chris Barron, (2010, Feb, 14).More Nuclear Power 'a No-Brainer' for Future, *PBMR*. [Online]. Available: **http://www.pbmr.co.za/index.asp?Content=217&Article=119&Year=2010** [Date of access: Aug. 2010].

[7] O Manyathi. (2004, Mar). Nuclear manufacturing blueprint emerging, *Engineering news* [Online]. Available: http://www.engineeringnews.co.za/article/nuclear-manufacturing-blueprint-emerging-2004-03-29 [Date of access: Sep. 2011].

[8] C McKune. ().Pebble bed modular reactor demonstration plant is funded but not constructed, *South African Journal of Science*, *106(5-6)* [Online]. Available: http://www.scielo.org.za/scielo.php?pid=S0038-23532010000300002&script=sci_arttext [Date of access: Sep. 2011].

[9] M Gosling. (2010, February) *iOLtechnology*. [Online]. Available: http://www.iol.co.za/scitech/technology/pbmr-company-running-out-of-money-1.473992 [Date of access: Sep. 2011].

[10] S. Burger.(2011, Aug). Nuclear research paralysis in SA despite nuclear build programme, *Engineering news* (South Africa) [Online]. Available:,

http://www.engineeringnews.co.za/print-version/nuclear-research-paralysis-in-sa-despite-nuclear-build-programme-2011-08-19

[11] J Holman. (2010, March). Desalination could comprise up to 10% of South Africa's urban water supply mix by 2030, *Engineering news.* [Online]. Available: http://www.engineeringnews.co.za/article/desalination-could-comprise-up-to-10-of-sas-water-supply-mix-by-2030-2010-03-05 [Date of access: Aug. 2009].

[12] (2011, July) *World Nuclear Association*. [Online]. Available: http://world-nuclear.org/info/inf04.html [Date of access: Nov. 2010].

[13] A. P. George, "Introduction to the Pebble Bed Modular reactor," PBMR, Pretoria, SA, Tech. Rep. 009949-185, 2001.

[14] K. Hu and J. Yuan. (2008). Multi-model predictive control method for nuclear steam generator water level, *Energy Conversion and Management*, *49*, pp. 1167-1174.

[15] H. Kwakernaak and R. Sivan, *Linear optimal control systems*. New York: Wiley, 1972.

[16] J. S. Qin and T. A. Badgwell. (2003) A survey of industrial model predictive control technology, *Control Engineering Practice* [Online], *11*, pp. 733–764. Available: www.sciencedirect.com

[17] C. E. Garcia, D. M. Prett, and M. Morari. (1989). Model predictive control: Theory and practice- a survey, *Automatica, 25(3)*, pp. 335-348.

[18] C. E. Garcia. (1986) *Advances in Model Predictive control*. [Online]. Available: http://drum.umd.edu/bitstream/1903/4475/1/TR_86-50.pdf [Date of access: Feb. 2010].

[19] J. B. Burl, *Linear Optimal Control, H2 and Hoo Methods*. Menlo Park, CA: Addison Wesley, 1999.

[20] T. B. S. Zhenhua, "Multiple Model Predictive Control framework for multi-input multi-output continuous processes," Ph.D. Thesis, Texas Tech. Univ., 2003.

[21] P. J. Antsaklis and A N MicUel, *Linear System*. New York: McGraw-Hill, 1997.

[22] T. KaUath, *Linear Systems*. Englewood Cliffs, NJ: Prentice-HalL, 1980.

[23] Y. Arkun and G. Stephenopoulos, "Studies in the Synthesis of control structures for chemical processes: Part IV. Design of steady state optimizing control structures for chemical process units," *AiCHE*, vol. 26, no. 975, 1980.

[24] C. R. Cutler and B. L. Ramaker, "Dynamic matrix control - a computer control algorithm," in *Automatic control conference*, 1980.

[25] S. M. Ranade and E. Torres. (2009, Mar). From Dynamic mysterious control to Dynamic manageable control, *Hydrocarbon Processing*, pp. 77 – 81.

[26] J. Doyle. (1982). Analysis of feedback systems with Structure uncertainities, *IEEE Proc*, *129*, pp. 242-250.

[27] J. A. Richalet, J L Rault, Testud, and J Papon. (1978). Model predictive heuristic control: Application to industrial processes, *Automatica*, *14*, pp. 413–428.

[28] C. Cutler, A. Morshedi, and J. Haydel, "Perspective on advanced control.," in *AICHE Ann. meet.*, Washington, DC, 1983.

[29] J. B. Froisy and T. Matsko, "IDCOM-M application to the Shell fundamental control problem," in *AIChE Ann. meet.*, 1990.

[30] B. J. Froisy, (2006, Jul). Model predictive control: Building a bridge between theory and practice, *Computers and Chemical Engineering* [Online], *30*, pp. 1426–1435. Available: www.sciencedirect.com

[31] L. Wang, *Advances in Industrial Control: Model Predictive Control System Design and Implementation using Matlab*. Melbourne, Australia: Springer-Verlag London Limited, 2009.

[32] M. G. Na .(2001, Feb). A Model Predictive Controller for the water level of nuclear steam generators, *Journal of the Korean Nuclear Society*, *33(1)*, pp. 102-110.

[33] M. G. Na.(2001, Oct). Auto-Tuned PID Controller Using a Model Predictive Control Method for the Steam Generator Water Level, *IEEE Transactions on Nuclear Science*, [Online], *48(5)*. pp. 1664 - 1671. Available; http://ieeexplore.ieee.org/stamp/stamp.jsp?arnumber=00960354

[34] E. Irving, C. Miossec, and J. Tassart, "Toward efficient full automatic operation of the pwr steam generator with water level adaptive control," in *2nd Int. Conf. Boiler Dynamics and Control in Nuclear Power Stations*, Bournemouth, U.K., 1979, pp. 309-329.

[35] M. G. Na, Y. R. Sim, and Y. J. Lee. (2003, Feb). Design of an Adaptive Predictive Controller for Steam Generators, *IEE Transactions on Nuclear Science*[Online], *50(1)*. Available: http://ieeexplore.ieee.org/stamp/stamp.jsp?arnumber=01178709

[36] M. G. Na, W. C. Kim, and S. H. Shin(2003, Oct) A model predictive controller for nuclear reactor power, *Journal of the Korean Nuclear Society* [Online],*35(5)*, pp. 399-411. Available: http://article.nuclear.or.kr/pub/jknspaper.php?jid=JK0350399

[37] M. G. Na. (2005, Aug). A Model Predictive Controller for Load-Following Operation of PWR Reactors, *IEEE Transactions on Nuclear Science* [Online], *52(4)*. pp. 1009 - 1020 Available: http://ieeexplore.ieee.org/xpls/abs_all.jsp?arnumber=1495798

[38] A Zuheir, "Fuzzy Model Predictive Control Algorithm Applied in Nuclear Power Plant," in *2006. ICTTA '06. 2nd Ann*. *Information and Communication Technologies, Damascus, SY*, pp. 1410 - 1415.

[39] HouSu-xia, LiChong and Z. T. Yun. (2010, Jun). An improved implicit multiple model predictive control used for movable nuclear power plant, *Nuclear Engineering and Design*.

[40] G. Xia, J. Xu and W. Zhang. (2008). Multivariable Integrated Model Predictive Control of Nuclear Power Plant, *International Journal of Control and Automation* [Online]. Available: www.sersc.org/journals/IJCA/vol1_no1/papers/01.pdf

[41] A. G. Parlos, S. Parthasarathy, and A. F. Atiya, (2001, sep). Neuro-Predictive Process Control Using On-Line Controller Adaptation, *IEEE Trans. Control Systems Technology* [Online], *9(5)*, pp. 741 - 755. Available: ieeexplore.ieee.org › ... › Journals › Control Systems Technology, IE

[42] A. J. S. Filho and E. Ruppert, "A predictive direct power control of doubly-fed induction generator," in *2010 IEEE Int. Conf. Industrial Technology* Vi a del Mar, pp. 1721 - 1726

[43] T. Peni and G. Szederkenyi. (2009). Model predictive control for the hybrid primary circuit dynamics of a pressurized water nuclear power plant, *Periodica Polytechnica Electrical Engineering* [Online]. *53*, pp. 37-44. Available: daedalus.scl.sztaki.hu/PCRG/works/publications/Peni2009.pdf

[44] M. Kuure-Kinsey and W. B. Bequette. (2010, Jul). Multiple Model Predictive Control Strategy for Disturbance Rejection, *Ind. Eng. Chem. Res*, *49(17)* [Online]. pp 7983-7989. Available: pubs.acs.org/doi/abs/10.1021/ie100093c

[45] M. Lundh and M. Molander, "State-Space Models in Model Predictive Control." *ABB Automation Products AB,* Västerås, CH, Rep. 721 59, 2000. Available: www05.abb.com/global/scot/scot267.nsf/.../tp_lundh_molander.pdf

[46] C. R. van Niekerk, J. F. Pritchard, G. van Schoor, and M. A. van Wyk. (2006, March). Linear model of a closed three shaft Brayton cycle, *South African institute of Electrical Engineers* [Online], *97(1)*. Available:

www.saiee.org.za/files/File/vol97_no1/Vol97_No1_7.pdf

[47] S. Thomas. (2005, September) The Economic Impact of the Proposed Demonstration Plant for the Pebble Bed Modular Reactor Design. [Online]. Available: www.psiru.org/reports/2005-09-E-PBMR.pdf [Date of access: July 2011].

[48] A. Haitham, "Analyzing State-Space Characteristics," Presentation,Dept. Elect. eng.,Kuwait University,. [Online] Available: http://electron1.eng.kuniv.edu.kw/LABVIEW/labview.html [Date of acceses: May 2011]

[49] R. C. Dorf and R. H. Bishop, *Modern Control Systems*, 9th ed., Marcian Horton, Jennie Diblasi, and Scott Dissano, Eds. UpperSaddle River, New Jersey, U.S.A: Prentice-Hall inc, 2001.

[50] T. Kailath, *Linear Systems*. Englewood Cliffs, NJ: Prentice Hall Inc, 1980.

[51] D. G. Luenberger, *Optimisation by Vector Space Methods*. New York: John Wiley and Sons, 1969.

[52] D. A. Wismer and R. Chattergy, *Introduction to Nonlinear Optimisation, a Problem Solving Approach*. New York: North-Holland, 1978.

[53] B. D. O. Anderson and J. B. Moore, *Linear Optimal Control*. Englewood Cliffs, NJ: Prentice-Hall, 1971.

[54] W. H. Kwon and S. Han, *Receding Horizon Control- model predictive control forstate models*. London, U.K. Springer, 2005.

[55] V Exadaktylos, C J Taylor, and A Chotai, "Model Predictive Control using a non-minimal state space form with an integral -of-error state variable," in *UKACC International Conference on Control 06*, Glasgor, UK, 2006, Paper 72.

[56] L. Wang and P. C. Young.(2006) "An inproved structure for model predictive control using non-minimal state space realizzation," *Journal of Process Control*, vol. 16, pp. 355-371. Available: linkinghub.elsevier.com/retrieve/pii/S0959152405000910

[57] D Dougherty and D. Cooper. (2003, Feb) "A practical multiple model adaptive strategy for single-loop MPC," *Control Engineering Practice* [Online], *11(2)*, pp. 141-159. Available: www.ingentaconnect.com/content/els/09670661/2003/.../art00106

[58] J. O. Trierweiler and L. A. Frarina. (2003, Mar). "RPN tuning strategy for model predictive control," *Journal of Process Control* [Online], *13(7)*, pp. 591-598. Available: www.sciencedirect.com/science/article/pii/S0959152402000938

[59] B. Vroemen, "Model Predictive Control of a Gas Turbine Installation," Eindhoven University of Technology, WFW report. 97.002, 1997.

[60] J. F. Pritchard, " Plant control: Development of a Linear Model of the Brayton Cycle," PBMR., 013202-318, 2002.

[61] *Process modelling*, 5th ed. NWU,Potchefstroom, South Africa, 2007.

[62] O. Rubin and J. Pritchard, "Dynamic modelling for control of a new generation nuclear power station," PBMR, 2002. [Online] Available: http://www.nt.ntnu.no/users/skoge/prost/proceedings/afcon03/Papers/095.pdf [Date of access: October 2010]

[63] 2007. Matlab® Version 7.5 Release 2007b, "Model predictive control Toolbox 2.3 Release notes".

[64] S. Skogestad. (2003, jun). Simple analytic rules for model reduction and PID controller tuning, *Journal of Process Control* [Online], 13(4), pp. 291–309. Available: www.nt.ntnu.no/users/skoge/publications/2003/tuningPID/.../mic.pdf

[65] A. J. Isakssona and S. F. Graebeb. (1999, Jun). Analytical PID parameter expressions for higher order systems, *Automatica* [Online] , 35(6), pp. 1121-1130. Available: www.sciencedirect.com/science/article/pii/S0005109899000096

[66] J. M. Robles. (2002) Simulation of a Gas power plant," Dept. Chem. Eng., Norwegian Univ. science and Tech. 2002[Online]. Available: http://www.nt.ntnu.no/users/skoge/diplom/prosjekt02/Robles-Pujals/gaspowerplant.pdf [Date of access: Jul 2011].

[67] B. Huang and R. Kadali, *Dynamic Modeling, Predictive Control and Performance Monitoring: A Data-driven Subspace Approach*. London, UK: Springer-Verlag London Limited , 2008.

[68] C. Wang, "Design, analysis and optimisation of the power conversion system for the modular pebble bed reactor system," Ph.D. dissertation, Nuc. Eng. dept.,Massechussets institute of technology, Cambridge, MA, 2003.

[69] C. Barton, "A Primier on Nuclear Safty: 2.5 Defence in depth," *Uncategorized*, October 2008. [Online] Available: http://energyfromthorium.com/2008/10/13/a-primer-on-nuclear-safety-2-1-defense-in-depth/

[70] A. Koster and D. Lee, "The PBMR containment system, "in *2nd International tropical Meeting on high temperature reactor technology*, Beijing, China, 2004.

[71] S. Shokooh, T. Khandelwal, F. Shokooh, J.s Tastet, and J. J. Dai, "Intelligent load shedding need for a fast optimal solution," in *IEEE Petroleum and Chemical Industry technical Conference*, Basel,CH, 2005.

[72] B Thompson. (2001, January) Calculate and measure noise values. *Test and measurement world*. [Online]. Available: http://www.tmworld.com/article/322275-Calculate_and_measure_noise_values.php [Date of access: September 2011].

[73] B. Carterand R Mancini, "Op Amp Noise Theory and Applications," in *Op Amps for Everyone,* 2nd ed. Dallas, TX, Texas instruments. 2008 [Online]. Available: http://www.ti.com/lit/ml/sloa082/sloa082.pdf [Date of access: October 2011].

[74] J S Bay, *Fundamentals of Linear State Space Systems*. Boston: WCB/McGraw-Hill, 1999.

[75] B. Majumdar, *Fluid Mechanics with laboratory manual*, New Delhi, India: PHI Learning private Ltd., 2011, pp. 386.

[76] S. V. Vaseghi, Advanced digital signal processing and noise reduction, *4*th ed. West Sussex, UK: Houghton Mifflin Company, 2009.pp. 37.

[77] "Choked Flow of Gases" [Online]. Available: http://www.therebreathersite.nl/04_Links/Downloads/Choked.pdf [Date of access: February 2012]

Appendix A

A.1 A state-space model

In our time-invariant state space equations, we write these matrices and their relationships as:

$$x_m(k+1) = A_m x_m(k) + B_m u(k)$$

$$y_m(k) = C_m x_m(k) + D_m u(k),$$

We have four constant matrices: A_m, B_m, C_m, and D_m. These matrices as described below [**50**]:

Matrix A_m,

is the **system matrix**, and relates the current state to the state change *x'* . A zero matrix implies that the state change is not dependent on the current state

Matrix B_m

is the **control matrix**, and determines how the system input relates to the state change. If the state change is independent of the system input, then *B* will be the zero matrix.

Matrix C_m,

is the **output matrix**. It determines the relationship between the system states and the system output.

Matrix D_m.

is the **feed-forward matrix**, showing how the system input affects the system output directly. The state space model of the system has the D_m matrix equal to the zero matrix.

A.2 Eigen values for the augmented model

The characteristic polynomial equation of the augmented plant model given by [**32**] is,

$$\rho(\lambda) = det\begin{bmatrix} \lambda I - A_m & o_m^T \\ C_m A_m & \lambda I - I_{q\times q} \end{bmatrix}$$

$$\rho(\lambda) = (\lambda - 1) det(\lambda I - A_m) = 0$$

The determinant of a block lower triangular matrix equals the product of the determinants of the matrices on the diagonal. Therefore, the eigenvalues of the augmented model are made up of the eigenvalues of the plant model and the *q* eigenvalues, $\lambda = 1$. This means that there are

q integrators embedded into the augmented design model [**32**].

A.3 Kalman filter

The Kalman filter is described in [**32**].For a multi-output system, the observer gain matrix, K_{ob}, is calculated recursively using the Kalman filter. The state space model is modified to include stochastic disturbance models as shown below:

$$x_m(k+1) = A_m P(i) C_m^T(k) + B_m u(k) + d(k)$$

$$y_m(k) = C_m x_m(k) + \xi(k).$$

Covariance matrices for the disturbance matrices are defined by,

$$E\{d(k)d(\tau)^T\} = \theta\delta(k-\tau)$$

$$E\{\xi(k)\xi(\tau)^T\} = \Gamma\delta(k-\tau),$$

where the impulse response $\delta(k-\tau) = 1$ for $k = \tau$ and zero otherwise. Riccati equations follow.

$$P(0) = E\{[x(0) - \hat{x}(0)][x(0) - \hat{x}(0)]^T\},$$

$$P(i+1) = A_m\{P(i) - P(i)C_m^T(\Gamma + C_m P(i) C_m^T)^{-1} C_m P(i)\}A_m^T + \theta,$$

The solution for the Riccati equation $P(i+1)$ need not be calculated in real time. Similarly, the observer is calculated offline. This is sufficient for predictive control applications.

$$K_{ob}(i) = A_m P(i) C_m^T \left(\Gamma + C_m P(i) C_m^T(k)\right)^{-1}.$$

When the all states are stable and can be seen at the output, the system (A_m, C_m) is detectable. In addition to this, if the system is stabilisable $\left(A_m, \theta^{1/2}\right)$ at time $k \to \infty$ the steady state solutions for $K_{ob}(i)$ and $P(i+1)$ satisfy the discrete time Riccati equation:

$$P(\infty) = A_m\{P(\infty) - P(\infty)C_m^T(\Gamma + C_m P(\infty) C_m^T)^{-1} C_m P(\infty)\}A_m^T + \theta \text{ and}$$

$$K_{ob}(\infty) = A_m P(\infty) C_m^T (\Gamma + C_m P(\infty) C_m^T)^{-1}.$$

A.4 Quadratic programming: Kuhn-Tucker conditions

An objective function J is defined as a Lagrange expression.

$$J = \frac{1}{2} x^T E x + x^T F + \lambda^T (Mx - \gamma)$$

Partial differentiation of J with respect to λ and x and equating the expressions to zero are a basis for necessary conditions for optimisation known as Kuhn -Tucker conditions. These can be expanded and used to specify active and inactive constraints. If S_{act} denotes the index set of active constraints these conditions are expressed as follows.

$$Ex + F + \sum_{i \in S_{act}} \lambda_i M_i^T = 0\,,$$

$$M_i x - \gamma_i = 0 \quad i \in S_{act}\,,$$

$$M_i x - \gamma_i < 0 \quad i \notin S_{act}\,,$$

$$\lambda_i \geq 0 \quad i \in S_{act}\,,$$

$$\lambda_i = 0 \quad i \notin S_{act}\,,$$

where the vector λ contains the Lagrange multipliers [**32**].

When a constraint is inactive i.e. $i \notin S_{act}$, the corresponding Lagrange multiplier is zero. Conversely, when a constraint is active i.e. $i \in S_{act}$, the corresponding Lagrange multiplier is non-negative. A constraint is inactive when it is satisfied. When all active constraints are known only inequality constraints would be used. Identifying these constraints together

with the programming procedure are not straight forward tasks. Active set methods or primal dual methods can be used. These can be found in literature.

A.5 Model characteristics

From the transfer functions in pole zero format the following information was extracted.

For transfer function $G_1(s)$, gain =-530.50×10^3,

Table A-1 Poles, zeros and gain of G_1(s)

Zeros	Poles	Time Constant (s)	Settling time (s)
-23.9895	-26.1052	0.003830654	0.1915
-6.0060	-9.9788	0.1002124504	0.501
12.0960×10^{-3}	-18.0527×10^{-18}	5.539×10^{16}	2.7697×10^{16}
$-755.39 \times 10^{-3}+452.86 \times 10^{-3}i$	-96.9114×10^{-3}	10.3187	51.5935
$-755.39 \times 10^{-3} - 452.86 \times 10^{-3}i$	$-795.83 \times 10^{-3}432.95 \times i$		
-677.062×10^{-3}	$-795.8266 \times 10^{-3} - 432.95 \times 10^{-3}i$		
	-953.23×10^{-3}	104.9061457	524.53

For transfer function $G_2(s)$, gain = -5.3696×10^3

Table A-2 Poles, zeros and gain of G_2(s)

Zeros	Poles	Time Constant (s)	Settling time (s)
-73.771	-26.1052	0.003830654	0.1915
39.0980	-9.9788	0.1002124504	0.501
-39.8468	-18.05×10^{-18}	5.539×10^{16}	2.7697×10^{16}
$-842.25 \times 10^{-3}+529.38 \times 10^{-3}i$	-96.91×10^{-3}	10.3187	51.5935
$-842.25e \times 10^{-3} - 529.38 \times 10^{-3}i$	$-795.83 \times 10^{-3} + 432.95 \times i$		
-795.0561×10^{-3}	$-795.83 \times 10^{-3} - 432.9488 \times 10^{-3}i$		
	-953.23×10^{-3}	104.9061457	524.53

There is a positive zero in both transfer functions and this is the cause of the minimum phase effect. Its effect is more apparent in $G_2(s)$ which has a larger positive value. There is a pole at -18.05$\times 10^{-18}$. In the true sense, this pole is actually a zero. The non-zero value is due to the fact that the extracted model is an approximation and not the exact model.

A.6 MPC controller

A.6.1 Design tool

When the MPC toolbox is opened and the plant being used is imported (Figure A-1), the designer can then specify the value for each parameter [**63**].

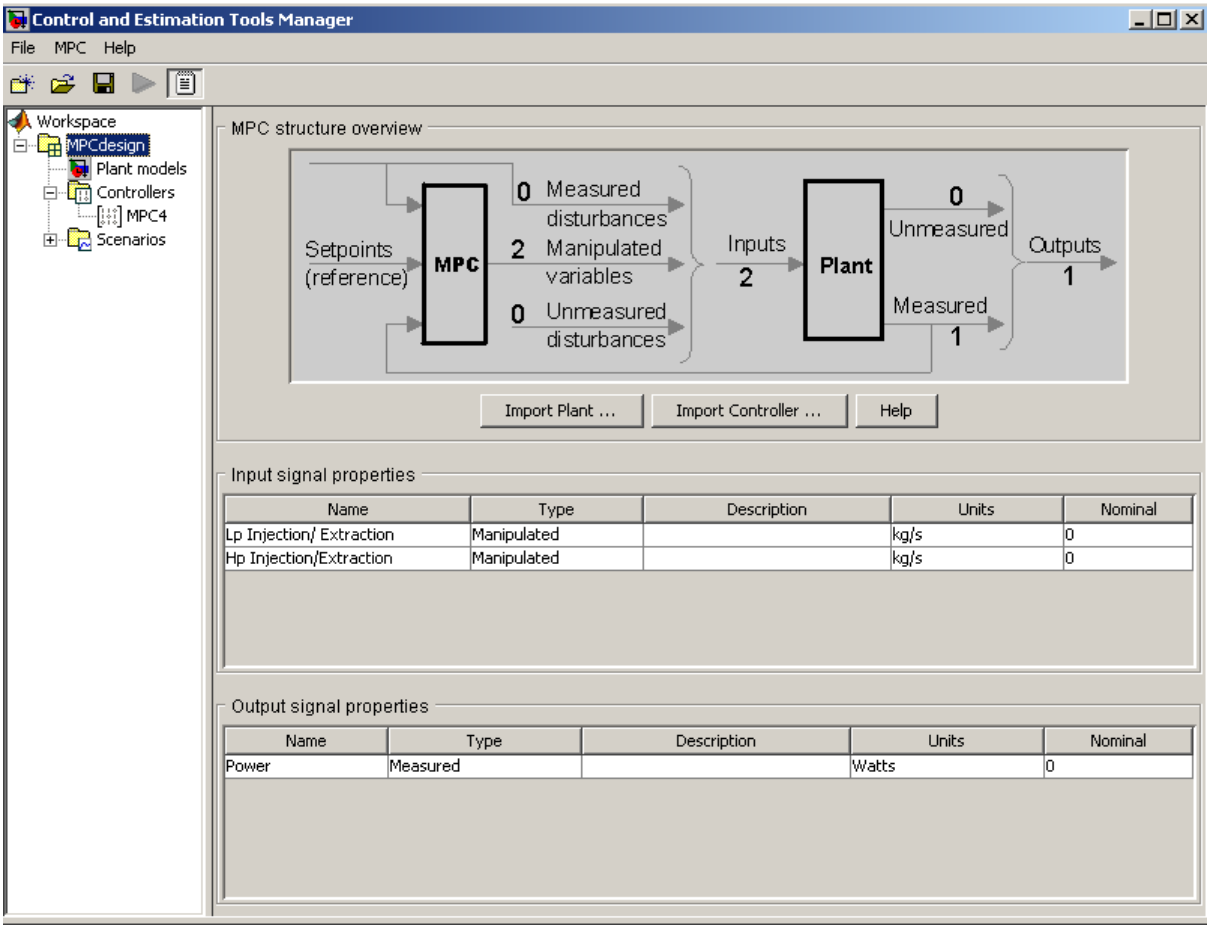

Figure A-1 Mpctool interface to specify the plant model

The first window deals with the control interval, the control horizon and the prediction horizon as shown in Figure A-2.

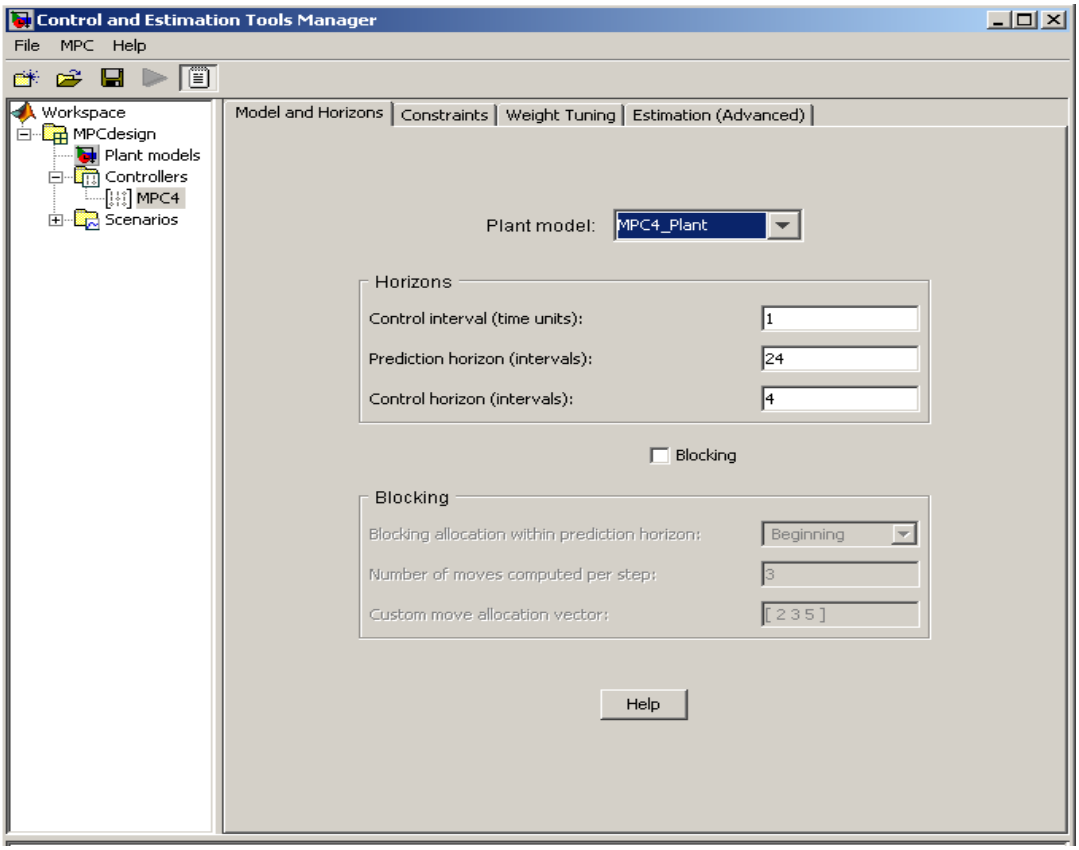

Figure A-2 Mpctool: Model horizons dialogue box

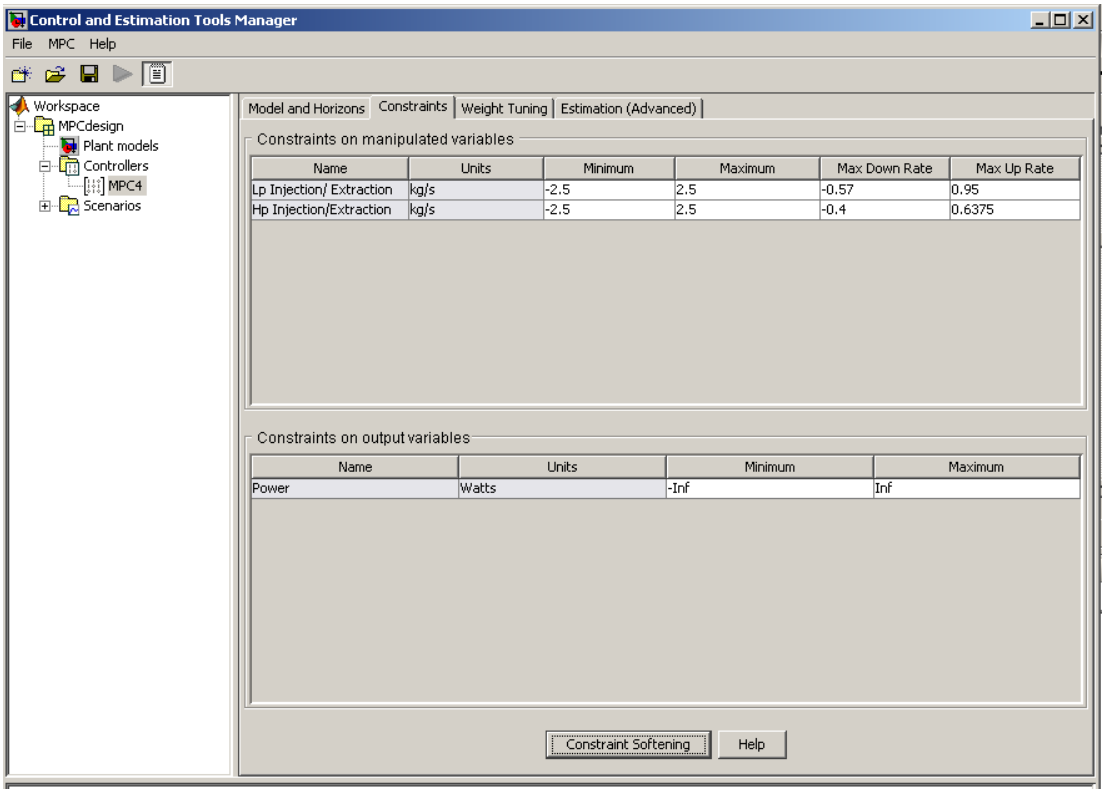

Figure A-3 Mpctool: Constraints specification

When the Constraint softening button is pressed a new window opens. The sliding bar at the bottom is used to specify the hardness of the constraints. Allowances to the constraints can also be specified within the “bands”.

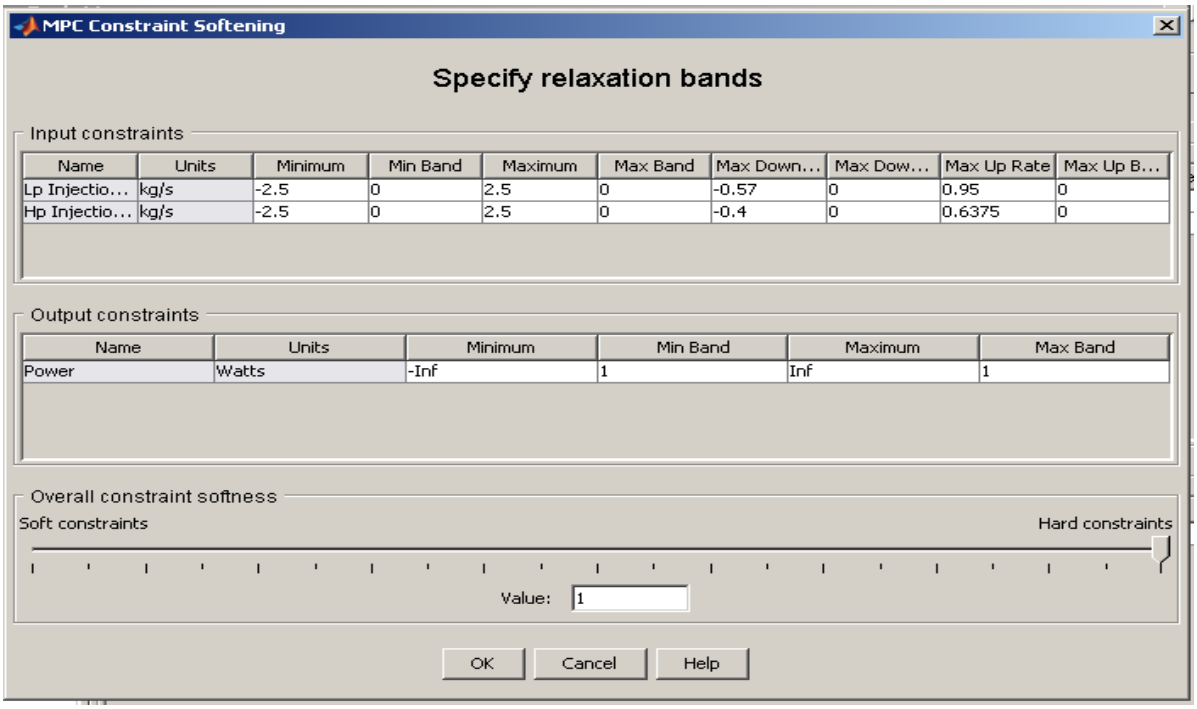

Figure A-4 Mpctool: Detailed constraints specification

The input weight,R, can also be specified. In this case, $R = 0.003$

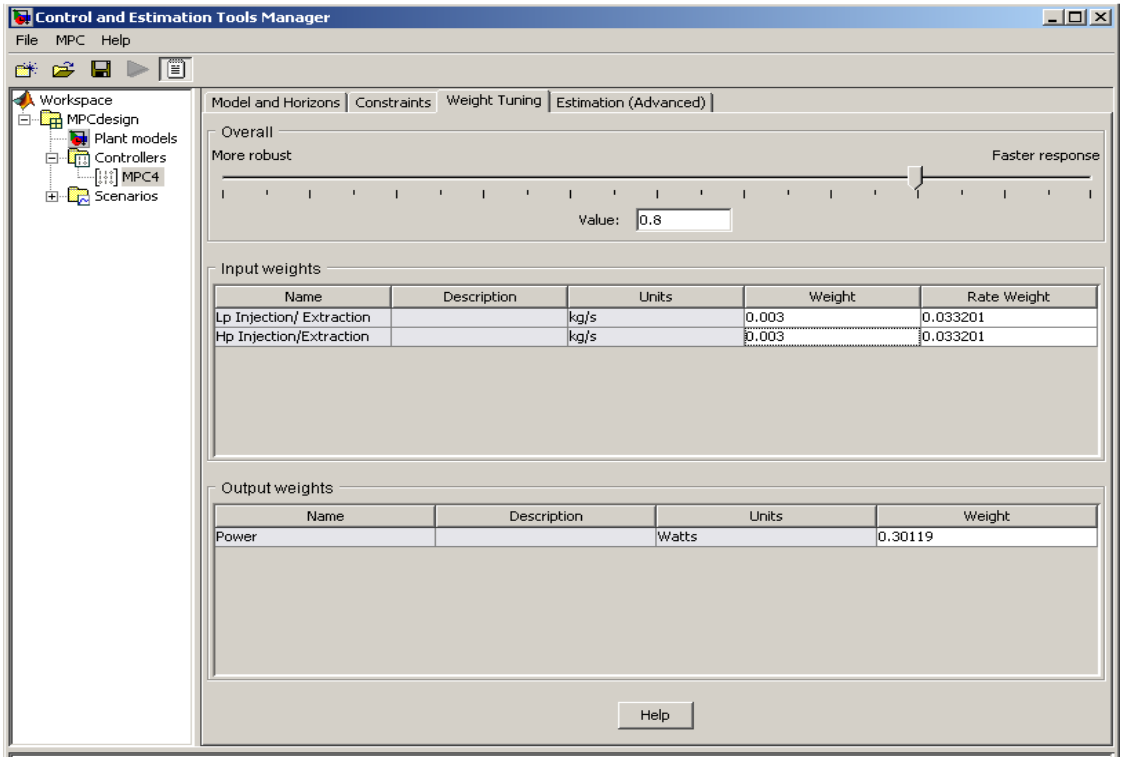

Figure A-5 Mpctool: Output and move suppression weights

No noise was specified initially. A noise free environment was assumed.

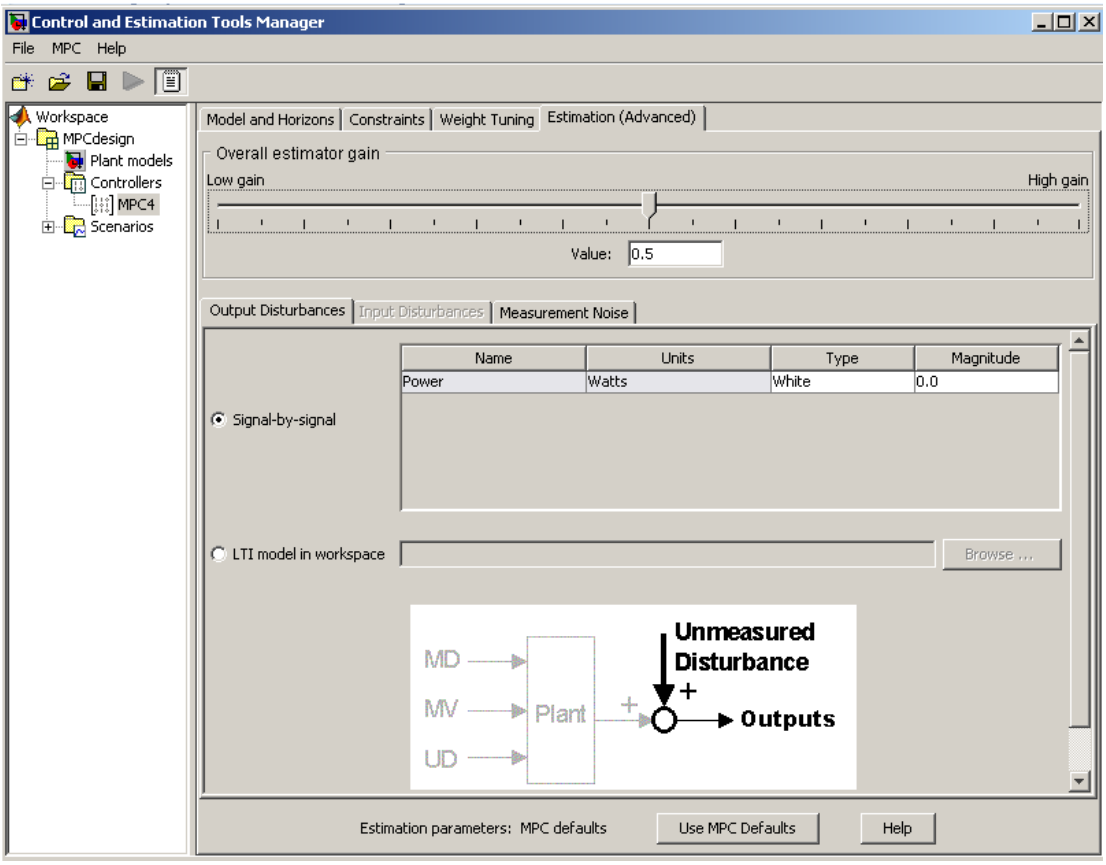

Figure A-6 Mpctool: Noise specification

A.6.2 Matlab® code for constraints specification

In the analysis, these parameters were changed via matlab® code. For example, for an MPC controller called MPC4, the following code can be used to manipulate the parameters in the controller.

Extract from an m-file

```
MPC4.Ts=ts(i);tt= MPC4.Ts; % alters Ts
MPC4.ControlHorizon=Mc(l);mm=MPC4.ControlHorizon;%
MPC4.P=Pr(k);pp=MPC4.P; %alters P
MPC4.W.ManipulatedVariables=[R(j) R(j)];% alters R
%MPC1.W.OutputVariables=1;
%MPC1.W.OutputVariables=1;
clear MPC4.MV
                    mv1rmin=MPC4.Ts.*(-0.57);
                    mv1rmax=MPC4.Ts.*(0.95);
                    mv2rmin=MPC4.Ts.*(-0.4);
                    mv2rmax=MPC4.Ts.*(0.6375);

MV(1)=struct('Min',2.5,'Max',2.5,'RateMin',mv1rmin,'RateMax',mv1rmax);
MV(2)=struct('Min',-2.5,'Max',2.5,'RateMin',mv2rmin,'RateMax',mv2rmax);
MPC4.MV=MV; % alters M
```

A.6.2 MPC controller block dialogue box.

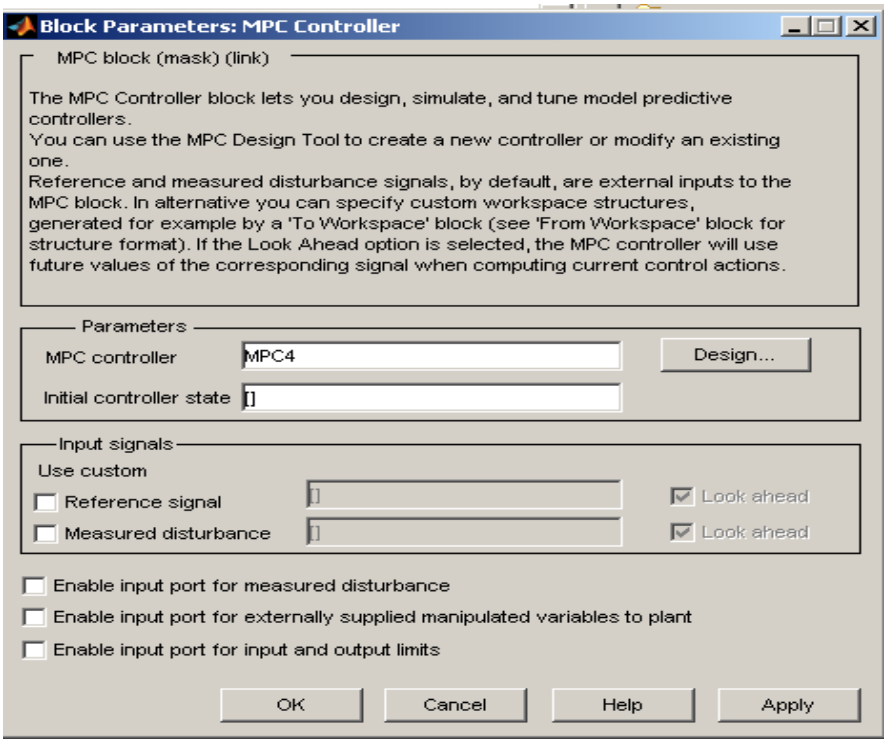

Figure A-7 MPC controller block dialogue box

A.7 Limitations

It was attempted to quantify the maximum load change that the controller could handle and to establish the limiting factors. It was found that to achieve a step up or down of 6 MW, the magnitude of helium input rate (controller output) should be greater than 2.27kg/s. TO achieve a step up of 10 MW, the input should be> abs(3.79kg/s). Results when the values max abs(input)=3.8kg/s were used are shown in Figure A-8 and Figure A-9 respectively. These limitations are the specifications of the valves used. Each valve has limit on the maximum flow-rate possible at a given temperature and pressure. These limitations are dependent on the manufacturing design specifications. For this work, it was assumed that a maximum rate of 2.5 kg/s was more realizable.

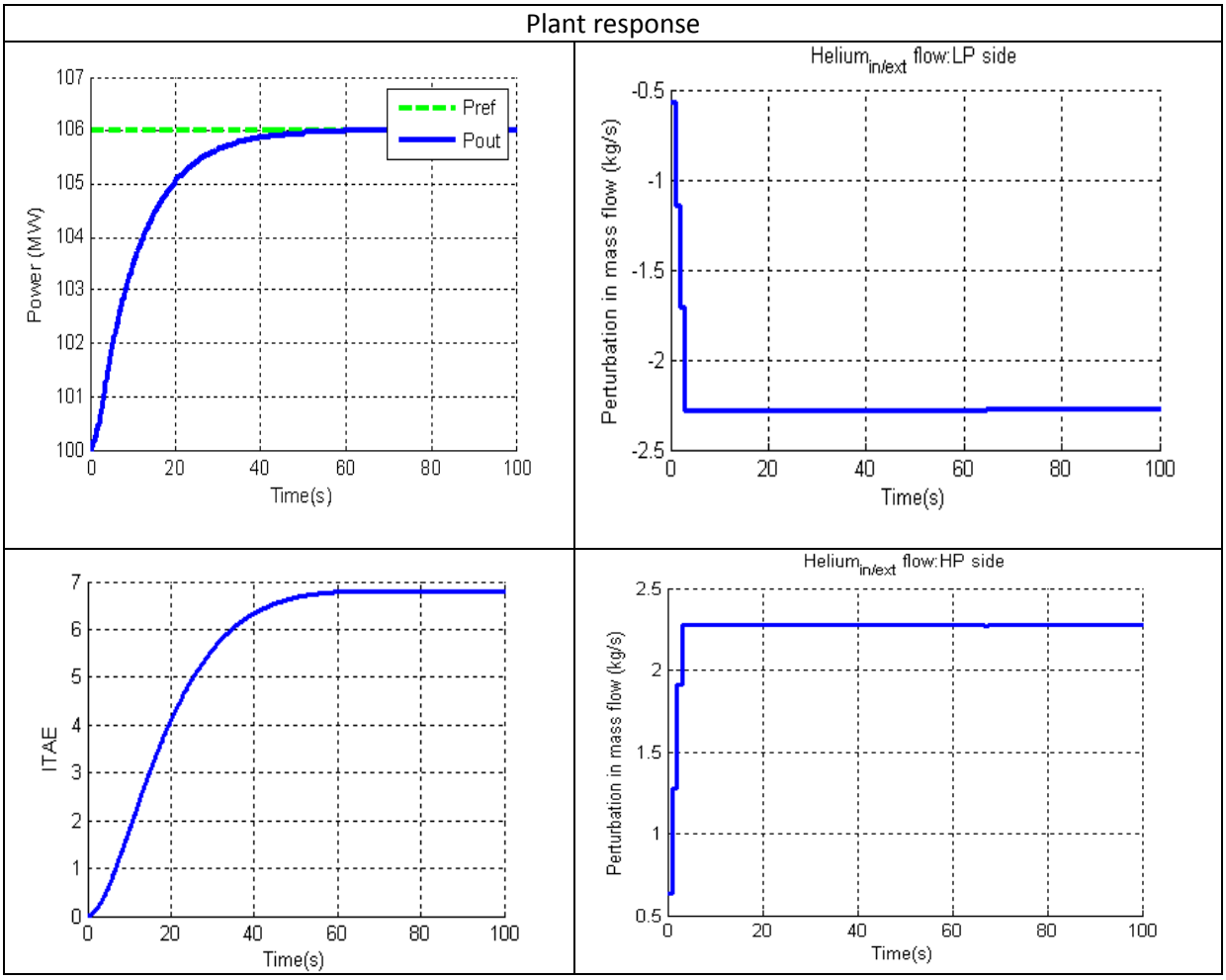

Figure A-8 Requirements for a 6 MW step change at in/out rate = 2.28kg/s

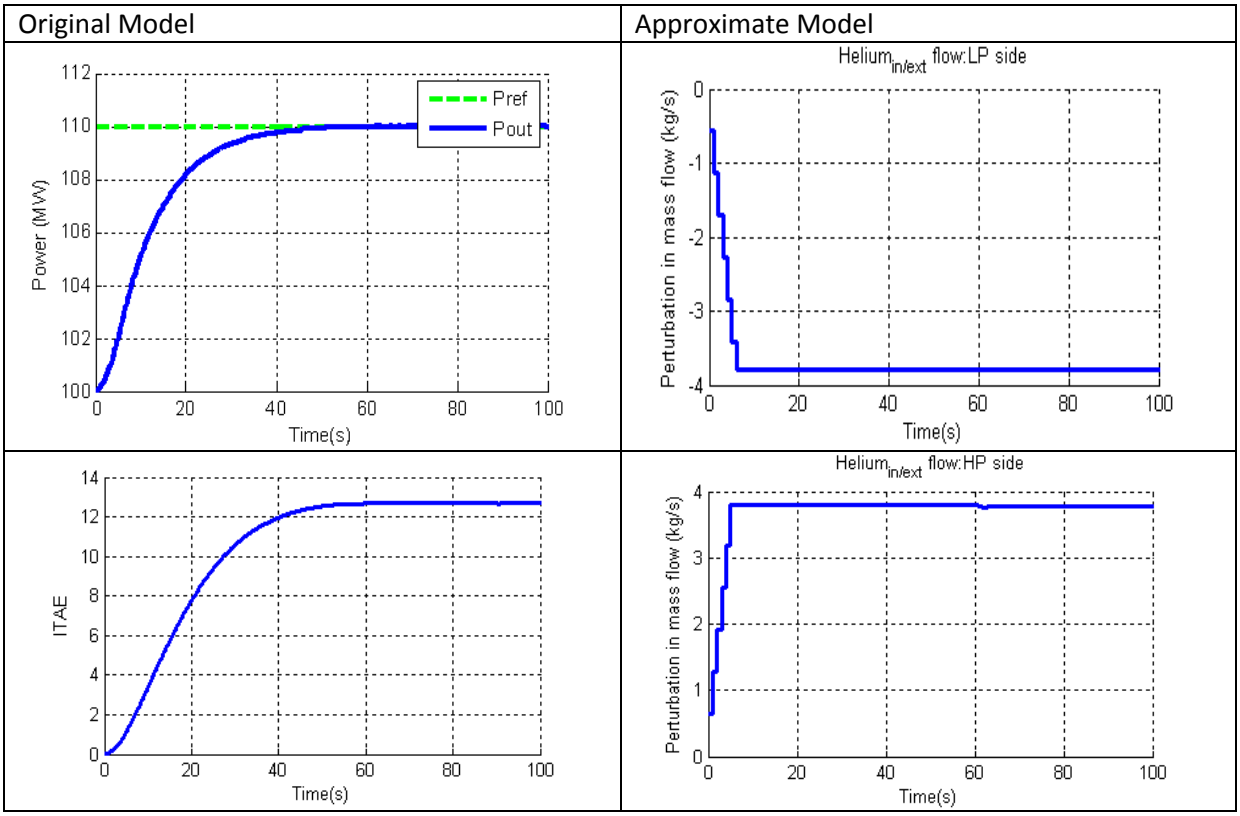

Figure A-9 Requirements for a 10 MW step change at in/out rate = 3.80kg/s

A.8 Reference Signals

A number of different reference trajectories were used to monitor the performance of the controller. This was in order to test the controller under all possible changes. The following reference signals were used to evaluate the controller performance.

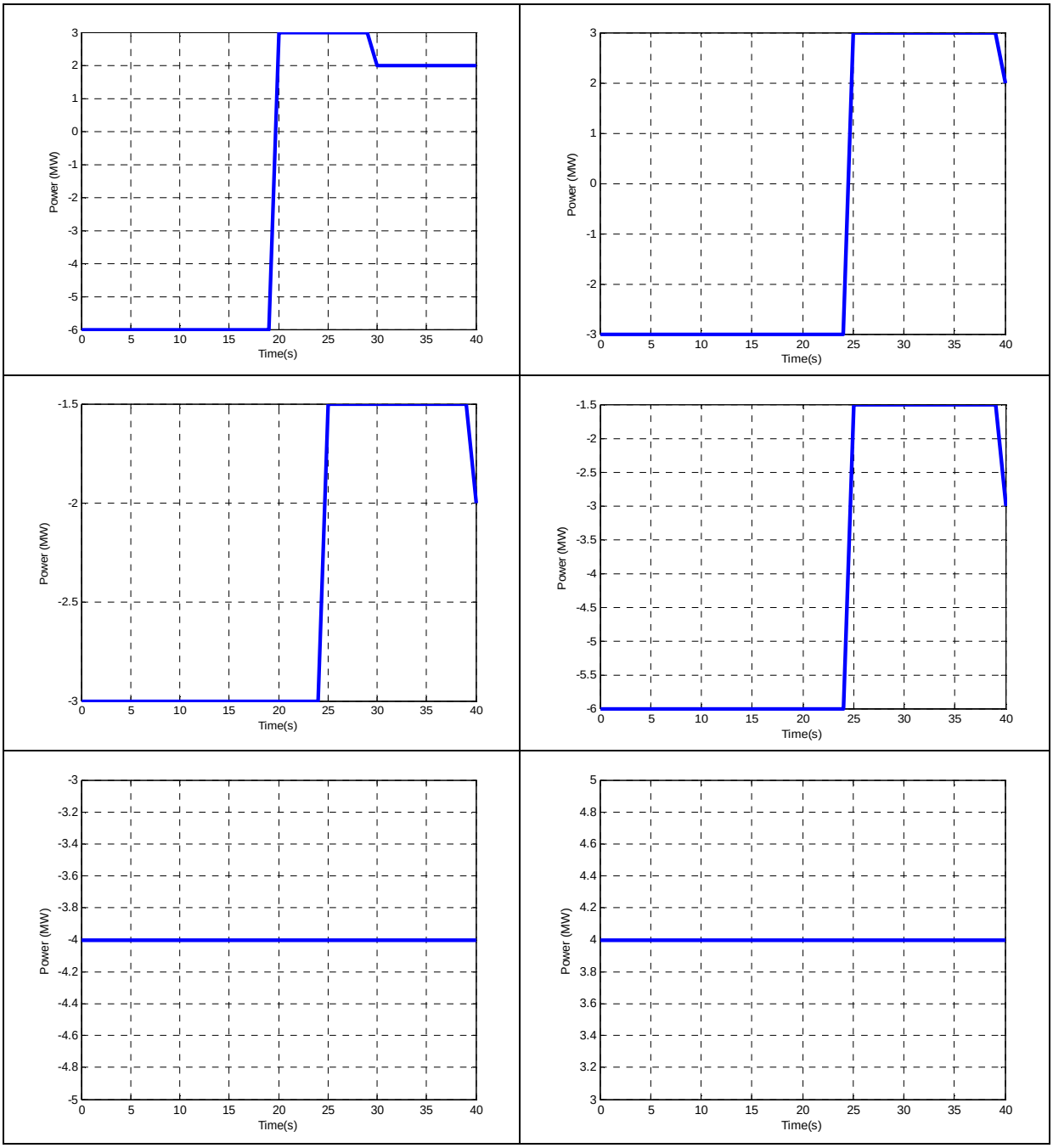

Figure A-10. Reference Signals

A.9 Mass flow-rate (Controller design)

Below is the mass flow-rate after injecting helium at a rate of 1kg/s for one second. The output flowrate stabilises at 0.01287 kg/s.

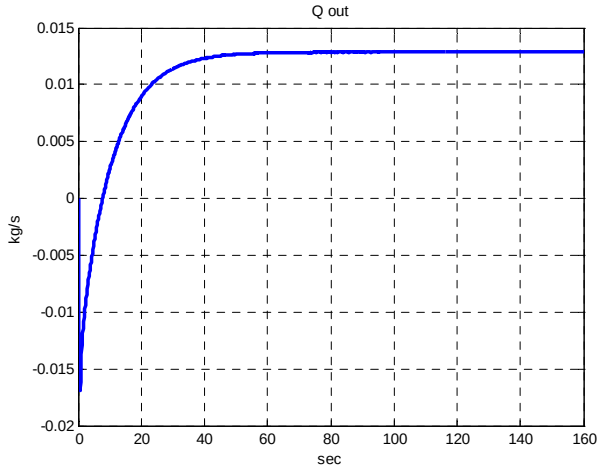

Figure A-11 Mass flow-rate of helium injection at a rate of 1kg/s for 1s

Below is the mass flow-rate after extracting helium at a rate of 1kg/s for one second. The output flowrate stabilises at 0.01288 kg/s.

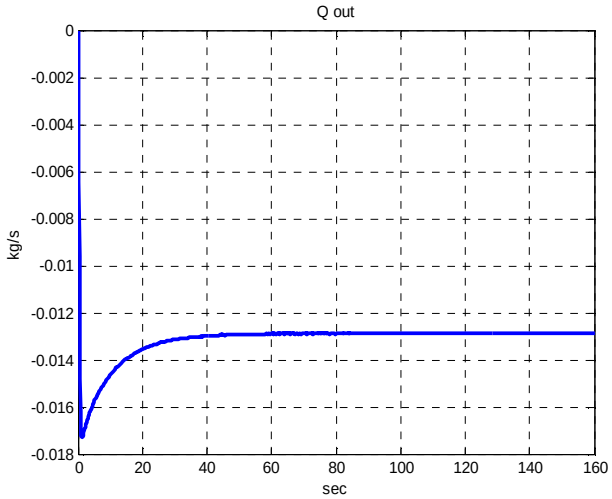

Figure A-12 Mass flow-rate during extraction of helium at a rate of 1kg/s for 1s

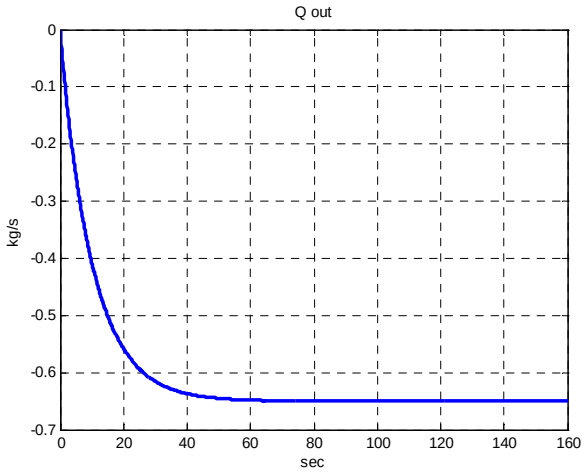

Figure A-13 Mass flow-rate during bypass at a rate of 1kg/s

A.10 Plant Disturbances

A.10.1 Leak flows in the system

The leak flows are incorporated in the system. These are represented using gains L1, L2 and L3. In Figure A-14 they are shaded. Their effect is also felt in other parts of the plant.

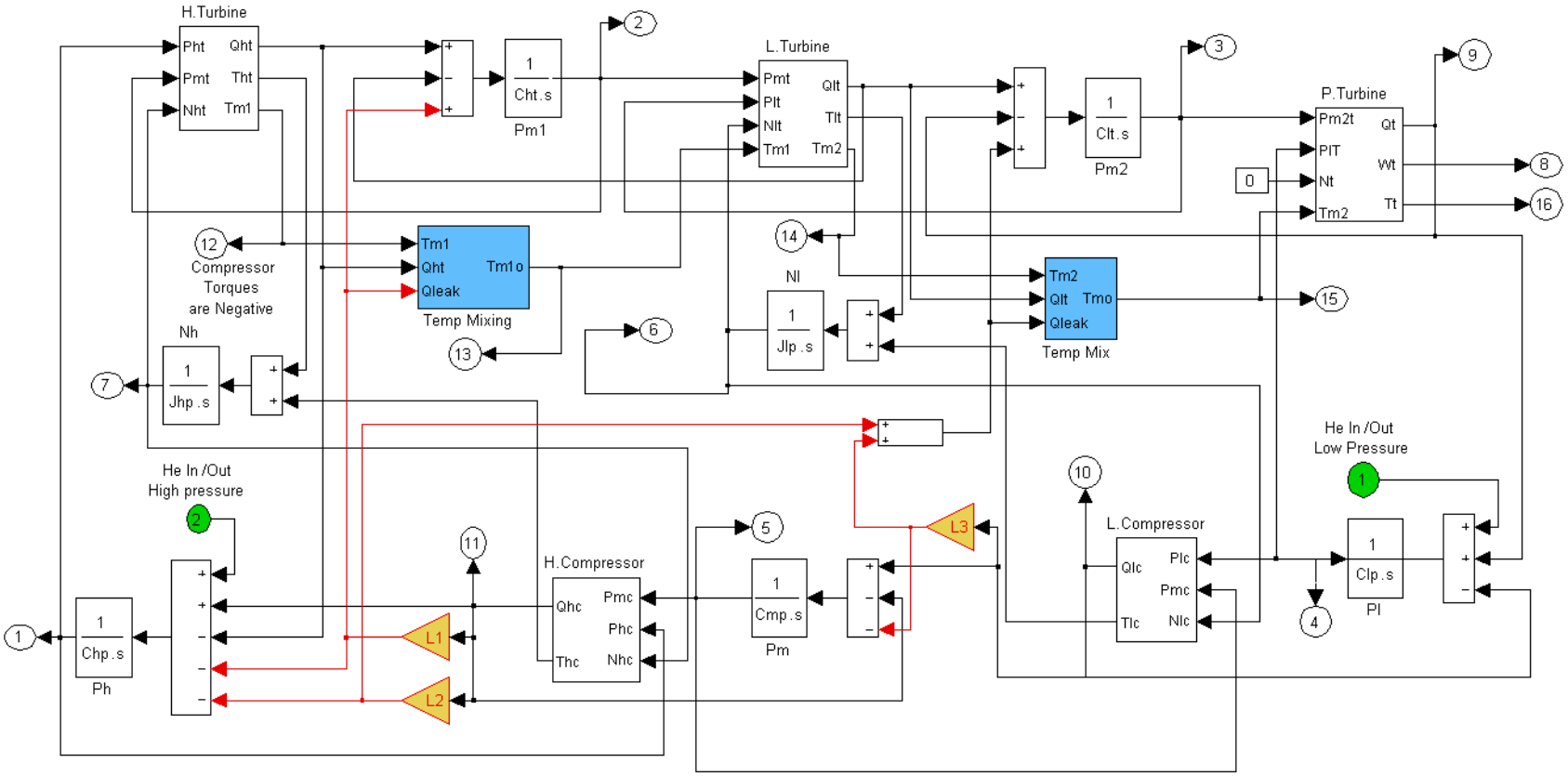

Figure A-14 Leak flow in the system

During recuperation, high temperature helium from the power turbine outlet is used to raise the temperature of helium flowing into the reactor. Heat exchange is dependent on the amount of helium flow which in turn is affected by leakages from the compressors to the turbines. In the figure below, the heat exchangers affected ("Temp mixing" and "Temp mix"), are shaded.

Leak flows L1, L2 and L3 are right after the low and high pressure compressors labelled as L. Compressor and H. Compressor respectively in the Simulink model.

A.10.2 White noise

The figures below show the response when white noise was added to the plant. The prediction horizon and control horizons were changed to see the effect that had in the presence of noise.

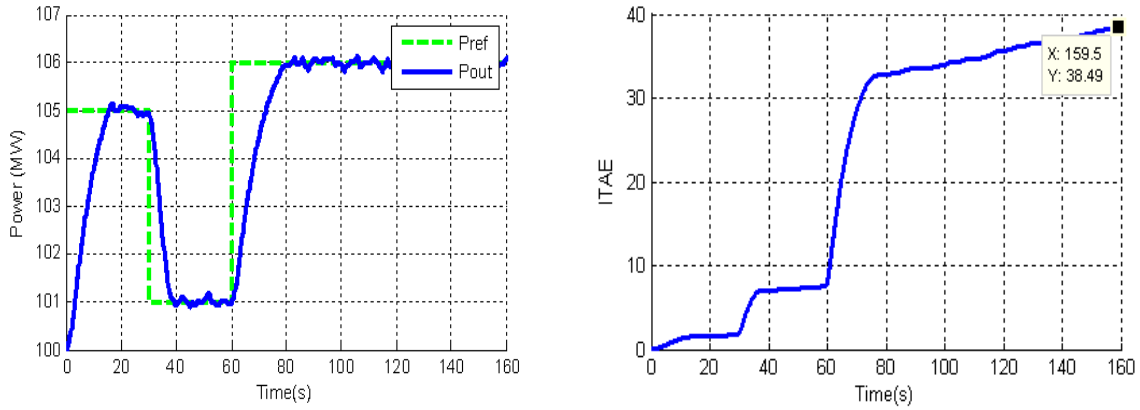

Figure A-15 Plant response in presence of white noise, P=73, M=4

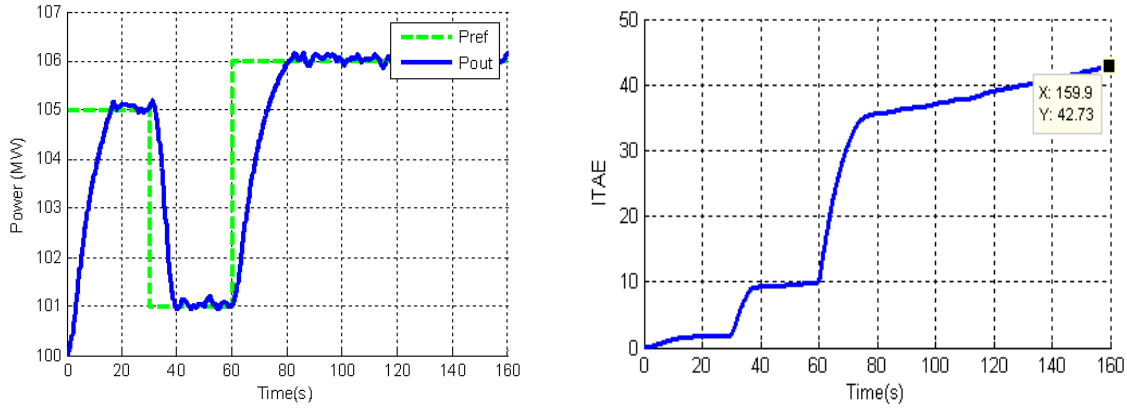

Figure A-16 Plant response in presence of white noise, P=24, M=9

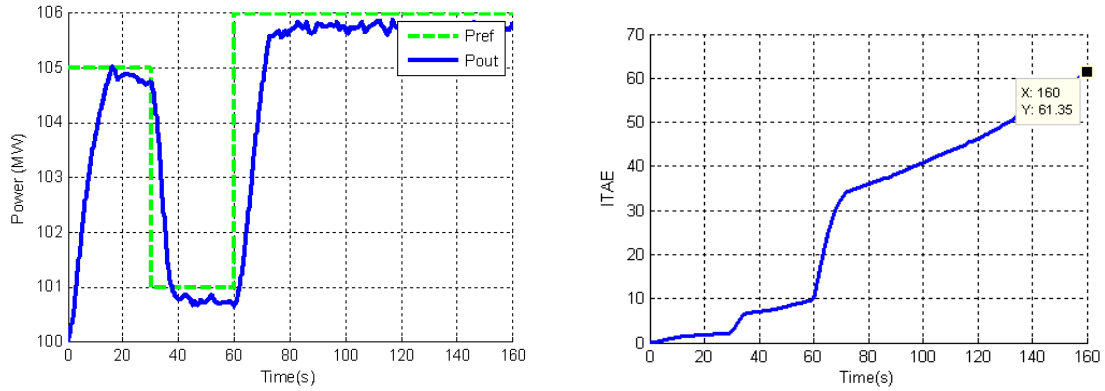

Figure A-17 Plant response in presence of white noise, P=24, M=14

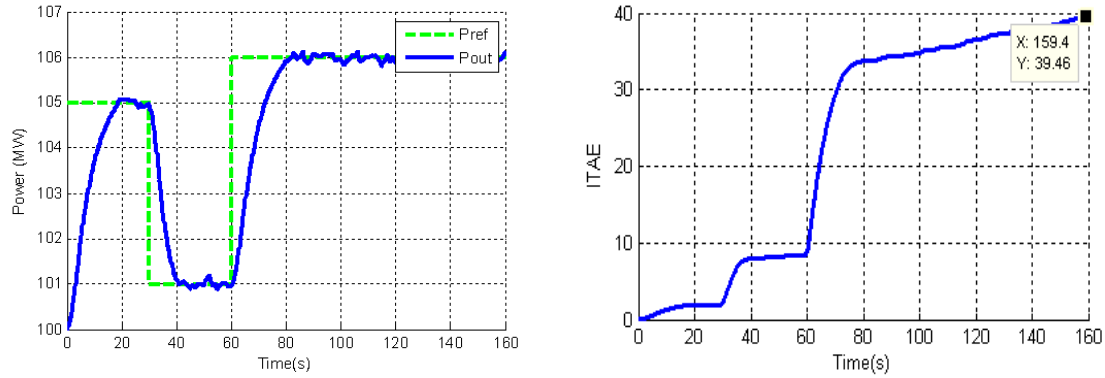

Figure A-18 Plant response in presence of white noise, P=20, M=2

A.10.3 Grid disturbance

The following is based on the grid disturbances. Below is a worst case scenario. A sampling rate of, $T = 0.1\ s$ was used. The system failed to track P_{ref} , the reference trajectory. When a sampling rate of, $T = 1\ s$ was used, the plant was able to track the reference trajectory.

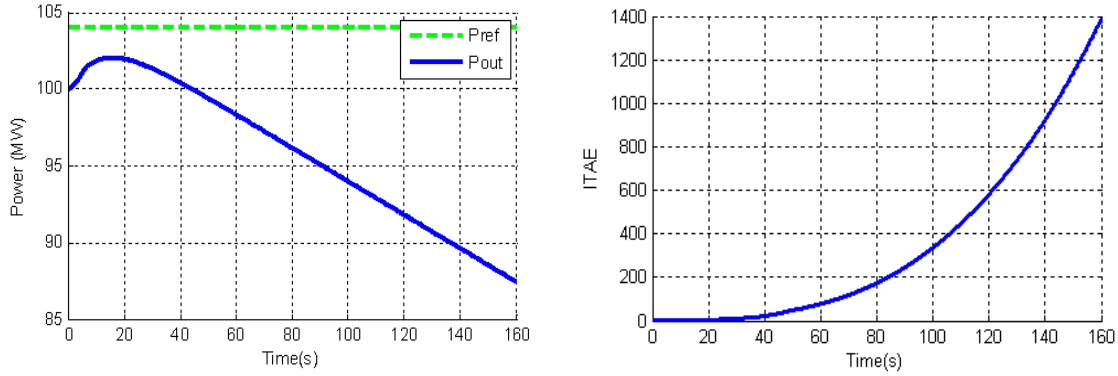

Figure A-19 Plant response & performance when a grid disturbance occurs at $T = 0.1s$

There are grid disturbances which result in an unstable plant response. Below are the control signals when a sampling rate of, $T = 0.1\,s$ is used. The response of the output is shown in Figure A-19.

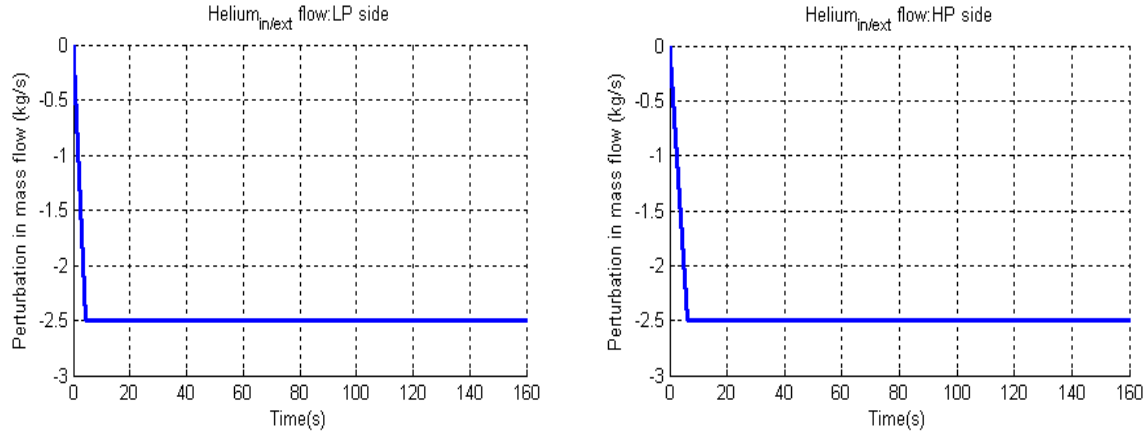

Figure A-19 Low and high pressure controller output for P=24, M=4

The figure below shows how the control horizon affects the plant response in the presence of an increase in the grid load.

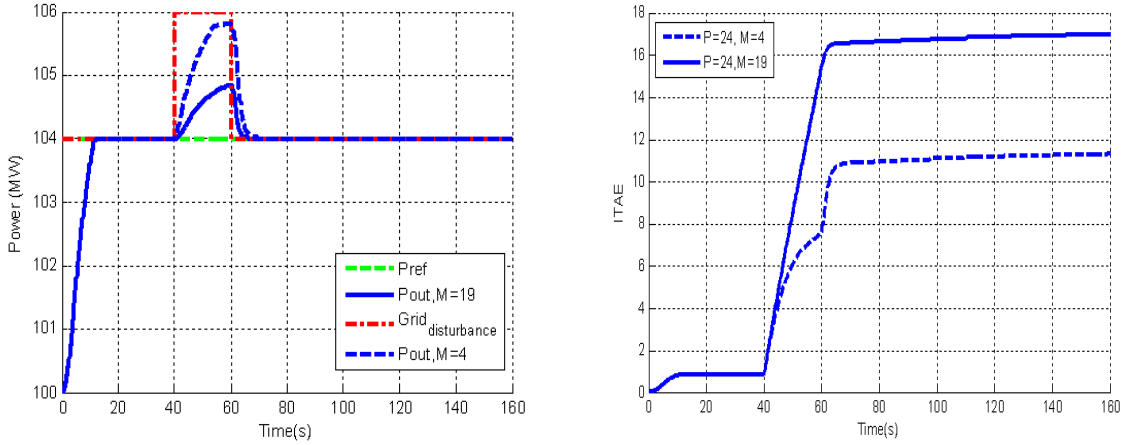

Figure A-20 Plant response and performance when control horizon is varied.

Disturbance reference signals

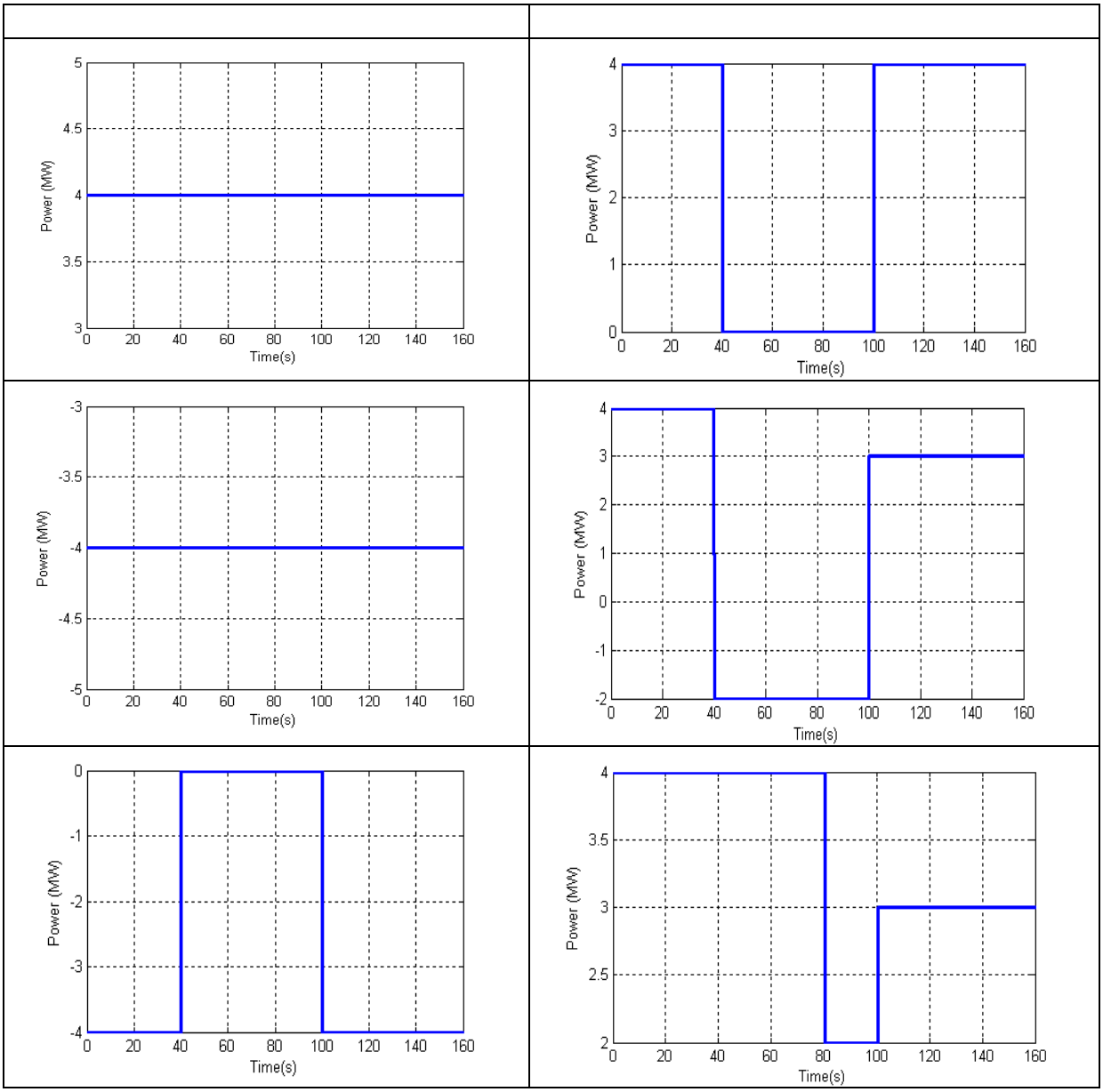

Figure A-21 Desired power output for disturbance analysis.

These signals were applied to the plant. The tables below show results of different disturbance signals applied to the plant. The column on the right shows the total ITAE value of all the responses. For the tables below, the colours blue, green and pink highlight the chosen, the best and the worst performance values respectively. In addition to the colour highlights, the "√" indicates best performance while "x" indicates worst performance. The asterisk shows the performance of the chosen parameter. The rows with results are divided into two. The top represent parameter values within the predetermined ranges.

Table A-3 Overall controller performance in presence of White noise

Control horizon	Prediction horizon	Pref 1 ITAE	Pref 2 ITAE	Pref 3 ITAE	Pref 4 ITAE	Pref 5 ITAE	Pref 6 ITAE	Total ITAE
4	73	8.39	8.39	39.01	38.28	54.72	14.23	163.018
4	60	8.40	8.40	39.06	38.30	54.96	14.22	163.337
14	45	510.34	513.66	350.92	347.97	349.22	398.44	2470.557
19	24	162.60	2.57E+11	2.57E+11	209.26	117.09	52.32	5.13E+11 x
14	24	34.37	27.26	238.41	67.62	81.10	41.65	490.401
9	24	10.66	9.98	38.51	38.95	55.29	16.54	169.927
4	24	8.45	8.46	39.31	37.82	54.71	14.16	162.914 *√
2	20	8.90	8.87	42.09	42.78	58.29	16.10	177.028
4	10	8.62	8.66	40.54	37.38	53.64	14.28	163.117
2	10	8.53	8.56	39.47	37.80	54.14	14.88	163.392
4	6	8.48	8.47	39.54	37.71	53.90	14.06	162.158

Table A-4 Overall controller performance in presence of a grid load decrease

Control horizon	Prediction horizon	Pref 1 ITAE	Pref 2 ITAE	Pref 3 ITAE	Pref 4 ITAE	Pref 5 ITAE	Pref 6 ITAE	Total ITAE
4	73	12.39	14.27	48.54	48.62	69.07	20.87	192.882
4	60	11.75	13.84	49.13	47.73	68.07	19.96	190.521
14	45	9.4	10.21	30.99	45.98	66.12	16.54	162.691√
19	24	9.86	9.43	27.86	130.11	80.47	20.47	257.730 x
14	24	8.86	14.42	45.17	45.53	71.55	16.22	185.528
9	24	9.04	12.06	36.16	45.59	68.19	16.30	171.036
4	24	9.6	12.33	46.14	44.64	66.02	16.80	178.730*
2	20	11.51	12.42	35.41	49.39	69.07	17.50	177.804
4	10	8.89	11.96	36.09	46.78	66.84	17.76	170.564
2	10	10.14	11.86	34.20	51.70	69.27	18.38	177.174
4	6	9.65	13.75	45.09	57.08	67.77	20.15	193.334

Table A-5 Overall controller performance in presence of a grid load increase

Control horizon	Prediction horizon	Pref 1 ITAE	Pref 2 ITAE	Pref 3 ITAE	Pref 4 ITAE	Pref 5 ITAE	Pref 6 ITAE	Total ITAE
4	73	13.6757	12.16	51.96	34.63	46.72	22.77	159.141
4	60	13.0095	11.42	50.86	33.90	45.92	21.70	155.0971
14	45	12.9481	8.50	47.96	31.41	271.58	20.27	372.394 x
19	24	16.9771	8.17	67.64	34.66	175.14	24.44	302.5846
14	24	9.2132	9.22	209.21	29.62	43.09	16.59	300.3549
9	24	10.2761	8.69	67.01	29.61	42.82	17.38	158.4091
4	24	11.3153	9.25	51.88	31.11	43.67	18.59	147.23*√
2	20	11.4483	11.46	161.26	32.00	43.37	18.67	259.5484
4	10	11.5334	8.54	157.70	33.29	44.40	20.12	255.4599
2	10	11.6273	9.83	149.30	33.08	44.60	19.98	248.4509
4	6	14.3936	9.59	226.53	34.88	46.13	24.12	331.5273

Table A-6 Overall controller performance in presence of control disturbance

Control horizon	Prediction horizon	Pref 1 ITAE	Pref 2 ITAE	Pref 3 ITAE	Pref 4 ITAE	Pref 5 ITAE	Pref 6 ITAE	Total ITAE
4	73	6.27	6.50	35.74	32.36	49.09	11.08	141.043√
4	60	6.31	6.52	35.74	32.30	353.66	11.08	445.620
14	45	531.51	492.49	343.02	366.19	353.66	417.51	2504.38 x
19	24	48.60	43.71	64.44	211.37	125.62	51.15	544.892
14	24	36.17	41.19	219.55	65.40	79.65	41.32	483.275
9	24	6.57	6.91	35.31	43.68	54.20	10.82	157.494
4	24	6.46	6.70	36.01	32.09	49.32	11.23	141.825*
2	20	7.03	7.45	40.52	37.02	54.47	12.83	159.311
4	10	6.67	7.02	37.42	32.16	49.01	11.60	143.898
2	10	6.85	7.23	39.01	32.54	49.45	12.20	147.285
4	6	5.97	6.55	36.71	32.03	48.44	10.92	140.622